UNIVERSITÀ DEGLI STUDI DI PADOVA

Sede Amministrativa: Università degli Studi di Padova

DIPARTIMENTO DI GEOSCIENZE

SCUOLA DI DOTTORATO DI RICERCA IN: SCIENZE DELLA TERRA

CICLO: XXV

WHAT GARNET, CLINOPYROXENE AND DIAMOND POTENTIAL CAN TELL US ABOUT THE EVOLUTION OF SUB-CRATONIC MANTLE SECTIONS: A CASE STUDY OF THE ZAGADOCHNAYA KIMBERLITE (YAKUTIA)

Direttore della Scuola: Ch.mo Prof. Massimiliano Zattin

Supervisore: Ch.mo Prof. Paolo Nimis

Dottorando: Luca Ziberna

ABSTRACT

This PhD provides major and trace element compositions for a new suite of Cr-rich garnet xenocrysts and associated minerals from the diamond-free Zagadochnaya kimberlite, Daldyn Field, Yakutia (Russia). Interpreting the nature and evolution of the underlying lithospheric mantle from these samples requires a good understanding of relationships between pressures and temperatures of formation, upper mantle phase relations and trace element signatures of petrochemical processes. I addressed these issues by integrating three main lines of research.

i) *Evaluation of single-clinopyroxene geobarometry for garnet peridotites.* Single-clinopyroxene thermobarometry represents the most reliable method among single-mineral thermobarometric techniques for mantle rocks, but the geobarometer tends to produce considerable scatter in P–T estimates when applied to clinopyroxenes with unfavourable compositions. Multiple electron microprobe analyses on compositionally diverse clinopyroxenes, using different analytical conditions, demonstrated that this scatter is mostly related to propagation of analytical errors on the calculated Cr-in-cpx pressure. The results of this analytical tests were used to calculate model analytical errors and propagated P uncertainties for a large set of published analyses of mantle-derived, xenolith-borne clinopyroxenes. I found that the parameter a_{Cr}/Cr# [where a_{Cr} = Cr–0.81•Na•Cr#, Cr#=Cr/(Cr+Al), atoms per 6-oxygen formula unit] can be used to discriminate clinopyroxenes for which analytical errors alone will propagate unacceptable P uncertainties (i.e., higher than ±0.25 GPa) for several combinations of analytical conditions. I therefore defined a new optimized analytical procedure for single-clinopyroxene geobarometry, which significantly decreases the pressure uncertainties and allows a better definition of clinopyroxene-based geotherms.

ii) *Thermodynamic modeling of natural peridotitic systems.* Calculations of phase equilibria in Cr-bearing peridotitic systems were used to predict the effects of P, T and bulk compositional variations on garnet–spinel relations in fertile and depleted mantle compositions. Calculations showed that in cratonic lithospheric sections the width of the garnet–spinel transition strongly depends on bulk composition: in a fertile mantle, spinel can coexist with garnet to about 120 km depth, while in an ultra-depleted harzburgitic mantle it can be stable to over 180 km depth. In the garnet+spinel stability field the calculated modes of spinel are very low (0.1–2.8 %), suggesting that spinel grains may be easily overlooked in mantle xenoliths. The model also suggests a significant potential role of P–T conditions on the distribution of garnets in the popular Ca–Cr discrimination diagram.

iii) *Interpretation of the mantle record in the Zagadochnaya kimberlite.* A suite of 28 garnet xenocrysts, often containing polymineralic inclusions, were selected from a heavy-mineral concentrate of the Zagadochnaya kimberlite for detailed electron microprobe analysis and laser-ablation inductively-coupled mass spectrometry. Robust P–T estimates for the garnets and associated clinopyroxenes and the Ca and Cr contents in the garnets indicate that the kimberlite sampled only a shallow mantle portion (< 130 km), which was mainly composed by fertile to depleted lherzolites and essentially corresponds to the shallow, lherzolite-rich layer previously defined on the basis of xenoliths/xenocrysts from the neighbor, highly diamondiferous Udachnaya kimberlite. The less (Ca, Cr)-rich garnets show chondrite-normalized Rare Earth Elements (REE) patterns, characterized by very low Light REE (LREE) increasing through the Middle REE (MREE) to the Heavy REE (HREE). With increasing Ca and Cr the garnets show increasing LREE and decreasing HREE, eventually resulting in sinusoidal patterns. Numerical simulations of melt/rock reactions demonstrated that such REE variability can be produced by a unique episode of melt injection and percolation through a refractory mantle column. Most garnet grains were partially replaced by low-Cr garnets + Cr-spinel + diopside (± hydrous minerals and Ti-oxides). The textures and mineralogy of these secondary mineral assemblages, the calculated trace element compositions of the equilibrium melts, and the Ca concentration profiles across garnet zoning, indicate pervasive reaction with melts strictly related to the host kimberlite. A relatively slow ascent of the kimberlite up to shallow mantle levels before eruption is suggested, which would explain the lack of xenocrysts from depths > 130 km, the absence of diamond, the Mg-rich composition of the kimberlite, and the pervasive reactions that produced the secondary assemblages.

RIASSUNTO

Nella presente tesi di dottorato vengono riportate le composizioni chimiche in elementi maggiori e in tracce di una nuova serie di xenocristalli a granato e minerali associati provenienti dalla kimberlite di Zagadochnaya, Daldyn Field, Yakutia (Russia). Per interpretare la natura e l'evoluzione geochimica del mantello litosferico sottostante è importante capire le condizioni di temperatura e pressione di formazione dei vari frammenti di mantello, le relazioni di fase nel mantello superiore, e le evidenze dei processi petrogenetici registrate negli elementi in tracia. In questa tesi, queste problematiche sono state affrontate in tre diverse linee di ricerca.

i) *Valutazione del geobarometro a clinopirosseno per le peridotiti a granato*. Tra i vari metodi termobarometrici basati sulla composizione di una singola fase mineralogica, il termobarometro a clinopirosseno rappresenta il metodo più affidabile per le rocce di mantello. Nonostante ciò, è stato visto che il geobarometro può essere molto impreciso se applicato a certi clinopirosseni con composizione sfavorevole, e questo si riflette in una considerevole incertezza nella stime delle geoterme. In questo lavoro ho effettuato ripetute analisi tramite microsonda elettronica su clinopirosseni a diverse composizioni, utilizzando diverse condizioni analitiche. I risultati dimostrano che le buona parte delle incertezze sono legate alla propagazione degli errori analitici sulle pressioni calcolate con il geobarometro. I dati ottenuti dal test analitico sono stati poi utilizzati per stimare gli le incertezze analitiche e la loro propagazione sulle pressioni calcolate per un gran numero di analisi di clinopirosseni di mantello riportate in letteratura. Il parametro a_{Cr}/Cr# [dove a_{Cr} = Cr–0.81•Na•Cr#, Cr#=Cr/(Cr+Al), atomi per unità di formula, 6 ossigeni] può essere utilizzato per discriminare i clinopirosseni per i quali la propagazione dell'errore analitico è troppo elevata (i.e., deviazione standard > 0.25 GPa). Ciò mi ha permesso di definire una nuova procedura analitica che permette di diminuire notevolmente le incertezze sulle pressioni calcolate e quindi definire meglio le geoterme basate su clinopirosseni di mantello.

ii) *Modellizzazione termodinamica di sistemi peridotitici con composizioni naturali.* Per comprendere l'effetto della pressione, temperatura e composizione sulle relazioni tra granato e spinello nel mantello superiore, ho effettuato dei calcoli termodinamici per sistemi peridotitici contenenti Cr. I calcoli hanno mostrato che nella litosfera cratonica la transizione da facies a spinello a facies a granato dipende dalla composizione totale della peridotite: in un mantello fertile, lo spinello può coesistere con il granato fino a ca. 120 km di profondità, mentre in un mantello molto impoverito lo spinello può essere stabile fino a 180 km di profondità. Nella facies granato+spinello, l'abbondanza modale dello spinello è molto bassa

(0.1–2.8%). Il modello suggerisce anche un maggiore influenza della pressione e della temperatura nella distribuzione dei granati nei classici diagrammi classificativi basati sul contenuto in Cr e Ca.

iii) *Interpretazione dei campioni di mantello della kimberlite di Zagadochnaya*. Una serie rappresentativa di 28 xenocristalli di granato, spesso contenenti inclusioni di diverse fasi mineralogiche, è stata caratterizzata per gli elementi maggiori e in tracce tramite microsonda elettronica e spettrometria di massa associata a microsonda laser. Le stime termobarometriche più affidabili per i granati e i clinopirosseni associati, assieme al contenuto in Cr e Ca dei granati, indicano che la kimberlite ha campionato solo una porzione superficiale del mantello (< 130 km), composta da lherzoliti variamente fertili fino a impoverite. In termini litologici, questa porzione è equivalente a alla porzione più superficiale del mantello campionato dalla vicina kimberlite diamantifera di Udachnaya. I granati meno ricchi in Cr e Ca mostrano dei pattern normalizzati delle terre rare (REE) con un aumento progressivo dalle terre rare leggere (LREE) alle pesanti (HREE). Con l'aumento di Ca e Cr, si nota anche un arricchimento in LREE e impoverimento delle HREE, fino ad avere dei pattern delle REE sinusoidali. Grazie alle simulazioni numeriche delle reazioni fuso/roccia, è stato possibile dimostrare che queste variazioni delle REE possono essere il risultato di un unico episodio di percolazione di fuso in una colonna di mantello originariamente refrattaria. La maggior parte dei granati mostrano evidenze di ricristallizzazione con formazione di granato impoverito in Cr + cromite + diopside (± minerali idrati e ossidi di Ti). La tessitura e la mineralogia di questi domini secondari, la composizione calcolata dei fusi in equilibrio, e i profili di concentrazione attraverso le zonature del granato, indicano che questi sono dei prodotti di reazione con fusi strettamente legati alla kimberlite di Zagadochnaya. Viene qui suggerita una risalita relativamente lenta della kimberlite fino ai livelli superficiali del mantello prima dell'evento eruttivo. Questo spiegherebbe la mancanza di xenocristalli da profondità > 130 km, l'assenza di diamante, l'arricchimento in Mg della kimberlite, e le reazioni spinte che hanno prodotto gli assemblaggi secondari.

ACKNOWLEDGEMENTS

This PhD was funded by Fondazione Cassa di Risparmio di Padova e Rovigo – “Progetto Dottorati di Ricerca 2009”.

I would like to gratefully thank
Prof. Paolo Nimis, Prof. Fabrizio Nestola, Prof. Stephan Klemme, Prof. Andrea Marzoli, Dott. Alberto Zanetti, Raul Carampin, Dott. Angelo de Min, Dott. Davide Lenaz, Prof. Andrew Putnis,
for providing carefully considered advice and for the valuable discussions throughout the duration of the project

I doubt I could have gotten through the PhD without you, Sula. It’s all thanks to you, keeping me on the right path, picking me up when I fell down, and always being with me.

THESIS LAYOUT

The main section of the present thesis consists of a collection of two manuscripts which have been submitted to peer-reviewed journals (*Manuscripts 2* and *3*) and one manuscript in preparation (*Manuscript 1*). The manuscripts develop and discuss in detail specific lines of research that have been pursued during the PhD. Before the manuscripts, an introduction chapter provides a brief overview of the current state of knowledge on the sub-cratonic lithospheric mantle, with particular emphasis on issues addressed in this work, and outlines the particular focuses and aims of the individual lines of research and of the thesis as a whole. A chapter on the methodological approach describes the rationale of the methodologies used in this work. After the manuscripts, I discuss the main results of the work and their bearing on future studies on mantle samples from cratonic settings.

CONTENTS

INTRODUCTION

Cratons and the samples of sub-cratonic mantle

The flat, tectonically stable interior of a continent was called *cratogen* for the first time in 1921 by the Viennese geologist Leopold Kober (Kober 1921). This word derives from the Greek *kratos*, meaning strong and unyielding. Now the term *craton* is generally used to indicate a segment of continental crust that has attained and maintained long-term stability since the Archean or, at least, the Proterozoic, with tectonic reworking being confined to its margins (Bleeker 2003; Cawood et al. 2013). Cratons extend laterally for hundreds of kilometers (Fig. 1), and are underlain to depths of 180–250 km by mantle roots that are chemically and physically distinct from the surrounding mantle. Despite continental collisions and other tectonic events and limited interactions with asthenospheric melts and fluids during Earth's history, the mantle roots of the cratons have largely survived since their formation and are characterized by relatively cold thermal regimes. Extensive reviews on the nature and origin of cratons and their underlying lithospheric mantle, from different perspectives, can be found in, e.g., Pearson and Nowell (2002), Griffin et al. (2003a), Lenardic et al. (2003), Sleep (2004), Pearson and Wittig (2008), and Lee et al. (2011).

Much of what we know of sub-cratonic mantle roots comes from the study of kimberlites. Kimberlites are volatile-rich (dominantly CO_2) potassic ultrabasic volcanic rocks which occur mostly in cratons and their margins (Mitchell 1995; Woolley et al. 1996). They are the major host of diamonds and have received special attention over the last century from both the scientific community and mineral exploration companies. Thanks to their deep-seated origin and their violent eruption style, kimberlites carry abundant mantle fragments from depths as great as 200–250 km to the surface. These fragments, which occur as xenoliths or xenocrysts, are unique samples that reveal the mineralogical and geochemical composition of the sub-cratonic lithospheric mantle and its evolution through Earth's history (e.g. Boyd 1989; Pearson et al. 1995; Boyd et al. 1997; Pearson and Nowell 2002; Pearson et al. 2003; Simon et al. 2007).

The vast literature on kimberlite-borne mantle xenoliths and kimberlite mineral concentrates indicates that the dominant rock type forming the lithospheric mantle beneath cratons is peridotite. Only a minor part (less than 2 vol%) is represented by eclogite and pyroxenite (cf. Harte 1983; Schulze 1989; Nixon 1987; Pearson et al. 2003). The majority of peridotites are clinopyroxene-poor lherzolites and harzburgites, which typically contain spinel at moderate pressures and garnet at high pressures.

In order to develop a full understanding of the physico-chemical structure of the sub-cratonic lithospheric mantle, it is critical to integrate the studies on natural samples with geological and geophysical data, high-P and high-T experiments, and thermodynamic studies (e.g. Chatterjee and Terhart 1985; Nickel and Green 1985; James et al. 2004; Menzies et al. 2007; Klemme et al. 2009; Afonso et al. 2010; Bascou et al. 2011; Mather et al. 2011; Herzberg and Rudnick, 2012). In this respect, however, it is important to realize the particular nature of the samples upon which much of the study of the lithospheric mantle is based. Firstly, mantle fragments included in kimberlites generally range from 20-30 cm (in rare cases up to 1–2 m) to less than 1 cm and are composed by mineral grains as large as 1 cm (Boyd & Mertzman, 1987; Nixon, 1987; Boyd et al., 1997; MacKenzie & Canil, 1999; Ionov et al., 2010). Therefore, one may question whether these fragments are truly representative of the mantle sections traversed by the kimberlite. This issue is even more problematic when the only available mantle fragments in a given kimberlite consist of isolated xenocrysts of mantle minerals (such as garnets, clinopyroxenes, and chromites), which can be a consequence of both the disaggregation of the xenoliths during the violent transport to the surface and later hydrothermal alteration. Secondly, the original geochemical and mineralogical features of the

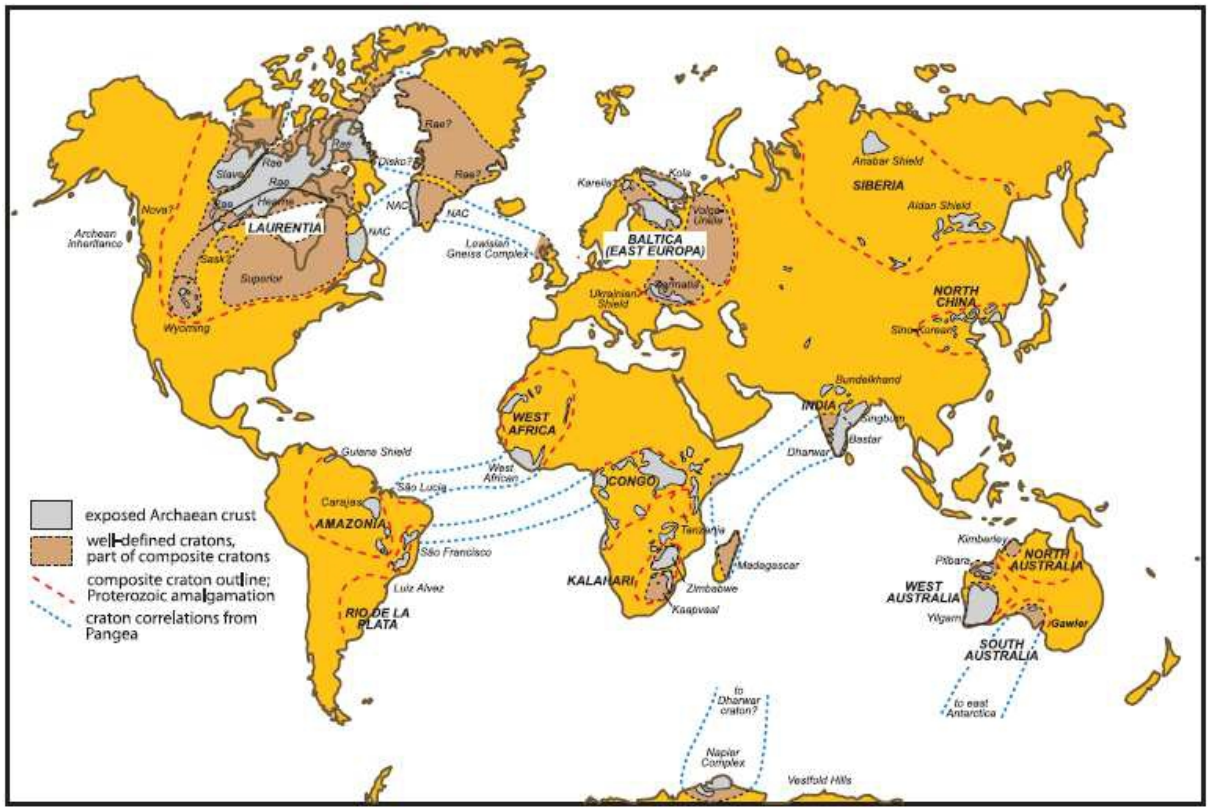

Fig. 1: *Global distribution of cratons (Pearson and Wittig 2008, modified after Bleeker 2003). Outcrops of Archaean crustal rocks are indicated in grey and other definable fragments of composite cratons in brown. Red dashed lines show the estimated extent of cratonic regions amalgamated from Archaean blocks during the Proterozoic. Blue dotted lines extended across oceanic areas show links between cratonic fragments that are thought to have once formed single cratonic blocks. NAC, North Atlantic Craton.*

mantle sample are often strongly modified by processes that are directly or indirectly related to the host magma. It is therefore of primary importance that all the available mantle samples are properly characterized and that their geochemical and mineralogical evolution, from their origin to the entrapment in the host magma and eruption to the surface, is understood. An example of this type of survey is represented by *Manuscript 3* in this work.

Thermodynamics and thermobarometry of mantle peridotites

The variations in upper mantle mineralogy with changing pressure, temperature, and bulk composition is constrained by high-pressure, high-temperature experiments in model and natural systems. Thermodynamic models can be developed from the experimental data and can be used to predict phase relationships at conditions not yet achieved by experiments. The simplified model system CaO-MgO-Al_2O_3-SiO_2 has often been used to study the fundamental phase relationships in mantle rocks (e.g., MacGregor 1965; Jenkins and Newton 1979; O'Neill 1981; Gasparik 1984; Klemme and O'Neill 2000; Walter et al. 2002), but the significant influence of less abundant components such as FeO, Cr_2O_3 and Na_2O has long been recognized (e.g., O'Neill 1981; Nickel 1986; Webb and Wood 1986; Doroshev et al. 1997, Girnis et al. 2003; Klemme 2004). However, quantitative thermodynamic models that faithfully reproduce all phase relationships in complex, natural, mantle systems are still lacking. The development of improved thermodynamic models for peridotite compositions similar to those in Earth's mantle is one of the main lines of research in this work (cf. *Manuscript 2*).

Thanks to the rapid ascent rates of the host volcanics, the high-pressure and high-temperature equilibrium states of the mantle mineral assemblages are often preserved and recorded by the compositions of the minerals in the xenoliths. This allows the application of a variety of geothermobarometers to estimate the depth of provenance of the kimberlite-borne mantle samples (e.g., MacGregor 1974; Ellis and Green 1979; Harley and Green 1982; Nickel and Green 1985; Brey and Köhler 1990; Taylor 1998; Brey et al. 2008), as well as to define the mantle thermal state and geotherm at the time of eruption (e.g., Boyd 1973; Mather et al. 2011). Conventional geothermobarometers were calibrated on high-temperature, high-pressure experiments in simple and complex systems that approach the typical compositions of the mantle rocks. They are based on the partitioning of major elements between two minerals in chemical equilibrium and, therefore, require the coexistence of these minerals in the mantle xenolith. For what concern garnet peridotites, one of the most reliable method for temperature estimates is the two-pyroxene thermometer of Taylor (1998), while the Al-in-Opx geobarometer of Nickel and Green (1985), or its modification proposed by Carswell

(1991), are considered to be the most reliable geobarometers (cf. Nimis and Grütter 2010, 2012; Wu and Zhao 2011).

In some cases, thermobarometric formulations can be devised that allow estimation of P and T on the basis of the composition of a single mineral (e.g. Ryan et al. 1996; Nimis and Taylor 2000; Ashchepkov 2006; Grütter et al. 2006; Simakov 2008; Creighton 2009; Turkin and Sobolev 2009). In the case of disaggregated xenocrysts, heavy-mineral concentrates and monomineralic inclusions in diamonds, single-mineral thermobarometers are the only suitable methods. Although the composition of only one mineral is used in calculations, single-mineral methods are still based on the partitioning of major or minor components between two mineral phases, therefore chemical equilibrium with the missing mineral remains a necessary assumption. Problems in single-mineral thermobarometry may derive from simplified assumptions concerning the composition of the missing mineral and the effect of bulk chemical variations. As a consequence, most single-mineral thermobarometers tend to produce large uncertainties in the calculation of the P–T of equilibration. Based on the recent review of Nimis and Grütter (2010), the most reliable single-mineral thermometer for garnet peridotites is the enstatite-in-Cpx thermometer of Nimis and Taylor (2000). This method can be coupled with the Cr-in-Cpx barometer of Nimis and Taylor (2000) to obtain P–T pairs from a single clinopyroxene. Since the stability of diamond is primarily controlled by pressure and temperature, this method has become popular in diamond exploration programs (Cookenboo and Grütter 2010). The problem of the reliability of the Cr-in-Cpx barometer in common applications is explored in *Manuscript 1* of this work.

Geochemistry and mantle evolution

The major element composition of cratonic peridotitic xenoliths indicate a more *depleted* nature with respect to abyssal or orogenic peridotites (cf. Griffin et al. 2003: Pearson et al. 2003; Pearson and Wittig 2008). The term *depleted* and its antonym *fertile* are generally used to indicate low or, respectively, high contents of "basaltic" components, such as CaO, Al_2O_3, FeO, TiO_2, Na_2O and K_2O. There is wide consensus that the depletion of cratonic peridotites is a consequence of high degrees (> 30%) of melt extraction in Archean times (e.g. Boyd and Mertzman 1987; Boyd 1989; Walter 1998; Pearson and Wittig, 2008; Doucet et al. 2012). Controversy still revolves around the geotectonic environments that allowed melting to such extensive degrees (see, for example, the extensive review of Pearson and Witting, 2008 and Cawood et al. 2013). The two most favored scenarios are decompression melting in upwelling mantle, which sometimes is linked to mantle plumes (e.g. Griffin et al. 1999a; Aulbach et al. 2007; Arndt et al. 2009; Doucet et al. 2012), and melting in a supra-subduction zone setting,

with or without prior melting at ridges (e.g. Parman et al. 2004; Canil 2004; Lee 2006; Simon et al. 2007; Pearson and Wittig 2008).

Xenoliths only rarely have simple depleted mantle signatures and almost always record some degree of metasomatic enrichment due to reactions with ascending melts or fluids. Metasomatism is commonly invoked to explain increased contents of incompatible elements in both whole-rock and constituent minerals, which may be accompanied by modal enrichments in "fertile" minerals, such as clinopyroxene and garnet, hydrous minerals (i.e. phlogopite and amphibole), Ti-oxides, sulphides and, sometimes, diamond (Menzies 1983; Dawson 1984; Erlank et al. 1987; Pearson et al. 2003; Grégoire et al. 2002; Stachel et al., 2004; Giuliani et al. 2013). Understanding the nature of the metasomatic agent(s), the style of metasomatism, and its bearing on diamond potential (e.g. diamond precipitation vs. resorption; cf. Malkovets et al. 2007) is not straightforward. Numerous studies of individual suites of metasomatized xenoliths suggested that typical metasomatic agents in the mantle include alkaline-basaltic melts (Burgess and Harte 2004), melts with kimberlitic to carbonatitic affinity (Erlank et al. 1987; Kinny and Dawson 1992; Grégoire et al. 2002; Simon et al. 2007; Weiss et al. 2011), as well as C-O-H-bearing fluids (Andersen et al. 1984; Stachel et al. 2004; Giuliani et al. 2013). One of the most difficult tasks in studies of individual mantle sections is to understand if different geochemical signatures in mantle xenoliths reflect metasomatism operated by different, genetically unrelated melts/fluids, or are related to a unique metasomatic event operated by a melt/fluid with progressively changing composition due to chemical differentiation. A case study is described in detail in *Manuscript 3* of the present work.

AIMS OF THE WORK

Among the peridotitic fragments transported to the surface as xenoliths, xenocrysts or inclusions in diamonds, garnet and clinopyroxene are particularly sensitive to chemical processes and physical conditions in the mantle and therefore represent fundamental tools to tackle all the issues described above. They are the major host of trace elements in peridotites and therefore contain important information about the melting/metasomatic history of the host rocks. Even when they occur as isolated grains, they can be used to map the distribution of rock types in the sub-cratonic lithospheric mantle and to constrain the geochemical processes that operated before or after their entrapment in the host kimberlites (e.g. Griffin et al. 1999b, 2002; Malkovets et al. 2007; Creighton et al. 2008; O'Reilly et al. 2010; Nimis et al. 2009; Pivin et al. 2009; Hunt et al. 2012; Ivanic et al. 2012). In addition, they can provide information on the thickness and thermal state of the lithosphere at the time of eruption, and therefore represent extraordinary deep-seated probes for diamond exploration (Sobolev et al. 1973, 1990; Dawson and Stephens 1975; Griffin and Ryan 1995; Ryan et al. 1996; Nimis and Taylor, 2000; Schulze 2003; Grütter et al. 2004, 2006). The present thesis aims to explore in more detail the potential of garnet and clinopyroxene as indicators of mantle processes and physico-chemical conditions.

The ideas behind the present thesis build in part on recognized issues in current mantle research (see above) and in part on specific problems that arose during a preliminary study of the Zagadochnaya kimberlite (Daldyn field, Yakutia). The Zagadochnaya kimberlite is a Type-II, micaceous kimberlite in which the only available mantle samples are represented by eclogitic xenoliths and Cr-garnet and Cr-diopside xenocrysts and microxenoliths (Sobolev et al., 1968; Nimis et al., 2009). Despite its being located only 30 km from the highly diamondiferous Udachnaya kimberlite, the Zagadochnaya kimberlite is free of diamonds. It thus represents an interesting case to understand short-scale variability of diamond potential in kimberlites. However, given the absence of discrete ultramafic xenoliths, interpreting the mantle record in the Zagadochnaya kimberlite is a challenging task. A detailed characterization of garnet and diopside xenocrysts remains the best way to gain an insight into the mineralogical and geochemical composition of the mantle beneath Zagadochnaya, to understand its evolution through geological time, and to explore possible relationships with its low diamond potential. Nimis et al. (2009) previously performed a detailed major and trace element study of chromian diopside xenocrysts from this kimberlite and proposed a complex metasomatic history and a relatively shallow mantle derivation. The correctness of their conclusions heavily depend on the correct interpretation of the geochemical variability of a

single mineral phase (in the absence of petrographic constraints!) and on the reliability of the single-mineral thermobarometers used. Both aspects demand further verification.

In the present thesis, I tried to improve the knowledge on the Zagadochnaya mantle by using a multidisciplinary approach aimed at:

- improving the reliability of single-clinopyroxene thermobarometry (*Manuscript 1*);
- exploring the thermodynamics of phase relationships and compositional variability in clinopyroxene-bearing peridotitic systems (*Manuscript 2*);
- extending the study of the mantle fragments by focusing on the major and trace element geochemistry of garnet xenocrysts and garnet–clinopyroxene microxenoliths, building in part on results from the two previous lines of activity, (i) to better *constrain the paragenesis of the parental rocks and the variability of ultramafic lithologies in the sampled mantle section*, ii) to better *constrain the pressure and temperature of formation* and depth of mantle sampling, iii) to better *reconstruct the metasomatic history* by defining the relationships between the trace element chemistry of the garnets and the geochemical processes in the lithospheric mantle, and iv) to *shed more light on the factors that controlled the diamond potential* (*Manuscript 3*).

The rationale of these three main lines of research is briefly outlined here and the reader is referred to the attached manuscripts for a full description of methods, results and implications.

Improving the reliability of single-clinopyroxene thermobarometry (Manuscript 1)

In case studies such as Zagadochnaya, the single-clinopyroxene thermobarometers of Nimis and Taylor (2000), i.e., the enstatite-in-Cpx geothermometer and the Cr-in-Cpx geobarometer, represent the only reliable methods for estimating the P *and* T conditions of equilibrium of the sampled mantle fragments and their depth of derivation. Although the enstatite-in-Cpx geothermometer has proved to be of very good quality compared with conventional two-phase geothermometers (Nimis and Grütter 2010), the Cr-in-Cpx geobarometer suffers from two major drawbacks: (i) it progressively underestimates with increasing pressures at P > ca. 4.5 GPa (Nimis 2002); (ii) it tends to produce considerable scatter in P–T estimates when applied to clinopyroxenes with unfavourable compositions (Nimis and Taylor, 2000; Grutter 2009; this work). The latter drawback is reflected by deviations from the garnet–orthopyroxene geobarometer (Nickel and Green 1985, or its modification by Carswell 1991), which are very large for clinopyroxenes with low values of a_{Cr} [= Cr – 0.81·Na·Cr/(Cr+Al), atoms per 6-oxygen formula unit] (Fig. 2). To investigate the origin of these drawbacks, in an attempt to improve the reliability of the geobarometer, I performed a quantitative evaluation of single-clinopyroxene geobarometry by using both an analytical and a thermodynamic approach.

As a first step, I carried out multiple electron microprobe analyses on compositionally different clinopyroxenes, using different analytical conditions, and I performed a statistical analysis of the propagation of analytical errors on the calculated Cr-in-Cpx pressures. I found that the geobarometer is very sensitive to analytical errors when applied to particular clinopyroxene compositions characterized by low values of the parameter of a_{Cr} and/or too low or too high values of the parameter Cr# [= Cr/(Cr + Al)]. This can account for most of the increased P–T scatter observed in previous works. I therefore defined a new optimized analytical procedure for single-clinopyroxene geobarometry, which significantly decreases the pressure uncertainties and allows a better definition of clinopyroxene-based geotherms.

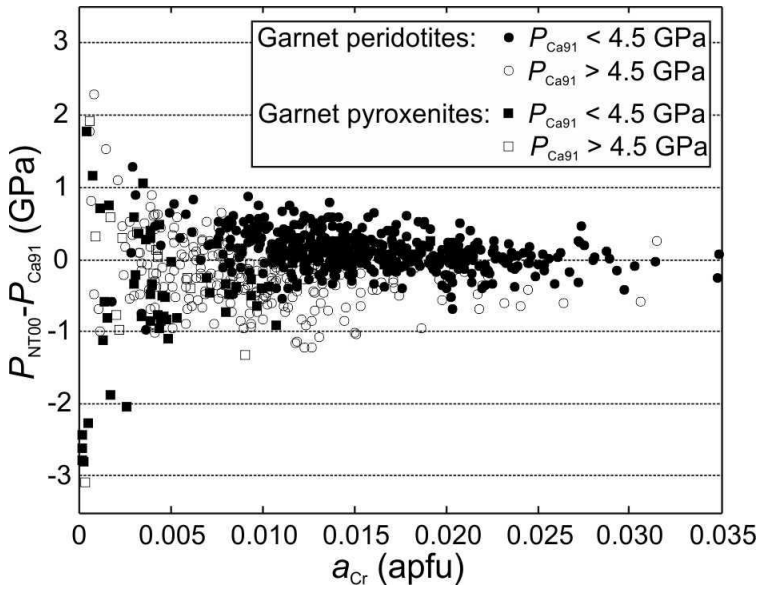

Fig. 2: *Discrepancies between the Cr-in-Cpx barometer (Nimis and Taylor 2000; P_{NT00}) and the orthopyroxene-garnet barometer (Nickel and Green 1985, as modified by Carswell 1991; P_{Ca91}) vs. the clinopyroxene parameter a_{Cr}. Clinopyroxene compositions from the compilation of well-equilibrated garnet peridotite and pyroxenite xenoliths of Nimis and Grutter (2010). The overall shift of high-P clinopyroxenes towards negative values can be ascribed to the known underestimation of Cr-in-Cpx pressures at high P (cf. Nimis 2002). Same Figure as Fig. 1 in Manuscript 1.*

Exploring the thermodynamics of phase relationships and compositional variability in clinopyroxene-bearing peridotitic systems (Manuscript 2)

The new optimized analytical procedure defined in the present thesis (*Manuscript 1*) does not eliminate the known progressive underestimation of P using the Cr-in-Cpx barometer of Nimis and Taylor (2000) at high pressure (Nimis 2002). This drawback may hamper correct definition of the shape of a mantle geotherm and recognition of thermal perturbation in the deep lithospheric mantle. In an attempt to improve the accuracy of the barometer at high P, I used a thermodynamic approach to investigate phase equilibria in clinopyroxene-bearing

peridotitic assemblages. I performed phase equilibria calculations using free energy minimization techniques using the 'Perple_X' set of computer programs (Connolly and Petrini 2002) and the most recent thermodynamic datasets for mantle minerals, partly modified to improve agreement with experimental constraints (see Supplementary Table 1 in *Manuscript 2*).

Unfortunately, discrepancies between the model compositions and the experimental compositions of the clinopyroxene (Fig. 3) indicated inconsistencies in the thermodynamic data for Cr- and Na-bearing clinopyroxenes. Therefore, improvement of the single-clinopyroxene barometer based on a robust thermodynamic approach was not possible. Nonetheless, such inconsistencies did not appear to significantly affect phase relations and compositional variations in orthopyroxene, garnet, and spinel. Therefore, I could use the thermodynamic model to predict the effect of P, T and bulk compositional variations on garnet–spinel relations in fertile and depleted mantle compositions. The results provided unprecedented constraints on the spinel peridotite-to-garnet peridotite transition and on the compositional variability of garnet and spinel as a function of pressure, temperature and bulk composition in a variety of mantle settings. Some of these results could be used later on for a more robust understanding of compositional variability in garnet xenocrysts from Zagadochnaya (cf. *Manuscript 3*).

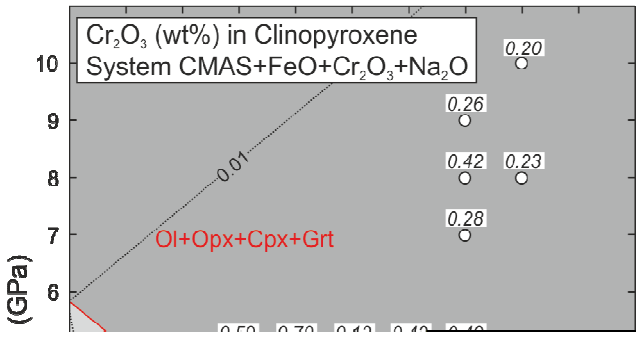

Extending the study of the mantle fragments in the Zagadochnaya kimberlite (Manuscript 3)

The heavy-mineral concentrates from the Zagadochnaya kimberlite were known to contain a significant amount of chromian diopsides and chromian garnets, often macroscopically inhomogeneous, due to the presence of polymineralic inclusions, mineral intergrowths, and chemical zonation (Kostrovitsky and de Bruin 2004; Nimis et al. 2009; Sobolev NV, pers. comm.). Following the work of Nimis et al. (2009) on the isolated clinopyroxene grains, for the present work I focused on the garnets and their inclusions. A detailed petrographic, major and trace element characterization revealed a wide textural and compositional variability, which may be the result of a complex geochemical history of the source rocks. Some garnet grains are optically and compositionally homogeneous, and are sometimes associated with subround chromian diopside. Other garnet grains are optically inhomogeneous, due to the presence of whitish-purple domains rich in polymineralic inclusions (Fig. 4). The textural relationships suggest a secondary origin of the inclusion-rich domains with respect to the host, inclusion-free garnets.

The source rocks of primary garnets (i.e. homogeneous grains and inclusion-free domains in the heterogeneous grains) were inferred by using the most common classification schemes (Sobolev et al., 1973; Schulze, 2003), further integrated by comparison with the major and trace element compositions of garnets from peridotites and megacryst suites from other kimberlites, and by investigating the geochemical and (where available) petrographic relationships with the chromian diopside xenocrysts studied by Nimis et al. (2009). To provide a reference framework for the geochemical variability, I subdivided the garnets into three main groups (Fig. 5a,b): the variably (Cr, Ca, LREE)-depleted, HREE-enriched Group A and B garnets (and group II clinopyroxenes of Nimis et al., 2009) were interpreted as fragments of fertile, variably metasomatized lherzolites, while the more (Cr, Ca, LREE)-rich, HREE-depleted Group C garnets were interpreted to have originated from depleted, weakly metasomatized lherzolites. To obtain reliable informations on the depths of provenance and temperatures of equilibration of the xenocrysts, I used the various versions of the Ni-in-garnet thermometer (Ryan et al., 1996; Canil, 1999) and, where primary clinopyroxenes were associated with the garnets, the single-clinopyroxene thermobarometers (Nimis and Taylor, 2000). The results indicated a shallow origin (< 130 km), and a substantial P–T overlap of garnet and clinopyroxene groups. The results of the previous lines of research developed in *Manuscripts 1* and *2* helped to assess the robustness of these data and of their interpretation.

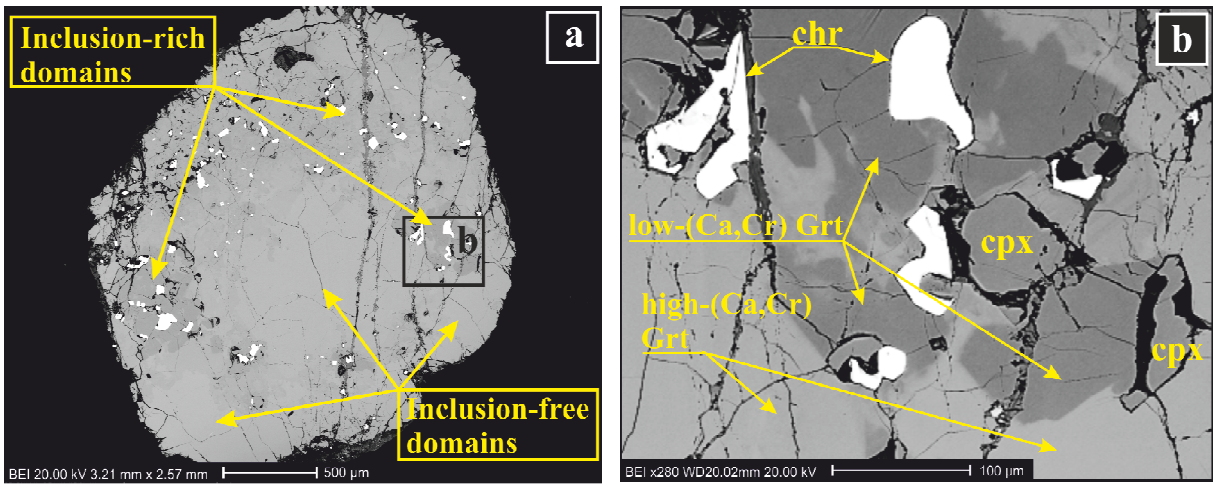

Fig. 4: *a) Back-scattered electron images of one of the analyzed garnets containing domains rich in polymineralic inclusions of chromian diopside (cpx) and chromite (chr); b) magnification of the same garnet showing the patchy zoning with transition from high-(Ca, Cr) (lighter areas) to low-(Ca-Cr) (darker areas). Same Figure as Fig. 2 in Manuscript 3.*

In a further step, I aimed to understand the processes that lead to the wide spectrum of REE variability in the primary garnets. Various degrees of REE fractionation such as those observed in Zagadochnaya garnets are commonly interpreted as a result of reactions between peridotite and different fluids or melts (Shimizu and Richardson, 1987; Hoal et al., 1994; Shimizu et al. 1997; Griffin et al., 1999b; Stachel et al., 2004; Grégoire et al., 2002; Burgess and Harte, 2004; Simon et al., 2007; Gibson et al., 2008), but understanding their genetic relationships is not straightforward, especially in the absence of strong petrographic constraints and isotopic measurements. To address this issue, I performed numerical simulations of peridotite/melt interaction (Plate Model; Vernières et al. 1997). This allowed me to model the trace element variation in the garnets, taking into account potentially important processes, such as chromatographic ion exchange, fractional crystallization, and assimilation of peridotitic minerals.

Then, I focused on the secondary garnets and associated inclusions, and performed a detailed petrographic, mineralogical and geochemical study. This allowed me to interpret these assemblages as products of dissolution/precipitation processes, driven by reaction with percolating melts. The very short geological time scale ($\leq 10^4$ years) required to preserve measured zoning profiles in the garnets (Fig. 4b) and the trace element compositions of the calculated liquids in equilibrium with the secondary minerals demonstrated that the metasomatic melts were genetically related the host kimberlite.

The above results were used to provide new constraints on the metasomatic history of the mantle section sampled by the Zagadochnaya kimberlite, as well as on the horizontal and vertical heterogeneity of the Daldyn lithospheric mantle. The previously hypothesized shallow

origin of Zagadochnaya mantle samples (cf. Nimis et al. 2009), which provides a simple explanation for the absence of diamonds, could be confirmed on the basis of a more robust assessment of the lithological variability of the Zagadochnaya mantle and of thermobarometric uncertainties.

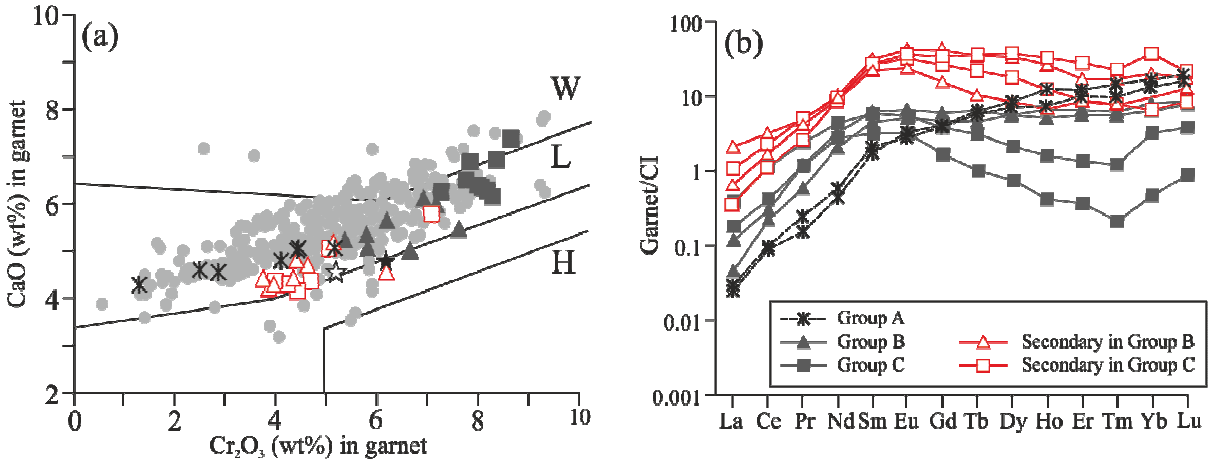

Fig. 5: *Main compositional features of Zagadochnaya garnets.* ***(a)*** *CaO vs. Cr_2O_3 discrimination diagram (Sobolev, 1971); the grey circles represent garnets from Zagadochnaya kimberlite concentrate (Sobolev NV, pers. com.); H, harzburgite; L, lherzolite; W, wehrlite; same figure as Fig. 3 in Manuscript 3.* ***(b)*** *Representative CI-normalized (Anders & Grevesse, 1989) REE patterns for Zagadochnaya garnets.*

METHODOLOGICAL APPROACH

The analytical approach to evaluating single-clinopyroxene geobarometry (Manuscript 1)

To establish if the large deviations of single-clinopyroxene geobarometry from the garnet–orthopyroxene geobarometry reflect an excessive sensitivity to analytical errors on Al, Cr and Na in clinopyroxene, I performed an analytical test on compositionally different clinopyroxenes (six chromian diopsides with different a_{Cr} and Cr# values). Each clinopyroxene was analysed in five analytical sessions, changing the operating conditions of the electron microprobe (beam current and counting times). During each session, 15 points were analyzed on the same, unzoned area of the clinopyroxene. This procedure allowed to evaluate the precision of the analyses, and of the P estimates, for the different analytical settings and the different clinopyroxene compositions. The results clearly showed that (i) propagation of analytical errors on Al, Cr and Na can explain the increased pressure uncertainties observed for clinopyroxenes with low a_{Cr}, and (ii) these uncertainties can be minimized if appropriate analytical conditions are adopted.

The results of the analytical test were then used to model the analytical errors for a large (N = 764) set of published analyses of mantle-derived, xenolith-borne clinopyroxenes. For each clinopyroxene, I calculated the analytical error for five combinations of analytical conditions. Assuming normal error propagation, I then calculated the propagated P uncertainties for each clinopyroxene and for each combination of analytical condition. This exercise allowed me to define the minimum analytical conditions for optimum single-clinopyroxene geobarometry as a function of clinopyroxene composition (see Table ??? in Manuscript 1).

Thermodynamic modeling (Manuscript 2)

Thermodynamic modeling is commonly used in petrology to study the chemical behavior of rock-forming minerals on the basis of phase equilibria constraints. In particular, thermodynamic modeling can be used to compare experimental results with data from other studies and to extrapolate experimental results in P–T–X space. Assuming that endmember and mixing parameters data are available for all phases, once an appropriate thermodynamic model is derived, it is possible to determine the chemical compositions and modal abundances of the phases present in a system at any given P–T–X condition. If applied to natural rocks in which the observed mineral assemblage is assumed to preserve the state of chemical

equilibrium, thermodynamics can also help translate the compositional data of the coexisting minerals into temperature and pressure of their equilibration.

Here I used the thermodynamic approach to investigate phase relations in model and natural peridotitic systems, at pressure and temperature conditions relevant for the upper mantle. Thermodynamic calculations were performed using the Perple_X set of Fortran programs (http://www.perplex.ethz.ch/), which is based on free-energy minimization techniques (Connolly 1990; Connolly and Petrini, 2002). The reliability of the calculations strongly depend on the consistency of the thermodynamic data of mineral endmembers and solid solutions used. Here I employed the thermodynamic database of Holland and Powell (1998), integrated with some recently determined thermodynamic properties of Cr-bearing spinel, garnet and pyroxenes. In a first step, I adopted the same database used by Klemme et al. (2009). To verify the consistency of the model, I compared the results of the calculations with available experiments in Cr-bearing peridotitic systems (e.g., Nickel 1986, 1989; Brey et al. 1990, 1999, 2008; Robinson and Wood 1998). Particular attention was given to Cr variations in garnet, spinel, and pyroxenes, as a function of pressure, temperature and bulk composition. As the model did not reproduce Cr variations in pyroxenes and garnets, I modified some thermodynamic properties for chromium endmembers of pyroxenes and for chromium-bearing garnet solid solutions, which are still not constrained by experiments. After numerous attempts, the model reproduced satisfactorily phase relations and Cr-Al variations in garnet, spinel and orthopyroxene. Although clinopyroxene compositions were still not reproduced adequately (Fig. 3), the model could be applied with reasonable confidence to investigate phase relations and chemical variations in Cr-bearing garnets and spinels in natural peridotitic systems.

Analyses of garnet and associated minerals from the Zagadochnaya kimberlite (Manuscript 3)

In order to understand the origin of, and the processes recorded by these garnets, a detailed characterization at a sub-millimeter scale was needed. 46 garnet grains (supplied by N.V. Sobolev, Novosibirsk) were prepared for petrographic and chemical analyses. They were mounted on epoxy resin, cut to about half their thickness and polished.

Preliminary petrographic analysis was carried out using back-scattered electron images of the grains, which were obtained with a CamScan MX2500 scanning electron microscope (SEM),. This preliminary survey allowed me to investigate the textural relationships between the host garnets and their mineral inclusions, and to characterize the distinctive chemical zonation in the inhomogeneous garnets. As a second step, the same grains were analysed with

a Cameca SX-50 electron microprobe equipped with four WDS spectrometers, to characterize the major and minor element composition of the garnets and associated minerals and their chemical zonation trends[1]. On the basis of petrographic observations and major element compositions, 28 representative grains were selected and further analyzed for trace elements by Laser Ablation Inductively Coupled Plasma Mass Spectrometry (LA-ICP-MS) at IGG-CNR, Pavia (Italy). This in-situ technique has the advantage to require minimal sample preparation (for this work I used the same samples analysed by electron microprobe), high spatial resolution at the sub-mm scale (to 30 μm), high sensitivity and detection limits below the ppm level, and rapid analysis times (typically 2 min per point analysis).

Numerical simulations of trace element transfer during melt/peridotite reactions were performed using the Plate Model of Vernières et al. (1997). The simulations were devised to reproduce the trace element variability observed in Zagadochnaya primary garnets (groups A, B, and C). The simulations require the knowledge of several parameters, such as the compositions of both infiltrating melt and ambient peridotite, the topology of the reactions, the mode of the segregated/assimilated minerals, the instantaneous melt/rock ratios (i.e., porosity), and the solid-liquid partition coefficients. Even if some of these data were missing in the studied case, mostly due to the lack of discrete peridotitic xenoliths, the successful reproduction of REE variability of Zagadochnaya garnets provided important insight into the petrochemical evolution of the sampled mantle section. The rationale of the numerical model and of the selection of input parameters is reported in detail in the Appendix of *Manuscript 3*.

The concentration profiles across garnet zoning were used to constrain the timing of the formation of the secondary garnets relative to the eruption of the kimberlite. A garnet grain in which the boundary between primary and secondary garnets looked particularly sharp (Fig. 3b) was re-analysed for Ca along a traverse parallel to the maximum concentration gradient, to obtain a concentration profile with a spatial resolution of 3 μm. The timescales were estimated by comparing the measured profile with theoretical profiles predicted by the binary diffusion model (Crank 1975). This model requires the knowledge of the element interdiffusion coefficients, which in turn depend on pressure, temperature and garnet composition (Vielzeuf et al. 2007; Ganguly 2010). I have performed various calculations, using interdiffusion coefficients from different sources (Vielzeuf et al. 2007; Ganguly 2010) and assuming P and T conditions relevant to process studied here (i.e., P ~ 3.5 GPa and T = 800–1100°C) to bracket the possible timescale interval.

[1] Detailed major and minor element concentration profiles, additional to those reported in *Manuscript 3*, are reported in the *Appendix 1* of the thesis. The related dataset is reported in the *Appendix 2* of the thesis.

MANUSCRIPT 1

(*In preparation*)

OPTIMUM ELECTRON MICROPROBE ANALYSIS FOR SINGLE-CLINOPYROXENE GEOBAROMETRY

ABSTRACT

Clinopyroxenes from garnet peridotites and pyroxenites are commonly used to estimate the pressure (*P*) of equilibration using the Cr-in-Cpx barometer. When compared to the orthopyroxene–garnet barometer, the Cr-in-Cpx method shows decreased precision for clinopyroxenes with low a_{Cr} (i.e., Cr – 0.81·Na·Cr#), with discrepancies up to 3.0 GPa for a_{Cr}<0.002 atoms per formula unit (apfu). Multiple electron microprobe analyses on compositionally diverse clinopyroxenes using different analytical conditions demonstrate that such discrepancies are mostly related to propagation of analytical errors on the calculated Cr-in-Cpx *P*. The results of the analytical tests were used to calculate model analytical errors and propagated *P* uncertainties for a large set of published analyses of mantle xenolith-borne clinopyroxenes. The resulting *P* uncertainties are negatively correlated with the a_{Cr} parameter and positively correlated with the Cr/(Cr + Al) ratio (Cr#). The a_{Cr}/Cr# parameter can thus be used to discriminate clinopyroxenes for which analytical errors alone will propagate unacceptable *P* uncertainties (i.e., higher than ±0.25 GPa) for several combinations of analytical conditions. For clinopyroxenes with a_{Cr}/Cr# > 0.024 apfu, "standard" analyses using a beam current of 15 nA, an accelerating voltage of 20 kV, and counting times of 10 s for peak and 5 + 5 s for background, will result in acceptable *P* uncertainties. In all other cases, higher beam currents and counting times are needed. Using a beam current of 40 nA, an accelerating voltage of 20 kV, and counting times of 40 s for peak and 40 + 40 s for background for measurement of Cr, Al and Na concentrations extends the applicability of the Cr-in-Cpx barometer to clinopyroxenes with a_{Cr}/Cr# as low as 0.013 apfu. Application of the barometer to clinopyroxenes with Cr# < 0.1 remains unwarranted in all cases, owing to limitations in the barometer calibration. Using appropriate analytical conditions, the barometer can thus be applied to at least 90% of clinopyroxene-bearing garnet peridotites and pyroxenites, 80% of clinopyroxene inclusions in lherzolitic diamonds, and 23% of clinopyroxene inclusions in websteritic diamonds. Evaluation of *P* uncertainties for clinopyroxenes included in diamonds from the Premier kimberlite shows that propagation of analytical errors produces biased *P–T* distributions. If only low-

uncertainty *P* estimates are selected, the *P*–*T* distribution is essentially compatible with that of mantle xenoliths from the same kimberlite, indicating that (i) diamond formation occurred when the lithospheric mantle had already attained a thermal state comparable with that extant at the time of kimberlite eruption, and (ii) the majority of Premier lherzolitic diamonds most likely formed in the cratonic lithosphere under virtually unperturbed thermal conditions.

INTRODUCTION

Single-clinopyroxene thermobarometry uses a combination of the enstatite-in-Cpx thermometer and Cr-in-Cpx barometer (Nimis and Taylor 2000). This method allows one to retrieve both the pressure (*P)* and the temperature (*T)* of formation of a mantle-derived chromian diopside from its electron microprobe (EMP) chemical analysis and has become a popular tool in mantle studies and diamond exploration (e.g., Read and Janse 2009; Cookenboo and Grütter 2010; Mather et al. 2011). The enstatite-in-Cpx thermometer has proved a top-quality method when compared to other mantle geothermometers (Nimis and Grütter 2010). Significant uncertainties on *T* estimates (>50°C) due to analytical errors can be expected only at low *T* (<900°C) in response to unusually large errors on CaO, SiO_2 (≥2% rel.) or Na_2O (≥10% rel.) determinations (Nimis 2002). The Cr-in-Cpx barometer (Nimis and Taylor 2000) is expressed as

$$P(\text{kbar}) = -\frac{T(\text{K})}{126.9}\cdot \ln a_{Cr} + 15.483\cdot \ln\left(\frac{\text{Cr\#}}{T(\text{K})}\right) + \frac{T(\text{K})}{71.38} + 107.8 \qquad (1)$$

where a_{Cr} = Cr – 0.81·Na·Cr# and Cr# = Cr/(Cr+Al), with elements in atoms per 6-oxygen formula unit (hereafter apfu). It represents the best alternative to the orthopyroxene–garnet barometer for garnet-bearing ultramafic rocks and the only viable method for isolated chromian diopside grains included in diamonds or recovered during mineral exploration programs.

Unfortunately, the Cr-in-Cpx barometer suffers from two major drawbacks. First, evaluations against experiments have shown progressive underestimation of the equilibrium pressures above ca. 4.5 GPa (Nimis 2002). Such systematic bias at high *P* evidently is a consequence of the simplified, single-mineral formulation of the Cr-in-Cpx barometer. Second, the deviations from results of orthopyroxene–garnet barometry can be very large for clinopyroxenes characterized by low values of a_{Cr} (Fig. 1). Based on a limited set of data, Nimis and Taylor (2000) suggested that the Cr-in-Cpx barometer should not be used if a_{Cr} is < 0.003 apfu, thus cutting off a significant fraction of naturally occurring clinopyroxenes,

especially those belonging to the pyroxenitic suite. Figure 1 shows that this threshold may be even too optimistic: at a_{Cr} = 0.010 apfu deviations from the orthopyroxene–garnet pressures may be as high as ±1.0 GPa, reaching ±3.0 GPa for a_{Cr} < 0.003 apfu. The decreased precision of the Cr-in-Cpx barometer at low a_{Cr} may be due to an oversimplified treatment of Cr equilibria between clinopyroxene and garnet or it may reflect an excessive sensitivity of the method to analytical errors on Al, Cr and Na or to departures from chemical equilibrium.

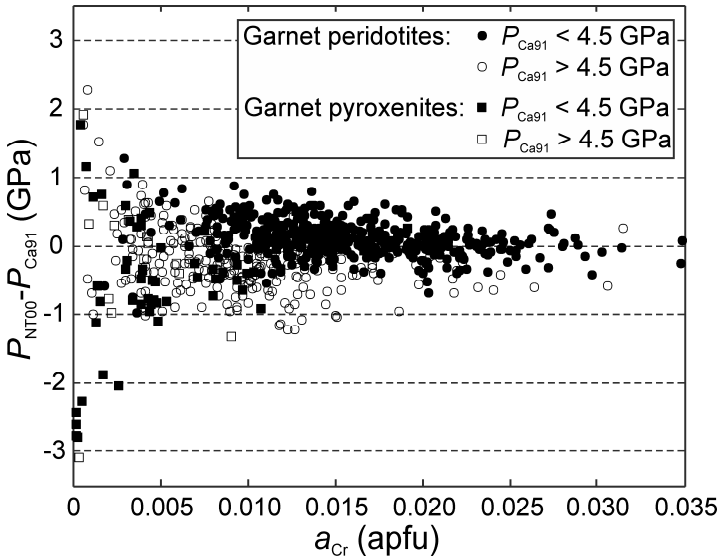

Fig. 1: *Discrepancies between the Cr-in-Cpx barometer (Nimis and Taylor 2000; P_{NT00}) and the orthopyroxene-garnet barometer (Nickel and Green 1985, as modified by Carswell 1991; P_{Ca91}) vs. the clinopyroxene parameter a_{Cr}. Clinopyroxene compositions from the compilation of well-equilibrated garnet peridotite and pyroxenite xenoliths of Nimis and Grutter (2010). The overall shift of high-P clinopyroxenes towards negative values can be ascribed to the known underestimation of Cr-in-Cpx pressures at high P (cf. Nimis 2002).*

Despite the obvious need of high-quality chemical analyses for reliable thermobarometry, the EMP analytical conditions employed in garnet peridotite or diamond inclusion studies are often not optimized for this specific purpose. Moreover, in many cases, the analytical conditions are not reported or only partial documentation is given. Of seventeen published papers in which the Cr-in-Cpx barometer is applied to clinopyroxene EMP analyses and documentation of analytical conditions is provided, sixteen used relatively low beam currents (≤20 nA) and/or low peak counting times (≤20 s) (e.g. Wang and Gasparik 2001; Menzies et al. 2004; Donnelly et al. 2007; Faryad et al. 2009; Nimis et al. 2009; Sand et al. 2009). This cast doubts on the reliability of many existing single-Cpx thermobarometric data and demands proper evaluation of propagation of analytical errors on P estimates.

Mather et al. (2011) made a qualitative evaluation of the errors propagated by analytical uncertainties on single-Cpx thermobarometry, but without a rigorous statistical assessment.

A more quantitative evaluation would be desirable to assess the reliability of existing thermobarometric data and help direct analytical procedures in future thermobarometric surveys. Assuming random error sources, the uncertainties on pressure estimates can be expressed with a normal error propagation function, i.e.,

$$\sigma P = \sqrt{\left(\frac{\partial P}{\partial \mathrm{Cr}} \cdot \sigma \mathrm{Cr}\right)^2 + \left(\frac{\partial P}{\partial \mathrm{Al}} \cdot \sigma \mathrm{Al}\right)^2 + \left(\frac{\partial P}{\partial \mathrm{Na}} \cdot \sigma \mathrm{Na}\right)^2 + \left(\frac{\partial P}{\partial T} \cdot \sigma T\right)^2} \quad (2)$$

Calculation of σP requires knowledge of analytical uncertainties on Cr, Al, Na and *T*. Uncertainties on *T* estimates can be derived from reproducibility of temperatures of experiments (±30–40°C; Nimis and Taylor 2000). Accurate evaluation of EMP uncertainties is not straightforward, because analytical errors primarily depend on the absolute element concentrations and on the analytical conditions adopted for the EMP analysis.

In this paper, we investigate the effect of EMP uncertainties on pressure estimates for compositionally diverse clinopyroxenes using both a direct and an indirect approach. In the *direct* approach, we evaluate the analytical errors for different analytical conditions and for a specific set of clinopyroxene compositions through repeated EMP measurements on the same samples, and evaluate the consequent uncertainties on *P* estimates by calculating *P* for each analysis. In the *indirect* approach, we apply the error propagation function (Equation 2) to a great variety of natural clinopyroxene compositions, assuming model analytical uncertainties derived from our direct test. We will show that, for particular compositions, standard analytical conditions may propagate very large uncertainties on pressure estimates, which account well for the lower observed precision of the Cr-in-Cpx barometer at low a_{Cr}. Minimum conditions for electron microprobe analysis of low-a_{Cr} clinopyroxenes will also be provided, which minimize the effect of analytical uncertainties and extend the applicability of the Cr-in-Cpx barometer to clinopyroxenes with a_{Cr} as low as 0.0014 apfu.

SAMPLE SELECTION AND ANALYTICAL PROCEDURES FOR THE DIRECT TEST

For the direct test we selected six clinopyroxenes having a_{Cr} between 0.0013 and 0.0188 apfu, characterized by various proportions of Al, Cr and Na, and equilibrated in a wide range of *P*–*T* conditions (Table 1). Appropriate compositions were found in two compositionally homogeneous clinopyroxenes and in two zoned clinopyroxenes from four well studied garnet peridotites.

Peridotite sample 160-4-8 is an orogenic, poikiloblastic garnet lherzolite from Cima di Gagnone, Adula–Cima Lunga nappe, Central Alps (Evans and Trommsdorff 1978). The

garnet peridotite forms a lens-shaped body within partly migmatitic gneisses, which include bodies of eclogites, marbles and ophicalcitic rocks. It was formed during prograde, high-pressure, Alpine metamorphism of serpentinitic protoliths to ca. 740°C and 3.0 GPa (Nimis and Trommsdorff 2001). It shows a weakly foliated texture and contains anhedral poikiloblastic garnets concentrated along pyroxene-rich layers. Garnet is surrounded by a matrix of idioblastic mosaic olivine, orthopyroxene, clinopyroxene and amphibole. Evans and Trommsdorff (1978) reported pronounced mineral zonations towards the rims of the first-generation porphyroclasts, due to re-equilibration under retrograde, hydrous conditions. For our test we selected an elongated clinopyroxene crystal (ca. 0.2 x 2.0 mm) which is almost totally enclosed in a poikilitic garnet with thin kelyphitic outer margins. Preliminary EMP analysis of the clinopyroxene indicated significant zoning. Two compositionally distinct, homogeneous areas could be found in the core and near the rim to garnet, which yielded a_{Cr} = 0.0014 apfu and a_{Cr} = 0.0040 apfu, respectively.

Table 1: *Results of preliminary clinopyroxene analyses adopting standard analytical conditions (15 nA, 20 kV, 10 s peak + 10 s background counting times). For each analysis, pressure (P_{NT00}) and temperature (T_{NT00}) were calculated using the single-clinopyroxene thermobarometers of Nimis and Taylor (2000). Pressures and temperatures for the host peridotites were also calculated with a combination of the Taylor (1998) thermometer (T_{Ta98}) and the Nickel and Green (1985; with modifications after Carswell 1991) barometer (P_{Ca91}), using published orthopyroxene and garnet compositions (Evans and Trommsdorff 1978; Canil and O'Neill 1996; Franz et al. 1996; Boyd, personal communication) and clinopyroxene compositions reported here.*

Sample	160-4-8 core	160-4-8 rim	FRB1031	KGG-65	Uv61/91 high-a_{Cr}	Uv61/91 low-a_{Cr}
SiO_2	55.17	54.49	55.69	54.57	54.88	55.28
TiO_2	0.06	0.08	0.25	0.28	0.05	0.12
Al_2O_3	1.55	1.50	2.46	2.65	0.61	0.65
Cr_2O_3	0.70	0.49	1.32	2.4	0.94	0.82
FeO_{tot}	3.13	2.28	3.26	2.26	2.45	2.62
MnO	0.09	0.06	0.11	0.06	0.10	0.10
MgO	16.55	17.36	19.23	16.15	19.20	18.98
CaO	22.18	22.95	16.74	19.5	20.92	20.93
Na_2O	1.42	0.98	1.89	2.32	0.65	0.82
Sum	100.85	100.19	100.95	100.19	99.80	100.32
Cr#	0.23	0.18	0.27	0.39	0.51	0.46
aCr	0.0013	0.0040	0.0092	0.0188	0.0081	0.0021
T_{NT00} (°C)	769	732	1270	912	1180	1185
P_{NT00} (GPa)	4.70	3.20	5.22	3.69	6.01	7.43
T_{Ta98} (°C)	728	728	1265	972	1190	1190
P_{Ca91} (GPa)	3.26	3.26	5.62	3.84	6.09	6.09

Sample FRB1031 is a high-*T* garnet lherzolite xenolith from the Jagersfontein kimberlite, South Africa, which was studied by Boyd and Mertzman (1987). It shows a mosaic porphyroclastic texture, with garnet porphyroclasts reaching 1 cm in size and orthopyroxene, clinopyroxene and olivine porphyroclasts never exceeding 5 mm. The matrix is mainly composed by serpentinized olivine neoblasts. Clino- and orthopyroxene porphyroclasts are often fractured or completely broken. For the test we selected an unzoned clinopyroxene fragment with a_{Cr} = 0.0094 apfu.

Sample KGG-65 is a clinopyroxene-bearing garnet harzburgite xenolith from the Gibeon kimberlite, Namibia, which was studied by Franz et al. (1996). It shows a coarse equant texture. Garnet, often with small kelyphitic rims, can reach 5 mm in size, while the other minerals never exceed 2 mm. Orthopyroxene grains are granoblastic to short prismatic. Most of the clinopyroxenes have serrated spongy rims containing numerous fine melt inclusions, but the cores are homogeneous and compositionally unzoned. For the test we have selected a clinopyroxene core with a_{Cr} = 0.0185 apfu.

Sample Uv-61/91 is a high-*T* sheared garnet lherzolite xenolith from the Udachnaya kimberlite, Yakutia, Russia, which was previously studied for petrology (Boyd et al. 1997), redox conditions (Canil et al. 1994), and isotope geochemistry (Pearson et al. 1995). Garnets are round and mm-sized, and are usually mantled by kelyphite. Orthopyroxenes are segregated into bands, giving the rock foliation. Partially serpentinized olivine neoblasts (0.1–0.3 mm) compose the groundmass and olivine porphyroclasts are often broken into a mosaic of grains (0.5–1.0 mm). Primary clinopyroxene porphyroclasts commonly have a blotchy alteration along margins and fractures. The clinopyroxene grain studied here was taken from a mineral separate, which was kindly supplied by D.G. Pearson. Preliminary EMP analyses indicated that the separated clinopyroxene grains were compositionally inhomogeneous. For the test we selected two homogeneous areas with significantly different a_{Cr}, one close to a partially altered portion (a_{Cr} = 0.0024 apfu) and the other far from it (a_{Cr} = 0.0080 apfu).

Clinopyroxene analyses were carried out with a CAMECA “CAMEBAX” electron microprobe (IGG–CNR, Padua, Italy), equipped with four wavelength-dispersive spectrometers. Natural and synthetic minerals (diopside for Ca and Si, albite for Na, orthoclase for K, and pure Al, Mg, Cr, Fe, and Mn-Ti oxides) were used as standards. X-ray counts were converted into weight percent oxides by using the CAMECA-PAP program. Each clinopyroxene grain/portion was first analyzed for all elements adopting standard analytical condition, i.e., 1 μm electron beam, 20 kV accelerating voltage, 15 nA beam

current, and a counting time of 10 s for peak and 10 + 10 s for background. This preliminary investigation allowed us to select compositionally homogeneous areas and provided us average compositions to be used for calculation of matrix effects in subsequent analytical sessions and preliminary thermobarometry (Table 1). The same clinopyroxenes were then analyzed again for Al, Cr and Na using different beam currents and counting times (Table 2). Five analytical sessions were carried out, during which 15 individual point analyses were acquired on the same, homogeneous areas of the clinopyroxenes. The analyses were carried out on a grid of 3 x 5 analytical spots (maximum side 20 μm). To limit element migration under the electron beam, before each session the grid was translated by 3–4 μm, within the previously defined homogeneous areas. Calcium measurements were also conducted on the same spots as a further check for compositional homogeneity of the analyzed area. Observed variations in CaO weight percentages were always less than 0.8%. To further minimize the effect of any minor compositional inhomogeneity, analyses for which any measured concentration departed by more than 3 standard deviations from the mean of the same session were rejected. Only in one case more than a single analysis had to be discarded. The number of accepted analyses and the average compositions obtained during the five test sessions on each selected clinopyroxene grain/portion are reported in Table 3.

Table 2 *Electron microprobe operating conditions for the different analytical sessions. Accelerating voltage was fixed to 20 kV. The last row indicates the minimum* a_{Cr}*/Cr# values required to maintain the propagated pressure uncertainties within ±0.25 GPa (σ)*

Session	15-10/5	15-20/20	40-10/5	40-20/20	40-40/40
Beam current (nA)	15	15	40	40	40
Peak (sec)	10	20	10	20	40
Background (sec)	5 + 5	20 + 20	5 + 5	20 + 20	40 + 40
*a*Cr/Cr#	0.024	0.019	0.018	0.015	0.013

Single-clinopyroxene *P–T* estimates (Nimis and Taylor 2000) for samples FRB1031 and KGG-65, for the rim composition of sample 160-4-8, and for the high-a_{Cr} composition of sample Uv61/91 compare well with those obtained using a combination of the Taylor (1998) two-pyroxene thermometer and the Nickel and Green (1985) orthopyroxene–garnet barometer (with modifications after Carswell 1991[1]) and published mineral compositions for the same samples (Table 1). The core composition of clinopyroxene 160-4-8 yields a much

[1] The combination of the Taylor (1998) thermometer and Nickel and Green (1985) barometer follows recommendations by Nimis and Grütter (2010). Carswell's (1991) modification only affects *P* estimates for highly sodic orthopyroxene compositions and was preferred here because it reproduces best pressures of experiments in peridotitic systems (cf. Fig. 1 in Nimis and Grütter 2010).

higher *P* (4.7 GPa vs. 3.3 GPa), suggesting disequilibrium with the garnet. This clinopyroxene core may retain a relict composition, which formed during prograde metamorphism at sub-garnet conditions. The low-a_{Cr} composition of sample Uv61/91 yields a significantly higher Cr-in-Cpx pressure than the high-a_{Cr} composition of the same sample (7.4 GPa vs. 6.0 GPa), which may again reflect disequilibrium, possibly related to late-stage clinopyroxene alteration. Although these compositions probably are out of equilibrium with the garnet, and thus yield meaningless Cr-in-Cpx *P* estimates, they still lie within the compositional space of clinopyroxenes from natural garnet peridotites and therefore may still serve as useful test cases to evaluate the propagation of analytical uncertainties on calculated pressures.

RESULTS OF THE DIRECT TEST

For each point analysis, Cr#, a_{Cr} and Cr-in-Cpx pressure estimates were calculated. Pressures were calculated using fixed input temperature values, which were obtained by applying the enstatite-in-Cpx thermometer, at *P* given by the Cr-in-Cpx barometer, on the compositions derived from the preliminary analyses of the samples (Table 1). Statistical parameters (mean values, standard deviations, quantiles) for all relevant variables are reported in Table 3 and illustrated in Fig. 2.

Relative uncertainties on the measured Al, Cr and Na concentrations decrease smoothly with increasing beam current, counting times, and element abundances (Table 3). This allowed us to model analytical uncertainties as linear functions of clinopyroxene composition for each set of analytical conditions (Table 4). The standard deviations on *P* estimates drastically change with changing analytical conditions (σ as high as 0.8 GPa using the lowest beam current and counting times) and clinopyroxene composition (Table 3 and Fig. 2). The relationships between *P* uncertainties and composition can be explained considering the topology of the Cr-in-Cpx barometer expression (Equation 1).

In equation (1), *P* is related to a_{Cr} and Cr# through two logarithmic functions. This enhances error propagation with decreasing a_{Cr} and Cr#. Owing to its greater weight in the equation, the effect of the a_{Cr} logarithmic term tends to be dominant in terms of error propagation. This accounts well for the larger *P* uncertainties obtained for the core of clinopyroxene 160-4-8 (a_{Cr} = 0.0013 apfu) with respect to clinopyroxene FRB1031 (a_{Cr} = 0.0092 apfu), in spite of their similar a_{Cr} uncertainties (Table 3). It also explains the progressively larger deviations from orthopyroxene–garnet pressures at lower a_{Cr} (Fig. 1). Moreover, because of the logarithmic relation, the distribution of propagated errors due to a_{Cr} uncertainties will tend to be skewed towards the positive side. This explains the

progressive decrease in mean *P* estimates for clinopyroxenes with very low a_{Cr} values when improved analytical conditions are adopted (see sample 160-4-8 core, $a_{Cr} \approx 0.0015$ apfu, in Table 3 and Fig. 2).

Whereas the effect of the Cr# logarithmic term on error propagation is marginal, Cr# has a major effect on the uncertainties of the a_{Cr} parameter. In particular, a higher Cr# will enhance

Table 3: *Results of analytical sessions on selected Cpx's using different operating condition (cf. Table 2). N: number of analyses; av.: average*

Sample	Session	N	Al_2O_3			Cr_2O_3			Na_2O			*Cr#*		a_{Cr}		*P* (GPa)	
			av.	σ	σ %	av.	σ	σ %	av.	σ	σ %	av.	σ	av.	σ	av.	σ
160-4-8 core	15-10/5	15	1.56	0.05	3.2%	0.72	0.05	7.3%	1.43	0.05	3.7%	0.238	0.015	0.0013	0.0010	4.99	0.78
	15-20/20	14	1.56	0.03	2.1%	0.71	0.04	5.6%	1.44	0.05	3.4%	0.233	0.011	0.0012	0.0008	4.79	0.46
	40-10/5	15	1.56	0.03	2.1%	0.71	0.03	4.5%	1.42	0.05	3.8%	0.235	0.009	0.0014	0.0008	4.71	0.44
	40-20/20	15	1.56	0.03	1.9%	0.72	0.02	2.6%	1.42	0.05	3.4%	0.235	0.005	0.0015	0.0006	4.62	0.31
	40-40/40	15	1.56	0.03	1.9%	0.72	0.02	3.4%	1.39	0.03	2.2%	0.237	0.008	0.0018	0.0004	4.45	0.18
160-4-8 rim	15-10/5	15	1.52	0.06	4.0%	0.48	0.05	11.3%	0.97	0.05	4.8%	0.176	0.018	0.0042	0.0006	3.14	0.14
	15-20/20	15	1.53	0.02	1.4%	0.49	0.02	3.8%	0.99	0.04	4.3%	0.178	0.006	0.0041	0.0005	3.17	0.08
	40-10/5	15	1.53	0.03	2.1%	0.49	0.02	3.1%	0.98	0.05	5.2%	0.176	0.006	0.0041	0.0006	3.16	0.14
	40-20/20	14	1.52	0.02	1.5%	0.48	0.02	4.4%	1.01	0.03	3.4%	0.173	0.006	0.0037	0.0005	3.22	0.09
	40-40/40	14	1.52	0.03	1.8%	0.47	0.02	4.5%	0.99	0.03	3.3%	0.173	0.007	0.0038	0.0005	3.18	0.10
FRB1031	15-10/5	15	2.49	0.06	2.4%	1.37	0.08	5.7%	1.88	0.03	1.6%	0.270	0.013	0.0102	0.0012	5.13	0.12
	15-20/20	15	2.46	0.04	1.6%	1.34	0.04	2.7%	1.91	0.03	1.7%	0.267	0.005	0.0092	0.0010	5.24	0.12
	40-10/5	15	2.48	0.03	1.1%	1.32	0.07	5.0%	1.90	0.02	1.3%	0.262	0.010	0.0093	0.0009	5.20	0.07
	40-20/20	15	2.47	0.02	0.9%	1.32	0.02	1.6%	1.89	0.02	0.8%	0.264	0.004	0.0093	0.0004	5.20	0.04
	40-40/40	15	2.48	0.01	0.5%	1.33	0.02	1.7%	1.89	0.02	0.8%	0.264	0.003	0.0094	0.0004	5.19	0.04
KGG65	15-10/5	15	2.65	0.04	1.5%	2.40	0.08	3.2%	2.31	0.05	2.0%	0.378	0.008	0.0192	0.0018	3.67	0.07
	15-20/20	15	2.63	0.03	1.1%	2.39	0.05	2.2%	2.31	0.04	1.5%	0.379	0.005	0.0184	0.0012	3.71	0.05
	40-10/5	15	2.63	0.03	1.0%	2.36	0.06	2.4%	2.31	0.03	1.2%	0.376	0.006	0.0182	0.0010	3.71	0.04
	40-20/20	15	2.63	0.02	0.8%	2.36	0.04	1.9%	2.30	0.02	1.0%	0.376	0.005	0.0184	0.0009	3.70	0.04
	40-40/40	15	2.62	0.01	0.5%	2.35	0.02	1.0%	2.30	0.02	0.8%	0.376	0.003	0.0181	0.0005	3.71	0.02
Uv61/91 low-a_{Cr}	15-10/5	15	0.65	0.03	4.7%	0.85	0.06	7.6%	0.81	0.04	5.5%	0.466	0.026	0.0029	0.0016	7.29	0.80
	15-20/20	15	0.66	0.02	2.6%	0.81	0.04	4.9%	0.82	0.03	3.8%	0.452	0.012	0.0021	0.0010	7.53	0.60
	40-10/5	15	0.66	0.03	5.0%	0.84	0.05	5.7%	0.83	0.02	2.7%	0.462	0.019	0.0023	0.0009	7.41	0.50
	40-20/20	14	0.66	0.02	3.6%	0.84	0.02	1.8%	0.82	0.03	3.5%	0.460	0.009	0.0024	0.0005	7.31	0.25
	40-40/40	8	0.64	0.01	1.5%	0.85	0.01	1.6%	0.82	0.02	2.1%	0.471	0.005	0.0024	0.0005	7.33	0.25
Uv61/91 high-a_{Cr}	15-10/5	15	0.61	0.02	3.8%	0.95	0.07	7.2%	0.66	0.04	5.6%	0.512	0.020	0.0081	0.0018	6.06	0.26
	15-20/20	15	0.61	0.03	4.1%	0.93	0.05	5.7%	0.64	0.03	4.8%	0.504	0.021	0.0082	0.0016	6.00	0.20
	40-10/5	15	0.60	0.02	3.2%	0.92	0.02	2.7%	0.64	0.03	4.8%	0.505	0.010	0.0080	0.0013	6.02	0.19
	40-20/20	15	0.61	0.01	2.4%	0.90	0.02	2.8%	0.63	0.02	3.0%	0.498	0.006	0.0080	0.0008	5.99	0.11
	40-40/40	15	0.61	0.01	1.3%	0.88	0.02	2.7%	0.63	0.01	2.2%	0.493	0.007	0.0076	0.0005	6.03	0.06

propagation of Na uncertainties on a_{Cr} and, therefore, on *P*. This explains the lower *P* uncertainties (and their less pronounced variations between different analytical sessions) obtained for 160-4-8 rim composition, which is characterized by low a_{Cr} (0.004 apfu) *and* low Cr# (0.17), compared with those obtained for compositions with higher Cr# values (Table 3 and Fig. 2).

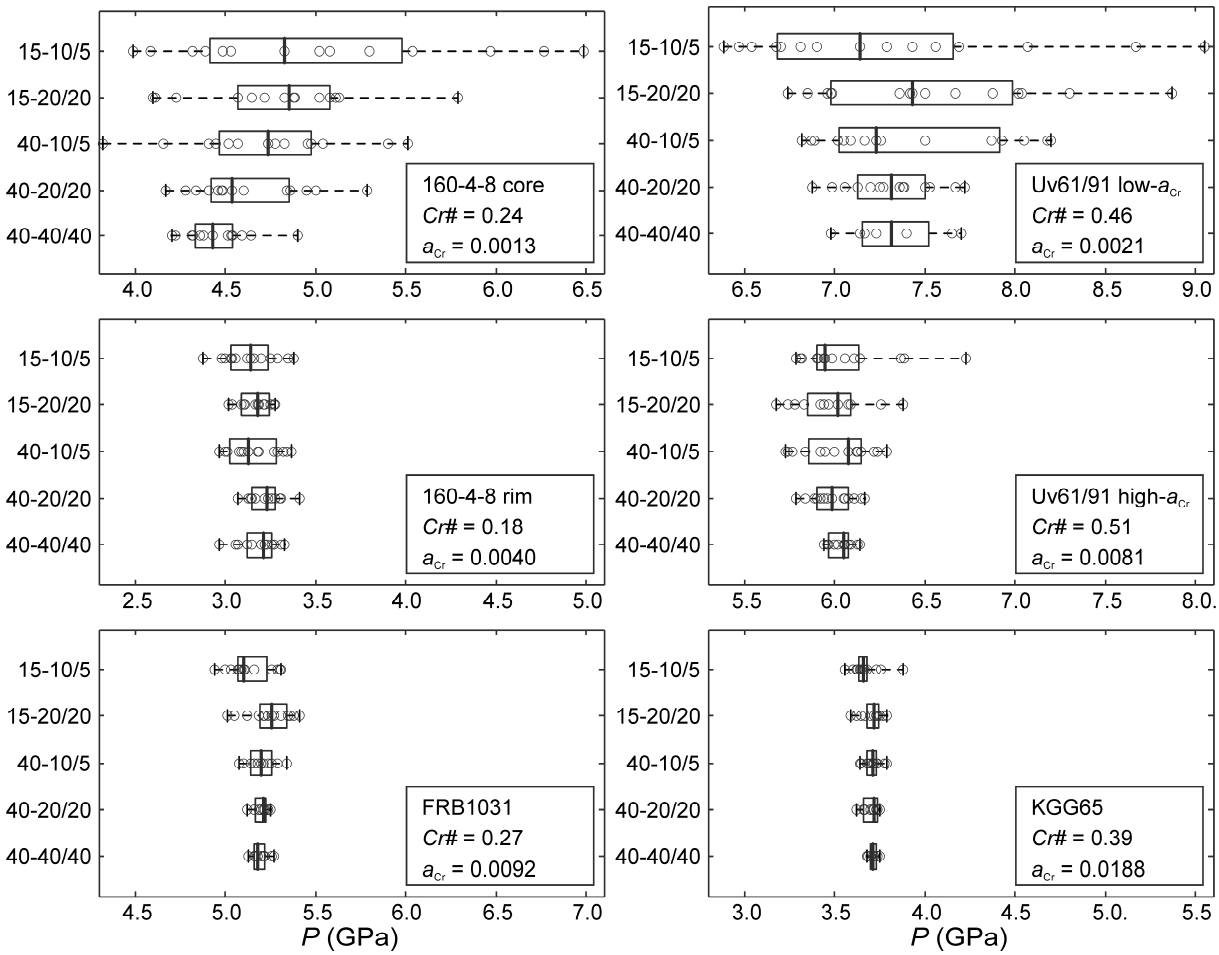

Fig. 2: *Box-plots of calculated pressures for the test clinopyroxenes analyzed using different operating conditions (cf. Table 2). Median values (thicker vertical line), interquartile range (box), whiskers (dashed lines) and individual pressure estimates for each point analyses (empty circles) are reported.*

P UNCERTAINTIES FOR NATURAL CLINOPYROXENES AND OPTIMUM ANALYTICAL CONDITIONS FOR CLINOPYROXENE BAROMETRY

The previous test indicates that the effect of analytical errors on the precision and accuracy of the calculated pressure strongly increases with *decreasing* a_{Cr} and with *increasing* Cr#. For any clinopyroxene composition, minimum analytical conditions should be defined for which analytical errors propagate acceptable errors on pressure estimates. For this purpose, a more extended test on comprehensive set of clinopyroxene compositions is needed. Here we use the

database of well-equilibrated xenoliths of Nimis and Grütter (2010) as our test material. Temperatures for each xenolith were calculated using the thermometer of Taylor (1998) at *P* given by the orthopyroxene–garnet barometer of Nickel and Green (1985; with modifications by Carswell 1991). The *T* uncertainty was fixed at 40 K (cf. Nimis and Taylor 2000). Uncertainties on clinopyroxene Cr, Al and Na analyses were calculated for each xenolith for five combinations of analytical conditions, taking into account the results of our previous analytical tests (Table 4). Uncertainties on Cr-in-Cpx pressures were then calculated by normal error propagation of the five resulting sets of analytical uncertainties (Equation 2).

Table 4 *Equations for estimating relative analytical errors (σ %) on oxide (wt%) and element (apfu) concentrations as a function of their abundances and analytical conditions, based on results of our analytical tests (Table 3). The analytical errors for wt% values >2.5% (corresponding to Al > 0.12 apfu, Cr > 0.08 apfu, Na > 0.18 apfu) become virtually independent of concentrations and can be considered equal to the estimated error for 2.5 wt% (or for the corresponding element concentrations)*

An. session	15-10/5	15-20/20	40-10/5	40-20/20	40-40/40
Al_2O_3 err %	$-1.1 \cdot Al_2O_3 + 4.8$	$-1.4 \cdot Al_2O_3 + 4.4$	$-1.4 \cdot Al_2O_3 + 4.5$	$-0.8 \cdot Al_2O_3 + 2.8$	$-0.6 \cdot Al_2O_3 + 2.3$
Al err %	$-0.26 \cdot Al + 0.048$	$-0.22 \cdot Al + 0.035$	$-0.34 \cdot Al + 0.046$	$-0.20 \cdot Al + 0.028$	$-0.26 \cdot Al + 0.033$
Cr_2O_3 err %	$-3.1 \cdot Cr_2O_3 + 10$	$-1.6 \cdot Cr_2O_3 + 6.0$	$-0.9 \cdot Cr_2O_3 + 5.0$	$-1.0 \cdot Cr_2O_3 + 3.6$	$-1.4 \cdot Cr_2O_3 + 3.7$
Cr err %	$-0.90 \cdot Cr + 0.093$	$-0.57 \cdot Cr + 0.060$	$-0.26 \cdot Cr + 0.047$	$-0.31 \cdot Cr + 0.034$	$-0.35 \cdot Cr + 0.034$
Na_2O err %	$-2.6 \cdot Na_2O + 7.4$	$-1.8 \cdot Na_2O + 5.7$	$-2.0 \cdot Na_2O + 5.7$	$-1.7 \cdot Na_2O + 4.8$	$-0.9 \cdot Na_2O + 3.0$
Na err %	$-0.32 \cdot Na + 0.067$	$-0.28 \cdot Na + 0.058$	$-0.32 \cdot Na + 0.062$	$-0.22 \cdot Na + 0.045$	$-0.19 \cdot Na + 0.037$

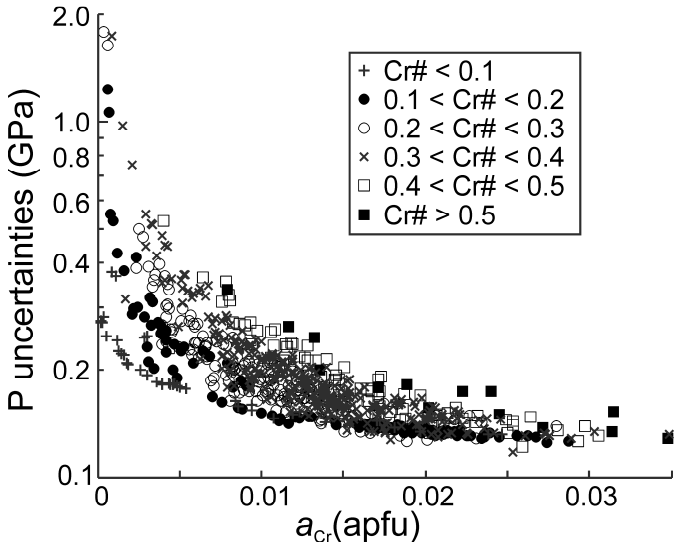

Fig. 3: *Calculated pressure uncertainties (σ) vs. aCr for clinopyroxenes from well-equilibrated garnet peridotites and pyroxenites (database of Nimis and Grütter 2010). The pressure uncertainties were calculated from normal propagation of temperature uncertainties (±40°C) and analytical errors derived from equations reported in Table 4, assuming the lowest beam current (15 nA) and counting times (10 s peak, 5 + 5 s background)*

As expected, the calculated uncertainties increase with decreasing a_{Cr} and increasing Cr# values (Fig. 3), reaching 1.8 GPa when a_{Cr} is <0.002 apfu and the lowest current and counting times are assumed. These results can be used to determine an approximate compositional threshold below which pressure estimates become too sensitive to analytical errors. We considered a maximum propagated uncertainty of ±0.25 GPa on the calculated *P*, including the effect of both analytical and thermometric errors, to be a reasonable limit. Taking into account the standard error of estimate of the barometer calibration (±0.23 GPa), this limit should ensure an overall uncertainty smaller than ±0.4 GPa. We found that simplified thresholds based on the a_{Cr} /*Cr#* ratio (Table 2) are capable to discriminate compositions for which *P* uncertainties are acceptable with a confidence of 95%. Although these thresholds are strictly applicable to analyses acquired using an electron microprobe similar to that used for the present work, we expect them to reproduce with reasonable approximation the performance of most WDS electron microprobes. The same thresholds can thus be used in common practice to derive minimum analytical conditions for thermobarometric applications or to help select the most reliable analyses from published datasets. Note that if the *lowest* beam current and counting times are assumed, the safety threshold is a_{Cr} /*Cr#* > 0.024 apfu. Such threshold would cut off 17% of the 764 records in the mantle xenolith database of Nimis and Grütter (2010) and 40% of reported clinopyroxene inclusions in ultramafic-type diamonds (cf. Stachel and Harris 2008). Assuming the highest beam current and counting times the threshold decreases to > 0.013 apfu, thus cutting off only 5% of the xenolith records and 18% of the inclusions.

IMPLICATIONS ON THERMOBAROMETRY OF MANTLE XENOLITHS AND DIAMOND INCLUSIONS AND ON ESTIMATED PALAEOGEOTHERMS

The above results suggest that many published clinopyroxene analyses may not be of sufficient quality for single-clinopyroxene thermobarometry. Accordingly, we have refined the xenolith database of Nimis and Grütter (2010) by excluding those analyses for which the estimated *P* uncertainties were above our recommended limit of ± 0.25 GPa. For each record, the analytical errors on Al, Cr, and Na concentrations were calculated taking into account the analytical conditions used for the analysis as reported in the source papers. If the reported analytical conditions did not match exactly any of those utilized here, the errors were estimated by interpolation of values obtained by assuming lower and higher beam currents or counting times. For records for which analytical details had not been reported, we cautiously assumed the beam current and counting times to be the lowest possible ones (i.e., 15 nA, 10 s peak, 5 + 5 s background).

Figure 4 shows that the discrepancies between Cr-in-Cpx and orthopyroxene–garnet pressures are greatly reduced for the refined database, especially at pressures above 3 GPa. At lower pressures, significant deviations are still observed only for a few samples with Cr# < 0.1 (Fig. 4b). This systematic bias for Cr-poor clinopyroxenes cannot be ascribed to propagation of analytical errors and suggests poor reliability of the Cr-in-Cpx barometer for low-Cr# compositions. Notably, the Cr-in-Cpx barometer was calibrated on 120 experimental clinopyroxenes with Cr# in the range 0.09–0.44, with only 6 of them having Cr# < 0.1 (Nimis and Taylor 2000). Rejecting such low-Cr# clinopyroxenes results in cutting off further 5% of clinopyroxenes from xenoliths, further 2% of inclusions in lherzolitic diamonds and further 58% (!) inclusions in websteritic diamonds.

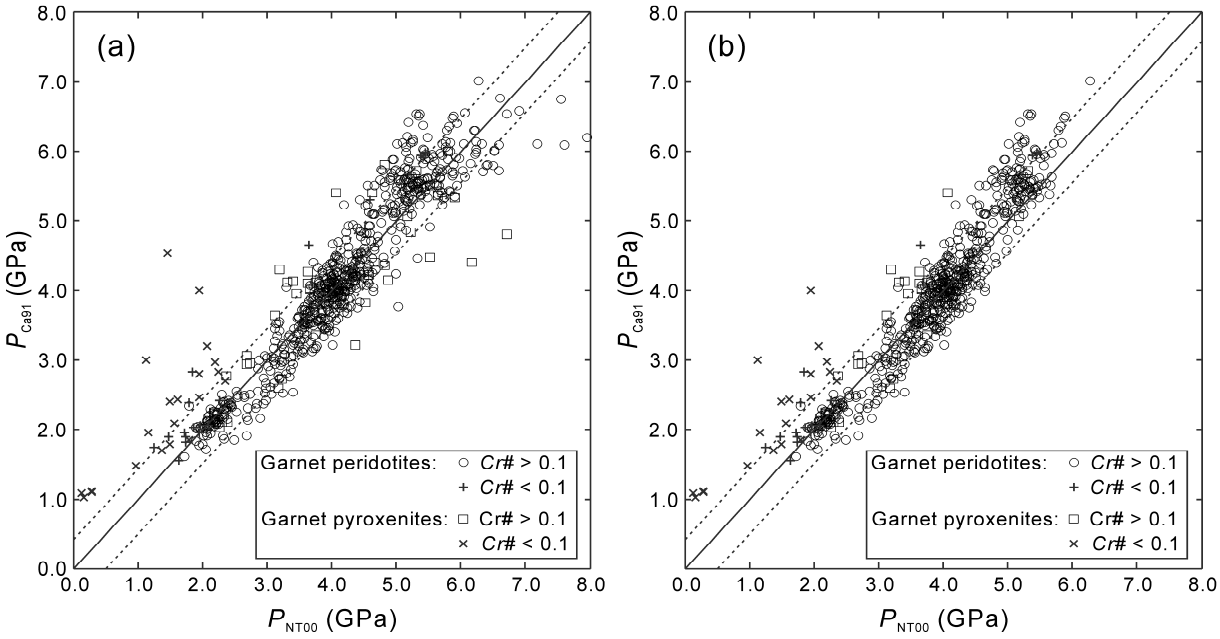

Fig. 4: *P estimates using the Cr-in-Cpx barometer plotted versus P estimates using the orthopyroxene–garnet barometer of Nickel and Green (1985, as modified by Carswell 1991) for (a) the entire dataset of well equilibrated garnet peridotites and pyroxenites of Nimis and Grutter (2010), and (b) the same dataset cleaned from samples with calculated pressure uncertainties greater than ±0.25 GPa.*

The refined dataset shows a progressive *negative* deviation of Cr-in-Cpx pressure estimates relative to orthopyroxene–garnet pressures estimates at $P > 4.5$ GPa. This confirms the tendency of the Cr-in-Cpx barometer to underestimate at high P, which was previously observed against experimental data (cf. Nimis 2002) (Fig. 4b)[2]. Moreover, a slight *positive*

[2] This systematic deviation would almost disappear if the native expression of the Nickel and Green (1985) orthopyroxene–garnet barometer was used.

deviation of Cr-in-Cpx pressures (<0.5 GPa on average) is observed at *P* around 3 GPa, which partly confirms observations by Grütter and Moore (2003) and Grütter (2009). It is unclear if this small discrepancy at moderate *P* is due to inaccuracy of the Cr-in-Cpx barometer, of the orthopyroxene–garnet barometer, or of both. Owing to these systematic deviations, mantle palaeogeotherms calculated on the basis of single-Cpx thermobarometry will tend to show slightly different shapes than those based on orthopyroxene–garnet barometry. The most important discrepancies will affect the deepest portion of the lithosphere, where single-Cpx geotherms will tend to show slightly overestimated *T*/*P* gradients, leading to underestimation of lithosphere thickness. As discussed by Nimis (2002), this drawback will not hamper recognition of samples coming from the diamond window.

Nimis (2002) discussed results of single-Cpx thermobarometry of isolated inclusions in diamonds from worldwide localities. In most cases, *P–T* estimates were similar to those obtained with the same method for mantle xenoliths from the same locality, suggesting that diamond crystals formed when the lithospheric mantle had already attained a conductive thermal regime comparable to that extant at the time of emplacement of the host kimberlite/lamproite. Occasional deviations from the local xenolith geotherms were ascribed to secular cooling or to thermal perturbation or relaxation of the lithosphere after encapsulation of the inclusions in their host diamond. Figure 5 illustrates one such example for a relatively large suite of inclusions in diamonds from the Premier kimberlite, South Africa. Low-*T* mantle xenoliths from this locality fall along a ~42-mWm^{-2} Pollack and Chapman (1977)-type conductive geotherm, while high-*T* xenoliths plot on or slightly above a ~44-mWm^{-2} geotherm. *P–T* estimates for the diamond-hosted clinopyroxenes mostly follow a similar trend as the xenoliths, but several high-*P* inclusions depart from the xenolith trend and remain close to the ~42-mWm^{-2} geotherm. Nimis (2002) interpreted this distribution as the result of thermal perturbation of the deep lithosphere *after* diamond formation. However, if clinopyroxenes analyses for which the estimated *P* uncertainties are higher than ±0.25 GPa are excluded, all *P–T* pairs departing from the xenolith trend are removed (Fig. 5). Using the same filtering criterion, a significant fraction of high-*T* xenoliths is also eliminated, thus considerably reducing the overall scatter (Fig. 5). Most remaining inclusions plot at *P–T* conditions compatible with those indicated by the xenoliths within the resolution of the thermometer (±40°C). This exercise indicates that the apparent discrepancies between *P–T* estimates for xenoliths and inclusions are probably an analytical artifact and that the majority of Premier lherzolitic diamonds most likely formed in the cratonic lithosphere under virtually unperturbed thermal conditions.

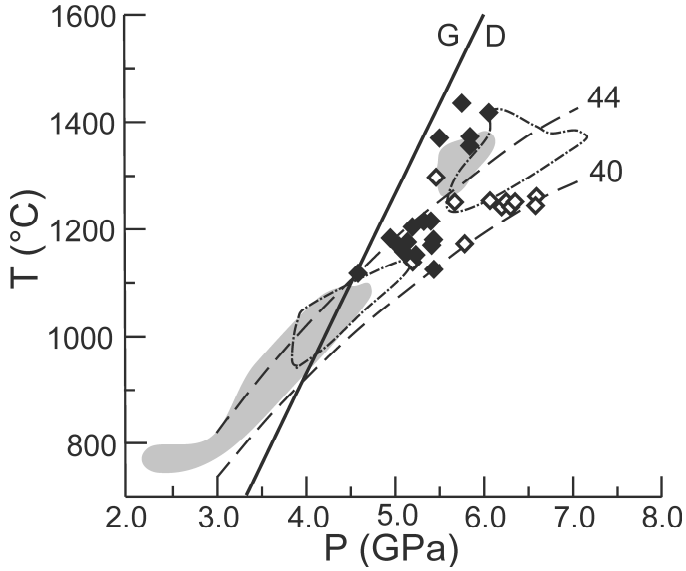

Fig 5 *P–T estimates for clinopyroxenes from the Premier kimberlite (Kaapvaal craton). Only clinopyroxenes plotting in the on-craton garnet peridotite field of Ramsay and Tompkins (1994) were included. Diamonds indicate clinopyroxenes from diamond inclusions (Gurney et al. 1986; Richardson et al. 1993). Shaded fields refer to clinopyroxenes from garnet peridotite xenoliths (Danchin 1979; Canil and O'Neill 1996; Smith 1999; Dludla et al. 2006) and xenocryst concentrates (Nimis, unpublished data). Open diamonds and dash-dot fields refer to clinopyroxenes for which the calculated* σP *is higher than ±0.25 GPa. Dashed curves are reference conductive geotherms for different surface heat-flows (*mWm^{-2}*) after Pollack and Chapman (1977). The graphite-diamond boundary (solid curve) is after Day (2012)*

CONCLUSIONS

The Cr-in-Cpx barometer can be extremely sensitive to analytical uncertainties for particular clinopyroxene compositions. In critical cases, *P* uncertainties can be as high as ±3 GPa. However, if appropriate analytical conditions are adopted during EMP analysis, the errors can be minimized and the barometer can be applied with reasonable confidence to a wide variety of compositions well beyond the limits originally recommended by Nimis and Taylor (2000), thus incorporating also a large proportion of pyroxenitic clinopyroxenes. Application to clinopyroxenes with Cr# < 0.1 remains unwarranted in all cases, owing to inconsistencies of the barometer outside the compositional field originally considered for its calibration. Simplified thresholds based on compositional parameters reported in Table 2 may help to select the most appropriate analytical conditions for optimum thermobarometry. High-quality analyses will *not* eliminate recognized underestimation of pressure at $P > 4.5$ GPa, but will considerably reduce scatter of *P–T* estimates for a great variety of natural clinopyroxenes, allowing better definition of mantle thermal state and diamond potential.

REFERENCES

- Boyd FR, Mertzman SA (1987) Composition and structure of the Kaapvaal lithosphere, southern Africa. In: Mysen BO (ed) Magmatic processes: physicochemical principles. Geochem Soc Spec Publ 1, pp 13–24
- Boyd FR, Pokhilenko NP, Pearson DG, Mertzman SA, Sobolev NV, Finger LW (1997) Composition of the Siberian cratonic mantle: evidence from Udachnaya peridotite xenoliths. Contrib Mineral Petrol 128:228–246
- Canil D, O'Neill HStC (1996) Distribution of ferric iron in some upper-mantle assemblages. J Petrol 37:609–635
- Canil D, O'Neill HStC, Pearson DG, Rudnick RL, McDonough WF, Carswell DA, (1994) Ferric iron in peridotites and mantle oxidation states. Earth Planet Sci Lett 123:205–220
- Carswell DA (1991) The garnet–orthopyroxene Al barometer: problematic application to natural garnet lherzolite assemblages. Mineral Mag 55:19–31
- Cookenboo HO, Grütter HS (2010) Mantle-derived indicator mineral compositions as applied to diamond exploration. Geochem Explor Environ Anal 10:81–95
- Danchin RV (1979) Mineral and bulk chemistry of garnet lherzolite and garnet harzburgite xenoliths from the Premier Mine, South Africa. In: Boyd FR, Meyer HOA (eds) The mantle sample: inclusion in kimberlites and other volcanics. AGU, Washington DC, pp 104–126
- Day HW (2012) A revised diamond-graphite transition curve. Am Mineral 97:52–62
- Dludla S, le Roux AP, Gurney JJ (2006) Eclogite xenoliths from the Premier kimberlite, South Africa: geochemical evidence for a subduction origin. S Afr J Geol 109:353–368
- Donnelly CL, Stachel T, Creighton S, Muehlenbachs K, Whiteford S (2007) Diamonds and their mineral inclusions from the A154 South pipe, Diavik Diamond Mine, Northwest territories, Canada. Lithos 98:160–176
- Evans BW, Trommsdorff V (1978) Petrogenesis of garnet lherzolite, Cima di Gagnone, Leopontine Alps. Earth Planet Sci Lett 40:333–348
- Faryad SW, Dolejš D, Machek M (2009) Garnet exsolution in pyroxene from clinopyroxenites in the Moldanubian zone: constraining the early pre-convergence history of ultramafic rocks in the Variscan froge. J Metamorphic Geol 27:655–671
- Franz L, Brey GP, Okrusch M (1996) Steady-state geotherm, thermal disturbances, and tectonic development of the lower lithosphere underneath the Gibeon Kimberlite Province, Namibia. Contrib Mineral Petrol 126:181–198
- Grütter H, Moore R (2003) Pyroxene geotherms revisited - an empirical approach based on Canadian xenoliths. Extended Abstract 8th International Kimberlite Conference no. 272 (CDROM)
- Grütter HS (2009) Pyroxene xenocryst geotherms: techniques and application. Lithos 112:1167–1178
- Gurney JJ, Harris JW, Rickard RS, Moore RO (1986) Premier Mine diamond inclusions. University of Cape Town, Internal Rep 4
- Mather KA, Pearson DG, McKenzie D, Kjarsgaard BA, Priestley K (2011) Constraints on the depth and thermal history of cratonic lithosphere from peridotite xenoliths, xenocrysts and seismology. Lithos 125(1-2):729–742
- Menzies A, Westerlund K, Grütter H, Gurney J, Carlson J, Fung A, Nowicki T (2004) Peridotitic mantle xenoliths from kimberlites on the Ekati Diamond Mine property,

N.W.T., Canada: major element compositions and implications for the lithosphere beneath the central Slave craton. Lithos 77:395– 412

- Nickel KG, Green DH (1985) Empirical geothermobarometry for garnet peridotites and implications for the nature of the lithosphere, kimberlites and diamonds. Earth Planet Sci Lett 73:158–170
- Nimis P (2002) The pressures and temperatures of formation of diamond based on thermobarometry of chromian diopside inclusions. Can Mineral 40:871–884
- Nimis P, Grütter H (2010) Internally consistent geothermometers for garnet peridotites and pyroxenites. Contrib Mineral Petrol 159:411–427
- Nimis P, Taylor WR (2000) Single-clinopyroxene thermobarometry for garnet peridotites. Part I. Calibration and testing of a Cr-in-Cpx barometer and an enstatite-in-Cpx thermometer. Contrib Mineral Petrol 139:541–554
- Nimis P, Trommsdorff V (2001) Revised thermobarometry of Alpe Arami and other garnet peridotites from the Central Alps. J Petrol 42:103–115
- Nimis P, Zanetti A, Dencker I, Sobolev NV (2009) Major and trace element composition of chromian diopsides from the Zagadochnaya kimberlite (Yakutia, Russia): Metasomatic processes, thermobarometry and diamond potential. Lithos 112:397–412
- Pearson DG, Shirey SB, Carlson RW, Boyd FR, Pokhilenko NP, Shimizu N (1995) Re–Os, Sm–Nd and Rb–Sr isotope evidence for thick Archaean lithospheric mantle beneath the Siberia craton modified by multistage metasomatism. Geochim Cosmochim Acta 59:959–977
- Pollack HN, Chapman DS (1977) On the regional variations of heat flow, geotherms and lithospheric thickness. Tectonophysics 38:279–296
- Ramsay RR, Tompkins LA (1994) The geology, heavy mineral concentrate mineralogy, and diamond prospectivity of the Boa Esperança and Cana Verde pipes, Corrego D'anta, Minas Gerais, Brazil. In: Meyer HOA, Leonardos OH (eds) Kimberlites, Related Rocks and Mantle Xenoliths CPRM, Spec Publ, Brasilia, Brazil, pp 329-345
- Read GH, Janse AJA (2009) Diamonds: Exploration, mines and marketing. Lithos 112:1-9
- Richardson SH, Harris JW, Gurney JJ (1993) Three generations of diamonds from old continental mantle. Nature 366:256–258
- Sand KK, Waight TE, Pearson DG, Nielsen TFD, Makovicky E, Hutchison MT (2009) The lithospheric mantle below southern West Greenland: A geothermobarometric approach to diamond potential and mantle stratigraphy. Lithos 112S:1155–1166
- Smith D (1999) Temperatures and pressures of mineral equilibration in peridotite xenoliths: review, discussion, and implications. In: Fei Y, Bertka CM, Mysen BO (eds) Mantle petrology: field observations and high pressure experimentation: a tribute to Francis R. (Joe) Boyd, vol 6. Geochem Soc Spec Publ, pp 171–188
- Stachel T, Harris JW, (2008) The origin of cratonic diamonds – constraints from mineral inclusions. Ore Geol Rev 34:5–32
- Taylor WR (1998) An experimental test of some geothermometer and geobarometer formulations for upper mantle peridotites with application to the thermobarometry of fertile lherzolite and garnet websterite. N Jb Min Abh 172:381–408
- Wang W, Gasparik T (2001) Metasomatic clinopyroxene inclusions in diamonds from the Liaoning province, China. Geochim Cosmochim Acta 65:611–62

MANUSCRIPT 2

(*Submitted to: Contributions to Mineralogy and Petrology*)

GARNET AND SPINEL IN FERTILE AND DEPLETED MANTLE: INSIGHTS FROM THERMODYNAMIC MODELLING

Luca Ziberna[1], Stephan Klemme[2], Paolo Nimis[1,3]

[1]Dipartimento di Geoscienze, Università di Padova, Italy; [2]Institut für Mineralogie, Universität Münster, Germany; [3]IGG–CNR, Padova, Italy

ABSTRACT

We performed thermodynamic calculations on model and natural peridotitic compositions at pressure and temperature conditions relevant to the Earth's upper mantle, using well-established free energy minimization techniques. The model is consistent with the available experimental data in Cr-bearing peridotitic systems, and can therefore be used to predict phase relations and mineral compositions in a wide range of realistic mantle compositions. The generated phase diagrams for six different bulk compositions, representative of fertile, depleted and ultra depleted peridotitic mantle, show that the garnet+spinel stability field is always broad at low temperatures and progressively narrows with increasing temperatures. In lithospheric sections with hot geotherms (ca. 60 mW/m^2) garnet coexists with spinel across an interval of 10–15 km, at ca. 50–70 km depths. In colder, cratonic, lithospheric sections (e.g., along a 40 mW/m^2 geotherm), the width of the garnet–spinel transition strongly depends on bulk composition: in fertile mantle, spinel can coexist with garnet to about 120 km depth, while in an ultra-depleted harzburgitic mantle it can be stable to over 180 km depth. In particular, formation of chromian spinel inclusions in diamonds is restricted to pressures between 4.0 and 6.0 GPa. The modes of spinel decrease rapidly to less than 1 vol% when it coexists with garnet, hence spinel grains can be easily overlooked during the petrographical characterization of small mantle xenoliths. The very Cr-rich nature of many spinels from xenoliths and diamonds from cratonic settings may be simply a consequence of their low modes in high-pressure assemblages, thus their composition does not necessarily imply an extremely refractory composition of the source rock. The model also shows that large Ca and Cr variations in lherzolitic garnets in equilibrium with spinel can be explained by variations of pressure and temperature along a continental geotherm and do not necessarily imply variations of bulk composition. The slope of the Cr# [i.e., Cr/(Cr + Al)mol] isopleths in garnet in equilibrium with spinel changes significantly at high temperatures, posing serious limitations to the applicability of empirical geobarometric methods calibrated on cratonic mantle xenoliths in hotter, off-craton, lithospheric mantle sections.

INTRODUCTION

Knowing the nature of the lithospheric and asthenospheric mantle is critical for our understanding of the seismic structure of the Earth's interior (Revenaugh and Jordan 1991; Ringwood 1991; Stixrude 1997; Stixrude and Lithgow-Bertelloni 2005; Afonso et al. 2010), of the generation of melts in the mantle (Green 1973; Asimow et al. 1995; Herzberg and Zhang 1996; Kinzler 1997), and of the tectonic evolution of the overlying crust (McKenzie 1978; Wood and Yuen 1983; Podladchikov et al. 1994; Kaus et al. 2005; Simon and Podladchikov 2008). Phase relations in the upper mantle are, in principle, well understood (e.g., Green and Ringwood 1967). Upper mantle peridotites usually consist of four major mineral phases, i.e., olivine, orthopyroxene, clinopyroxene, and an aluminous phase (i.e., feldspar at low pressures, spinel at medium pressures, and garnet at higher pressures). The transition from plagioclase to spinel in lherzolitic compositions occurs at about 0.6–0.8 GPa (Green and Ringwood 1967; Presnall et al. 1978; Borghini et al. 2010). The transition from spinel to garnet lherzolite, which can be described by the generalized reaction spinel + pyroxene(s) = garnet + olivine, occurs at much higher pressures. The vast experimental and thermodynamic work on mantle phase relations in simplified chemical compositions, such as MgO-Al_2O_3-SiO_2 (MAS) (MacGregor 1974; Danckwerth and Newton 1978; Perkins et al. 1981; Gasparik and Newton 1984) and CaO–MgO–Al_2O_3–SiO_2 (CMAS) (e.g., MacGregor 1965; Jenkins and Newton 1979; O'Neill 1981; Gasparik 1984; Klemme and O'Neill 2000a; Walter et al. 2002) has shown that the spinel–garnet transition has a positive Clapeyron slope, and crosses the solidus at about 1570°C and 3.0 GPa (Milholland and Presnall 1998; Klemme and O'Neill 2000a; Walter et al. 2002). In more complex compositions, phase relations are more complicated and, due to the Gibbs phase rule, the higher variance opens a *P*–*T* area where garnet and spinel coexist (Chatterjee and Terhart 1985). Further experimental investigations have shown that the addition of Fe^{2+} decreases the spinel stability field (O'Neill 1981), whereas the addition of Fe^{3+} and Cr^{3+} stabilizes spinel relative to garnet (O'Neill 1981; Nickel 1986; Webb and Wood 1986; Doroshev et al. 1997). In very Cr-rich bulk compositions, Cr-spinel may be stable to pressure of more than 10 GPa (Klemme 2004).

Although the existing data already provide a good overall picture of phase relations in the upper mantle, our understanding of the effect of bulk compositional variations on mantle mineralogy is still incomplete. This is particularly important, because evidence from natural mantle samples, such as orogenic peridotite massifs and mantle xenoliths (e.g., Nixon 1987; Bodinier and Godard 2003; Pearson et al. 2003), and constraints from high-pressure, high-temperature experiments (e.g., Green and Ringwood 1967; Ringwood 1991) indicate that the lithospheric mantle is rather heterogeneous in terms of chemical and mineralogical composition, ranging from fertile lherzolite to variably depleted harzburgite and dunite. The aim of this paper is to investigate multi-phase and multi-component phase relations in simplified compositions and in complex, near-natural peridotite compositions, ranging from fertile lherzolite to depleted harzburgite, using thermodynamic calculations.

THERMODYNAMIC DATABASE, CALCULATION METHODS AND MODEL VALIDATION

Phase relations for different bulk compositions were carried out using well-established free energy minimization techniques and the *Perple_X* set of computer programs (Connolly 1990; Connolly and Petrini 2002). We employed the internally consistent thermodynamic database of Holland and Powell (1998), which was augmented for relevant Cr-bearing mantle minerals. Details of the model can be found at *http://www.perplex.ethz.ch* and in Klemme et al. (2009). We follow the approach of Klemme et al. (2009), who used new measured thermodynamic endmember data for Cr-bearing pyroxenes, garnets and spinels (e.g., Chatterjee et al. 1982; Oka et al. 1984; Mattioli and Bishop 1984; Klemme and O'Neill 1997, 2000b; Klemme et al. 2000, 2005; Klemme 2004) together with new mixing properties for Cr-bearing garnets and pyroxenes. Some endmember data for Cr-bearing pyroxenes and mixing proprieties for Cr-bearing garnets were further fitted by hand, so as to improve agreement with available experimental data in complex fertile and depleted, Cr-bearing mantle compositions (Nickel 1986, 1989; Brey et al. 1990, 1999, 2008; Robinson and Wood 1998). The refined thermodynamic database with endmember data and mixing models for Cr-bearing phases is available online as electronic supplement Table S1.

Figure 1 shows a comparison between the calculated garnet (Grt), spinel (Spl) and orthopyroxene (Opx) compositions and those determined by experiments in depleted and fertile mantle compositions. There is good overall agreement between the calculated and experimentally determined mineral compositions. In the Grt + Spl stability field, the calculated Cr/(Cr + Al) molar ratio (hereafter Cr#) in garnet increases with increasing pressure and temperature (Fig. 1a,c), in good agreement with experiments in complex Cr-bearing systems (Nickel 1986; Webb and Wood 1986; Doroshev et al. 1997; Brey et al. 1999; Girnis et al. 2003). In the garnet stability field (i.e. in spinel-free assemblages), the calculated $Cr\#_{Grt}$ remains almost constant, in excellent agreement with the experiments in natural compositions of Brey et al. (1990, 2008), in which garnets show no significant Cr# variations over the range 900 °C < *T* < 1500 °C and 2.5 < *P* < 10.0 GPa. The $Cr\#_{Spl}$ isopleths also agree well with the experimental data (Fig. 1b). For natural compositions, in the garnet-free assemblages the calculated $Cr\#_{Spl}$ decreases with increasing temperature and without significant pressure dependency. In the Grt+Spl stability field, $Cr\#_{Spl}$ increases rapidly with increasing pressure and slightly with increasing temperature (Fig. 1b), again in good agreement with experiments (Webb and Wood 1986; Brey et al. 1999; Girnis et al. 2003).

Reliable experimental data on Cr in orthopyroxene are scant, especially at pressures and temperatures where garnet and spinel coexist (Nickel 1989; Brey et al. 1999). When orthopyroxene coexists with spinel, its calculated Cr_2O_3 content increases with increasing temperature (Fig. 1d). In the Grt + Spl facies, Cr_2O_3 in Opx slightly decreases with increasing pressure (Fig. 1d). These relationships are not well constrained by experimental data, considering the low concentrations of Cr_2O_3 in opx and the large associated uncertainties (Nickel 1989; Brey et al. 1999; Klemme and O'Neill 2000b). In the garnet-only field, Cr_2O_3

in Opx decreases with increasing pressure and decreasing temperature, in good agreement with the experiments of Brey et al. (1990, 2008).

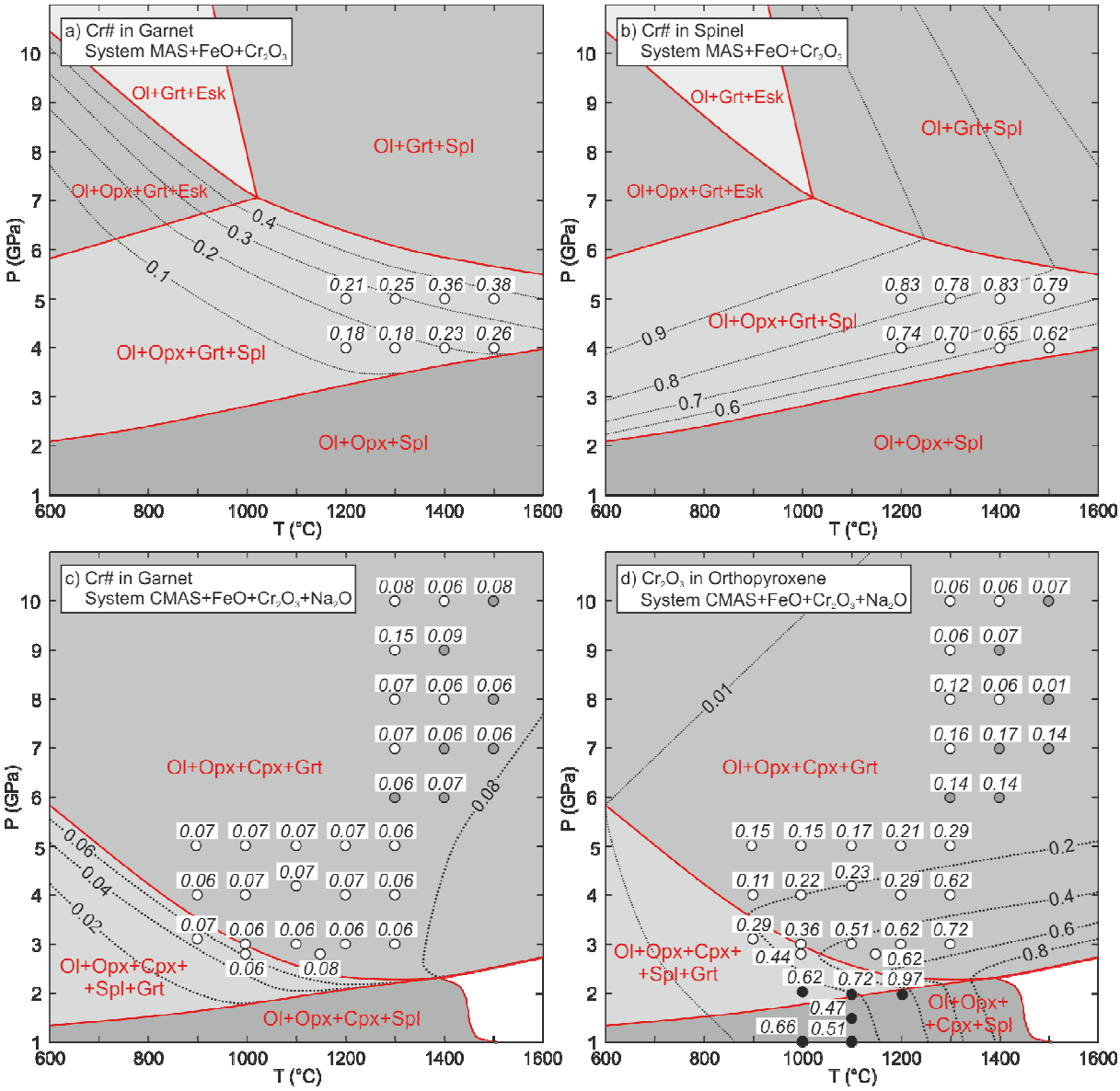

Fig. 1: *Calculated phase diagrams (solid lines) and isopleths of mineral composition (dashed lines) compared with experimental data (circles). Ol = olivine, Opx = orthopyroxene, Cpx = clinopyroxene, Spl = spinel, Grt = garnet, Esk = eskolaite).* ***a-b*** *Cr-rich system (composition ABC; Brey et al. 1999); the mineral assemblage in the experimental products was Ol+Opx+Grt+Sp.* ***c-d*** *Cr-poor systems (composition SC-1; Brey et al. 1990, 2008); the mineral assemblages in the experimental products were Ol+Opx+Cpx+Grt (white circles), Ol+Opx+Grt (grey circles) and Ol+Opx+Cpx+Sp+melt (black circles); minor melt and/or magnesite were reported in the run products at P ≥ 6 GPa (Brey et al. 2008). Bulk compositions are reported in Table 1. Note that the thermodynamic model does not allow for melting, so the results in the high-T and low-P regions of the diagrams may not be accurate.*

Despite the encouraging results of our validation test, we would like to caution the reader that the thermodynamic database used here is still far from being complete. Although it includes good recently determined thermodynamic data for major Cr-bearing mantle minerals (e.g., Klemme and O'Neill 1997, 2000b; Klemme et al. 2000, 2005, Klemme 2004), the

thermodynamic parameters for Cr-bearing pyroxenes and garnet refined in the present work are based on a set of relatively high-T experiments, which do not fully cover *P–T* conditions relevant to the shallowest mantle sections (Fig. 1). Furthermore, the employed model does not currently allow for Ca in orthopyroxene. This will not significantly affect phase relations in fertile bulk compositions, in which clinopyroxene (Cpx) and garnet dominate the Ca-budget of the rock, and will be even less problematic in depleted, low-Ca bulk compositions. Nevertheless, neglecting Ca in orthopyroxene will lead to a slight overestimation of the garnet stability and to somewhat increased calculated Ca contents in the garnet. A rough sensitivity analysis of the aforementioned issues showed that neglecting Ca in orthopyroxene determines a negative shift of the Grt-in reaction of about 0.15 GPa. Finally, Cr–Al variations in clinopyroxene are not well constrained by experiments and the thermodynamic model for clinopyroxene still needs improving, which requires more and better experiments than currently available. However, owing to the small modal amounts of, and low Al and Cr contents in clinopyroxene in typical mantle rocks, the obvious shortcomings in the Cpx thermodynamic model did not significantly affect modelling of garnet, orthopyroxene and spinel phase relations and compositions (Fig. 1).

PHASE RELATIONS IN FERTILE AND DEPLETED MANTLE

It is well known that the increase of Cr# in peridotites increases the pressure of the Grt-in reaction and expands the Grt + Spl stability field to higher pressures, as demonstrated by thermodynamic and experimental studies in synthetic systems (O'Neill 1981; Webb and Wood 1986; Doroshev et al. 1997; Brey et al. 1999; Klemme 2004). Our improved thermodynamic model allows to investigate the effect of bulk Cr# for more realistic mantle compositions. Calculations were performed in six different bulk compositions (Table 1), which encompass most of the chemical variability of the peridotitic upper mantle. We restricted the calculations to subsolidus conditions (no melt or fluid phase was allowed), at pressures between 1.0 and 10 GPa and temperatures between 600 and 1600 °C.

Compositions JSL266 and JSL261 are based on two mantle xenoliths from the Letlhakane kimberlite, Botswana (van Achterbergh et al. 2001). Their bulk compositions were calculated from reported mineral modal abundances and mineral compositions (van Achterbergh et al. 2001). The sample JSL266 is a clinopyroxene-free garnet harzburgite. Given its high bulk Cr# ratio (0.32) and the low CaO and high Cr_2O_3 contents of garnet (2.4 and 11.0 wt%, respectively), this sample can be considered as representative of a highly refractory, harzburgitic, sub-cratonic lithospheric mantle (cf. Nixon 1987; Griffin et al. 2003; Pearson et al. 2003). The sample JSL261 is a clinopyroxene-bearing peridotite, has lower bulk Cr# ratio (0.24) and contains garnets with "lherzolitic" major element compositions (e.g., Cr_2O_3 = 7.6 wt% and CaO = 6.2 wt%). This composition was chosen to represent a refractory sub-cratonic mantle that underwent low degrees of refertilization (cf. Nixon 1987; Griffin et al. 2003; Pearson et al. 2003).

Table 1: *Bulk compositions of experimental and natural samples used in thermodynamic models. SC-1: natural mineral mixtures used in the experiments of Brey et al. (1990, 2008). ABC: synthetic mineral mixtures of Brey et al. (1999). JSL266 and JSL261: mantle xenoliths from the Letlhakane kimberlite (Botswana); bulk compositions calculated from reported mineral modal abundances and compositions (van Achterbergh et al. 2001). R893, R347 and R123: natural samples from the Ronda peridotite massif; bulk composition obtained by X-ray fluorescence (Frey et al. 1985). MPY: MORB-Pyrolite (Robinson et al. 1998). Cr# and Ca# are Cr/(Cr+Al) and Ca/(Ca+Mg+Fe_{tot}) molar ratios, respectively.*

	SC-1	ABC	JSL266	JSL261	R893	R347	R123	MPY
SiO_2	45.37	41.18	44.88	45.2	42.94	44.37	45.66	44.95
Al_2O_3	4.16	9.08	1.82	1.71	0.89	1.88	4.85	4.39
Cr_2O_3	0.45	12.50	1.29	0.80	0.29	0.34	0.31	0.45
FeO	7.87	6.16	5.83	6.14	7.98	8.11	8.81	7.59
MgO	38.23	31.08	45.89	45.3	47.09	43.70	35.85	38.81
CaO	3.56	0.00	0.29	0.67	0.78	1.49	4.08	3.40
Na_2O	0.36	0.00	0.00	0.05	0.03	0.11	0.45	0.40
Cr#	0.07	0.48	0.32	0.24	0.18	0.11	0.04	0.06
Ca#	0.06	0.00	0.00	0.01	0.01	0.02	0.07	0.05

Compositions R893, R347 and R123 are based on well-characterized samples of the Ronda peridotite massif (Frey et al. 1985) and range from depleted (R893) to fertile (R123) peridotite. These compositions cover most of the chemical variations of the sub-continental lithospheric mantle in more fertile sub-cratonic sections (CaO = 0.4–1.0 wt%, Al_2O_3 = 0.8–1.8 wt%; Griffin et al. 2003) and beneath off-craton, Phanerozoic and Proterozoic mobile belts (CaO = 1.3–3.4 wt%, Al_2O_3 = 1.5–4.0 wt%; Griffin et al. 2003). Composition MPY (MORB-Pyrolite after Robinson et al. 1998) is thought to represents the primary composition of oceanic mantle before MORB extraction (cf. Ringwood 1979; Green and Falloon 1998).

Figure 2 depicts *P–T* sections calculated for the selected bulk compositions. As predicted by the phase rule (Gibbs 1875–1878) a Grt + Spl field is always present, regardless of the bulk composition used. The Grt-in reaction is always positively sloped in P–T space, while the Spl-out reaction has a marked negative slope, as already shown by previous experiments and thermodynamic calculations in simple systems (O'Neill 1981; Doroshev et al. 1997; Girnis and Brey 1999; Klemme 2004). At high temperatures, the transition from spinel to garnet peridotite becomes very narrow. For the bulk composition MPY the transition at the solidus lies at 1400 °C and 2.4 GPa, in good agreement with experiments with analogous pyrolitic compositions (1400 °C and 2.6 GPa; Robinson and Wood 1998; Walter 1998).

In fertile compositions (MPY, R123), the Grt + Spl stability field is narrower, especially at high temperatures (Fig. 2a–b). In depleted compositions, spinel is stable to higher pressures and coexists with garnet to 5.5 GPa and 1000 °C (composition JSL266; Fig. 2f). As a rule, with increasing bulk Cr# and decreasing Ca#, the pressure of the Grt-in reaction increases only slightly, while the pressure of the Spl-out reaction increases significantly, thus broadening the Grt + Spl stability field.

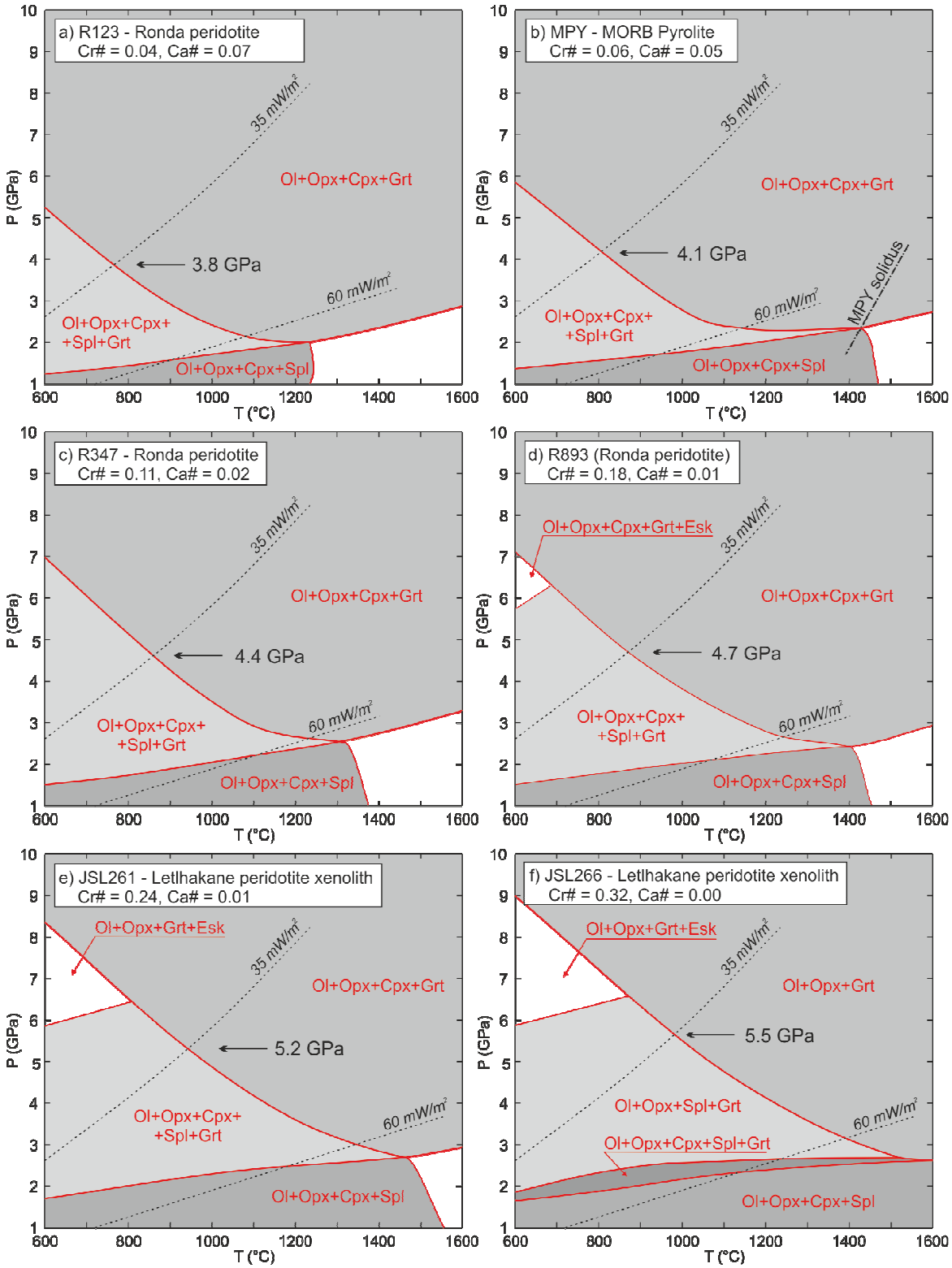

Fig. 2: *Phase diagrams calculated for model and natural peridotitic compositions, arranged in order of increasing Cr# and decreasing Ca# (cf. Table 1). Mineral abbreviations as in Fig. 1. The thermodynamic model does not allow for melting and therefore the predicted assemblages for T > 1250 °C and P < 3.0 GPa (white fields) were not considered. The dash-dot line in* ***(b)*** *is the solidus for MORB-Pyrolite (MPY) derived from the experiments of Robinson and Wood (1998); no melting experiments are available for the other peridotitic compositions. Dotted curves are steady-state conductive geotherms after Hasterok and Chapman (2011). Note that on a 35-mW/m^2 geotherm, the pressure of the spinel-out reaction (arrows) progressively increases with increasing depletion of the peridotite.*

The effect of temperature on spinel stability plays a crucial role on the variation of the spinel to garnet peridotite transition in the upper mantle under different thermal regimes. For a relatively hot 60 mW/m^2 steady-state geotherm, the Grt + Spl stability field is always narrow, regardless of the bulk composition (Fig. 2). Garnet and spinel coexist between about 1.5 and 2.1 GPa in the most fertile bulk compositions (R123), and between 2.4 and 3.0 GPa in the most depleted bulk composition (JSL266). For a 35 mW/m^2 geotherm, representative of the coldest cratonic mantle sections, garnet and spinel coexist over a wide range of pressures and this range increases with the degree of depletion (Fig. 2).

COMPOSITION AND MODE OF GARNET AND SPINEL IN FERTILE AND DEPLETED MANTLE

Figure 3 shows calculated Cr# isopleths for garnet for the most fertile (R123) and most depleted (JSL266) natural compositions reported in Table 1. Garnet becomes increasingly enriched in Cr with increasing pressure and temperature as long as spinel is also stable. In the Grt-only field the composition of the garnet remains virtually constant. This is because the Al and Cr contents in the pyroxenes are very low at high pressure and, therefore, pyroxene modal or compositional variations do not affect garnet Cr# significantly. The Cr content in garnet (or its Cr#) can therefore be a useful barometer when spinel is present, as already empirically observed by Ryan et al. (1996), Grütter (2006), and Turkin and Sobolev (2009). The present modelling, however, shows that the slope of the Cr#$_{Grt}$ isopleths changes significantly at high temperatures (Figs. 1a,c and Fig. 3), posing serious limitations to the applicability of empirical barometric methods derived from cratonic mantle xenoliths in hotter (e.g., off-craton) lithospheric mantle sections.

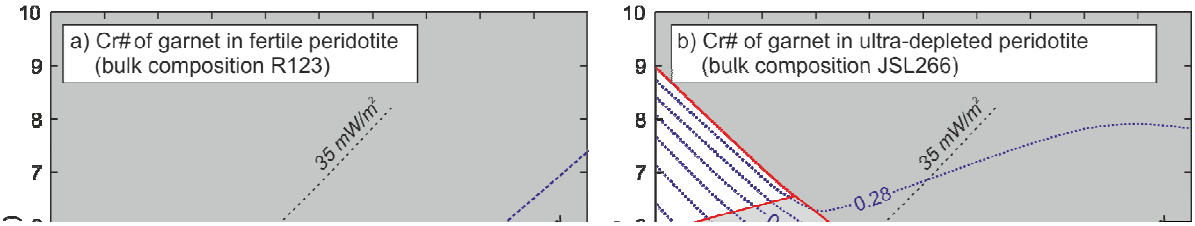

Calculation of garnet composition at different *P* and *T* provides further insights into the large compositional variability observed in natural garnets from mantle xenoliths and heavy mineral concentrates from kimberlites. We have calculated garnet compositions at different *P–T* conditions along a 35 mW/m^2 steady state geotherm (typical of the coldest cratonic sections), using fertile and depleted bulk compositions. The calculated garnet compositions are shown in a Ca–Cr diagram (Fig. 4). It appears that, for a fixed bulk composition and in the presence of spinel, very large variations in garnet composition may simply be caused by variation of *P* and *T* along a continental geotherm. In particular, a garnet with high Cr_2O_3 does not necessarily imply a highly depleted composition, but may well indicate a high pressure origin. For fertile to moderately depleted lherzolitic bulk compositions (bulk Cr# ≤ 0.24 and Ca# ≥ 0.01), the change in garnet chemistry with increasing *P–T* in the presence of spinel produces an almost linear trend that mimics in slope and extension the classic lherzolitic trend in Ca–Cr diagrams (e.g., Sobolev et al. 1973; Gurney 1984) (Fig. 4). The increase in Cr and, for lherzolitic compositions, also in Ca reflects the progressive reaction of spinel and clinopyroxene components to garnet with increasing pressure (see also Klemme et al. 2009). Only when spinel is completely exhausted, the garnet compositional variations with changing *P–T* become minimal (Fig. 4).

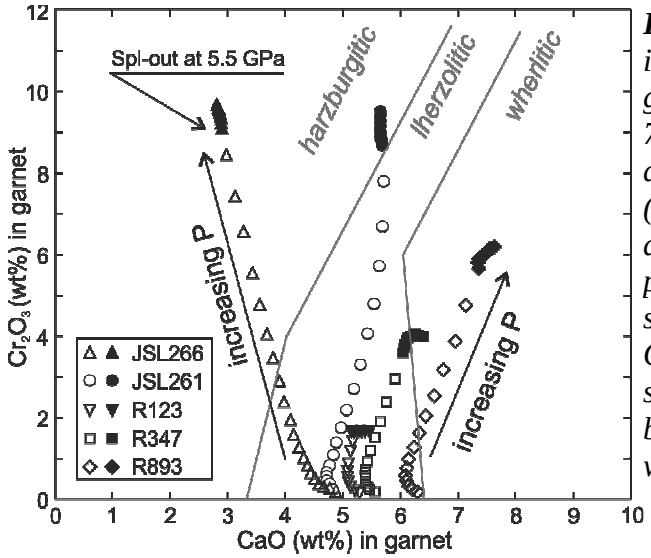

Fig. 4: *Calculated CaO and Cr_2O_3 contents in garnet along a 35 mW/m^2 steady-state geotherm (from 600 °C, 2.5 GPa to 1200 °C, 7.0 GPa), for fertile (R893) to strongly depleted (JSL266) bulk rock compositions (see Table 1). Note that Cr_2O_3 contents drastically increase with increasing pressure and temperature in the Grt + Spl stability field (empty symbols), while in the Grt-only stability filed (filled symbols) they show only small variations. Compositional boundaries for harzburgites, lherzolites and wherlites are after Sobolev et al. (1973).*

Figure 5 shows calculated modes and Cr# ratios in spinel for the most depleted (JSL266) and fertile (R123) bulk compositions. Spinel modes are low in ultra-depleted compositions (< 2.8 %) and even lower in fertile compositions (< 1.5 %). In the Grt + Spl stability field, spinel modes decrease rapidly with increasing pressure and temperature to less than 1.0 %, regardless of the bulk composition (Fig. 5). At such low modes, spinel grains may be easily overlooked in mantle xenoliths, especially if the xenoliths are small and the grain size is large. Therefore, we conclude that many garnet-peridotite xenoliths reported in the literature may in fact be garnet–spinel peridotites. A review of existing literature data on mantle xenoliths with reported mineral modes indicates that 73 % of 764 records have no reported spinel and 99 % have spinel modes lower than 3.0 vol%, which is consistent with the model. Doubts are cast on the petrological significance of several garnet–spinel peridotite xenoliths with abundant

modal spinel (up to 7 vol%; e.g., Nixon and Boyd 1979; Murav'yeva et al. 1985): these elevated modes are likely to reflect either a non-representative mantle sampling, due to the small size of the xenoliths (cf. Nixon and Boyd 1979), or the occurrence of relict spinels (e.g., from higher-*T*, garnet-free parageneses) that did not fully re-equilibrate with the surrounding garnet-bearing assemblage.

Our data show that the Cr# ratio in the spinel increases rapidly with pressure and decreases only slightly with temperature (Fig. 5). Along a cold continental geotherm (35–45 mW/m^2), Cr# in spinel can be as high as 0.85 even in fertile compositions (Fig. 5). Therefore, Cr-rich spinels in mantle xenoliths do not necessary imply ultra-depleted bulk compositions, but may also reflect decreased spinel modes in relatively fertile compositions.

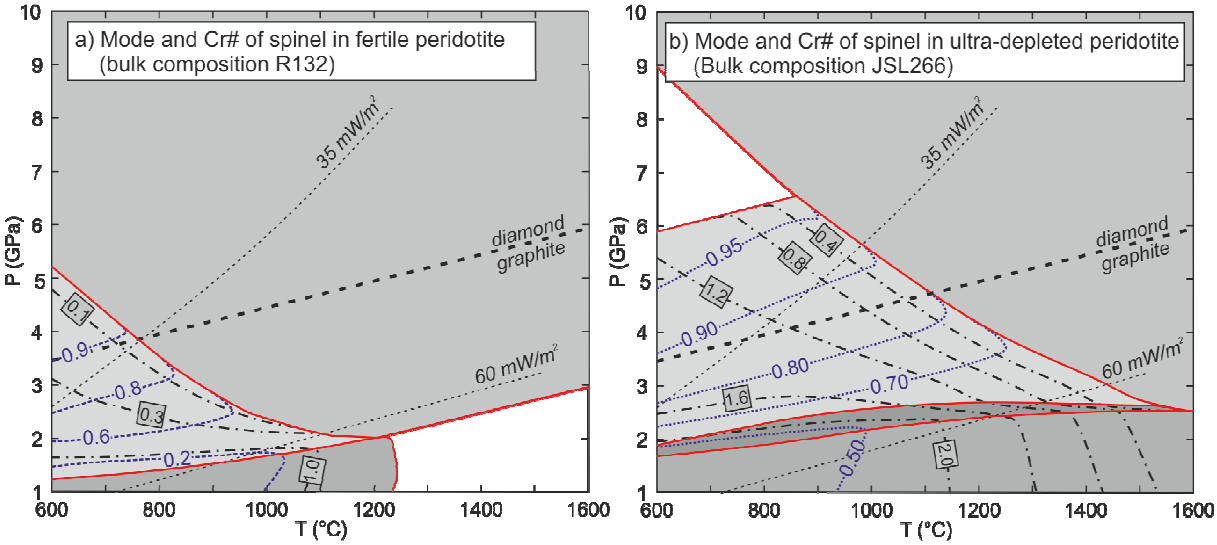

Fig. 5: *Isopleths of modes (vol%; dash-dot curves) and Cr# (dotted curves) in spinel from* ***(a)*** *fertile (R123) and* ***(b)*** *strongly depleted (JSL266) bulk compositions. Assemblages, phase boundaries, and reference geotherms as in Figure 2. The graphite–diamond boundary is after Day (2012). Along a cold geotherm, in the low-P, low-T region, spinel modes are higher in the strongly depleted bulk compositions, yet spinels in fertile and strongly depleted peridotite have almost the same Cr# values.*

IMPLICATIONS FOR THE SPINEL PERIDOTITE TO GARNET PERIDOTITE TRANSITION

The transition from spinel peridotite to garnet peridotite is one of the most important phase boundaries in the upper mantle, which has important effects on the tectonic evolution of the lithosphere (Yamasaki and Nakada 1997; Kaus et al. 2005; Simon and Podladchikov 2008) and on deep magmatic processes (Wood 1979; Allègre et al. 1984; Salters and Hart 1989; LaTourette et al. 1993; Asimow et al. 1995). Our calculated phase diagrams (Fig. 2) show that the depth of the spinel-to-garnet transition strongly depends on the thermal state of the lithosphere and that the effect of bulk composition is relevant only in a cold lithosphere. According to our calculations, in a relatively hot lithosphere the transition occurs across an interval of 10–15 km, at ca. 50–70 km depth, regardless of the bulk composition. In a colder lithosphere, the transition occurs across a broader pressure interval and at much greater

depths: in a fertile mantle, spinel can coexist with garnet to about 120 km depth, while in an ultra-depleted harzburgitic mantle it remains stable to some 180 km depth.

These results have interesting bearing on the interpretation of the so-called "Hales discontinuity" or "Hales gradient zone", a seismic impedance increase observed over wide areas around the world, which is usually attributed to the spinel-to-garnet transition (Green and Hales 1968; Hales 1969; Wood and Yuen 1983; Revenaugh and Jordan 1991; Lebedev et al. 2009; Ayarza et al. 2010). In principle, a sharp Hales discontinuity should only be observed when the Grt + Spl stability field is small. This would most likely be the case in a very hot lithosphere (e.g., under mid-ocean ridges), independently of bulk composition (Fig. 2). In colder lithospheric sections, where the Grt + Spl stability field is wider (Fig. 2), a Hales gradient zone should be observed. This is in agreement with the observed extension of the Hales gradient zone in various geodynamic settings. In continental regions with relatively hot geotherms, such as the Variscan Orogen in the SW Iberian Peninsula (Palomeras et al. 2011), the Hales gradient zone is only 10–20 km thick and lies at around 70 km depth (Ayarza et al. 2010). In cratonic blocks with colder geotherms, it appears at greater depths and over broader intervals, i.e., from the Moho to 150 km depth (Lebedev et al. 2009). We further predict that bulk composition may control the extension of the Hales gradient zone in cold, cratonic settings, but its influence will progressively decrease at higher geothermal gradients.

GARNET AND SPINEL IN THE DIAMOND STABILITY FIELD

Under typical cratonic geothermal gradients (i.e., 35–45 mW/m^2 mean surface heat flow), Cr# in garnet increases with pressure solely in the Grt + Spl stability field, while it remains almost constant at higher pressures where only garnet is stable (Fig. 3). Using our new model, we can determine the minimum Cr#$_{Grt}$ needed for garnet to be in the diamond stability field. According to our model, when considering a 35 mW/m^2 geotherm and depleted to very depleted bulk compositions (R893, JSL266), the minimum Cr# for a garnet in the diamond stability field (P > ca. 4 GPa; T > ca. 800°C) is 0.06. For fertile compositions (R123), the minimum Cr# in garnet decreases to 0.04. On a hotter 45 mW/m^2 geotherm, the minimum Cr# jumps to 0.16 for depleted compositions (R893) and to 0.22 for very depleted compositions (JSL266). For fertile compositions, the same change in the geothermal gradient does not produce any appreciable change in the minimum Cr#$_{Grt}$, because spinel reacts out with increasing P–T before entering the diamond stability field (Fig. 3).

Figure 5 shows that, for depleted compositions, the stability field of chromian spinel extends well into the diamond stability field, in agreement with the relatively common finding of chromian spinel inclusions in diamonds (e.g., Stachel and Harris 2008). According to our calculations, for typical cratonic geotherms (35–45 mW/m^2), the Cr# ratios of spinel in the diamond stability field is 0.87–0.90 for depleted bulk compositions (R893) and 0.84–0.92 for ultra-depleted compositions (JSL266). This is in good agreement with Cr# data for spinel inclusions in diamonds, which are mostly between 0.82 and 0.92 (Stachel and Harris 2008).

In an ultra depleted mantle rock (e.g., composition JSL266; bulk Cr# = 0.32), we calculate that spinel can be stable up to 5.5 GPa. This value decreases with decreasing bulk Cr# ratio (Fig. 2). As the typical bulk Cr# values of sub-cratonic lithospheric peridotites range between 0.15 and 0.35 (cf. Pearson et al. 2003), it can be argued that spinel inclusions in diamonds cannot originate at pressures greater than about 6.0 GPa.

CONCLUSIONS

The new thermodynamic model for chromium-bearing peridotites enables phase equilibria calculations from fertile to strongly depleted mantle compositions. The model successfully reproduces experimentally determined phase equilibria between 2.0–10.0 GPa and 900–1500 °C, and allows calculations of phase relations in a high *P* and low *T* regime difficult to investigate by experiments, but relevant for *P–T* conditions in the cratonic upper mantle.

Our calculations for natural peridotitic compositions show that garnet and spinel coexist across a restricted depth interval (ca. 10–15 km) between 50 and 70 km in regions with hot geotherms and extends to 120–180 km depth in regions with cold geotherms, in good agreement with seismic observations. The very low calculated modes of spinel (0.1–2.8 %) in the garnet+spinel stability field suggest that many mantle xenoliths described in the literature as garnet peridotites may in fact be garnet–spinel peridotites. Our thermodynamic model also provides a quantitative explanation of the empirically-determined compositional variations in peridotitic garnets coexisting with spinels. The model also suggests a significant potential role of *P–T* conditions on the distribution of garnets in the popular Ca–Cr discrimination diagram. Finally, formation of chromian spinel inclusions in diamonds is restricted to pressures between 4.0 and 6.0 GPa, and their very high Cr contents do not necessarily imply ultra-depleted bulk compositions.

REFERENCES

- Afonso JC, Ranalli G, Fernàndez M, Griffin WL, O'Reilly SY, Faul, U (2010) On the Vp/Vs–Mg# correlation in mantle peridotites: Implications for the identification of thermal and compositional anomalies in the upper mantle. Earth Planet Sci Lett 289:606–618
- Allègre CJ, Hamelin B, Dupré B (1984) Statistical analysis of isotopic ratios in MORB: the mantle blob cluster model and the convective regime of the mantle. Earth Planet Sci Lett 71:71-84
- Asimow PD, Hirschmann MM, Ghiorso MS, O'Hara MJ, Stolper EM (1995) The effect of pressure-induced solid-solid phase transitions on decompression melting of the mantle. Geochim Cosmochim Acta 59:4489-4506
- Ayarza P, Palomeras I, Carbonell R, Afonso JC, Simancas F (2010) A wide-angle upper mantle reflector in SW Iberia: Some constraints on its nature. Phys Earth Planet Inter 181:88-102
- Bodinier J-L, Godard M (2003) Orogenic, Ophiolitic, and Abyssal Peridotites. In: Holland HD, Turekian KK (eds) Treatise on Geochemistry, Elsevier, Amsterdam, pp 103-170

- Borghini G, Fumagalli P, Rampone E (2010) The stability of plagioclase in the Upper Mantle: Subsolidus experiments on fertile and depleted Lherzolite. J Petrol 51:229-254
- Brey G, Köhler T, Nickel K (1990) Geothermobarometry in four-phase lherzolites I. Experimental results from 10 to 60 kb. J Petrol 31:1313-1352
- Brey GP, Doroshev AM, Girnis AV, Turkin AI (1999) Garnet-spinel-olivine-orthopyroxene equilibria in the FeO-MgO-Al_2O_3-SiO_2-Cr_2O_3 system: I. Composition and molar volumes of minerals. Eur J Mineral 11:599-617
- Brey GP, Bulatov VK, Girnis V (2008) Geobarometry for Peridotites: Experiments in simple and natural systems from 6 to 10 GPa. J Petrol 49:3-24
- Chatterjee ND, Terhart L (1985) Thermodynamic calculation of peridotite phase relations in the system MgO-Al_2O_3-SiO_2-Cr_2O_3, with some geological applications. Contrib Mineral Petrol 89:273-284
- Chatterjee ND, Leistner H, Terhart L, Abraham K, Klaska R (1982) Thermodynamic mixing properties of corundum eskolaite, alpha-$(Al,Cr^{+3})_2O_3$, crystalline solutions at high-temperatures and pressures. Am Mineral 67:725-735
- Connolly JAD (1990) Multivariable phase diagrams: An algorithm based on generalized thermodynamics. Am J Sci 290:666-718
- Connolly JAD, Petrini K (2002) An automated strategy for calculation of phase diagram sections and retrieval of rock properties as a function of physical conditions. J Metamorph Geol 20: 697-708
- Danckwerth PA, Newton RC (1978) Experimental determination of the spinel peridotite to garnet peridotite reaction in the system MgO– Al_2O_3–SiO2 in the range 900 – 1100 °C and Al_2O_3 isopleths of enstatite in the spinel field. Contrib Mineral Petrol 66:189-201
- Day HW (2012) A revised diamond-graphite transition curve. Am Mineral 97:52-62.
- Doroshev A, Brey G, Girnis A, Turkin A, Kogarko L (1997) Pyrope-knorringite garnets in the Earth's mantle: Experiments in the MgO-Al_2O_3-SiO_2-Cr_2O_3 system. Russ Geol Geophys 38:559-586
- Frey FA, Suen CJ, Stockman HW (1985) The Ronda high temperature peridotite: Geochemistry and petrogenesis. Geochim Cosmochim Acta 49:2469-2491
- Gasparik T (1984) Two-pyroxene thermobarometry with new experimental data in the system CaO-MgO-Al_2O_3-SiO_2. Contrib Miner Petrol 87:87-97
- Gasparik T, Newton RC (1984) The reversed alumina contents of orthopyroxene in equilibrium with spinel and forsterite in the system MgO–Al_2O_3–SiO_2. Contrib Mineral Petrol 85:186-196
- Gibbs JW (1874–1878) On the Equilibrium of Heterogeneous Substances. Trans Conn Acad Arts Sci 3:108-248, 343-524
- Girnis AV, Brey GP (1999) Garnet–spinel–olivine–orthopyroxene equilibria in the FeO–MgO–Al_2O_3–SiO_2–Cr_2O_3 system: II. Thermodynamic analysis. Eur J Mineral 11:619-636
- Girnis AV, Brey GP, Doroshev AM, Turkin AI, Simon N (2003) The system MgO-Al_2O_3-SiO_2-Cr_2O_3 revisited: reanalysis of Doroshev et al.'s (1997) experiments and new experiments. Eur J Mineral 15:953-964
- Green DH (1973) Contrasted melting relations in a pyrolite upper mantle under mid-oceanic ridge, stable crust and island arc environments. Tectonophysics 17:285-297
- Green DH, Falloon TJ (1998) Pyrolite: a Ringwood concept and its current expression. In: Jackson I (ed) The Earth's mantle – composition, structure and evolution. Cambridge University Press, Cambridge, pp 311-378

- Green RWE, Hales AL (1968). Travel times of P waves to 30 degrees in Central United States and upper mantle structure. Bull Seismol Soc Am 58:267-278
- Green DH, Ringwood AE (1967) The stability fields of aluminous pyroxene peridotite and garnet peridotite and their relevance in upper mantle structure. Earth Planet Sci Lett 3:151-160
- Griffin WL, O'Reilly SY, Abe N, Aulbach S, Davies RM, Pearson NJ, Doyle BJ, Kivi K (2003) The origin and evolution of Archean lithospheric mantle. Precambrian Res 127:19-41
- Grütter H (2006) Cr-saturation arrays in concentrate garnet compositions from kimberlite and their use in mantle barometry. J Petrol 47:801-820
- Gurney JJ (1984) A correlation between garnets and diamonds in kimberlites. In: Glover JE, Harris PG (Eds) Kimberlites: Occurrence and Origin: A Basis for Conceptual Models in Exploration. University of Western Australia, Extension Services, Perth, pp 143-166
- Hales A (1969) A seismic discontinuity in the lithosphere. Earth Planet Sci Lett 7:44-46
- Hasterok D, Chapman DS (2011) Heat production and geotherms for the continental lithosphere. Earth Planet Sci Lett 307:59-70
- Herzberg C, Zhang J (1996) Melting experiments on anhydrous peridotite KLB-1: Compositions of magmas in the upper mantle and transition zone. J Geophys Res 101:8271-8295
- Holland TJB, Powell R (1998) An internally consistent thermodynamic data set for phases of petrological interest. J Metamorph Geol 16:309-343
- Irifune T, Ohtani E, Kumazawa M (1982) Stability field of knorringite $Mg_3Cr_2Si_3O_{12}$ at high pressure and its implication to the occurrence of Cr-rich pyrope in the upper mantle. Phys Earth Planet Inter 27:263-272
- Jenkins DM, Newton RC (1979) Experimental determination of the spinel peridotite to garnet peridotite inversion at 900°C and 1000°C in the system CaO-MgO-Al_2O_3-SiO_2, and at 900°C with natural garnet and olivine. Contrib Mineral Petrol 68:407-419
- Kaus B, Connolly J, Podladchikov Y, Schmalholz S (2005) Effect of mineral phase transitions on sedimentary basin subsidence and uplift. Earth Planet Sci Lett 233:213-228
- Kinzler RJ (1997) Melting of mantle peridotite at pressures approaching the spinel to garnet transition: Application to mid-ocean ridge basalt petrogenesis. J Geophys Res 102:853-874
- Klemme S (2004) The influence of Cr on the garnet–spinel transition in the Earth's mantle: experiments in the system MgO–Cr_2O_3–SiO_2 and thermodynamic modelling. Lithos 77:639-646
- Klemme S, O'Neill HSC (1997) The reaction $MgCr_2O_4+SiO_2=Cr_2O_3+MgSiO_3$ and the free energy of formation of magnesiochromite ($MgCrO_4$). Contrib Mineral Petrol 130:59-65
- Klemme S, O'Neill HSC (2000a) The near-solidus transition from garnet lherzolite to spinel lherzolite. Contrib Mineral Petrol 138:237-248
- Klemme S, O'Neill HSC (2000b) The effect of Cr on the solubility of Al in orthopyroxene: experiments and thermodynamic modelling. Contrib Mineral Petrol 140:84-98
- Klemme S, O'Neill HSC, Schnelle W, Gmelin E (2000) The heat capacity of $MgCr_2O_4$, $FeCr_2O_4$, and Cr_2O_3 at low temperatures and derived thermodynamic properties. Am Mineral 85:1686-1693

- Klemme S, van Miltenburg JC, Javorsky P, Wastin F (2005) Thermodynamic properties of uvarovite garnet ($Ca_3Cr_2Si_3O_{12}$). Am Mineral 90:663-666
- Klemme S, Ivanic TJ, Connolly JAD, Harte B (2009) Thermodynamic modelling of Cr-bearing garnets with implications for diamond inclusions and peridotite xenoliths. Lithos 112:986-991
- LaTourette TK, Kennedy AK, Wasserburg GJ (1993) Thorium-uranium fractionation by garnet evidence for a deep source and rapid rise of oceanic basalts. Science 261:739-742
- Lebedev S, Boonen J, Trampert J (2009) Seismic structure of Precambrian Lithosphere: new constraints from broad-band surface-wave dispersion. Lithos 109:96-111
- MacGregor ID (1965) Stability fields of spinel and garnet peridotites in the synthetic system MgO–CaO–Al_2O_3–SiO_2. Carnegie Inst Wash Year Book 64:126-134
- MacGregor ID (1974) The system MgO–Al_2O_3–SiO_2: solubility of Al_2O_3 in enstatite for spinel and garnet peridotite compositions. Am Mineral 59:110-119
- Mattioli GS, Bishop FC (1984) Experimental-determination of the chromium–aluminum mixing parameter in garnet. Geochim Cosmochim Ac 48:1367-1371
- McKenzie D (1978) Some remarks on the development of sedimentary basins. Earth Planet Sci Lett 40:25-32
- Milholland CS, Presnall DC (1998) Liquidus phase relations in the aluminous pyroxene thermal divide and high-pressure fractionation of picritic and komatiitic magmas. J Petrol 39:3-27
- Murav'yeva NS, Polyakov AI, Senin VG (1985) Physicochemical conditions and mechanism of formation of garnet-spinel lherzolite from the Vitim Plateau, Baikal rift zone. Doklady Akademii Nauk SSSR 283:1458-1462 (in Russian)
- Nickel KG (1986) Phase equilibria in the system SiO_2–MgO–Al_2O_3–CaO–Cr_2O_3 (SMACCR) and their bearing on spinel/garnet lherzolite relationships. Neues Jahrb Mineral Abh 155:259-287
- Nickel KG (1989) Garnet-pyroxene equilibria in the system SMACCR (SiO_2–MgO–Al_2O_3–CaO–Cr_2O_3): The Cr-geobarometer. In: Ross J, Jaques AL, Ferguson J, Green DH, O'Reilly SY, Danchin RV, Janse AJA (eds) Kimberlites and Related Rocks, Vol. 2, Their Mantle/Crust Setting, Diamonds and Diamond Exploration. Geological Society of Australia Special Publication 14. Blackwell Scientific, Victoria, pp 901-912
- Nixon PH (1987) Mantle xenoliths. John Wiley, Chichester.
- Nixon PH, Boyd FR (1979) Garnet bearing lherzolites and discrete nodule suites from the Malaita alnoite, Solomon Islands, S.W. Pacific, and their bearing on oceanic mantle composition and geotherm. In: Boyd FR, Meyer HOA (eds) The mantle sample: inclusions in kimberlites and other volcanics. American Geophysical Union, Washington, DC, pp 400-423
- O'Neill HSC (1981) The transition between spinel lherzolite and garnet lherzolite, and its use as a geobarometer. Contrib Mineral Petrol 77:185-194
- Oka Y, Steinke P, Chatterjee ND (1984) Thermodynamic mixing properties of Mg(Al, $Cr)_2O_4$ spinel crystalline solution at high-temperatures and pressures. Contrib Mineral Petrol 87:196-204
- Palomeras I, Carbonell R, Ayarza P, Fernández M, Simancas F, Martínez-Poyatos D, González-Lodeiro F, Pérez-Estaún A (2011) Geophysical model of the lithosphere across the Variscan Belt of SW Iberia: Multidisciplinary assessment. Tectonophysics 508:42-51

- Pearson DG, Canil D, Shirey SB (2003) Mantle Samples Included in Volcanic Rocks : Xenoliths and Diamonds. In: Holland HD, Turekian KK (eds) Treatise on Geochemistry. Elsevier, Amsterdam, pp 171-275
- Perkins DP, Holland TJB, Newton RC (1981) The Al_2O_3 contents of enstatite in equilibrium with garnet in the system $MgO–Al_2O_3–SiO_2$ at 15–40 kbar and 900– 1600 °C. Contrib Mineral Petrol 78:99-109
- Podladchikov YY, Poliakov ANB, Yuen DA (1994) The effect of lithospheric phase-transitions on subsidence of extending continental lithosphere. Earth Planet Sci Lett 124:95-103
- Presnall DC, Dixon SA, Dixon JR, O'Donnell TH, Brenner NL, Schrock RL, Dycus DW (1978) Liquidus phase relations on the join diopside–forsterite–anorthite from 1 atm to 20 kbar; their bearing on the generation and crystallization of basaltic magma. Contrib Mineral Petrol 66:203-220
- Revenaugh J, Jordan TH (1991) Mantle Layering From ScS Reverberations 3. The Upper Mantle. J Geophys Res 96:19781-19810
- Ringwood AE (1979) Origin of the Earth and Moon. Springer-Verlag, New York
- Ringwood AE (1991) Phase transformations and their bearing on the constitution and dynamics of the mantle. Geochim Cosmochim Acta 55:2083-2110
- Robinson JAC, Wood BJ (1998) The depth of the spinel to garnet transition at the peridotite solidus. Earth Planet Sci Lett 164:277-284
- Robinson JAC, Wood BJ, Blundy JD (1998) The beginning of melting of fertile and depleted peridotite at 1 . 5 GPa. Earth Planet Sci Lett 155:97-111
- Ryan CG, Griffin WL, Pearson NJ (1996) Garnet geotherms: pressure–temperature data from Cr-pyrope garnet xenocrysts in volcanic rocks. J Geophys Res 101:5611-5625
- Salters VJM, Hart SR (1989) The hafnium paradox and the role of garnet in the source of mid-ocean-ridge basalts. Nature 342:420-422
- Simon NSC, Podladchikov YY (2008) The effect of mantle composition on density in the extending lithosphere. Earth Planet Sci Lett 272:148-157
- Sobolev NV, Lavrent'ev YG, Pokhilenko NP, Usova LV (1973) Chrome-rich garnets from the kimberlites of Yakutia and their paragenesis. Contrib Mineral Petrol 40:39-52
- Stachel T, Harris J (2008) The origin of cratonic diamonds – Constraints from mineral inclusions. Ore Geol Rev 34:5-32
- Stixrude L (1997) Structure and sharpness of phase transitions and mantle discontinuities. J Geophys Res 102:14835-14852
- Stixrude L, Lithgow-Bertelloni C (2005) Thermodynamics of mantle minerals- I. Physical properties. Geophys J Int 162:610-632
- Turkin AI, Sobolev NV (2009) Pyrope–knorringite garnets: overview of experimental data and natural parageneses: Russ Geol Geophys 50:1169-1182
- Van Achterbergh E, Griffin WL, Stiefenhofer J (2001) Metasomatism in mantle xenoliths from the Letlhakane kimberlites : estimation of element fluxes. Contrib Mineral Petrol 141:397-414
- Walter MJ (1998) Melting of Garnet Peridotite and the Origin of Komatiite and Depleted Lithosphere. J Petrol 39:29-60
- Walter M, Katsura T, Kubo A, Shinmei T, Nishikawa O, Ito E, Lesher C, Funakoshi K (2002) Spinel–garnet lherzolite transition in the system $CaO-MgO-Al_2O_3-SiO_2$ revisited: an in situ X-ray study. Geochim Cosmochim Acta 66:2109-2121

- Webb SAC, Wood BJ (1986) Spinel-pyroxene-garnet relationships and their dependence on Cr/Al ratio. Contrib Mineral Petrol 92:471-480
- Wood BJ, Yuen DA (1983) The role of lithospheric phase transitions on seafloor flattening at old ages. Earth Planet Sci Lett 66:303-314
- Wood DA (1979) A variably veined sub-oceanic upper mantle genetic significance for mid-ocean ridge basalts from geochemical evidence. Geology 7:499-503
- Yamasaki T, Nakada M (1997) The effects of the spinel–garnet phase transition on the formation of rifted sedimentary basins. Geophys J Int 130:681-692

MANUSCRIPT 3

(*Submitted to: Journal of Petrology*)

GEOCHEMICAL GRADIENTS DURING REFERTILISATION OF THE SIBERIAN SUB-CRATONIC MANTLE AS RECORDED BY GARNETS AND ASSOCIATED MINERALS FROM THE ZAGADOCHNAYA KIMBERLITE, DALDYN FIELD (YAKUTIA)

Luca Ziberna[1], Paolo Nimis[1,2], Alberto Zanetti[3], Andrea Marzoli[1,2], Nikolai V. Sobolev[4]

[1]Dipartimento di Geoscienze, Università di Padova, Italy; [2]IGG–CNR, Padova, Italy; [3]IGG–CNR, Pavia, Italy; [4]V.S. Sobolev Institute of Geology and Mineralogy, Novosibirsk, Russia

ABSTRACT

Garnet xenocrysts (N = 386) and associated minerals from the diamond-free Zagadochnaya kimberlite (Daldyn field, Yakutia) were studied to provide new insights into mantle processes beneath this sector of the Siberian Craton. Electron microprobe analyses on the whole set of samples indicate that the great majority of the garnets follow the "lherzolitic" trend in the CaO vs Cr_2O_3 diagram (Cr_2O_3 = 0.5–9.3 wt%, CaO = 3.2–10.3 wt%), with less than 10% falling in the wehrlitic field and less than 3% falling in a transitional region between the lherzolitic and harzburgitic field. A representative subset of the garnets (N = 28) was further analysed for trace elements by laser-ablation inductively-coupled mass spectrometry. Based on both major and trace element data, three main compositional groups are distinguished: Group A garnets (Cr_2O_3 = 1.3–5.2 wt%) are often associated with chromian diopsides and are characterised by progressively increasing, chondrite (CI)-normalized Rare Earth Elements (REE) abundances from La to Lu; Group B garnets (Cr_2O_3 = 5.4–8.6 wt%) are less depleted in Light REE (LREE) and show nearly flat patterns from Sm to Lu; Group C garnets (Cr_2O_3 = 7.3–8.4 wt%) are characterized by humped to strongly sinusoidal REE patterns, with Yb between 0.5 and 3.0 xCI. Numerical simulations of melt–rock interactions show that the wide spectrum of REE compositions observed from Group A to Group B to Group C can be produced by a unique episode of melt injection and percolation through a refractory mantle column, whereby the melt progressively changes its composition due to chromatographic ion exchange, fractional crystallisation, and assimilation of peridotitic minerals, under decreasing melt/rock ratios. The calculated composition of the metasomatising melt has a kimberlitic affinity, but is distinct from the composition of the host Zagadochnaya kimberlite. Most of Group B and C garnets show evidence of replacement by a secondary mineral assemblage made of (Ca, Cr)-poor garnet, chromian diopside, and chromite (± phlogopite ± amphibole).

The (Ca, Cr)-poor garnets are enriched in almost all incompatible trace elements, and often show humped CI-normalized REE patterns. The textures and mineralogy of these secondary mineral assemblages, the calculated compositions of the melts in equilibrium with the secondary garnets and clinopyroxenes, and Ca concentration profiles across garnet zoning, indicate deep-seated (90–130 km) pervasive reaction with melts strictly related to the host kimberlite. The lack of mantle materials from depth greater than 130 km, the absence of diamond, the abundance of secondary mineral assemblages, and the high-Mg composition of the kimberlite are consistent with a relatively slow ascent of the melts to shallow lithospheric levels and extensive melt–mantle interactions before eruption.

INTRODUCTION

Garnet peridotites are the most abundant lithologies in cratonic mantle xenoliths and may record a variety of petrochemical processes from Archean to Phanerozoic times. It is now widely accepted that, during its initial stages of formation, the sub-cratonic lithospheric mantle underwent extensive partial melting, which produced MgO-rich melts, such as komatiites or picrites, and dunitic to harzburgitic refractory residua with low FeO and high Mg# [100*Mg/(Mg + Fe)$_{mol}$] values (e.g. Efimova & Sobolev, 1977; Sobolev, 1977; Hanson & Langmuir, 1978; Boyd, 1989; Walter, 1998; Stachel *et al.*, 1998; Griffin *et al.*, 2003; Malkovets *et al.*, 2007). Later on, the strongly-depleted mantle sectors experienced variable degrees of cryptic and modal metasomatism, owing to migration of fluids and melts (e.g. Harte, 1983; Dawson, 1984; Erlank *et al.*, 1987; Boyd *et al.*, 1997; Malkovets *et al.*, 2007; Foley, 2008).

Studying the trace element compositions of mantle garnets is particularly useful to gain insights into these mantle processes. In particular, the Rare Earth Element (REE) composition shows strong relationships with the melting and metasomatic history of their host rocks (e.g. Shimizu & Richardson, 1987; Hoal *et al.*, 1994; Shimizu *et al.*, 1997a, b; Griffin *et al.*, 1999a; Stachel *et al.*, 1998, 2004; Grégoire *et al.*, 2002; Burgess and Harte, 2004; Simon *et al.*, 2007; Gibson *et al.*, 2008). For instance, sub-calcic garnets of the harzburgitic paragenesis (Sobolev *et al.*, 1969, 1973) typically show strongly to mildly sinusoidal chondrite (CI)-normalized REE patterns. In the more fertile (or refertilised) lherzolitic garnets, “normal” REE patterns with positive slopes for the Light REE (LREE) and nearly flat to positive slopes for the Middle REE (MREE) and the Heavy REE (HREE) are the most frequent, although sinusoidal to humped patterns have also been reported (e.g. Stachel *et al.*, 1998; Grégoire *et al.*, 2002; Ionov *et al.*, 2010). The interpretation of the sinusoidal or humped REE patterns has long

been debated (see Gibson *et al.*, 2008, for exhaustive reviews). It is now generally accepted that they represent transient compositions produced by interactions of former depleted peridotites with melts or fluids with high LREE/HREE ratios (e.g. Stachel *et al.*, 1998, 2004; Burgess & Harte, 2004). Stachel *et al.* (1998, 2004) suggested that the metasomatism that produced the sub-calcic harzburgitic garnets was driven by CHO fluids, while the enrichment in both major and trace elements recorded by the more calcic lherzolitic garnets should imply metasomatism operated by melts. Burgess & Harte (2004) further pointed out that the overall variation in REE patterns in lherzolitic garnets (i.e., from normal to sinusoidal) can be produced by a percolative fractional crystallization process, dominated by fractional crystallization of garnet and clinopyroxene. As yet, however, no quantitative modelling of these variations has been provided, which takes into account the combined effects of fractional crystallization *and* of chromatographic and assimilation processes during percolation of metasomatic melts through the mantle column (cf. Harte *et al.*, 1993; Dick & Natland, 1996; Bodinier *et al.*, 1990; Vernières *et al.*, 1997; Bedini *et al.*, 1997).

The lack of a comprehensive quantitative modelling can be a significant drawback for our understanding of metasomatic processes. For instance, numerous studies on kimberlite-borne mantle xenoliths, xenocrysts, and diamond inclusions allowed the identification of compositionally different metasomatic melts and fluids operating in the cratonic lithosphere (e.g. Gurney & Harte, 1980; Erlank *et al.*, 1987; Menzies *et al.*, 1987; Shimizu *et al.*, 1997b; Stachel *et al.*, 1998; Grégoire *et al.*, 2002). Hence, one of the key questions that need to be answered is whether the different metasomatic signatures recorded in mantle xenoliths from a given mantle section are the products of genetically unrelated metasomatic agents or of a unique episode of melt or fluid injection (e.g. Harte *et al.*, 1993; Burgess & Harte, 1999, 2004; Ionov *et al.*, 2002, 2006; Simon *et al.*, 2007; Gibson *et al.*, 2008). Without a rigorous quantitative support, the answer remains largely conjectural.

In this work, we tackle this problem by examining petrographic and geochemical features of "lherzolitic" garnet xenocrysts from the Zagadochnaya kimberlite, a diamond-free kimberlite from the highly diamondiferous Daldyn kimberlite field (Yakutia, Russia; Bobrievich *et al.*, 1960: Sobolev *et al.*, 1968, Sobolev, 1977). The absence of discrete ultramafic xenoliths has long hampered reconstruction of mantle conditions and processes before eruption of the kimberlite and interpretation of its barren nature. Nonetheless, the Zagadochnaya kimberlite is rich in garnet and diopside xenocrysts, which show a wide range of textures and major and trace element compositions, as a result of a complex metasomatic history (Nimis *et al.*, 2009). The aim of the present study is manifold: (i) to define the source

rocks of the garnet xenocrysts and their relationships with the chromian diopside xenocrysts studied by Nimis *et al.* (2009); (ii) to place new constraints on the metasomatic history of the Zagadochnaya lithospheric mantle, as well as on the horizontal and vertical heterogeneity of the Daldyn lithospheric mantle; (iii) to improve the knowledge of the petrochemical processes that drive the evolution of the sub-cratonic mantle, using numerical modelling of the trace element variability in the garnets; (iv) to explain the absence of diamond in the Zagadochnaya kimberlite.

GEOLOGICAL SETTING OF THE ZAGADOCHNAYA KIMBERLITE AND PREVIOUS WORK ON MANTLE-DERIVED XENOLITHS AND XENOCRYSTS

The Zagadochnaya kimberlite is a diamond-free kimberlite, located in the southern cluster of the Daldyn kimberlitic field, ca. 30 km from the highly diamondiferous Udachnaya kimberlite (Fig. 1). The Zagadochnaya kimberlite consists of two small pipes of high-Mg, low-Ti, micaceous (or Type II) kimberlite intruded in Lower Ordovician limestones (Sobolev, 1977; Kostrovitsky *et al.*, 2007). Fission track data on zircons and whole-rock K–Ar radioisotopic data suggest an emplacement age of 370 ± 19 Ma and 420 ± 20 Ma, respectively (see review by Griffin *et al.*, 1999b). The former estimate is in good agreement with U–Pb ages of zircons (from 344 ± 2Ma to 358 ± 2Ma; Davis et al., 1980) and of perovskites (from 355 ± 5 Ma to 367 ± 5 Ma; Kinny et al., 1997) in other kimberlites from the Daldyn field, as well as with Rb-Sr isochron method for neighbouring Alakit and Nakyn fields which also include important diamond mines (from 358 ± 5Ma to 364 ± 5Ma; Agashev et al., 2004). The Zagadochnaya kimberlite contains kyanite-bearing eclogitic and grospyditic xenoliths (Bobrievich *et al.*, 1960; Sobolev *et al.*, 1968, 2011; Tomilenko *et al.*, 2011), as well as abundant xenocrysts of chromian diopside and lesser amounts of garnet and spinel (Sobolev *et al.*, 1968; Egorov *et al.*, 1992; Kostrovitsky & de Bruin, 2004; Nimis *et al.*, 2009). No discrete peridotitic

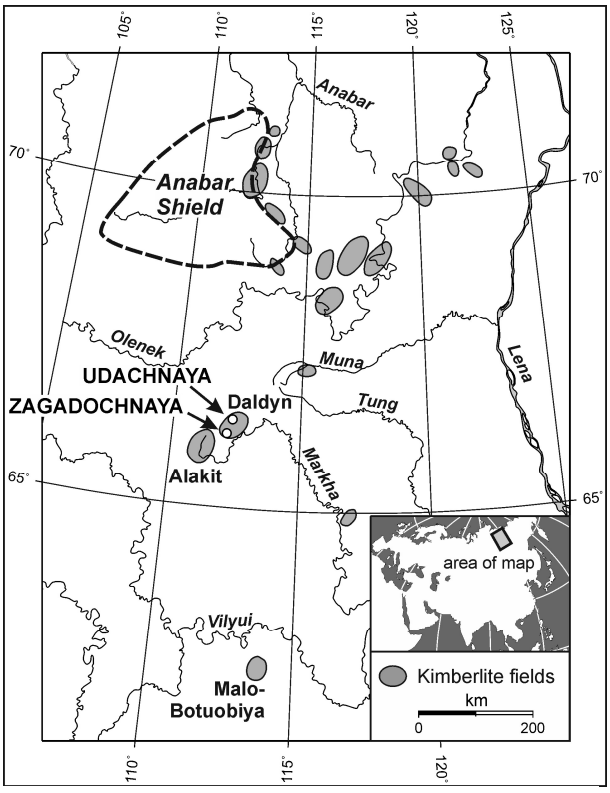

Fig.1: *Location of the Zagadochnaya kimberlite and of major Yakutian kimberlite fields (after Nimis et al., 2009)*

xenoliths have been found, probably owing to strong fragmentation of the xenoliths and extensive post-emplacement hydrothermal alteration (Sobolev, 1977; Nimis *et al.*, 2009).

Egorov *et al.* (1992) suggested that Zagadochnaya chromian diopsides crystallised from a kimberlitic melt. This hypothesis was based on the composition and appearance of the clinopyroxene grains, as well as on the absence of peridotitic xenoliths. Kostrovitsky & de Bruin (2004) proposed for the garnets an origin by magmatic segregation or by kimberlite metasomatism on pre-existing large garnet xenocrysts. More recently, Nimis *et al.* (2009) reported major and trace element compositions of sixty-one diopside xenocrysts and three diopside-bearing garnet xenocrysts. Based on geochemical data and limited petrographic evidence, they concluded that only a minor amount of chromian diopsides could represent direct magmatic segregates (their Group I), while the others (their Groups II and III) were fragments of variously metasomatized garnet peridotites or pyroxenites. Nimis *et al.* (2009) suggested that the low diamond potential of the Zagadochnaya kimberlite is a consequence of a shallow interval of mantle sampling and, possibly, of a strong metasomatic overprint on the sampled mantle section.

MATERIALS AND ANALYTICAL METHODS

We have selected 386 red-purple garnet grains (<0.6 cm) from heavy mineral concentrates of the Zagadochnaya kimberlite. The garnets were mounted on epoxy resin, cut to about half their thickness and polished. Preliminary major element analyses were performed using electron microprobes CAMEBAX-micro and JXA 8100 at standard conditions (e.g. Sobolev *et al.,* 2009a). Twenty-eight garnets from the same concentrate were then selected for a detailed petrographic and geochemical investigation.

The petrographic study was performed by using back-scattered electron images of the grains, which were obtained with a CamScan MX2500 scanning electron microscope (SEM), at the Department of Geosciences, University of Padua (Italy). The SEM was equipped with a tungsten cathode, a four-quadrant solid-state BSE detector and an EDX-EDAX system for qualitative microanalysis. The working distance was ~21 mm and the accelerating voltage was 20 kV.

Detailed major element analyses of the garnets and associated minerals were performed with a Cameca SX-50 electron microprobe (IGG-CNR, Padua, Italy), equipped with four wavelength-dispersive spectrometers. Natural and synthetic minerals (wollastonite for Ca and Si, albite for Na, orthoclase for K, and pure Al, Mg, Cr, Fe, and Mn–Ti oxides) were used as standards. Analytical conditions were a 20 kV accelerating voltage, a 20 nA beam current,

and a beam size of about 1 μm. Time counting was 10 s for peak and 5 s for background. X-ray counts were converted into weight percent oxides by using the CAMECA-PAP program. Estimated precision of the analysis are within ± 1–2 relative % for major and ± 2–5 relative % for minor oxides.

In-situ trace element analyses were carried out using Laser-Ablation Inductively-Coupled-Plasma Mass-Spectrometry (LA-ICP-MS) at IGG-CNR, Pavia (Italy). The laser probe consists of a Q-switched Nd:YAG laser, model Quantel (Brilliant), whose fundamental emission in the near-IR region (1064 nm) was converted into 266 nm wavelength using two harmonic generators. The spot diameter was typically 50 μm. The ablated material was analyzed using a double-focusing sector-field ICP-MS model Element I (ThermoFinnigan MAT), in which the standard field regulator power stage of the magnet and the ICP torch were upgraded to those of the Element II model. Helium was used as carrier gas and mixed with Ar downstream of the ablation cell. Data reduction was undertaken by means of the GLITTER software. NIST SRM 610 was used as external standard, whereas CaO has been used as internal standard for garnet, clinopyroxene, amphibole and calcite, SiO_2 for phlogopite and MgO for chromite. Precision and accuracy were assessed from repeated analyses of the BCR-2g standard and resulted usually better than 10% for concentration at ppm level. Detection limits were typically in the range of 10–100 ppb for Sc, Sr, Zr, Ba, Gd and Pb, 1–10 ppb for Y, Nb, La, Ce, Nd, Sm, Eu, Dy, Er, Yb, Hf and Ta, and usually <1 ppb for Pr, Th and U.

PETROGRAPHY

The garnet xenocrysts, purplish red in colour, are subround or subangular in shape and measure 2 to 6 mm across. Coatings of altered kimberlitic material (with calcite, phlogopite, apatite, serpentine, and minor perovskite) are common (Fig. 2d). Veinlets cutting thorough the garnet grains may be filled by the same fine-grained kimberlitic material, by an undefined silica-rich material, or by coarser phlogopite and/or amphibole associated with euhedral to sub-euhedral spinel. Many garnets contain subround, 0.2–1.0 mm-sized inclusions made of silica-rich material, serpentine (Fig. 2e) and/or calcite, which may represent alteration products after former olivine or orthopyroxene, caused by interaction with late-stage kimberlitic melts or fluids.

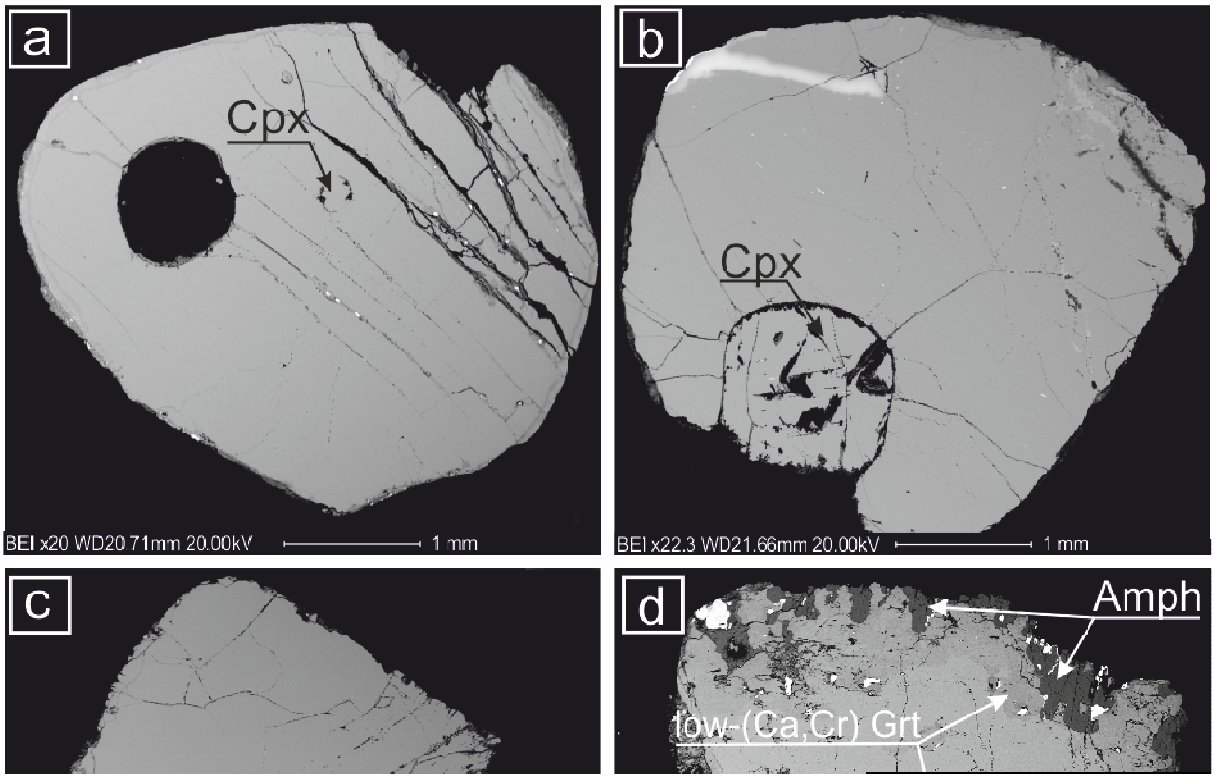
a
Cpx
BEI x20 WD20 71mm 20.00kV
1 mm
b
Cpx
BEI x22.3 WD21.66mm 20.00kV
1 mm
c
d
Amph
low-(Ca,Cr) Grt

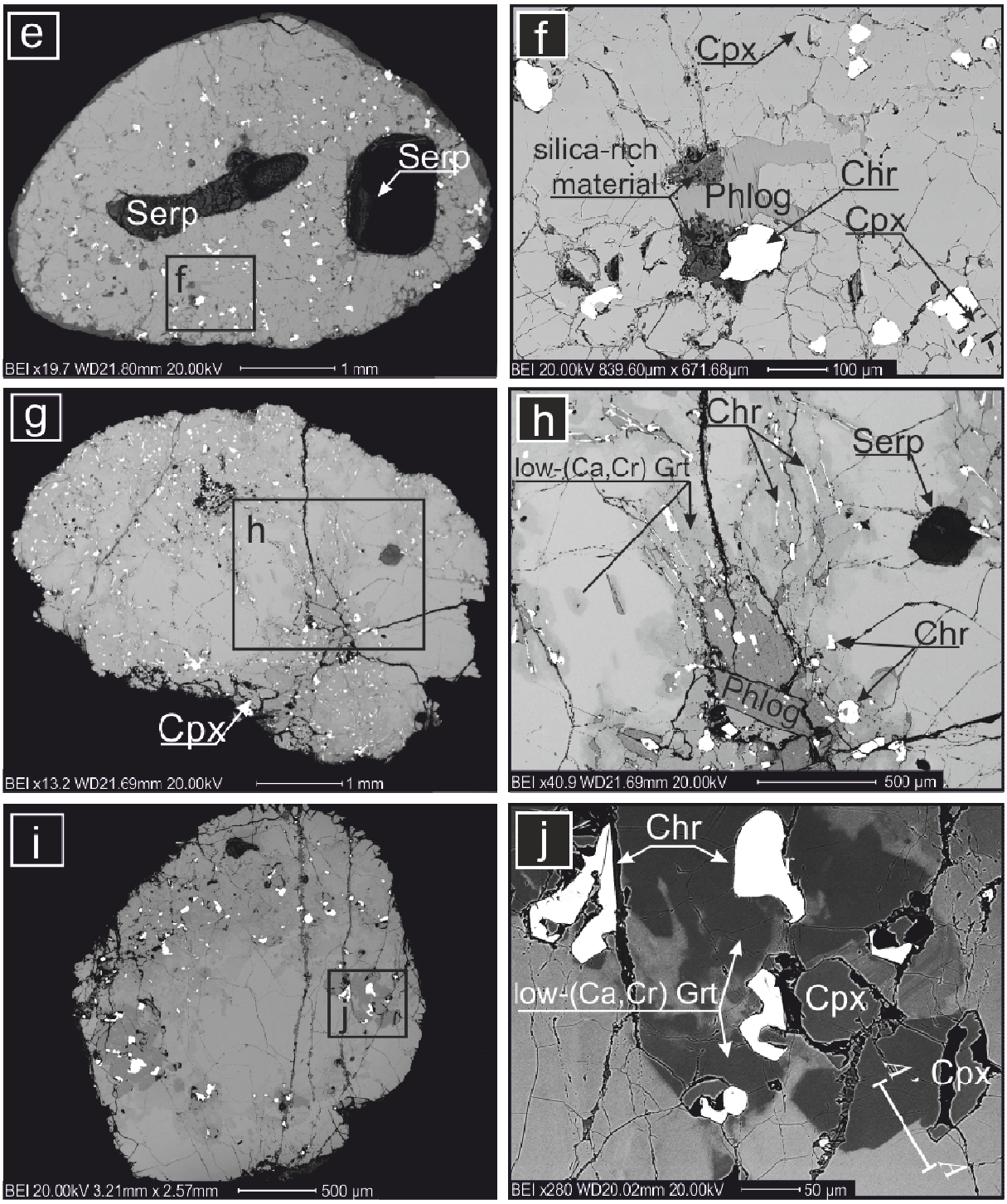

Fig. 2: *Continued.*

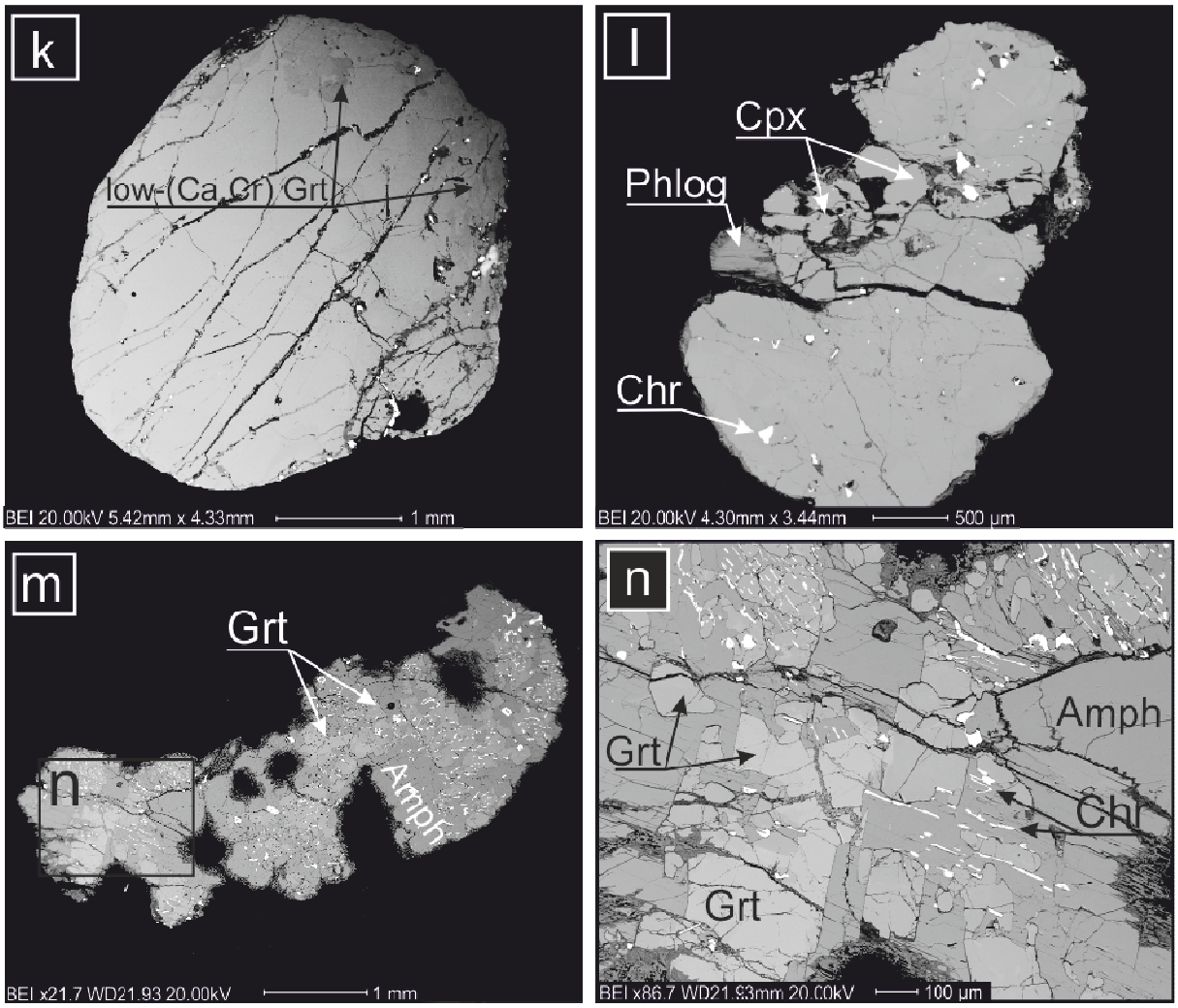

Fig. 2: *Continued.*

Some garnets are optically and compositionally homogeneous (Fig. 2a–c). These garnets are sometimes associated with homogeneous, subround chromian diopside grains (0.3–1.0 mm) and occasionally contain small (up to 50 µm) inclusions of rutile. Other garnets are optically strongly zoned, due to the presence of whitish-purple domains rich in polymineralic inclusions made of anhedral, often mutually intergrown, sub-millimetric grains of chromian diopside and chromite (± serpentine ± phlogopite ± amphibole) (Fig. 2d–l). These domains may also contain rare sub-elongated inclusions (<40 µm) of Ti-rich oxides of the crichtonite series. The composition of the garnets near the inclusion-rich domains is strongly inhomogeneous and shows irregular patches with distinctly low Ca and Cr contents, identified by darker areas in back-scattered electron images (e.g. Fig. 2d,h,j). Transition from high-(Ca, Cr) to low-(Ca, Cr) areas is generally sharp (Fig. 2h,j and Supplementary Fig. 1).

The distribution of the inclusion-rich domains in the garnet grains is variable. They are often located at the edges of the grains (Figs. 2d,i,k). In some cases they appear as bands

cutting through the host crystal, possibly following healed fractures within the garnet (Fig. 2d,g). In some samples (Z4-7, Z5-3, Z6-12), these domains apparently extend pervasively throughout the garnet grain (Fig. 2e,l). All of these features suggest a secondary origin of the low-(Ca, Cr) patches and of the associated inclusions.

One of the analysed garnet grains (Z4-11) showed unusual features. This grain consists of a polycrystalline amphibole–garnet intergrowth, containing oriented elongated, vermicular, and atoll-shaped chromite inclusions (Fig. 2m,n). The garnet shows (Ca, Cr)-zoning similar to the heterogeneous garnets described above, although it is devoid of diopside. Some of the low-(Ca, Cr) portions contain chromite inclusions with the same shape and orientation as those included in the adjacent amphibole, as well as remnants of high-(Ca, Cr) garnet showing cusp-and-caries outlines (Fig. 2m,n).

MAJOR AND TRACE ELEMENT COMPOSITIONS

Major element analyses for the complete dataset of 386 garnet grains are reported in Supplementary Table 1. All garnets classify as chromian pyropes, with Cr_2O_3 contents between 0.5 and 9.3 wt% and CaO contents between 3.2 and 10.3 wt%. TiO_2 is generally low (0.0–0.4 wt%) and the mg# values are quite variable (62.8–84.9), although 97% of the garnets lie in the range 78.0–84.9. In the CaO vs. Cr_2O_3 discrimination diagram (Sobolev *et al.*, 1969, 1973; Sobolev, 1971), most garnets plot within or very close to the lherzolitic field and show a positive correlation between these elements (Fig. 3). A small fraction of the garnets plots in the high-Ca wehrlitic field (e.g. Sobolev *et al.,* 1970), and an even smaller fraction falls into a transitional region between the lherzolitic and harzburgitic fields. Major and trace element data for garnets and associated minerals from the 28 selected grains are given in the Supplementary Table 2. Based on petrographic and geochemical features, these selected grains have been subdivided into three main groups.

Group A garnets

Group A garnets are compositionally homogeneous and are sometimes associated with subround chromian diopside (e.g. Fig. 2a,b). Major element concentration profiles (Supplementary Fig. 2) across garnet–diopside boundaries show no chemical zoning in either mineral. The main geochemical features are moderate Cr_2O_3 (1.3–5.2 wt%) and CaO (4.3–5.0 wt%) contents (Fig. 3) and CI-normalized REE patterns (cf. Anders & Grevesse, 1989) showing increasing values from La (0.03–0.07 xCI) to Lu (7.9–29 xCI), with a steeper slope from La to Sm and a flatter profile from Sm to Lu (La_{CI}/Sm_{CI} = 0.01–0.02; Sm_{CI}/Lu_{CI} = 0.08–

0.46) (Fig. 4a). The HREE show significant grain-to-grain variability (Yb = 8.1–24.9 xCI). TiO_2 contents are low (0.12–0.32 wt%) and mg# varies from 80.4 to 81.6. Primitive Mantle (PM)-normalized trace element patterns (cf. McDonough & Sun, 1995) show low abundances of highly incompatible elements, usually at 0.01–0.2 xPM, with Ba, Ta and Pb content often below the detection limits (Fig. 4b). However, U, and randomly Pb, show a positive anomaly up to 1.0 xPM. Zr and Hf show positive anomalies (Zr_{PM}/Nd_{PM} = 3.6–9.2), with the Zr_{PM}/Hf_{PM} ratio varying between 0.8 and 1.9. A pronounced negative Sr anomaly (Sr_{PM}/Sr^* = 0.02–0.05, where $Sr^* = (Pr_{PM}+Nd_{PM})/2$) and a minor negative Ti anomaly (Ti/Ti^* = 0.33–0.63, where $Ti^* = (Eu_{PM}/Gd_{PM})/2$) are present in all Group A garnets.

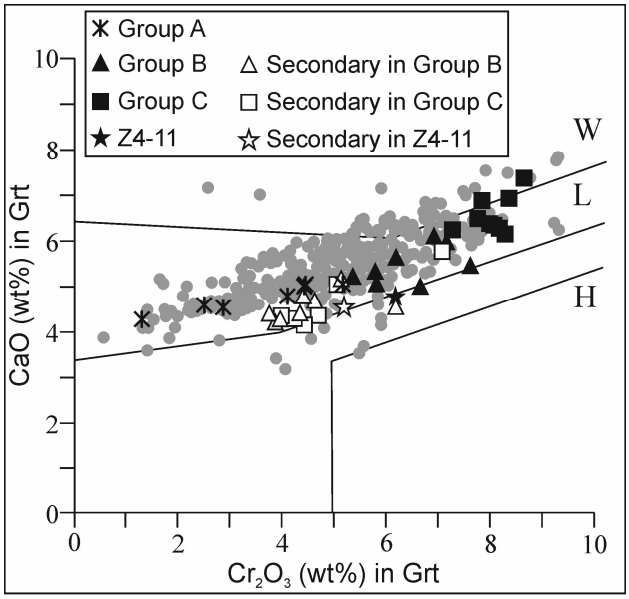

Fig. 3: *CaO vs. Cr_2O_3 discrimination diagram (Sobolev, 1971) for Zagadochnaya garnets. Grey circles: garnets from Zagadochnaya kimberlite concentrate. Other symbols: garnets analyzed by LAM–ICP–MS. H, harzburgite; L, lherzolite; W, wehrlite.*

Group B garnets

Group B comprises one subangular and unzoned garnet (Z5-6; Fig. 2c) and inclusion-free domains in some heterogeneous garnets (e.g. Fig. 2d,k). Group B garnets are distinguished from Group A by their higher Cr_2O_3 (5.4–7.6 wt%) and CaO (5.1–6.1 wt%) contents, higher LREE contents (La = 0.03–0.07 xCI, Sm = 2.37–4.54 xCI), and nearly flat REE patterns from Sm to Lu (Sm_{CI}/Lu_{CI} = 0.5–1.0; Lu = 7.86–29.2 xCI; Fig. 5). The mg# values vary over a restricted range (80.2–81.1), except for the unzoned garnet Z5-6, which has an mg# of 83.8. Group B garnets are also distinguished from Group A by their higher contents and larger grain-to-grain variations of highly incompatible elements (Fig. 5). Positive U anomalies are present. Unlike Group A, Pb is always above the detection limits and shows both positive and negative anomalies. Higher LREE abundances are not accompanied by significant variation in Zr and Hf concentrations with respect to Group A garnets, resulting in lower (Zr, Hf)/LREE ratios (Zr_{PM}/Nd_{PM} = 0.4–3.9 vs. 3.6–9.2). Negative anomalies of Ti (Ti/Ti^* = 0.26–0.68) and Sr (Sr/Sr^* = 0.01–0.02) are similar and slightly more pronounced, respectively, than in Group A.

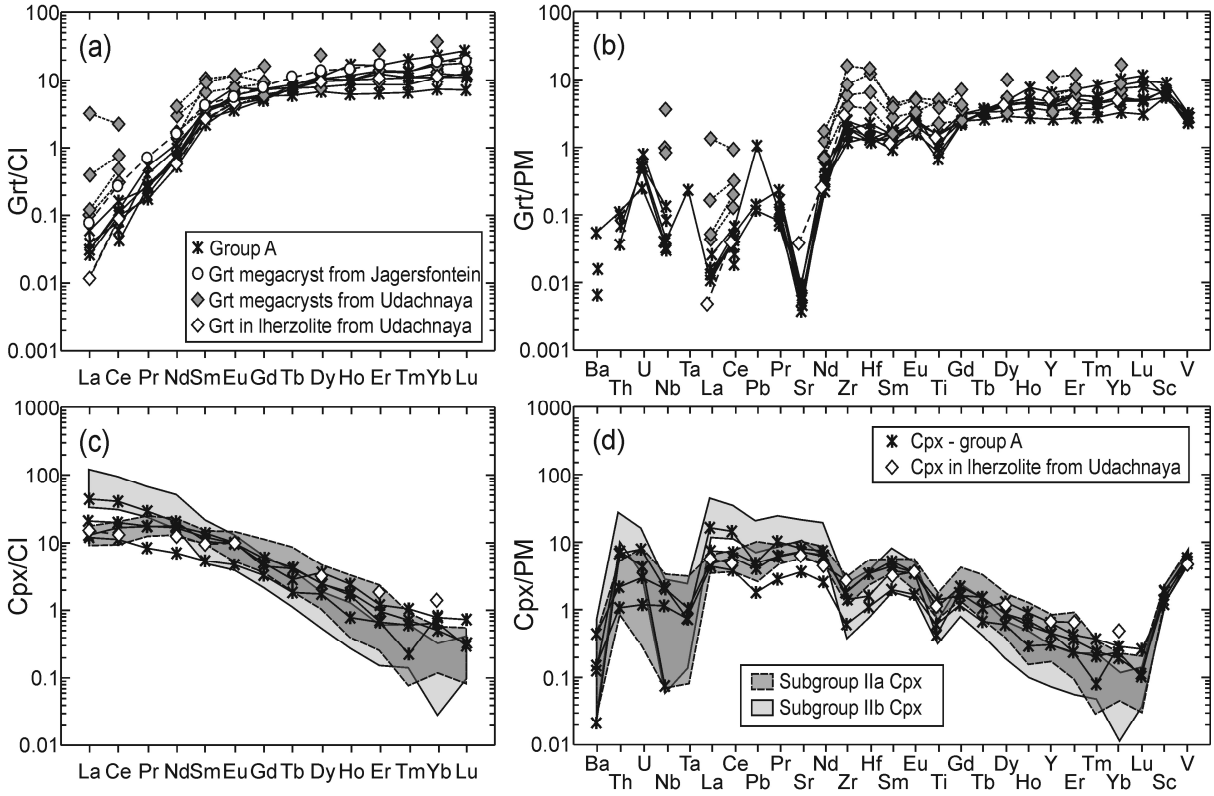

Fig. 4: *CI-normalized (Anders & Grevesse, 1989) REE patterns and PM-normalized (McDonough & Sun, 1995) extended trace element patterns for* ***(a) (b)*** *Group A garnets and* ***(c) (d)*** *associated clinopyroxenes from the Zagadochnaya kimberlite. Subgroup IIa and IIb clinopyroxenes (grey fields) are from the same kimberlite (Nimis et al., 2009). The data of garnet and clinopyroxene in lherzolite from Udachnaya (sample 417/89) are from Shimizu et al. (1997). Other data are from Burgess & Harte (2004), and Solov'eva et al. (2008).*

Group C garnets

Group C comprises inclusion-free domains in some of the heterogeneous garnets (e.g. Fig. 2g,i). Distinctive features of this group are the high contents of Cr_2O_3 (7.3–8.6 wt%) and CaO (6.2–7.4 wt%), and the humped to sinusoidal CI-normalized REE patterns (Fig. 6). The mg# values (80.3–81.7) are similar to Group A and Group B, except for the slightly more ferroan garnets Z4-4 (mg# = 78.7) and Z5-14 (mg# = 79.0). Almost all Group C garnets have CI-normalized profiles enriched in L-MREE, with a maximum at Sm (at Eu for garnets Z4-1 and Z6-11), and depleted in HREE, with minimum at Er–Tm (at Tb for Z5-14). The most strongly sinusoidal pattern is displayed by garnet Z4-4, which is extremely depleted in HREE (minimum at Tm = 0.21 xCI). Samples Z5-14, Z6-9 and Z6-10 are distinguished by their higher La_{CI}/Sm_{CI} ratios (0.06–0.08) and flatter patterns from Sm to Tm (Sm_{CI}/Tm_{CI} = 2.0–2.8). Negative Sr and Ti anomalies and Zr/LREE ratios are similar to Group B garnets, but Zr_{PM}/Hf_{PM} ratios are slighly higher and more variable (0.96–2.04 vs. 0.98–1.27). The concentrations of trace elements more incompatible than La are similar to those of Group B.

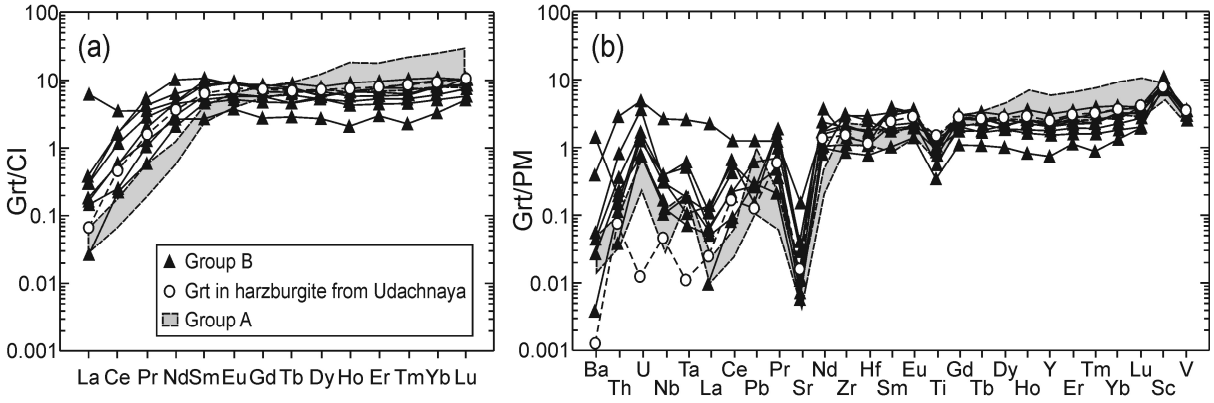

Fig. 6: (a) *CI-normalized REE patterns and* ***(b)*** *PM-normalized extended trace element patterns for Group B garnets. Field of Group A garnets is shown for comparison. The data of garnet in harzburgite from Udachnaya (sample U501) are from Ionov et al. (2010).*

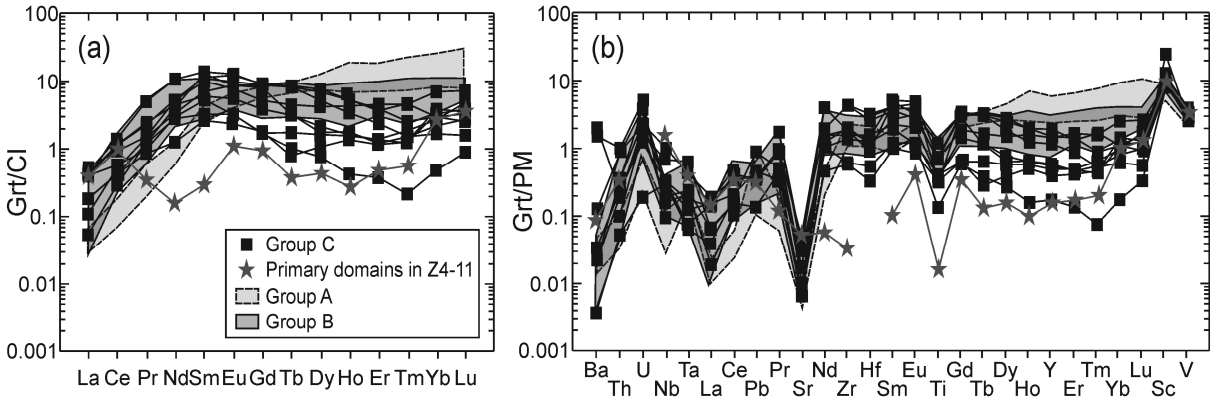

Fig. 6. (a) *CI-normalized REE patterns and* ***(b)*** *PM-normalized extended trace element patterns for Group C garnets and high-(Ca, Cr) garnet in the peculiar garnet–amphibole intergrowth Z4-11. Fields of Group A and B garnets are shown for comparison.*

Secondary garnet domains

Secondary domains are present in both Group B and Group C garnets. Their most evident feature is the significantly lower Cr_2O_3 (3.7–7.1 wt%) and CaO (4.2–5.8 wt%) contents and higher mg# values (80.4–83.28) with respect to the host primary garnets. Major element profiles across garnet zoning are step-like to S-shaped (e.g. Supplementary Fig. 1). These low-(Ca, Cr) domains are enriched in almost all trace elements. In most cases, the CI-normalized REE patterns are humped, with maximum at Eu (Fig. 7a). In two cases (Z5-3 and Z6-12), the secondary domains show progressively increasing CI-normalized REE values from Sm (20.6–21.2 x CI) to Lu (64.3–44.3 xCI). In general, grain-to-grain variation are relatively small for the LREE (Nd = 6.1–15.8 xCI), but high for the HREE (Nd_{CI}/Yb_{CI} = 0.1–2.0; Fig. 7a). With respect to the host primary garnets, Hf and Sc show minor variations, whereas Ti and V are systematically lower. As a consequence, PM-normalized trace element patterns show stronger, negative Ti anomalies (Ti/Ti* = 0.01–0.14 vs. 0.08–0.68), higher

Zr_{PM}/Hf_{PM} ratios (1.82–7.76 vs. 0.96–2.04) and slightly higher Sc_{PM}/V_{PM} ratios (2.91–6.71 vs 2.16–4.26; Fig. 7b).

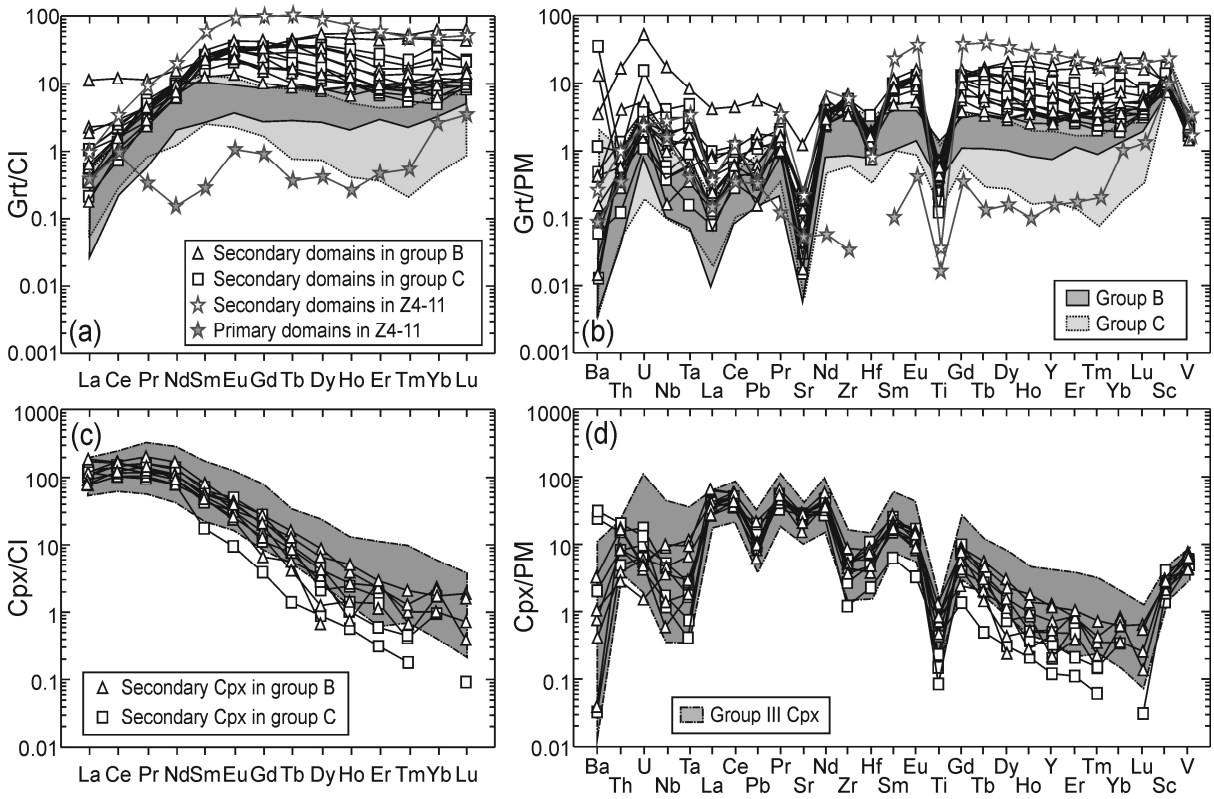

Fig. 7. *CI-normalized REE patterns and PM-normalized extended trace element patterns for* ***(a) (b)*** *secondary garnet domains and* ***(c) (d)*** *associated secondary clinopyroxenes. In* ***(a)*** *and* ***(b)*** *field of primary garnets of Group B and Group C are shown for comparison. In* ***(c)*** *and* ***(d)*** *the field of group III clinopyroxene from the same kimberlite (Nimis et al., 2009) is also reported.*

Amphibole-garnet intergrowth

The high-(Ca, Cr), *primary* garnet domains in grain Z4-11 have Cr_2O_3 contents similar to Group B garnets, but are slightly less calcic, straddling the boundary between the lherzolite field and the transitional field towards harzburgitic garnet compositions (Fig. 3). The CI-normalized REE patterns are unlike any of the other studied garnets, with very low MREE and three maxima at Ce, Eu and Lu (Fig. 6). The low-(Ca, Cr), *secondary* garnet domains show similar major and trace element composition to secondary domains in Group B and Group C garnets, but with stronger enrichment in MREE (Sm to Er), deeper negative Ti anomalies, and higher Sc_{PM}/V_{PM} ratios (Fig. 7).

Other minerals

Clinopyroxene

The *primary*, subround clinopyroxenes associated with Group A garnets (e.g. Fig. 2a,b) are compositionally homogeneous chromian diopsides with 2 to 8 mol% kosmochlor component and 9 to 12 mol% jadeite component (Supplementary Table 2). They are TiO_2-poor (<0.35 wt%) and have mg# values ranging from 92.6 to 94.0. The CI-normalized REE abundances progressively decrease from La (20.5–42.8 xCI) to Lu (0.29–0.71 xCI) (Fig. 4c). PM-normalized spidergrams show negative anomalies for the High Field Strength Elements (HFSE; i.e., Nb, Ta, Zr, Hf, and Ti) and Pb (Fig. 4d).

The *secondary* chromian diopside inclusions associated with the low-(Ca, Cr) garnet domains are enriched in kosmochlor component (7.0–13.8 mol%) and LREE, and show more variable jadeite contents (8–18 mol%) and mg# values (90.2–94.1) (Supplementary Table 2). Similarly to the associated garnets, grain-to-grain variations are small for the LREE (e.g. Nd = 79–171 xCI), but high for the MREE and HREE (Nd_{CI}/Yb_{CI} = 35–149; Fig. 7). PM-normalized trace element patterns show stronger Pb, Sr, and Zr–Hf negative anomalies and much stronger Ti negative anomalies than the primary clinopyroxenes (Fig. 7d). No major difference is observed between inclusions in Group B and those in Group C garnets, except for lower Nb_N/Ta_N ratios (0.8–1.2 vs. 1.9–2.9) and more pronounced negative Sr anomalies (0.40–0.78 vs. 0.50–0.91) in the former.

Amphibole

Amphiboles intergrown with garnet are present only in some Group B grains (Z4-3 and Z5-5) and in the peculiar grain Z4-11 (e.g. Fig. 2d,m,n). They are sodic-calcic amphiboles (magnesiokataphorites; Hawthorne & Oberti, 2007) with Na_2O contents of 4.6 to 5.4 wt%, Cr_2O_3 contents of 1.9 to 3.1 wt%, and Al_2O_3 contents of 7.9 to 9.4 wt%. Amphibole in the anomalous sample Z4-11 shows slightly lower contents of K_2O (0.97 vs. 1.4–1.5 wt%) and TiO_2 (0.04 vs. 0.20–0.26 wt%). PM-normalized trace element patterns for all analysed amphiboles are very similar to those of the secondary diopsides, except for the slightly less fractionated REE profiles and the expected (cf. Raffone *et al.*, 2009) positive Nb–Ta anomaly (Fig. 8b). Amphiboles in the late veinlets cutting the garnets are calcic amphiboles (pargasites; Hawthorne & Oberti, 2007). They are enriched in Al_2O_3 (11.3–16.9 wt%), have more variable Cr_2O_3 contents (1.8–4.9 wt%), and show lower Na_2O (1.1–3.8 wt%) and K_2O (0.28–0.38 wt%) contents. No trace element data are available for these amphiboles.

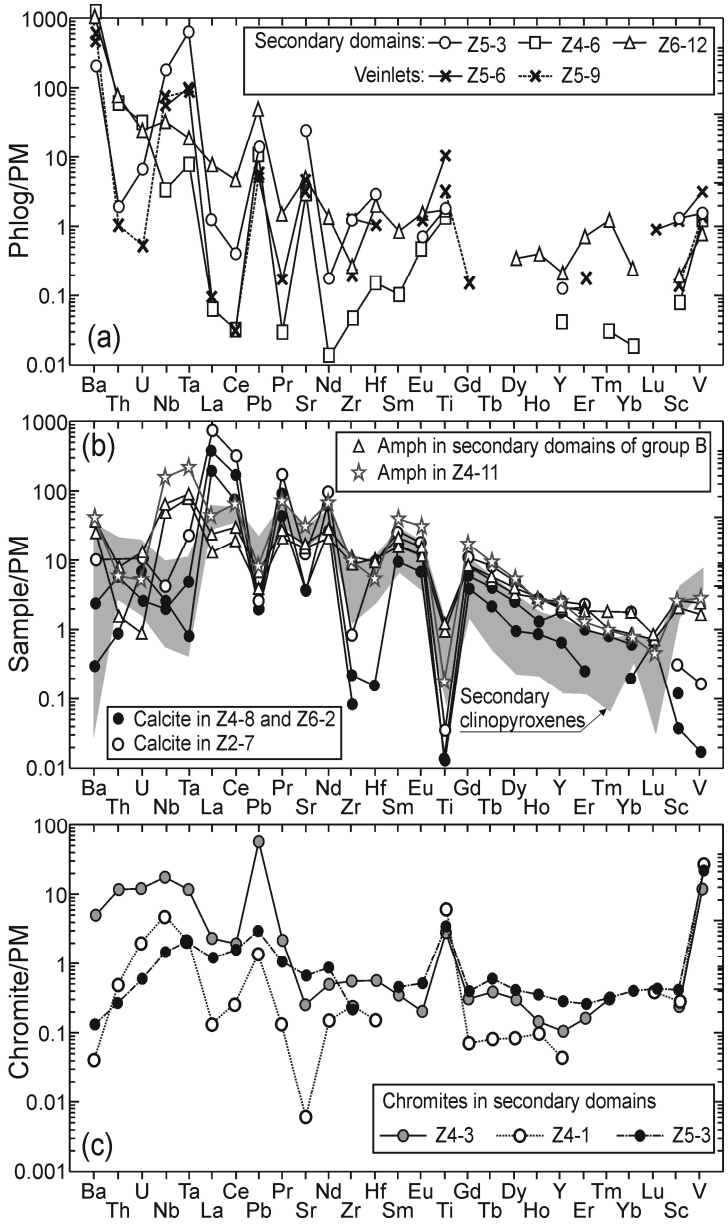

Fig. 8: *PM-normalized extended trace element patterns in representative* ***(a)*** *phlogopites,* ***(b)*** *amphiboles and calcites, and* ***(c)*** *chromites.*

Phlogopite

Phlogopites associated with low-(Ca, Cr) garnet domains (e.g. Fig. 2f,h) are unzoned and have low TiO_2 contents (0.07–0.90 wt%) and relatively high Cr_2O_3 contents (0.40–1.25 wt%) (Supplementary Table 2). Only minor variations are observed for Al_2O_3 contents (12.5–13.5 wt%) and mg# values (90.5–94.5). Ni, Rb and Ba abundances are high, while REE concentrations are low and frequently below detection limits. Phlogopites occurring within veinlets cutting the garnets and those associated with low-(Ca, Cr) garnet domains generally show similar major and trace element compositions (Fig. 8a and Supplementary Table 2). Note that some of these phlogopites contain up to 0.5 wt.% Cl, which is consistent with the

elevated Cl abundance in the unaltered Udachnaya East kimberlite (e.g. Kamenetsky *et al.*, 2004; Maas *et al.,* 2005). Phlogopite in veinlets cutting garnet Z5-6 has distinctly higher TiO_2 (2.62 wt%) and Cr_2O_3 (2.52 wt%) contents, and is similar in its composition with some lherzolitic phlogopite inclusions from diamonds (Sobolev *et al*., 2009a).

Chromian spinels

Spinel inclusions associated with secondary low-(Ca, Cr) garnet domains are chromites with Cr/(Cr+Al) molar ratios (Cr#) of 78.5 to 82.0 and mg# values of 45.2 to 48.9. TiO_2 content varies between 0.2 and 1.2 wt%, higher than in typical mantle spinels (TiO_2 < 0.5 wt%; Pearson *et al.*, 2003). We have analyzed the trace element abundances of chromites from five samples (Supplementary Table 2). Except for Ti, the HFSE and REE contents show grain-to-grain variations of up to one order of magnitude. Hf and the M-HREE are often near or below detection limits. Distinctive features of all the analysed chromites are the positive Pb and Ti anomalies and an almost constant Sc_{PM}/V_{PM} ratio (0.004–0.020; Fig. 8c). Zn contents vary between 1120 and 1484 ppm, while Ni varies between 714 and 1017 ppm.

Spinels in veinlets cutting the garnets have lower Cr# (21.7–64.8), higher mg# (44.9–73.1) and similar TiO_2 content (0.2–1.5 wt%) to those in the secondary domains. They are often zoned, showing a core-to-rim decrease in Cr# and increase in mg#, typical of groundmass spinels in kimberlites (c.f. Roeder & Schulze, 2008).

Ti-rich oxides

One sub-elongated Ti-oxide grain in a secondary domain of garnet Z4-1 was analysed by electron microprobe. It is Cr-rich (Cr_2O_3 = 20.8 wt%) and contains considerable amounts of Sr, Zr, La and Ce (Supplementary Table 2), suggesting a relationship with crichtonite-series minerals (cf. Haggerty *et al.*, 1983; Erlank *et al.*, 1987; Kalfoun *et al*., 2002), which are sometimes present as inclusions in Siberian diamonds (Sobolev *et al.,* 1997).

Carbonate

Carbonate filling an inclusion in grain Z4-8 and found in association with serpentine filling an inclusion in sample Z6-2 is nearly pure calcite. The trace element contents are similar to a calcite included in one of the diopside grains from the same kimberlite studied by Nimis *et al.* (2009) (Fig. 8b). With respect to secondary clinopyroxenes, all calcites are enriched in LREE, have lower Sc and V, and show much deeper Sr, Ti and Zr–Hf negative anomalies. The L-MREE contents are higher than in calcite-dolomite cumulates from primary carbonatites, and approach the high concentrations found in interstitial grains segregated from evolved carbonatite liquids (Ionov & Harmer, 2002). The compositional and textural features suggest

that all these calcites represent alteration products derived by late interaction of former mantle minerals with kimberlite-related hydrothermal fluids.

ORIGIN OF THE XENOCRYSTS

Primary garnets and associated clinopyroxenes

CaO vs. Cr_2O_3 relationships in the studied garnets are similar to those of garnets from lherzolitic xenoliths, indicating an origin from ultramafic rocks that were saturated or nearly saturated in calcic clinopyroxene (Sobolev *et al.*, 1973; Schulze, 2003; Grütter *et al.*, 2004; Fig. 3). Discrimination between an origin from lherzolites, Ca-rich harzburgites, pyroxenites, or kimberlite-segregated megacrysts is not straightforward on a major-element basis, as garnets from different protolith types may show significant compositional overlaps. In the compilations of worldwide garnet compositions of Schulze (2003) and Grütter *et al.* (2004), garnet megacrysts with Cr_2O_3 contents as high as 6.0 wt% (interpreted as high-pressure segregates from kimberlite-related melts or asthenospheric melts lato sensu; e.g. Dawson, 1980; Burgess & Harte, 2004; Moore & Belousova, 2005) generally have TiO_2 contents higher than 0.5 wt% and only rarely as low as 0.30 wt%. Based on the low TiO_2 contents of the garnets studied here (av. 0.17 wt%; range 0.04–0.35 wt%), a megacryst-like origin is unlikely for the Zagadochnaya garnets. Garnets with "lherzolitic" Cr_2O_3 vs. CaO relationships also occur in several pyroxenitic xenoliths (e.g. Roden *et al.*, 1999; Kopylova *et al.*, 1999; Pokhilenko *et al.*, 1999; Agashev *et al.*, 2001; Aulbach *et al.*, 2007), although Cr_2O_3 contents in these pyroxenitic garnets never exceed 5.2 wt%. Therefore, based on the major element compositions of the garnets studied here, a peridotitic origin is the most likely for both Group B and Group C garnets (Cr_2O_3 = 5.4–8.6 wt%), whereas Group A garnets (Cr_2O_3 = 1.3–5.2 wt%) are compatible with both a peridotitic or pyroxenitic origin. Further evidence in support of this conclusion and more specific information on the origin of the garnets are provided by trace element data.

Group A garnets show CI-normalized REE patterns characterized by depleted and fractionated LREE, and flattened to slightly sloped HREE (Fig. 4a), similar to those of many fertile lherzolitic garnets from both off- and on-craton settings (e.g. Griffin *et al.*, 2002; Pearson *et al.*, 2003). The REE patterns also broadly resemble those of some megacrysts from the Kaapvaal craton (cf. Burgess & Harte, 2004), but are more LREE-depleted (La = 0.03–0.07 vs. 0.06–0.5 xCI) than garnet megacrysts from Yakutian kimberlites and HFSE-depleted relative to megacrysts from Udachnaya (cf. Kostrovitsky *et al.*, 2008; Solov'eva *et al.*, 2008;

Fig. 4a). Moreover, in spite of their appreciable REE variability (e.g. Yb from 8 to 25 xCI), Group A garnets do not show the negative correlation between REE contents and mg# that was observed by Solov'eva *et al.* (2008) for megacrysts from Udachnaya, as well as by Kostrovitsky *et al.* (2008) for megacrysts from various Yakutian kimberlites.

Primary chromian diopsides associated with Group A garnets have major and trace element contents very similar to those of some diopside grains reported by Nimis *et al.* (2009) from the same kimberlite (Fig. 4c,d). In particular, they show an intermediate character between subgroup IIa and subgroup IIb diopsides of Nimis *et al.* (2009). Consistently, these authors did report several diopside grains with intermediate IIa–IIb compositions. They interpreted these diopsides as fragments of variably refractory peridotites that were metasomatised by kimberlitic melts with low LREE/(Zr, Hf) ratios, i.e., distinct from the host Zagadochnaya kimberlite (cf. Kostrovitsky *et al.*, 2007). They also found similarities between some of these diopsides and the most REE-enriched diopsides from Udachnaya coarse-grained garnet peridotites (cf. Shimizu *et al.*, 1997a), suggesting a common origin. Indeed, Group A garnets show very similar compositions to those of a coarse-grained, equigranular lherzolite of Shimizu *et al.* (1997a) (sample 417/89; Fig. 4a,b). Based on these considerations, we conclude that our Group A garnets and the intermediate IIa–IIb diopsides of Nimis *et al.* (2009) represent fragments of the same metasomatised (refertilised), lherzolitic protoliths, which are represented in both Zagadochnaya and Udachnaya upper mantle sections.

Only two garnets with *Group B* geochemical affinity were already reported from Zagadochnaya (cf. samples Z2-11 and Z3-21 of Nimis *et al.*, 2009). The flattened REE patterns from Nd–Sm to Lu (Fig. 5a) are common in lherzolitic garnets (e.g. Hoal *et al.*, 1994; Shimizu *et al.*, 1997a; Stachel *et al.*, 1998; Burgess & Harte, 2004; Ionov *et al.*, 2010). The most LREE-depleted Group B garnets show major and trace element similarities with a garnet from one clinopyroxene-bearing, granular garnet harzburgite from the nearby Udachnaya kimberlite (cf. sample U501 of Ionov *et al.*, 2010), but show higher concentrations of U, Nb and Ta (Fig. 5b).

With respect to Group A, Group B garnets are poorer in moderately incompatible elements (e.g. HREE and Ti) and richer in both compatible (e.g. Cr) and highly incompatible elements (LILE, LREE, Nb, Ta, Th and U; Fig. 5a, b). Group B garnets also show slightly stronger Ti negative anomalies and lower Zr–Hf contents relative to neighbouring REE (cf. Fig. 5b). A similar behaviour is shown by subgroup IIb diopsides with respect to subgroup IIa diopsides of Nimis *et al.* (2009) (Fig. 4c, d). These observations suggest that Group B garnets

belonged to the same Ca-rich (i.e., clinopyroxene-bearing) harzburgitic or lherzolitic protoliths of subgroup IIb diopsides.

Group C garnets show humped to sinusoidal CI-normalized REE patterns, which have never been reported in garnets from pyroxenites or garnet megacrysts (c.f. Kopylova *et al.*, 2009; Pokhilenko *et al.*, 1999; Burgess & Harte, 2004; Aulbach *et al.*, 2007; Kostrovitsky *et al.*, 2007), but are commonly observed in garnets from cratonic harzburgites and depleted lherzolites (e.g. Nixon *et al.*, 1987; Hoal *et al.*, 1994; Shimizu *et al.*, 1997a; Pearson *et al.*, 2003; Gibson *et al.*, 2008). No similar garnet has been previously reported from Zagadochnaya (cf. Kostrovitsky & de Bruin, 2004; Nimis *et al.*, 2009). No clinopyroxene has been found in association with Group C garnets and no clinopyroxene grains among those studied by Nimis *et al.* (2009) show trace element compositions compatible with equilibrium with such garnets. Nonetheless, the "lherzolitic" to even "wehrlitic" composition of the garnets (Fig. 3) still suggests an origin from clinopyroxene-saturated rocks. Indeed, the least HREE-depleted garnets of this group show REE patterns and CaO and Cr_2O_3 contents similar to some garnets from granular or fine-porphyroclastic harzburgites *and* lherzolites from Udachnaya (Shimizu *et al.*, 1997a; Solov'eva *et al.*, 2008, Ionov *et al.*, 2010) and from other kimberlites (e.g. Jagersfontein, South Africa; Burgess & Harte, 2004). We therefore conclude that Group C garnets derived from relatively depleted, moderately metasomatised peridotites, which contained only scarse and/or small clinopyroxene grains that were not recovered in the heavy mineral concentrates (1–3 mm size fraction) studied by Nimis *et al.* (2009).

Secondary garnets and associated inclusions

Inclusion-rich, low-(Ca, Cr) domains in Group B and Group C garnets show textural and chemical features that, in the Daldyn field, seem to be peculiar to samples from high-Mg, micaceous kimberlites (i.e., Zagadochnaya, Bukovinskaya, Gonyatskaya, and Kusov; Kostrovitsky & de Bruin, 2004). Nimis *et al.* (2009) already reported such inclusion-rich domains in three garnets from the Zagadochnaya kimberlite (samples Z2-11, Z3-11 and Z3-21) and, based on the geochemical affinity with their Group III diopside xenocrysts, suggested an origin by melt metasomatism related to the host kimberlite. The diopside inclusions in our secondary garnets show a clear geochemical affinity with Group III diopside xenocrysts of Nimis *et al.* (2009) (e.g. Fig. 7b), although the former are slightly more HREE-depleted, probably owing to preferred partitioning of such elements in the much bigger host garnet.

Replacement of mantle-derived garnets by chromite + Cr-diopside (± phlogopite ± orthopyroxene ± Ti-oxide) has already been reported in other kimberlites of the Kaapvaal and Siberian cratons (Erlank *et al.*, 1987; Solovjeva *et al*., 1997; Simon *et al.*, 2003; Kostrovitsky & de Bruin, 2004; Solov'eva *et al.*, 2010; Ivanic *et al.*, 2012), but chemical zoning in the associated garnet was not generally described. To our knowledge, the most similar reported analogues are the garnet-rich peridotitic microxenoliths from Newlands and Bobbejaan kimberlites (Kaapvaal Craton), studied by Ivanic *et al.* (2012). These authors report re-crystallisation of originally high-Cr garnets into an assemblage of low-(Ca, Cr) garnet, Cr-spinel, Cr-diopside and orthopyroxene (altered to serpentine), but with neither phlogopite nor amphibole. Based on the preferred crystallographic orientation of some inclusions, *P–T* estimates, and compositional zonation trends in the garnet, Ivanic *et al.* (2012) interpreted these intergrowths as products of solid-state reactions during a decompression event.

In our case, the presence of phlogopite, amphibole, and kosmochlor-rich diopside, the overall enrichment in both moderately and strongly incompatible trace elements, the distinct patchy Ca–Cr zoning in the garnets, and the distribution of these secondary products at the garnet rims or along healed fractures (cf. Matthews *et al.*, 1992) rather suggest formation by reactions with a percolating melt. The decrease in Ca and Cr in the secondary garnets would reflect the preferential re-distribution of these elements in secondary chromian diopsides and chromites during garnet–melt reactions. The relatively abrupt compositional zoning and frequent cusp-and-caries features (Fig. 2h,j) suggest formation of the low-(Ca, Cr) garnet by dissolution–precipitation rather than by diffusion (cf. Putnis, 2009).

The occasional presence of crichtonite series minerals in the secondary garnet domains is further evidence of metasomatism. These minerals are important reservoirs for LILE, LREE and HFSE (e.g. Erlank and Rickard, 1977; Haggerty *et al.*, 1983; Konzett *et al.*, 2005) to pressures extending into the stability field of diamond (e.g. Sobolev *et al.*, 1997), and are typically found in association with phlogopite and/or amphibole in peridotite xenoliths that show the most advanced degrees of metasomatism (e.g. Erlank and Rickard, 1977; Haggerty, 1983; Erlank *et al.*, 1987; Wang *et al.*, 1999; Grégoire *et al.*, 2000; Kalfoun *et al.*, 2002; Rivalenti *et al.*, 2004; Konzett *et al.*, 2005).

Amphibole-garnet intergrowth

The unusual texture and peculiar composition of the primary garnet in grain Z4-11 (Figs. 2m,n and 6) must be the result of complex processes. Very LREE- and MREE-depleted garnets similar to the primary garnet Z4-11 were already found in some clinopyroxene-

bearing granular peridotites from Udachnaya (Shimizu *et al.*, 1997a; Solov'eva, 2007; Ionov *et al.*, 2010). The extremely low REE contents were tentatively interpreted as a result of modification by reduced asthenospheric fluids related to the Middle Palaeozoic kimberlite event (Solov'eva, 2007) or as the closest approach to an unmetasomatised lithospheric mantle (Shimizu *et al.*, 1997a). In agreement with the hypothesis of Shimizu *et al.* (1997a), we suggest that the small maxima at Eu and Lu might reflect the development of an incipient, mildly sinusoidal REE profile. The degree of metasomatic enrichment and refertilisation at this stage was lower than in the more Ca-rich Group C garnets (Figs. 3 and 6).

Later metasomatic reactions produced an intergrowth of amphibole and low-(Ca, Cr) garnet, which partially replaced the original garnet (Figs. 2m,n). Considering the strict geochemical affinities, the metasomatic agent was cognate to the melts that produced the secondary domains in Group B and Group C garnets (Figs. 7a, b and 8b). Remnants of the primary garnets only partially re-equilibrated during this metasomatic stage and were selectively enriched in the most incompatible elements (Ba to Ce; Fig. 7b).

The significance of the oriented spinel grains (Fig. 2n) is uncertain. Similar spinels do occur in some secondary garnet domains in other grains (Fig. 2h), so they are probably related to the same late metasomatic event. Indeed, the observed textures resemble those found in some amphibole + spinel symplectites from South African peridotites (Field, 2008), which were interpreted as a result of metasomatic replacement of pre-existing clinopyroxene + spinel or clinopyroxene + orthopyroxene + spinel symplectites. We therefore speculate that their orientation was inherited from an intergrowth with an early (metasomatic?) mineral of uncertain nature (pyroxene?), which was completely replaced by the secondary garnet during a more advanced metasomatic stage.

GEOTHERMOBAROMETRY

Given the assumption that the garnets belonging to groups A, B and C coexisted with former olivine (i.e., they were of peridotitic origin), we have estimated the Ni-in-garnet temperatures using the geothermometers of Ryan *et al.* (1996) and Canil (1999) (Supplementary Table 2). Assuming a Ni content in olivine of 3100 ppm (average value for olivines from the nearby Udachnaya peridotites; Sobolev *et al.*, 2009b) the geothermometer of Canil (1999) gives temperatures of 900–928°C for Group A garnets, of 812–920°C for all but one Group B garnets, and of 839–931°C for Group C garnets. The unique, homogenous garnet Z5-6 (Group B) yields a higher temperature of 1037°C, as a consequence of its higher Ni content (48.3 vs. 12.0–26.7 ppm). This garnet is distinguished from all other primary garnets studied by its

higher mg# (83.8 vs. 78.7–81.7) and TiO_2 (0.35 wt% vs. 0.04–0.32 wt%). The geothermometer of Ryan *et al.* (1996) gives systematically lower temperatures, i.e., 811–853°C for Group A, 691–840°C for Group B (1020°C for garnet Z5-6), and 728–857°C for Group C.

The enstatite-in-Cpx geothermometer of Nimis & Taylor (2000) was applied to primary diopsides coexisting with Group A garnets (Supplementary Table 2), again assuming a peridotitic origin and equilibrium with orthopyroxene. The estimated temperatures (803–885°C) are in good agreement with those estimated with the Ni-in-garnet thermometer of Ryan *et al.* (1996) for the associated garnets. Clinopyroxene–garnet geothermometry, which yielded problematic, higher temperatures in previous studies of similar samples (see discussion in Nimis *et al.* 2009) was not attempted here, following recommendations of Nimis & Grütter (2010).

The low estimated temperatures suggest a relatively shallow origin for the garnets, in agreement with Cr-in-Cpx pressure estimates (Nimis & Taylor, 2000) for diopsides associated with Group A garnets (3.2–3.8 GPa; Supplementary Table 2) and previous estimates of 3.2–4.0 GPa (Nimis *et al.*, 2009) for Zagadochnaya diopside xenocrysts probably related to Group A and Group B garnets. *Minimum* pressures calculated using the Cr-in-garnet barometers of Grütter *et al.* (2006) and Turkin & Sobolev (2009) range between 1.9 and 3.6 GPa and between 1.3 and 3.4 GPa, respectively, consistent with the above results.

Owing to the absence of secondary olivine and orthopyroxene, quantitative estimates of *P–T* conditions could not be obtained for the secondary mineral assemblages in low-(Ca, Cr) garnet domains. Only *minimum P–T* conditions (730–888°C; 3.0–3.8 GPa; Supplementary Table 2) could be estimated for the secondary diopsides using single-clinopyroxene thermobarometers (Nimis & Taylor, 2000). These estimates are compatible with those obtained for the primary diopsides (741–848 °C; 3.2–4.0 GPa), suggesting that the formation of the secondary assemblages occurred at the same mantle depths. This further strengthens our interpretation that replacement of high-Cr garnets by low-Cr garnets + Cr-spinel + diopside (± other minerals) was not due to subsolidus decompressional reequilibration, as suggested by Ivanic *et al.* (2012) for microxenoliths from South African kimberlites, but was driven by non-isochemical reactions with percolating melts.

INSIGHT INTO THE EARLY REFERTILISATION PROCESSES

There is general consensus that the lithospheric mantle roots under cratons originated in the Archean after extensive extraction of high-Mg melts, which left refractory residua basically

consisting of harzburgite and dunite (e.g. Hanson & Langmuir, 1978; Boyd, 1989; Walter, 1998; Griffin *et al.*, 2003). Such scenario was proposed also for the lithospheric mantle beneath the Daldyn-Alakit Province (Griffin *et al.* 2003; Malkovets *et al.*, 2007; Ionov *et al.*, 2010). The high Cr_2O_3 contents (7.3–8.6 wt%) and low HREE contents (e.g. Yb = 0.07–1.07 ppm; Fig. 11) of our Group C garnets from Zagadochnaya are consistent with the strongly depleted nature of the pre-metasomatic protoliths. The high CaO contents of most garnets studied here (Fig. 3) imply subsequent refertilisation, which led to saturation in clinopyroxene. The enrichment in Ca suggests that metasomatism was at least in part driven by Ca-bearing melts rather than by fluids (Harte *et al.*, 1993; Grégoire *et al.* 2003; Burgess & Harte 1999, 2004; Stachel *et al.* 2004; Malkovets *et al.* 2007). Further information on the nature of the metasomatic agents can be obtained from the trace element distribution between garnets and clinopyroxenes and reconstruction of the equilibrium melt compositions.

Garnet–clinopyroxene equilibria and composition of the metasomatic melts

Textural features and absence of major element zoning across garnet–clinopyroxene boundaries suggest that Group A garnets were in chemical equilibrium with the associated clinopyroxenes (Figs. 2a,b and Supplementary Fig. 2). This is further supported by garnet/clinopyroxene partition coefficients ($^{Grt/Cpx}D = X_i^{Grt}/X_i^{Cpx}$, where X_i is the concentration of the element *i*), calculated for four garnet–diopside (Table 1 and Fig. 9). The calculated $^{Grt/Cpx}D$'s show little variations from grain to grain, except for Th, U and Nb. One sample (Z5-2) shows slightly higher D values for the REE from Tb to Tm. In general, the MREE and HREE are preferentially incorporated in the garnet ($^{Grt/Cpx}D > 1$), Zr and Ti have similar affinity for garnet and clinopyroxene ($^{Grt/Cpx}D \approx 1$), and Hf, Nb, Ta, Large Ion Lithophile Elements (LILE), and LREE from La to Eu show preferential partitioning in the clinopyroxene ($^{Grt/Cpx}D < 1$). The calculated $^{Grt/Cpx}D$'s are consistent, although slightly lower for the LREE, with the dataset of Zack *et al.* (1997), which was compiled for well equilibrated natural garnet pyroxenites with equilibration temperatures (920 ± 30 °C) similar to or slightly higher than those estimated for our samples.

In order to characterise the nature of the metasomatic agents and to investigate their possible relationships with the various primary mantle minerals, we have calculated the theoretical composition of the melts in equilibrium with the Zagadochnaya garnets and, where available, clinopyroxenes. Literature data show that garnet/melt ($^{Grt/melt}D$) and clinopyroxene/melt ($^{Cpx/melt}D$) partition coefficients depend on pressure, temperature and phase compositions (e.g. Hertogen & Gijbels, 1976; Harte *et al.*, 1996; Green, *et al.*, 2000;

Table 1: *Calculated garnet/clinopyroxene partition coefficients for well-equilibrated Group A microxenoliths*

Grt-cpx pair	**Z4-2**	**Z5-02**	**Z5-11**	**Z5-15**
Ti	1.27	1.31	1.00	1.47
Sc	3.33	4.53	3.23	4.44
V	0.51	0.50	0.49	0.49
Sr	0.0012	0.0012	0.0008	0.0007
Y	8.10	13.44	8.44	9.47
Zr	1.28	1.85	0.97	1.41
Nb	0.40	0.11	0.01	0.02
La	0.0021	0.0029	-	0.0007
Ce	0.0044	0.0114	0.0042	0.0028
Pr	0.012	0.039	0.025	0.006
Nd	0.048	0.114	0.061	0.029
Sm	0.29	0.56	0.30	0.23
Eu	0.64	0.85	0.58	0.51
Gd	1.33	1.80	1.49	1.10
Tb	2.22	4.50	1.96	3.15
Dy	4.55	6.25	4.81	3.45
Ho	6.08	14.55	6.91	7.61
Er	13.57	22.26	17.31	15.13
Tm	16.7	64.4	20.0	21.1
Yb	27.1	26.7	19.5	31.8
Lu	37.8	-	45.7	41.0
Hf	0.50	1.23	0.33	0.79
Ta	-	-	-	0.30
Th	-	0.059	0.043	0.015
U	-	0.40	-	0.03

Salters *et al.*, 2002; Blundy & Wood, 2003; van Westrenen & Draper, 2007; Lazarov *et al.*, 2012); therefore, the choice of the most appropriate $^{solid/melt}D$ dataset is not straightforward. Johnson (1998) determined the partition coefficients for the incompatible elements between clinopyroxene, garnet, and basaltic melt from experiments at 1300–1470°C and 2–3 GPa. Such high temperatures would be pertinent to processes of pervasive melt migration (e.g. Xu *et al.* 1998; Lenoir *et al.*, 1999, 2001). The Zagadochnaya samples show evidence of low equilibration temperatures, which may reflect either metasomatism by percolating melts that were thermally equilibrated with the ambient mantle or subsolidus reequilibration after metasomatism. In both cases, the $^{Grt/Cpx}D$'s of Johnson (1998) may not be appropriate. A comparison between the $^{Grt/Cpx}D$'s (calculated as $^{Grt/melt}D$ / $^{Cpx/melt}D$) in the high temperature experiments by Johnson (1998) and those measured on our Zagadochnaya samples (Table 1) suggests that with decreasing equilibration temperature the highly incompatible elements tend to redistribute into the clinopyroxene, while the HREE become only slightly more compatible in the garnet (Fig. 9). This is consistent with earlier observations by, e.g., Harte *et al.* (1996), Green *et al.* (2000) and Lazarov *et al.* (2012). As a consequence, using the experimentally derived $^{Grt/L}D$'s and $^{Cpx/L}D$'s to determine the

composition of the melts in equilibrium with Group A garnets and clinopyroxenes will respectively underestimate and overestimate the highly incompatible element in the melt, thus bracketing the real composition.

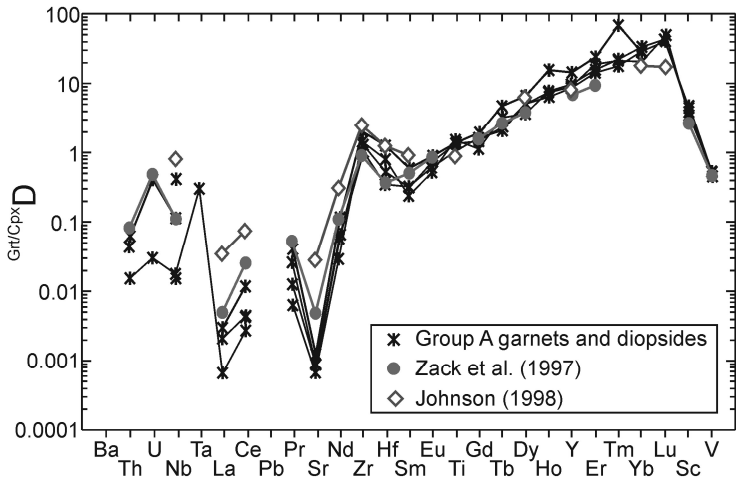

Fig. 9: *Comparison between garnet/clinopyroxene partition coefficients for well-equilibrated Group A microxenoliths (Table 1) and from literature.*

The calculated liquids in equilibrium with Group A garnets are enriched in LILE and LREE (e.g. La = 6.4–14.6 xPM) and show HREE values close to primitive mantle (e.g. Lu = 0.4–1.5 xPM) (Fig. 10a). The calculated liquids in equilibrium with Group A clinopyroxenes have similar trace element contents from Ti to Er, slighly lower Yb and Lu contents, but distinctly higher contents of highly incompatible elements from Nb to Sm (Fig. 10a). As discussed above, the actual trace element contents of the metasomatic agent should lie between the compositions of the melts calculated from the garnets and the clinopyroxenes, respectively. Compared with the compositions of Siberian kimberlites (Kostrovitsky *et al.*, 2007), the calculated melts have slightly lower contents of trace elements and show similar trace element fractionation with increasing element incompatibility, but with slightly less fractionated HREE (Fig. 10a). Other differences concern the negative Zr and Hf (and Ti) anomalies, which are less pronounced than in the kimberlitic melts.

Due to the lack of clinopyroxene in the studied samples, the composition of the metasomatic agent in equilibrium with Group B and Group C minerals could be calculated only from the compositions of the garnets (Fig. 10b). The melts in equilibrium with Group B garnets are richer in highly incompatible elements and more fractionated in HREE with respect to Group A. Negative anomalies also occur for Zr, Hf and Ta. Group C calculated melts are even more fractionated in HREE (e.g. Yb as low as 0.03 xPM), and often show negative anomalies in Ti and Zr_{PM}/Hf_{PM} ratios < 1. Because the $^{Grt/melt}D$'s used are probably

underestimated for the low-*T* Zagadochnaya samples (see discussion above), the melts in equilibrium with Group B and Group C garnets were even more HREE-fractionated and probably had similar or slightly higher contents of highly incompatible elements with respect to Siberian kimberlites (Fig. 10b).

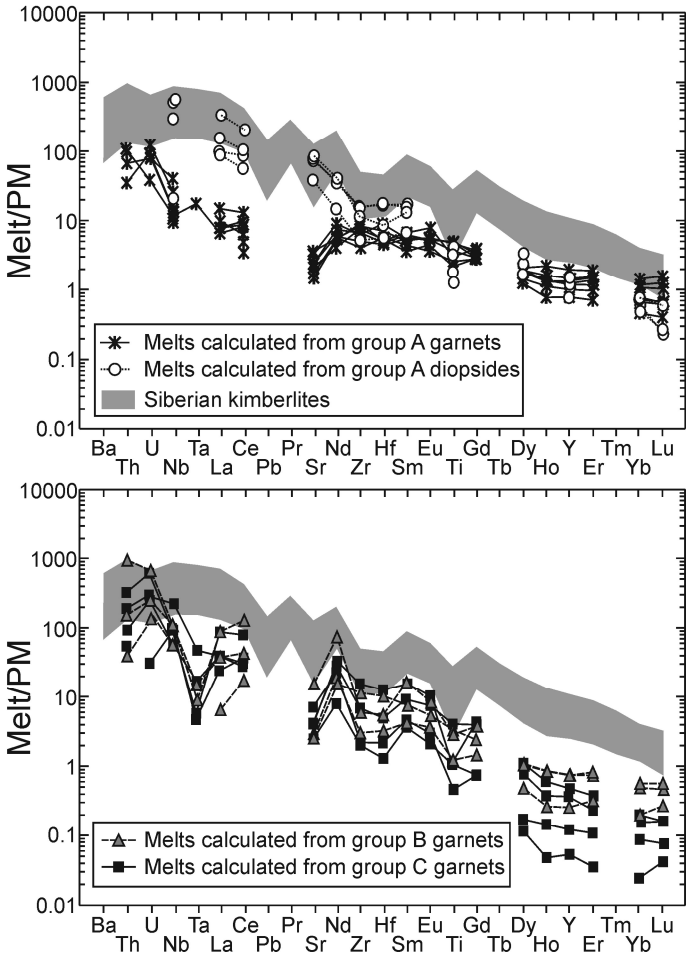

Fig. 10. *PM-normalized extended trace element patterns of representative calculated melt in equilibrium with (a) Group A garnets and clinopyroxenes and (b) Group B and Group C garnets. In (a) the actual melt composition should lie between those calculated from the clinopyroxenes and the garnets, respectively (see text for further explanation). The grey area covers the range of trace elements concentrations in Siberian kimberlites (Kostrovitsky et al., 2007).*

Evidence for a unique refertilisation event

As discussed above, the significant progressive increase in Ca and Cr from Group A through Group B to Group C garnets (Fig. 3) was controlled by changes in the bulk rock composition. The observation that this major-element trend is accompanied by a progressive increase of highly incompatible elements (e.g. LREE) and decrease of moderately incompatible elements (e.g. HREE and Y) (Fig. 11), suggests that the observed compositional "gradient" could be

the result of a unique refertilisation event, during which an uprising melt evolved through interaction with the ambient peridotite. The Cr-rich and HREE-depleted Group C garnets could thus represent the least refertilised peridotites, whereas the more Al- and HREE-rich Group A garnets should have originated from the most refertilised counterparts.

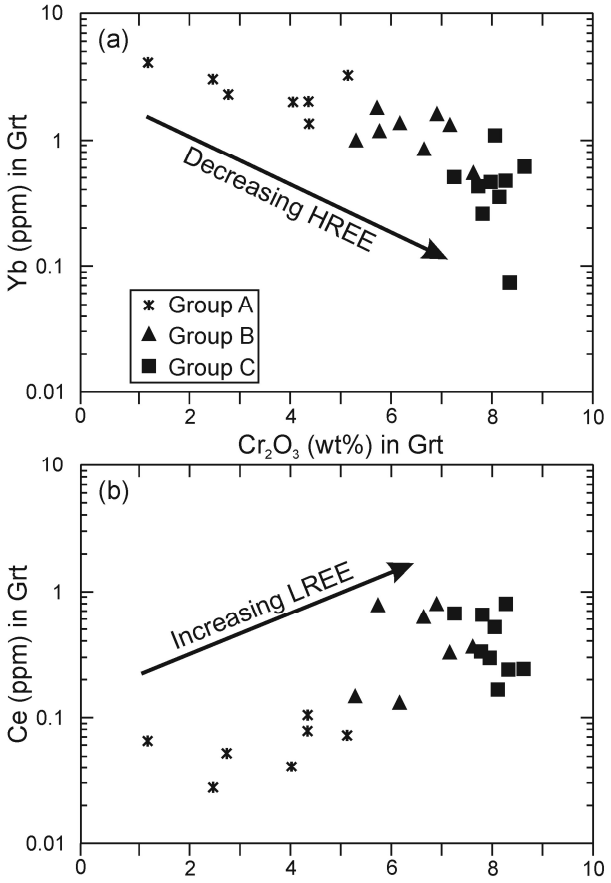

Fig. 11. *(a) Cr_2O_3 vs. Yb and (b) Cr_2O_3 vs. Ce in garnets from Groups A, B and C.*

To verify such hypothesis, a numerical simulation was performed using the Plate Model program (Vernières *et al.*, 1997), assuming that a melt in equilibrium with the garnet Z5-15 (i.e., the most HREE-rich of Group A garnets) percolated through a refractory mantle column consisting of clinopyroxene-bearing garnet harzburgite (*Model 1*). Details of the simulation and the rationale for the choice of the relevant input parameters are reported in Appendix 1. The results (Fig. 12a,b) show that fractional crystallisation of clinopyroxene and garnet (± olivine) and melt-peridotite chromatographic chemical exchange during melt percolation can reproduce the compositional transition from Group A to Group B garnets. In particular, the decrease in HREE observed in Group A garnets would reflect an initial interaction at high time-integrated melt/rock ratio, in the lower part of the mantle column (first cells in Fig. 12a,b). The increase in LREE observed in Group B garnets would reflect interaction at low time-integrated melt/rock ratios, in the upper part of the mantle column (last cells in Fig. 12a,b). The above process would bring about a significant increase of the modal contents of clinopyroxene and garnet in the mantle column, which could eventually be converted into a clinopyroxene-rich garnet lherzolite or even pyroxenite (cf. Grègoire *et al.*, 2003; Simon *et al.*, 2003, 2007; Ionov et al., 2005, 2006, 2010). The MREE and HREE contents and MREE/HREE fractionation of the calculated melts strongly depend on the $^{Grt/melt}D$'s used. In particular, the flat M-HREE pattern exhibited by Group B garnets implies little variation of $^{Grt/melt}D$'s from MREE to HREE, similar to what

predicted by Johnson's (1998) high-*T* dataset. Assimilation of peridotitic minerals (e.g. orthopyroxene) was found to be non influential at this stage (See Appendix 1).

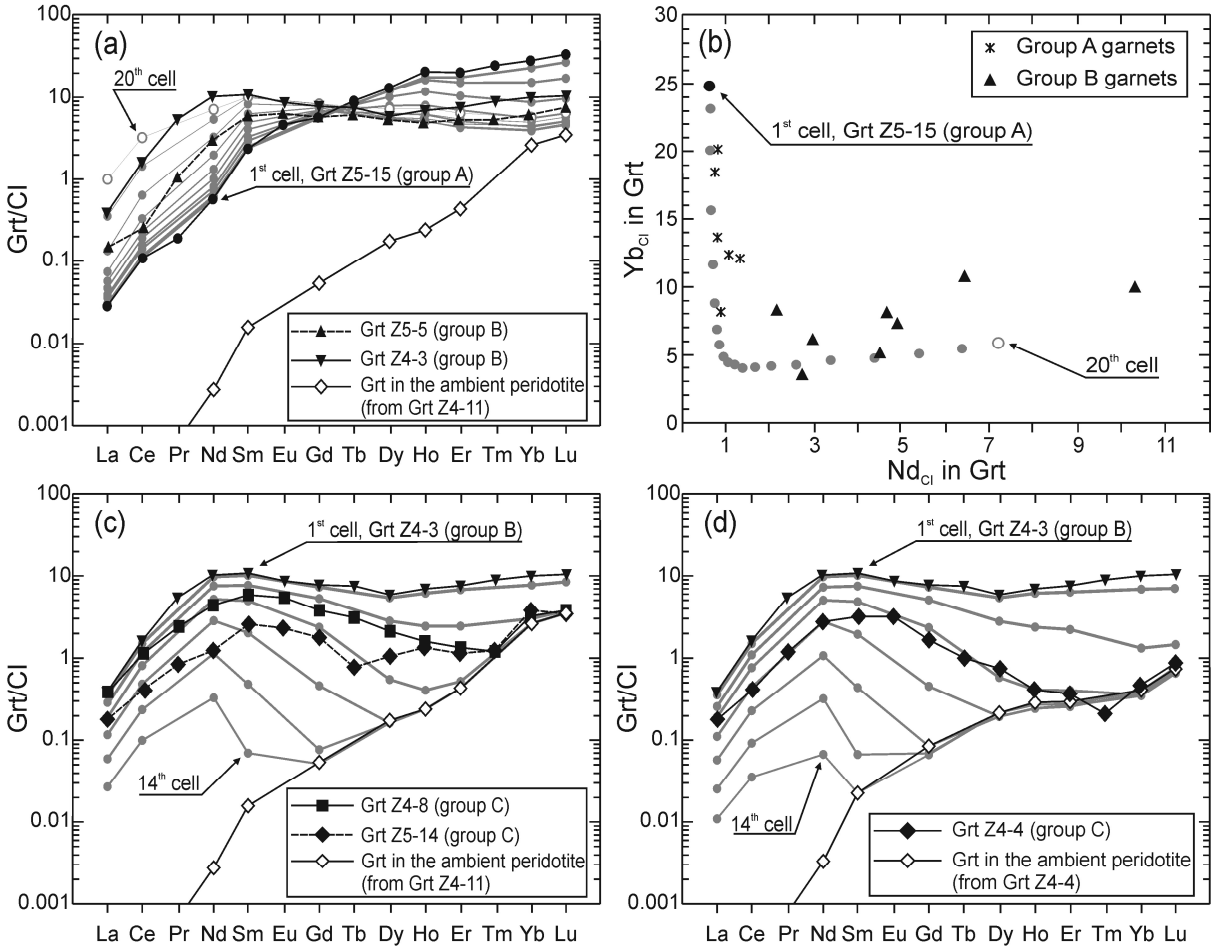

Fig. 12. *Comparison between CI-normalized REE abundances of representative primary garnets and those calculated by Plate Model numerical simulation (Vernières et al., 1997). (a, b) The transition from Group A to Group B garnets is reproduced by interaction between a melt in equilibrium with garnet Z5-15 (Group A) and a refractory garnet harzburgite containing a garnet with REE contents extrapolated from HREE abundance in garnet Z4-11 (Model 1). (c, d) The sinusoidal REE patterns of Group C garnets are obtained by interaction between a melt in equilibrium with the most LREE-rich garnet Z4-3 (considered as the residual melt after the reactions that produced Group B garnets) and refractory garnet harzburgites (Models 2 and 3). In (c) the REE contents of the peridotite garnet were extrapolated from the HREE abundance in garnet Z4-11 (Model 2); in (d) they were extrapolated from the HREE abundance in the most HREE-depleted garnet Z4-4 (Model 3). See appendix for further details.*

In Group C garnets, the highly incompatible elements (e.g. LREE) show no relevant changes with respect to Group B (Fig. 6), suggesting only minor involvement of fractional crystallisation processes. The more pronounced negative MREE fractionation and the observed inversion of the pattern slope in the heaviest REE region (Fig. 6) suggest that the percolating melts progressively approached chemical equilibrium with the country peridotite. This could occur by chromatographic-type chemical exchange at low time-integrated

melt/rock ratios (e.g. Xu *et al.*, 1998; Ionov *et al.*, 2002). Moreover, some Group C garnets show similar LREE fractionation, but variable LREE contents (Fig. 6). These features may reflect (i) changes in the composition of the infiltrating melts, (ii) variations in $^{solid/melt}D$'s, or (iii) assimilation of LREE-poor peridotite minerals (e.g. orthopyroxene; cf. Ionov *et al.*, 2005; Piccardo *et al.*, 2007). Assimilation of orthopyroxene in kimberlitic or proto-kimberlitic melts has been proposed by several authors to explain the scarcity of orthopyroxene xenocrysts in kimberlites (e.g. Brett *et al.*, 2009; Kamenetsky *et al.*, 2008, 2009; Arndt *et al.*, 2010; Russell *et al.*, 2012). In our case, a predominant role of assimilation would require a *T* of the melt high enough to avoid extensive concurrent crystallisation of magmatic minerals.

Numerical simulations of these processes were performed assuming percolation through the refractory mantle column of a melt in equilibrium with the most LREE-rich Group B garnet (sample Z4-3), which was assumed to represent the residual melt of the reactions that produced Group A and Group B garnets (cf. *Models 2* and *3* in Appendix). Allowing for orthopyroxene assimilation, during percolation at low time-integrated melt/rock ratios, the melt acquires transient chemical compositions, which closely approach those of Group C garnets and reproduce their sinusoidal REE patterns (Fig. 12c,d). In particular, the compositions of the most HREE-rich Group C garnets (samples Z4-8 and Z5-14) can be attained by assuming an ambient refractory peridotite with REE contents estimated on the basis of the peculiar garnet Z4-11 (*Model 2*; Fig. 12c). The most HREE-depleted compositions (sample Z4-4) are instead attained by assuming a more HREE-depleted original protolith, estimated on the basis of the HREE contents in garnet Z4-4 (*Model 3*; Fig. 12d). In these simulations, the compositions of the melts that reach the top of the mantle column are significantly different from that of the initial melt, mostly owing to assimilation of peridotite orthopyroxene. After these processes, the mantle column would consist of clinopyroxene-bearing garnet harzburgites with Group C garnets.

The above models simulate the formation of Group A, Group B, and Group C garnets by percolation of a single initial melt through a refractory mantle column. Such a process implies a progressive decrease in the melt/rock ratio and, therefore, a decreasing degree of refertilisation of the ambient peridotite in terms of bulk major element chemistry. In particular, given the likely low Cr_2O_3 content of the metasomatic melts (< 1.0 wt% for kimberlites; cf. Becker & Le Roex, 2006), and assuming an original depleted and homogenous mantle column, the higher the melt/rock ratio, the lower the Cr_2O_3 content in the metasomatised peridotite. This is consistent with the observed progressive decrease in Cr_2O_3 from the less refertilised Group C garnets to the more refertilised Group A garnets (Fig. 11).

LATE-STAGE METASOMATISM RELATED TO THE HOST KIMBERLITE

Time scales of the metasomatic event

In order to determine an order-of-magnitude timescale for the process responsible for the formation of the secondary garnet domains and estimate the residence time of these garnets in the mantle after the last metasomatic event, we have modelled the concentration profiles across the transitions between high-(Ca, Cr) and low-(Ca, Cr) garnet zones. For an optimal evaluation of the residence time, zoning should be perpendicular to the thin section surface. Any deviation from this condition would result in contamination of electron microprobe analyses near the high-(Ca, Cr) – low-(Ca, Cr) interface by the adjacent garnet and in apparent smoothing of the diffusion profiles. This would, in turn, determine an overestimation of the timescale, thereby only a maximum residence time can generally be retrieved. The most appropriate zoning profile was found in some areas of garnet Z6-10, in which the boundary between primary and secondary garnets looked particularly sharp (Supplementary Fig. 1). We measured the zoning profile of Ca across the high-(Ca, Cr) – low-(Ca, Cr) interface and compared it with theoretical profiles obtained through the binary diffusion model (Crank, 1975), i.e.,

$$C_i(x,t) = C_{i,0} + \frac{C_i^0}{2}\left\{1 - erf\frac{x}{2\sqrt{D_{i-j}t}}\right\}$$

where $C_i(x,t)$ is the concentration as a function of distance and time, C_i^0 is the initial concentration difference between the two sides of the couple, $C_{i,0}$ is the lower of the two initial values of concentration (here we used normalized concentrations, setting $C_{i,0} = 0$ and $C_i^0 = 1$) and D_{i-j} is the binary interdiffusion coefficient between the components *i* and *j*. To model Ca concentration profiles, we have considered a multicomponent diffusion only of Ca and Mg, since Fe abundances in these garnets show no variation along the zoning profiles (cf. Supplementary Fig. 1).

We have calculated the single interdiffusion coefficient $D_{Ca\text{-}Mg}$ from the molar fractions (X) and self-diffusion coefficients of Ca and Mg (Ganguly, 2010), using the formula

$$D_{Ca-Mg} = \frac{D_{Ca}D_{Mg}}{X_{Ca}D_{Ca} + X_{Mg}D_{Mg}}\left(1 + \frac{\partial ln\gamma_{Ca}}{\partial lnX_{Ca}}\right),$$

approximating the parenthetical term (thermodynamic factor) to unity. We used the Ca self-diffusion coefficient of Perchuk *et al.* (2009; with corrections in Ganguly, 2010) and the Mg self-diffusion coefficient of Ganguly *et al.* (1998), normalized to pressures and temperatures (Ganguly, 2010) relevant to processes studied here (i.e., $P \sim 3.5$ GPa and $T = 800–1100$°C).

Comparison of the modelled and measured Ca concentration profiles (Fig. 13a) indicates a maximum time-span of 10 years at 1100°C and less than 100 years at 900°C. Modelling using the Ca–(Mg, Fe) interdiffusion coefficients of Vielzeuf *et al.* (2007) yields slightly longer timescales (Fig. 13b), with a maximum of 10^4 years at 900°C. Regardless of the model parameter used, these results indicate that the secondary garnet domains and the associated inclusions formed shortly before the kimberlite eruption and therefore suggest a possible link between the reacting melt and the host kimberlite.

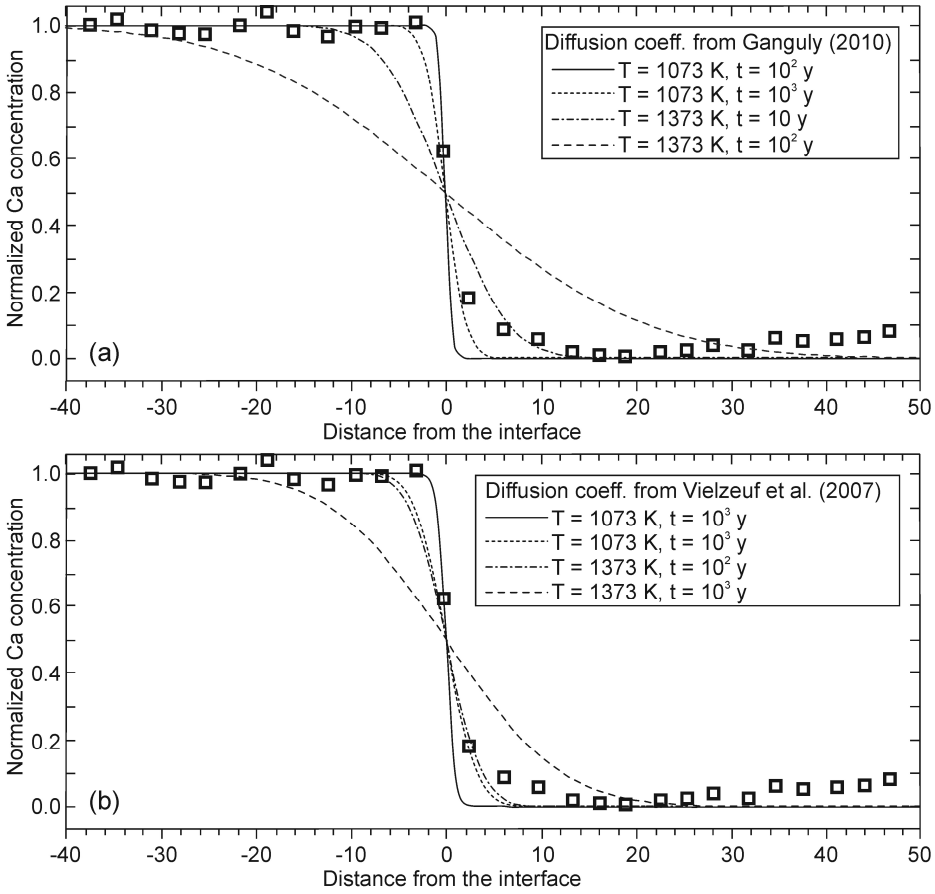

Fig. 13: *Measured Ca profile along the transect A-A' in garnet Z6-10 (cf. Figs. 2j and A1 of the Electronic Appendix), and corresponding modeled Ca diffusion profiles, using diffusion coefficients after (a) Ganguly (2010) and (b) Vielzeuf et al. (2007), normalized for pressure of 3.5 GPa and temperatures of 1073 and 1373 K.*

Composition and evolution of kimberlite-related melts

The secondary garnets and clinopyroxenes (as well as the geochemically analogous Group III chromian diopsides of Nimis *et al.*, 2009) show lower Ti_{PM}/Zr_{PM} ratios (0.02–0.20, av. = 0.09 for garnets; 0.03–0.28, av. = 0.12 for clinopyroxenes) than the primary minerals (0.08–0.70, av. = 0.40 for garnets; 0.31–1.00, av. = 0.68 for clinopyroxenes; Fig. 14). Most likely, this difference reflects the composition of the late metasomatic agent, which is therefore more

compatible with a Type II (similar to the host magma) rather than Type I kimberlite (cf. Shimizu *et al.*, 1997a). The presence of phlogopite in the secondary domains, even if not abundant, is also consistent with this hypothesis.

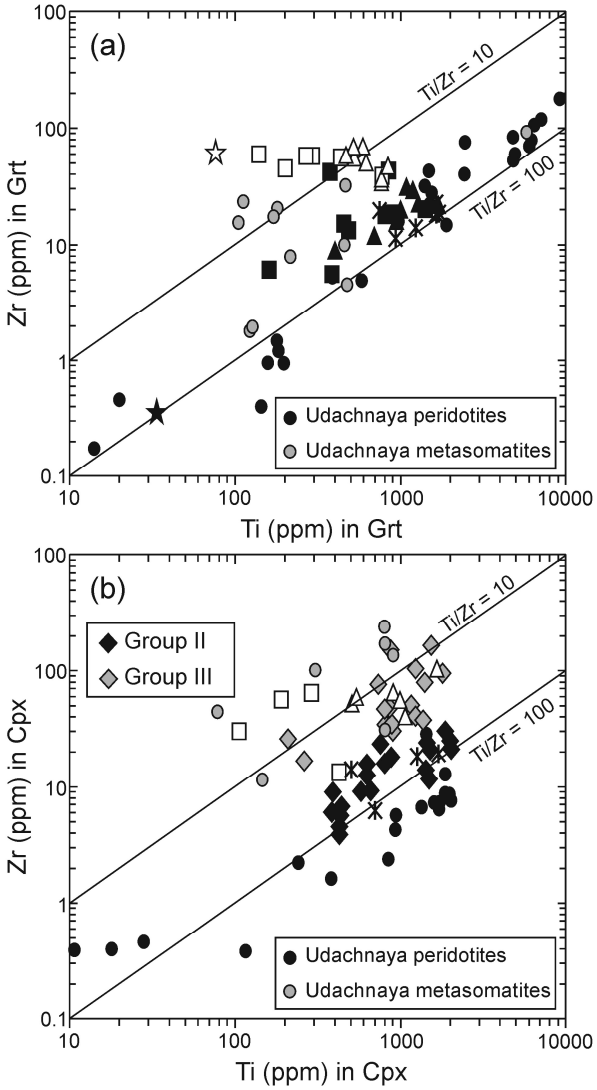

Fig. 14. *Ti vs. Zr covariation for the analyzed (a) garnets and (b) clinopyroxenes. Data for Group II and Group III clinopyroxenes are from Nimis et al. (2009). Data for Udachnaya peridotites and metasomatites are taken from Shimizu et al. (1997) and Solov'eva et al. (2010), respectively. Symbols as in Figs. 3 and 4, except for those reported in the legend.*

To further constrain the nature of the metasomatic agent, we calculated the compositions of the melts in equilibrium with the secondary garnets and clinopyroxenes, using again the $^{solid/melt}D$ dataset of Johnson (1998) (Fig. 15). The trace element patterns of the calculated melts broadly resemble that of the Zagadochnaya Type II kimberlite (Fig. 15). The most relevant discrepancies concern the trace element contents from Ti to Lu, which show a transition to progressively more fractionated compositions with respect to the kimberlite.

The significance of the variable Ti–Lu fractionation of the secondary garnets is well illustrated in Figure 16, which shows the REE patterns of primary and secondary domains in representative garnets, compared with the calculated REE pattern of a hypothetical garnet in equilibrium with the Zagadochnaya kimberlite. In garnet grains Z4-9 and Z4-8, which underwent only incipient melt reaction at the rim (Fig. 2k), the secondary domains are enriched only in LREE and MREE up to Dy–Er (Fig. 16). Garnet grain Z4-4 underwent more extensive reaction (secondary domains extend to most of the grain; Fig. 2g,h) and was enriched also in HREE, approaching more closely equilibrium with the Zagadochnaya kimberlite (Fig. 16). Finally, garnet Z6-12, which appears to have almost completely reacted with the melt (Fig. 2k), shows even higher HREE enrichment, effectively reaching equilibrium with the

Zagadochnaya kimberlite. The slightly higher LREE calculated for the garnet in equilibrium with the kimberlite (Fig. 16) may again reflect overestimation of $^{Grt/melt}D$'s using the high-*T* $^{Grt/melt}D$ dataset of Johnson (1988) (see discussion in chapter *Garnet–clinopyroxene equilibria and composition of the metasomatic melts*).

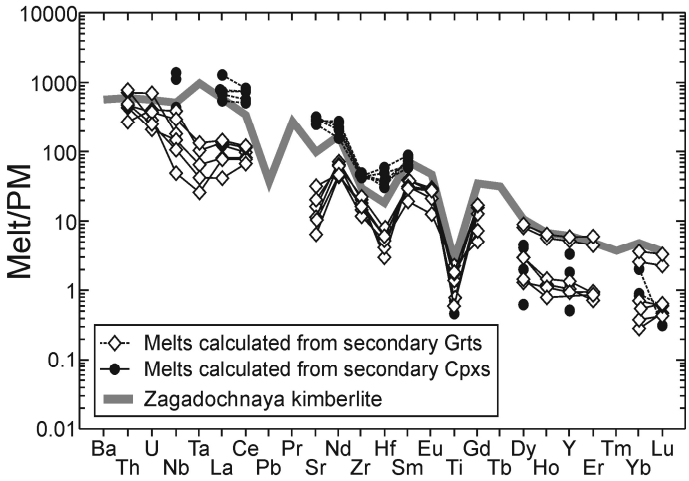

Fig. 15: *PM-normalized trace element patterns of representative calculated melts in equilibrium with secondary garnets and diopsides ($^{solid/melt}D$'s from Johnson, 1998). The composition of the Zagadochnaya kimberlite (Kostrovitsky et al., 2007) is reported for comparison.*

Other discrepancies from the composition of the Zagadochnaya kimberlite are the generally lower U, Nb and Ta contents, and variable Sr anomalies in the melts calculated from the garnets. The very low measured abundances and, therefore, low analytical precision of such highly incompatible elements can in part account for such discrepancies. Moreover, the variable Sr anomalies, which positively correlate with Nb abundances (Supplementary Table 2), suggest contamination of LA–ICP-MS analyses by sub-microscopic (Nb, Sr)-bearing phases, possibly belonging to the crichtonite series (e.g. lindsleyite; Haggerty *et al.*, 1983). Note also that the most realistic contents of the highly incompatible elements lie between those calculated from the garnets and those calculated from the clinopyroxenes (see

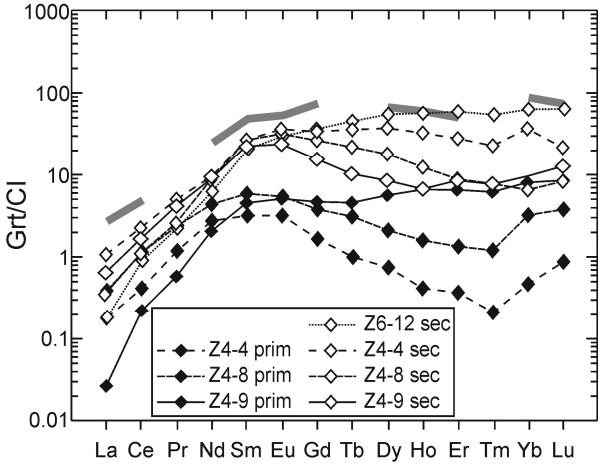

Fig.16. *CI-normalized REE patterns of some primary garnets (prim) and their secondary domains (sec). Grey line indicates the calculated REE pattern of garnet in equilibrium with the Zagadochnaya kimberlite ($^{Grt/melt}D$'s from Johnson, 1998). Data for the Zagadochnaya kimberlite after Kostrovitsky et al. (2007).*

discussion in chapter *Garnet–clinopyroxene equilibria and composition of the metasomatic melts*). For all these reasons, the observed discrepancies for the highly incompatible elements are not significant.

The relationships between grain textures and REE contents suggest that the variable degree of REE fractionation observed in the secondary garnets and clinopyroxenes (and in their calculated equilibrium melts) represent transient features related to percolation at depth of a melt related to the host kimberlite. Moreover, the close similarity between the calculated melts in equilibrium with the most reacted garnets and the host kimberlite suggests that the erupting kimberlitic magma did not significantly change its trace element contents from depths of 100–130 km.

DISCUSSION

Combining garnet and diopside records: overall evolution of the shallow lithospheric mantle beneath Zagadochnaya

The lithospheric mantle beneath the Daldyn field is believed to consist of a deep (ca. 180–230 km depth) layer in which moderately to strongly melt-metasomatised lherzolites are predominant, an intermediate, diamond-rich layer (ca. 140–180 km) in which harzburgites and depleted lherzolites are more abundant, and an upper layer (ca. 95–140 km) in which lherzolites (from depleted to strongly melt-metasomatised) dominate (Malkovets *et al.*, 2007, and reference therein; Ionov *et al.*, 2010; Agashev *et al.*, 2012). The major and trace element compositions of garnet groups A, B and C studied here, and of diopside Group II described by Nimis *et al.* (2009), are consistent with a derivation from variably metasomatised, formerly highly refractory peridotites. Metasomatism operated by Ca-bearing melts with kimberlitic affinity led to neo-formation of modal clinopyroxene, giving rise to variably re-fertilised lherzolites. Based on the geochemical compositions of the garnets and of the chromian diopsides and on thermobarometric data (cf. Nimis *et al.*, 2009, and this study), our Group C garnets may be representative for the shallow, weakly metasomatised, depleted lherzolites, whereas our Group A and Group B garnets (and Group II diopsides of Nimis *et al.*, 2009) may be part of the melt-metasomatised lherzolites from the same layer.

Plate model numerical simulations indicate that the overall geochemical variability observed in the studied garnets can be the result of a unique melt injection, whereby the liquid composition progressively changed due to reactions with the ambient peridotite and fractional crystallisation. The substantial *P–T* overlap of groups A, B and C indicates the heterogeneous distribution of metasomatism operated by the percolating melts, which led to formation of

variably refertilised lithologies at about the same lithospheric level. Similar metasomatic gradients were reported in several orogenic lherzolite massifs (e.g. Lherz and Ronda; Lenoir *et al.*, 2001; Le Roux *et al.*, 2007). Although the hypothesis of multi-stage metasomatism cannot be ruled out, the contribution of various unrelated melts operating in the lithosphere appears to be unnecessary to explain the observed compositional spectrum of the garnets.

Late reactions with ultra-alkaline melts cognate with the erupted Zagadochnaya kimberlite partially transformed Group B and Group C garnets into low-(Ca, Cr) garnet–clinopyroxene–chromite (± phlogopite ± amphibole) assemblages shortly before eruption. Group III diopsides of Nimis *et al.* (2009) were also formed by these processes. Minimum pressure estimates and the precipitation of secondary garnet and spinel indicate that these late reactions occurred at relatively great depth, shortly before entrainment in the erupting kimberlite. Group A garnets remained apparently unaffected during this late metasomatic stage. The reason for their preservation is unclear. On the one hand, the major element compositions of Group A garnets are the most similar to those of the secondary garnets, which possibly made them less prone to reactions with the percolating kimberlite. On the other hand, the trace element compositions of the two garnet types is so different that some compositional gradients would have been expected at least for the most incompatible elements. An alternative explanation could be the higher predicted modal content of pyroxenes in the host rocks, which could have decreased melt connectivity and thus hindered melt percolation (cf. Toramaro & Fuji, 1986; Schäfer and Foley 2002).

Migration of the pre-eruption kimberlitic melts to shallower mantle levels led to crystallisation of the (Al, Cr, Na)-poor Group I diopsides of Nimis *et al.* (2009). These diopsides have a megacryst-like geochemical signature and were interpreted to represent spinel-facies, orthopyroxene-free segregates from melts, which were related to the host kimberlite, but were partly modified by interaction with the ambient peridotites.

The latest interaction between the kimberlite and the mantle minerals is recorded by the precipitation of kimberlitic mineral assemblages in veinlets cutting Group II and Group III diopsides of Nimis *et al.* (2009) and by pargasite + phlogopite + chromite veinlets in many garnets reported in this study. The presence of pargasite constrains the pressure of formation of the garnet-hosted veinlets to < 3.0 GPa (Niida & Green, 1999). Given the higher pressure of formation estimated for the host garnets and clinopyroxenes (> 3.0 GPa), the veinlet assemblages in the garnets must have crystallised on route to the surface, after entrapment of the xenocrysts in the kimberlite.

Although the whole spectrum of garnet compositions observed at Zagadochnaya has not been reported at Udachnaya, compositional similarities of our Groups A, B and C with some Udachnaya garnets (cf. Shimizu *et al.*, 1997a; Ionov *et al.*, 2010) suggest that the lherzolite-rich, shallow mantle sections beneath Zagadochnaya and Udachnaya shared a common early geochemical history. The late, deep-seated, metasomatic event, which was operated by melts strictly related to the host kimberlite, has apparently no counterpart at Udachnaya (cf. Solov'eva *et al.*, 1997, 2010; Nimis *et al.*, 2009; Ionov *et al.*, 2010). Most likely, analogous processes did instead occur under other Daldyn localities, where Type II kimberlites similar to the Zagadochnaya kimberlite were erupted. These include the Bukovinskaya, Gornyatskaya and Kusov kimberlite pipes, in which several garnet–diopside–chromite aggregates petrographically and geochemically similar to those found at Zagadochnaya have been reported (cf. Kostrovitsky & de Bruin, 2004).

Implications on diamond potential and Type II kimberlite volcanology

The substantial rarity of harzburgitic materials, which contrasts with the abundance of highly refractory, low-Ca lithologies at intermediate mantle depths (140–180 km) in the Daldyn kimberlite field (Griffin *et al.*, 2002; Malkovets *et al.*, 2007), the low Ni-in-garnet temperatures (≤860°C or ≤950°C, depending on the preferred thermometric formulation, with only one exception at 1020°C or 1065°C, respectively), and the low Cr-in-Cpx estimated pressures for the associated clinopyroxenes (3.0–4.0 GPa) suggest derivation of Zagadochnaya xenocrystic material from a relatively shallow mantle section (ca. 100–130 km). Only a minor portion, if any, of the mantle sampled by the Zagadochnaya kimberlite may have been seated within the diamond stability field, thus providing a simple explanation for the absence of diamond at Zagadochnaya, as previously suggested by Nimis *et al.* (2009). This is in marked contrast with the xenolith record in the nearby, highly diamondiferous Udachnaya kimberlite, which extends to depths as great as 250 km (cf. Griffin *et al.*, 1996; Boyd *et al.*, 1997; Pokhilenko *et al.*, 1999; Shimizu *et al.*, 1997a; Solov'eva *et al.*, 2008; Ionov *et al.*, 2010).

The apparent absence of mantle material from depths greater than ca. 130 km is unusual for kimberlites and must be the result of particular volcanological processes. Most likely, the maximum depth of sampling reflects the depth at which the rising magma becomes fast enough to initiate the mechanical disaggregation and incorporation of xenoliths (Wilson & Head, 2007), which in turn may be controlled by exsolution of CO_2 (Arndt *et al.*, 2010; Russel *et al.*, 2012). Arndt *et al.* (2010) suggested that the exsolution level may be different

for Type I and Type II kimberlites. In Type II kimberlites, which are usually less CO_2-rich, exsolution may take place at shallower, lithospheric levels, allowing for extensive interaction with the lithospheric mantle before eruption and driving the melt to more magnesian compositions. On a qualitative basis, this scenario seems compatible with (i) the lack of deep mantle materials, (ii) the abundance of secondary assemblages, and (iii) the high-Mg composition of the Type II Zagadochnaya kimberlite. Considering the high dissolution rate of diamond in kimberlitic melts (cf. Fedortchouk *et al.*, 2005; Arima & Kozai, 2008), melt–rock reactions at depth may have led to resorption of any small diamond fraction originally present.

CONCLUDING REMARKS

(1) The shallow lithospheric mantle beneath Zagadochnaya (100–130 km) is mostly composed by moderately to strongly refertilised, formerly depleted peridotites, which are represented by garnets with progressively decreasing Cr, Ca, and LREE and increasing HREE contents, i.e., showing sinusoidal to normal CI-normalized REE patterns. These refertilised lithologies could be produced by a unique episode of melt injection through a former refractory mantle column. The evolution of the metasomatic melt by fractional crystallisation, assimilation, and chromatographic exchange during percolation through the mantle produced relatively small-scale geochemical gradients, which are recorded by xenocrysts sampled by the kimberlite across a restricted depth interval (ca. 30 km). This early-stage metasomatism affected a wide area under the Daldyn field, determining a high proportion of variously refertilised rock types sharing similar geochemical features.

(2) Late interaction between the mantle rocks and melts cognate to the host kimberlite occurred at depth shortly before eruption, forming shallow, spinel-facies, clinopyroxene segregates and deeper, secondary mineral assemblages made of low-(Ca, Cr) garnet, chromite and diopside (± amphibole and phlogopite) with distinct Type II kimberlite affinity. Similar secondary products are widespread in other Type II kimberlites within the Daldyn field.

(3) The lack of mantle materials from depth greater than 130 km, the absence of diamond, the abundance of secondary mineral assemblages, and the high-Mg composition of the kimberlite are consistent with a relatively slow ascent of the kimberlitic melts to shallow lithospheric levels and extensive melt–mantle interactions before eruption.

APPENDIX: PLATE MODEL NUMERICAL SIMULATION

Design of the numerical simulations

Numerical simulations were carried out using the Plate Model program of Vernières *et al.* (1997). In all simulations, the hypothetical mantle column was divided in 20 cells and 20 process increments were run. At each process increment, melt and peridotite were allowed to equilibrate with each other through ion exchange, after possible assimilation and/or fractional crystallisation. The chemical and modal parameters used in the final simulations (*Models 1, 2* and *3*) are reported in Supplementary Table 3.

The numerical simulation of melt–peridotite interactions requires the knowledge of several parameters, such as the compositions of both infiltrating melts and ambient peridotites, the topology of the reactions, the mode of the segregated/assimilated minerals, the instantaneous melt/rock ratios (i.e., porosity), and the solid-liquid partition coefficients. Most of these parameters may significantly vary depending on the *P–T* conditions and composition of the system. Most of these information are missing in the studied case, mostly due to the lack of discrete mantle xenoliths.

Taking into account these limitations, several numerical simulations were performed using different input data, in order to constrain the critical petrochemical and physical parameters that governed the incorporation and fractionation of trace elements in Zagadochnaya garnets. The rationale for these simulations and the main results are described here and may be used as reference for future studies on garnets from other cratonic settings.

Evaluating fractional crystallisation, assimilation, and melt/rock ratio

Our first model (*Model 1*) was devised to reproduce the transition from Group A to Group B garnets (Fig. 12a,b). Preliminary simulations showed that the progressive *increase* of the concentrations of *highly incompatible elements* from Group A to Group B can only be obtained by melt–peridotite reactions that involve strong fractional crystallisation and decreasing volumes of the percolating melts (see also Vernières *et al.*, 2007; Ionov *et al.*, 2002; Piccardo et al, 2007; Rivalenti *et al.*, 2004; 2007a,b). Preliminary modeling also showed that olivine crystallisation did not change significantly the trace element fractionation in the differentiated liquids. Thus, although it is likely that olivine segregation did occur, we only assumed segregation of clinopyroxene and garnet for simplicity.

The concomitant *decrease* of the *moderately incompatible elements* and *increase* of the *highly incompatible elements* from Group A to Group B (Fig. 12a,b) was obtained by progressively decreasing melt/rock ratios, i.e., by allowing a progressively more efficient

chemical buffering exerted by the ambient peridotite (cf. Vernières *et al.*, 2007; Ionov *et al.*, 2002; Piccardo et al, 2007; Rivalenti *et al.*, 2004; 2007a,b; Nimis *et al.*, 2009). Increasing amount of garnet in the system, either in the crystallizing mineral mode or in the host peridotite, induces a faster decrease of the HREE contents in the percolating liquid and was therefore adjusted to obtain the best fit with the observed data. The best reproduction of the observed REE trends was obtained assuming a crystallising mode of 80% clinopyroxene and 20% garnet (mass units). It is noteworthy that the simulation well reproduces also the variations of Th, U, Nb and Ti, but fails in reproducing the variations of Zr and Hf (Supplementary Table 3). No assimilation was allowed, because its simulated effects were not helpful in any way to explain the observed geochemical trends. We do not exclude that some assimilation did take place, but its effects were negligible compared to those of fractional crystallisation and chromatographic exchange.

Models 2 and *3* were devised to reproduce the transition between Group B and Group C (Fig. 12c,d). Owing to the absence of significant variations in the concentration of highly incompatible elements (e.g. LREE) between the two groups (Fig. 6), no fractional crystallisation was assumed. The existence of some Group C garnets showing similar LREE fractionation, but variable LREE contents (Fig. 6) was reproduced allowing for assimilation of peridotite orthopyroxene. The best fit was obtained assuming orthopyroxene assimilation varying from 1% of solid mass in the first cell at the bottom of the mantle column to 1‰ of solid mass at the top of the mantle column.

Mineral/liquid partition coefficients

The degree of MREE/HREE fractionation of the modeled garnet compositions was strongly dependent on the adopted $^{Grt/melt}D$ values. In our tests, the $^{Grt/melt}D$'s calculated from the $^{Grt/Cpx}D$'s measured on our Group A garnet–clinopyroxene pairs (Table 1) and the $^{Cpx/melt}D$'s of Ionov *et al.* (2002) produced HREE depletion rates and MREE/HREE fractionations higher than those observed in our Group A and Group B garnets. This observation suggests that during melt–peridotite interaction $^{Grt/melt}D_{HREE}$ values were lower than those estimated based on Grt/Cpx partitioning in the re-equilibrated Group A samples (T = 811–853°C), as expected for reactions operating at higher-T conditions. The high-T experimental $^{Grt/melt}D$ values of Johnson (1998) allowed us to obtain a much better fit with the observed data.

In the final simulations, mineral/melt partition coefficients for olivine, orthopyroxene and clinopyroxene were taken from Table 7 of Ionov *et al.* (2002), while the $^{Grt/melt}D$ were those of

Johnson (1998), with the exception of those for U and Th, which were taken from Hauri *et al.* (1994).

Composition of the ambient peridotite

The trace element composition of the ambient peridotite before the refertilisation processes is constrained by Group C garnets, being their high Cr/Al ratio and their extreme depletion in HREE evidence for strongly depleted original compositions. In the nearby Udachnaya kimberlite, abundant depleted garnet harzburgites occur at slightly greater depth (140–180 km; Boyd *et al.*, 1997; Shimizu *et al.*, 1997a; Ionov *et al.*, 2010) than those estimated for the Zagadochnaya xenocrysts (100–130 km; Nimis *et al.*, 2009, and this study). Bulk rock major element compositions for some fresh granular peridotites characterized by depletion in moderately incompatible trace elements similar to that of Group C garnets are reported in Ionov *et al.* (2010; cf. their samples U29 and U506). However, these granular peridotites show enrichments in highly incompatible elements in both bulk rock and minerals, as well as chemical disequilibrium between garnet and clinopyroxene, evidencing for late metasomatic interaction with melts or fluids. For sake of simplicity, the compositions of the ambient peridotites was recalculated assuming that their modal composition was identical to that of the very HREE-depleted granular harzburgite U506 studied by Ionov *et al.* (2010; 77.2 wt.% Ol, 16 wt.% Opx, 2.6 wt.% Cpx, and 4.2 wt.% Grt), but modifying the compositions of highly incompatible trace elements of the minerals. Thus, in *Model 1* and *Model 2*, the concentrations of the HREE from Ho to Lu (as well as Zr and Ti) of the garnet were assumed to be equal to those of our very depleted garnet Z4-11 (Fig. 12a,b); the contents of the other trace elements were extrapolated from those of the HREE, according to the trace element fractionation shown by minerals in equilibrium with komatiitic melts (komatiite melt 7-PPR-97; Hanski *et al.*, 2001) (Fig. 12a,c). In *Model 3*, the HREE composition of the garnet was assumed to be equal to that of our garnet Z4-4 (Fig. 12d); the contents of the other trace elements were again extrapolated from those of the HREE (Fig. 12d) and the fractionation calculated for minerals in equilibrium with komatiites. The influence of these artificial modifications, however, was found to be negligible at least for the numerical simulation of M*odel 1* and for the first 8–10 cells of *Models 2* and *3*, which were sufficient to approach the compositions of the Zagadochnaya garnets (Fig. 12 a,c,d). Similarly, moderate changes in the initial mineral modes (e.g. presence/absence of minor clinopyroxene) did not affect significantly the modeling results, which were much more strongly dependent on the assumed extent of fractional crystallisation and assimilation. In all models, the trace element

compositions of olivine, orthopyroxene and clinopyroxene were calculated from those of the garnet, using Grt/Cpx, Grt/Ol and Grt/Opx partition coefficients determined on the basis of the adopted $^{mineral/melt}D$'s.

Initial liquid compositions

In *Model 1*, the composition of the initial liquid (see Supplementary Table 3) was assumed to be that of the calculated melt in equilibrium with our garnet Z5-15, using the $^{Grt/melt}D$'s of Johnson (1998). This garnet is the richest in HREE among Group A garnets, therefore its calculated equilibrium liquid should be the closest to the hypothetical composition of the unmodified metasomatic melt. In *Models 2* and *3*, the composition of the liquid (see Supplementary Table 3) was assumed to be that of the calculated melt in equilibrium with Group B garnet Z4-3. This garnet is one of the richest in highly incompatible trace elements. Its calculated equilibrium liquid was chosen to represent the composition of the residual melt after the processes that formed Group A and Group B garnets.

REFERENCES

- Agashev, A. M., Watanabe, T., Kuligin, S. S., Pokhilenko, N. P. & Orihashi, Y. (2001). Rb-Sr and Sm-Nd isotopes in garnet pyroxenite xenoliths from Siberian kimberlites: an insight into lithospheric mantle. *Journal of Mineralogical and Petrological Science* **96**, 7-18.
- Agashev, A. M., Pokhilenko, N. P., Tolstov, A. V., Polyanichko, V. V., Malkovets, V. G. and
- Sobolev, N. V. (2004). New age data on kimberlites from the Yakutian Diamondiferous Province. *Doklady Earth Sciences* **399**, 1142-1145.
- Agashev, A. M., Ionov, D. A., Pokhilenko, N. P., Golovin, A. V., Cherepanova, Yu. & Sharygin, I. S. (2012). Metasomatism in lithospheric mantle roots: Constraints from whole-rock and mineral chemical composition of deformed peridotite xenoliths from kimberlite pipe Udachnaya. *Lithos* doi: 10.1016/j.lithos.2012.11.014.
- Anders, E. & Grevesse, N. (1989). Abundances of the elements: Meteoritic and solar. *Geochimica et Cosmochimica Acta* **53**, 197-214.
- Arima, M. & Kozai, Y. (2008). Diamond dissolution rates in kimberlitic melts at 1300–1500 ◦C in the graphite stability field. *European Journal of Mineralogy* **20**, 357-364.
- Arndt, N. T., Guitreau, M., Boullier, A.-M., Le Roex, A., Tommasi, A., Cordier, P. & Sobolev, A. (2010). Olivine, and the origin of kimberlite. *Journal of Petrology* **51**, 573-602.
- Aulbach, S., Pearson, N. J., O'Reilly, S. & Doyle, B. J. (2007). Origins of xenolithic eclogites and pyroxenites from the Central Slave Craton, Canada. *Journal of Petrology* **48**, 1843-1873.
- Becker, M. & Le Roex, A. P. (2006). Geochemistry of South African on- and off-craton, Group I and Group II kimberlites: petrogenesis and source region evolution. *Journal of Petrology* **47**, 673-703.
- Bedini, R. M., Bodinier, J. L., Dautria, J. M. & Morten, L. (1997). Evolution of LILE-enriched small melt fractions in the lithospheric mantle: a case study from the East African Rift. *Earth and Planetary Science Letters* **153**, 67-83.
- Blundy, J. D. & Wood, B. J. (2003). Partitioning of trace elements between crystals and melts. *Earth and Planetary Science Letters* **210**, 383-397.
- Bobrievich, A. P., Smirnov, G. I. & Sobolev, V. S. (1960). On the mineralogy of pyroxene-disthen rock (grospydite) from the kimberlites of Yakutia. *Geologiya i Geofizika* **3**, 51-60 (in Russian).
- Bodinier, J. L., Vasseur, G., Vernières, J., Dupuy, C. & Fabriès, J. (1990). Mechanisms of mantle metasomatism: geochemical evidence from the Lherz orogenic peridotite. *Journal of Petrology* **31**, 597-628.
- Boyd, F. R. (1989). Compositional distinction between oceanic and cratonic lithosphere. *Earth and Planetary Science Letters* **96**, 15-26.
- Boyd, F. R., Pokhilenko, N. P., Pearson, D. G., Mertzman, S. A., Sobolev, N.V. & Finger, L.W. (1997). Composition of the Siberian cratonic mantle: evidence from Udachnaya peridotite xenoliths. *Contributions to Mineralogy and Petrology* **128**, 228-246.
- Brett, R. C., Russell, J. K. & Moss, S. (2009). Origin of olivine in kimberlite: Phenocryst or Imposter? *Lithos* **112**, 201-212.
- Burgess, S. R. & Harte, B. (1999). Tracing lithosphere evolution through the analysis of heterogeneous G9/G10 garnet in peridotite xenoliths, I: Major element chemistry. In:

Gurney, J. J., Gurney, J. L., Pascoe, M. D. & Richardson, S. H. (eds) *Proceedings of the 7th Kimberlite Conference (Dawson volume)*. Cape Town: Red Roof Design, 66-80.

- Burgess, S. R. & Harte, B. (2004). Tracing lithosphere evolution through the analysis of heterogeneous G9-G10 garnets in peridotite xenoliths, II: REE chemistry. *Journal of Petrology* **45**, 609-634.
- Canil, D. (1999). The Ni-in-garnet geothermometer: calibration at natural abundances. *Contributions to Mineralogy and Petrology* **136**, 240-246.
- Crank, J. (1975). *The mathematics of diffusion, 2nd edition*. Oxford: Clarendon Press.
- Davis, G. L., Sobolev, N. V. & Kharkiv, A. D. (1980). New data on the age of Yakutian kimberlites obtained by the U-Pb method on zircons. *Doklady Akademii Nauk SSSR* **254**, 175-179 (in Russian).
- Dawson, J. B. (1980). *Kimberlites and their xenoliths*. Berlin: Springer-Verlag.
- Dawson, J. B. (1984). Contrasting types of upper mantle metasomatism. In: Kornprobst, J. (ed.) *Kimberlites II. The Mantle and Crust-Mantle Relationships*. Amsterdam: Elsevier, 289-294.
- Dick, H. J. B. & Natland, J. H. (1996). Late-stage melt evolution and transport in the shallow mantle beneath the East Pacific Rise. In: Mevel, C., Gillis, K. M., Allan, J. F. & Meyer, P. S. (eds.) *Proceedings of the Ocean Drilling Program, Scientific Results, 147*. College Station, TX: Ocean Drilling Program, 103-134.
- Efimova, E. S. & Sobolev, N. V. (1977). Abundance of crystalline inclusions in Yakutian diamonds. *Doklady Akademii Nauk SSSR* **237**, 1475-1478 (in Russian).
- Egorov, K. N., Bogdanov, G. V. & Paradina, L. F. (1992). Chemical evolution of clinopyroxene from the Zagadochnaya kimberlite pipe and their specific genesis. *Zapiski Vserossijskogo Mineralogicheskogo Obshchestva* **121**, 88-97 (in Russian).
- Erlank, A. J. & Rickard, R. S. (1977). Potassic richterite bearing peridotites from kimberlite and the evidence they provide for upper mantle metasomatism. *Extended Abstracts of the 2nd International Kimberlite Conference*. Santa Fe, USA.
- Erlank, A. J., Waters, F. G., Hawkesworth, C., J., Haggerty, S. E., Allsopp, H. L., Rickard, R. S. & Menzies, M. (1987). Evidence for mantle metasomatism in peridotite nodules from the Kimberley pipes, South Africa. In: Menzies, M. & Hawkesworth, C. J. (eds) *Mantle metasomatism*. New York; Academic, 221-311.
- Fedortchouk, Y., Canil, D. & Carlson, J.A. (2005). Dissolution forms in Lac de Gras diamonds and their relationship to the temperature and redox state of kimberlite magma. *Contributions to Mineralogy and Petrology* **150**, 54–69.
- Field, S.W. (2008). Diffusion, discontinuous precipitation, metamorphism, and metasomatism: the complex history of South African upper-mantle symplectites. *American Mineralogist* **93**, 618-631.
- Foley, S. F. (2008). Rejuvenation and erosion of the cratonic lithosphere. *Nature Geoscience* **1**, 503-510.
- Ganguly, J. (2010). Cation diffusion kinetics in aluminosilicate garnets and geological applications. *Reviews in Mineralogy & Geochemistry* **72**, 559-601.
- Ganguly, J., Cheng, W. & Chakraborty, S. (1998). Cation diffusion in aluminosilicate garnets: experimental determination in pyrope-almandine diffusion couples. *Contributions to Mineralogy and Petrology* **131**, 171-180.
- Gibson, S. A., Malarkey, J. & Day, A. A. (2008). Melt Depletion and Enrichment beneath the Western Kaapvaal Craton: Evidence from Finsch Peridotite Xenoliths. *Journal of Petrology* **49**, 1817-1852.

- Green, T. H., Blundy, J. D., Adam, J. & Yaxley, G. M. (2000). SIMS determination of trace element partition coefficients between garnet, clinopyroxene and hydrous basaltic liquids at 2–7.5 GPa and 1080–1200 °C. *Lithos* **53**, 165-187.
- Grégoire, M., Lorand, J. P., O'Reilly, S. Y. & Cottin, J. Y. (2000). Armacolite-bearing, Ti-rich metasomatic assemblages in harzburgitic xenoliths from the Kerguelen Islands: Implications for the oceanic mantle budget of high-field strength elements. *Geochimica et Cosmochimica Acta* **64**, 673-694.
- Grégoire, M., Bell. D.R. & Le Roex, A.P. (2002). Trace element geochemistry of phlogopite-rich mafic mantle xenoliths: their classification and their relationship to phlogopite-bearing peridotites and kimberlites revisited. *Contributions to Mineralogy and Petrology* **142**, 603-625.
- Grégoire, M., Bell, D. R. & Le Roex, A. P. (2003). Garnet lherzolites from the Kaapvaal Craton (South Africa): trace element evidence for a metasomatic history. *Journal of Petrology* **44**, 629-657.
- Griffin, W. L., O'Reilly, S. Y., Abe, N., Aulbach, S., Davies, R. M., Pearson, N. J., Doyle, B. J. & Kivi, K. (2003). The origin and evolution of Archean lithospheric mantle. *Precambrian Research* **127**,19-41.
- Griffin, W. L., Kaminsky, F. V., Ryan, C. G., O'Reilly, S. Y., Win, T. T. & Ilupin, I. P.(1996). Thermal state and composition of the lithospheric mantle beneath the Daldyn kimberlite field, Yakutia. *Tectonophysics* **262**, 19-33.
- Griffin, W. L., Shee, S. R., Ryan, C. G., Win, T. T. & Wyatt, B. A. (1999a). Harzburgite to lherzolite and back again: metasomatic processes in ultramafic xenoliths from the Wesselton kimberlite, Kimberley, South Africa. *Contributions to Mineralogy and Petrology* **134**, 232- 250.
- Griffin, W. L., Ryan, C. G., Kaminsky, F. V., O'Reilly, S. Y., Natapov, L. M., Win, T. T., Kinny, P. D., Ilupin, I. P. & (1999b). The Siberian lithosphere traverse. Mantle terranes and the assembly of the Siberian craton. *Tectonophysics* **310**, 1-35.
- Griffin, W. L., Fisher, N. I., Friedman, J. H., O'Reilly, S. Y. & Ryan, C. G. (2002). Cr-pyrope garnets in the lithospheric mantle 2. Compositional populations and their distribution in time and space. Geochemistry Geophysics Geosystems **3**, doi:10.1029/2002GC000298.
- Griffin, W. L., O'Reilly, S. Y., Abe, N., Aulbach, S., Davies, R. M., Pearson, N. J., Doyle, B. J. & Kivi, K. (2003). The origin and evolution of Archean lithospheric mantle. *Precambrian Research* **127**, 19-41.
- Grütter, H. S., Gurney, J. J., Menzies, A. H. & Winter, F. (2004). An updated classification scheme for mantle-derived garnet, for use by diamond explorers. *Lithos* **77**, 841-857.
- Grütter, H. S., Latti, D. & Menzies, A. (2006). Cr-saturation arrays in concentrate garnet compositions from kimberlite and their use in mantle barometry. *Journal of Petrology* **47**, 801-820.
- Gurney, J. J. & Harte, B. (1980). Chemical variations in upper mantle nodules from southern African kimberlites. *Philosophical Transactions of the Royal Society of London, Series A* **297**, 273-293.
- Haggerty, S. E. (1983). The mineral chemistry of new titanates from the Jagersfontein kimberlite, South Africa, implications for metasomatism in the upper mantle. *Geochimica et Cosmochimica Acta* **47**, 1833-1854.
- Haggerty, S. E., Smyth, J. R., Erlank, A. J., Rickard, S. & Danchin, R. V. (1983). Lindsleyite (Ba) and mathiasite (K): two new chromium-titanates in the crichtonite series from the upper mantle. *American Mineralogist* **68**, 494-505.

- Hanski, E., Huhma, H., Rastas, P. & Kamenetsky V. S. (2001). The Palaeoproterozoic komatiite-picrite association of Finnish Lapland. *Journal of Petrology* **42**, 855-876.
- Hanson, G. N. & Langmuir, C. H., 1978. Modelling of major elements in mantle-melt systems using trace element approaches. *Geochimica et Cosmochimica Acta* **42**, 725-741.
- Harte, B. (1983). Mantle Peridotites and processes–the kimberlite sample. In: Hawkesworth, C. J. & Norry, M. J. (Eds.) *Continental basalts and mantle xenoliths*. Cheshire: Shiva, 46-91.
- Harte, B., Hunter, R. H. & Kinny, P. D. (1993). Melt geometry, movement and crystallization in relation to mantle dykes, veins and metasomatism. *Philosophical Transactions of the Royal Society of London, Series A* **342**, 1-21.
- Harte, B., Fitzsimons, I. C. W. & Kinny, P. D. (1996). Clinopyroxene–garnet trace element partition coefficients for mantle peridotite and melt assemblages. *V. M. Goldschmidt Conference, Journal of Conference Abstracts*. Heidelberg.
- Hauri, E. H., Wagner, T. P. & Grove, T. L. (1994). Experimental and natural partitioning of Th, U, Pb and other trace elements between garnet, clinopyroxene and basaltic melts. *Chemical Geology* **117**, 149-166.
- Hawthorne, F. C. & Oberti, R. (2007). Classification of the amphiboles. *Reviews in Mineralogy and Geochemistry* **67**, 55-88.
- Hertogen, J. & Gijbels, R. (1976). Calculation of trace element fractionation during partial melting. *Geochimica et Cosmochimica Acta* **40**, 313-322.
- Hoal, K. E. O., Hoal, B. G., Erlank, A. J. & Shimizu, N. (1994). Metasomatism of the mantle lithosphere recorded by rare earth elements in garnets. *Earth and Planetary Science Letters* **126**, 303-313.
- Ionov, D. & Harmer, R. E. (2002). Trace element distribution in calcite–dolomite carbonatites from Spitskop: inferences for differentiation of carbonatite magmas and the origin of carbonates in mantle xenoliths. *Earth and Planetary Science Letters* **198**, 495-510.
- Ionov, D. A., Bodinier, J.-L., Mukasa, S. B. & Zanetti, A. (2002) Mechanisms and sources of mantle metasomatism: major and trace element compositions of peridotite xenoliths from Spitsbergen in the context of numerical modelling. *Journal of Petrology* **43**, 2219-2259.
- Ionov, D. A., Chanefo, I. & Bodinier, J. -L. (2005). Origin of Fe-rich lherzolites and wehrlites from Tok, SE Siberia by reactive melt percolation in refractory mantle peridotites. *Contributions to Mineralogy and Petrology* **150**, 335-353.
- Ionov, D. A., Chazot, G., Chauvel, C., Merlet, C. & Bodinier J. –L. (2006). Trace element distribution in peridotite xenoliths from Tok, SE Siberian craton: A record of pervasive, multi-stage metasomatism in shallow refractory mantle. *Geochimica et Cosmochimica Acta* **70**, 1231-1260.
- Ionov, D. A., Doucet, L. S. & Ashchepkov, I. V. (2010). Composition of the Lithospheric Mantle in the Siberian Craton: New Constraints from Fresh Peridotites in the Udachnaya-East Kimberlite. *Journal of Petrology* **51**, 2177-2210.
- Ivanic, T. J., Harte, B. & Gurney, J. J. (2012). Metamorphic re-equilibration and metasomatism of highly chromian, garnet-rich peridotitic xenoliths from South African kimberlites. *Contributions to Mineralogy and Petrology* **164**, 505-520.
- Johnson (1998). Experimental determination of partition coefficients for rare earth and high-field-strength elements between clinopyroxene, garnet, and basaltic melt at high pressures. *Contributions to Mineralogy and Petrology* **133**, 60-68.

- Kalfoun, F., Ionov, D. A., Merlet, C., 2002. HFSE residence and Nb/Ta ratios in metasomatised, rutile-bearing mantle peridotites. *Earth and Planetary Science Letters* **199**, 49-65.
- Kamenetsky, M. B., Sobolev, A. V., Kamenetsky, V. S., Maas, R., Danyushevsky, L. V., Thomas, R., Pokhilenko, N. P., Sobolev, N. V. (2004). Kimberlite melts rich in alkali chlorides and carbonates: a potent metasomatic agent in the mantle. *Geology* **32**, 845-848.
- Kamenetsky,V. S., Kamenetsky, M. B., Sobolev, A.V., Golovin, A.V., Demouchy, S., Faure, K., Sharygin, V. V. & Kuzmin, D.V. (2008). Olivine in the Udachnaya-East Kimberlite (Yakutia, Russia): types, compositions and origins. *Journal of Petrology* **49**, 823-839.
- Kamenetsky,V. S., Kamenetsky, M. B., Sobolev, A.V., Golovin, A.V., Sharygin,V.V., Pokhilenko, N. P. & Sobolev, N.V. (2009). Can pyroxenes be liquidus minerals in the kimberlite magma? *Lithos* **112S**, 213-222.
- Kinny, P. D., Griffin, B. J., Heaman, L. M., Brakhfogel, F. F. & Spetsius, Z. V. (1997). SHRIMP U–Pb ages of perovskite from Yakutian kimberlites. *Russian Geology and Geophysics* **38**, 97-105.
- Konzett, J., Hexiong, Y. & Frost, D. J. (2005). Phase relations and stability of magnetoplumbite- and crichtonite-series phases under upper-mantle P–T Conditions: an Experimental Study to 15 GPa with Implications for LILE Metasomatism in the Lithospheric Mantle. *Journal of Petrology* **46**, 749-781.
- Kopylova, M. G., Russell, J. K. & Cookenboo, H. (1999). Petrology of peridotite and pyroxenite xenoliths from the Jericho kimberlite: implications for the thermal state of the mantle beneath the Slave craton, Northern Canada. *Journal of Petrology* **40**, 79-104.
- Kopylova, M. G., Nowell, G. M., Pearson, D. G. & Markovic, G. (2009). Crystallization of megacrysts from protokimberlitic fluids: Geochemical evidence from high-Cr megacrysts in the Jericho kimberlite. *Lithos* **112S**, 284-295.
- Kostrovitsky, S. I. & de Bruin, D. (2004). Chromium assemblage of minerals in micaceous kimberlites of Yakutian province. *Russian Geology and Geophysics* **45**, 565–576.
- Kostrovitsky, S. I., Morikiyo, T., Serov, I. V., Yakovlev, D. A. & Amirzhanov, A.A. (2007). Isotope-geochemical systematics of kimberlites and related rocks from the Siberian Platform. *Russian Geology and geophysics* **48**, 272-290.
- Kostrovitsky, S. I., Alymova, N. V., Yakovlev, D. A., Solov'eva, L. V. & Gornova, M. A. (2008). Origin of garnet megacrysts from kimberlites. *Doklady Earth Sciences* **420**, 636-640.
- Lazarov, M., Brey, G. P. & Weyer, S. (2012). Evolution of the South African mantle – a case study of garnet peridotites from the Finsch diamond mine (Kaapvaal craton); Part 1: Inter-mineral trace element and isotopic equilibrium. *Lithos*, doi: 10.1016/j.lithos.2012.07.007.
- Le Roux, V., Bodinier, J. L., Tommasi, A., Alard, O., Dautria, J. M., Vauchez, A. & Riches, A. J. V. (2007). The Lherz spinel lherzolite: refertilized rather than pristine mantle. *Earth and Planetary Science Letters* **259**, 599-612.
- Lenoir, X., Garrido, C. J., Bodinier, J., Dautria J. & Gervilla, F. (2001). The recrystallization front of the Ronda Peridotite: evidence for melting and thermal erosion of subcontinental lithospheric mantle beneath the Alboran Basin. *Journal of Petrology* **42**, 141-158.
- Lenoir, X., Garrido, C. J., Bodinier, J. -L.,Dautria, J. -M. & Gervilla, F. (1999). Origin of petrological and geochemical zoning in the Ronda peridotite via thermal and chemical

erosion of subcontinental lithospheric mantle by upwelling asthenosphere. *Ofioliti* **24**, 125-126.

- Maas, R., Kamenetsky, M. B., Sobolev, A. V., Kamenetsky, V. S., Sobolev, N. V. (2005). Sr, Nd and Pb isotope evidence for a mantle origin of alkali chlorides and carbonates in the Udachnaya kimberlite, Siberia. *Geology* **33**, 549-552.
- Malkovets, V. G., Griffin,W. L., O'Reilly, S. Y. & Wood, B. J. (2007). Diamond, subcalcic garnet, and mantle metasomatism: Kimberlite sampling patterns define the link. *Geology* **35**, 339-342.
- Matthews, M., Harte, B. & Prior, D. (1992). Mantle garnets: a cracking yarn. *Geochimica et Cosmochimica Acta* **56**, 2633-2642.
- McDonough,W. F. & Sun, S. (1995). The composition of the Earth. *Chemical Geology* **120**, 223-253.
- Menzies, M. A., Rogers, N., Tindle, A. & Hawkesworth, C. J. (1987). Metasomatic and enrichment processes in lithospheric peridotites, an effect of asthenosphere–lithosphere interaction. In: Menzies, M. A. & Hawkesworth, C.J. (Eds.) *Mantle Metasomatism*. London: Academic Press, 313-361.
- Moore, A. & Belousova, E. (2005). Crystallization of Cr-poor and Cr-rich megacryst suites from the host kimberlite magma: implications for mantle structure and the generation of kimberlite magmas. *Contributions to Mineralogy and Petrology* **149**, 462-481.
- Niida, K. & Green, D. H. (1999). Stability and chemical composition of pargasitic amphibole in MORB pyrolite under upper mantle conditions. *Contributions to Mineralogy and Petrology* **135**, 18-40.
- Nimis, P. & Grütter, H. (2010). Internally consistent geothermometers for garnet peridotites and pyroxenites. *Contributions to Mineralogy and Petrology* **159**, 411-427.
- Nimis, P. & Taylor, W.R. (2000). Single clinopyroxene thermobarometry for garnet peridotites. Part I. Calibration and testing of a Cr-in-Cpx barometer and an enstatite-in-Cpx thermometer. *Contributions to Mineralogy and Petrology* **139**, 541-554.
- Nimis, P., Zanetti, A., Dencker, I. & Sobolev, N. V. (2009). Major and trace element composition of chromian diopsides from the Zagadochnaya kimberlite (Yakutia, Russia): Metasomatic processes, thermobarometry and diamond potential. *Lithos* **112**, 397-412.
- Nixon, P. H., van Calsteren, P. W. C., Boyd, F. R. & Hawkesworth, C. J. (1987). Harzburgites with garnets of diamond facies from southern African kimberlites. In: Nixon, P. H. (ed.) *Mantle Xenoliths*. NewYork: JohnWiley, 523-534.
- Pearson, D. G., Canil, D., Shirey, S. B., 2003. Mantle samples included in volcanic rocks: xenoliths and diamonds. In: Carlson R. W. (ed.) *Treatise in geochemistry, volume 2*. Amsterdam: Elsevier, 171-275.
- Perchuk, A. L., Burchard, M., Schertl, H. P., Maresch, W. V., Gerya, T. V., Bernhardt, H. J. & Vidal, O. (2009). Diffusion of divalent cations in garnet. *Contributions to Mineralogy and Petrology* **157**, 573-592.
- Piccardo, G. B., Zanetti, A. & Müntener, O. (2007). Melt/peridotite interaction in the Southern Lanzo peridotite: Field, tectural and geochemical evidence. *Lithos* **94**, 181-209.
- Pokhilenko, N. P., Sobolev, N. V., Kuligin, S. S. & Shimizu, N. (1999). Peculiarities of distribution of pyroxenite paragenesis garnets in Yakutian kimberlites and some aspects of the evolution of the Siberian craton lithospheric mantle. In: Gurney, J. J., Gurney, J. L., Pascoe, M. D. & Richardson, S. H. (eds) *Proceedings of the 7th International Kimberlite Conference, Vol. 2*. Cape Town: Red Roof Design, 689-698.

- Putnis, A. (2009). Mineral replacement reactions. *Reviews in Mineralogy and Geochemistry* **70**, 87-124.
- Raffone, N., Chazot, G., Pin, C., Vannucci, R. & Zanetti A. (2009). Metasomatism in the lithospheric mantle beneath Middel Atlas (Morocco) and the origin of Fe- and Mg-rich wehrlites. *Journal of Petrology* **50**, 197-249.
- Rivalenti, G., Zanetti, A., Mazzucchelli, M., Vannucci, R. & Cingolani, C. A. (2004). Equivocal carbonatite markers in the mantle xenoliths of the Patagonia backarc: the Gobernador Gregores case (Santa Cruz Province, Argentina). *Contributions to Mineralogy and Petrology* **147**, 647-670.
- Rivalenti, G., Mazzucchelli, M., Zanetti, A., Vannucci, R., Bollinger, C., Hémond, C., Bertotto, G.W. (2007a). Xenoliths from Cerro de los Chenques (Patagonia): An example of slab-related metasomatism in the backarc lithospheric mantle. *Lithos* **99**, 45-67.
- Rivalenti, G., Zanetti, A., Girardi, V. A. V., Mazzucchelli, M., Tassinari, C. C. G. & Bertotto, G. W. (2007b). The effect of the Fernando de Noronha plume on the mantle lithosphere in north-eastern Brazil. *Lithos* **94**, 111-131.
- Roden, M. F., Lazko, E. E. & Jagoutz, E. (1999). The role of garnet pyroxenites in the Siberian lithosphere: evidence from the Mir kimberlite. In: Gurney, J. J., Gurney, J. L., Pascoe, M. D. & Richardson, S. H. (eds) *Proceedings of the 7th International Kimberlite Conference, Vol. 2*. Cape Town: Red Roof Design, 714-720.
- Roeder, P. L. & Schulze, D. J. (2008). Crystallization of groundmass Spinel in kimberlite. *Journal of Petrology* **49**, 1473-1495.
- Russel, J. K., Porritt, L. A., Lavallèe, Y. & Dingwell, D. B. (2012). Kimberlite ascent by assimilation-fuelled buoyancy. *Nature* **481**, 352-356.
- Ryan, C. G, Griffin, W. L. & Pearson, N. J. (1996). Garnet geotherms: pressure-temperature data from Cr-pyrope garnet xenocrysts in volcanic rocks. *Journal of Geophysical Research* **101**, 5611-5626.
- Salters, V. J. M., Longhi, J. E. & Bizimis, M. 2002. Near mantle solidus trace element partitioning at pressures up to 3.4 GPa. *Geochemistry Geophysics Geosystems* **3**, doi: 10.1029/2001GC000148.
- Schäfer, F. N. & Foley, S.F. (2002). The effect of crystal orientation on the wetting behaviour of silicate melts on the surfaces of spinel peridotite minerals. *Contributions to Mineralogy and Petrology* **143**, 254-261.
- Schulze, D. J. (2003). A classification scheme for mantle-derived garnets in kimberlite: a tool for investigating the mantle and exploring for diamonds. *Lithos* **71**, 195-213.
- Shimizu, N. & Richardson, S. H. (1987). Trace element abundance patterns of garnet inclusions in peridotite suite diamonds. *Geochimica et Cosmochimica Acta* **51**, 755-758.
- Shimizu, N., Pokhilenko, N. P., Boyd, F. R. & Pearson, D. G. (1997a). Geochemical characteristics of mantle xenoliths from the Udachnaya kimberlite pipe. *Russian Geology and Geophysics* **38**, 205-217.
- Shimizu, N., Sobolev, N. V. & Yefimova, E. S. (1997b). Chemical heterogeneity of garnet inclusions and juvenility of peridotite diamonds from Siberia. *Russian Geology and Geophysics* **38**, 356-372.
- Simon, N. S. C., Irvine, G. J., Davies, G. R., Pearson, D. G. & Carlson, R. W. (2003). The origin of garnet and clinopyroxene in 'depleted' Kaapvaal peridotites. *Lithos* **71** 289-322.
- Simon, N. S. C., Carlson R. W., Pearson, D. G. & Davies, G. R. (2007). The origin and evolution of the Kaapvaal cratonic lithospheric mantle. *Journal of Petrology* **48**, 589-625.

- Sobolev, N. V. (1971). On mineralogical criteria for the presence of diamonds in kimberlites. *Geologiya I Geofizika* **3**, 70-79.
- Sobolev, N. V. (1977). *Deep-Seated Inclusions in Kimberlites and the Problem of the Composition of the Upper Mantle*. Washington: American Geophysical Union.
- Sobolev, N. V., Kuznetsova, I. K. & Zyuzin, N. I. (1968). Petrology of grospydite xenoliths from the Zagadochnaya kimberlite pipe in Yakutia. *Journal of Petrology* **9**, 253-280.
- Sobolev N. V., Lavrent'ev Y. G., Pospelova, L. N. & Sobolev, E. V. (1969). Chrome pyropes from Yakutian diamonds (in Russian). *Doklady Akademii Nauk SSSR* **189**, 162-165.
- Sobolev, N. V., Bartoshinsky, Z. V., Yefimova, E. S., Lavrent′ev, Y. G. & Pospelova, L. N. (1970). Olivine-garnet-chrome diopside assemblage from Yakutian diamond. *Doklady Akademii Nauk SSSR* **192**, 1349-1352 (in Russian).
- Sobolev, N. V., Lavrent'ev, Y. G., Pokhilenko, N. P. & Usova, L. V. (1973). Chrome-rich garnets from the kimberlites of Yakutia and their parageneses. *Contributions to Mineralogy and Petrology* **40**, 39-52.
- Sobolev, N. V., Kaminsky, F. V., Griffin, W. L., Yefimova, E. S., Win, T. T. & Botkunov, A. I. (1997). Mineral inclusions in diamonds from the Sputnik kimberlite pipe, Yakutia. *Lithos* **39**, 135-157.
- Sobolev, N. V., Logvinova, A. M., Efimova, E. S. (2009a). Syngenetic phlogopite inclusions in kimberlite-hosted diamonds: implications for role of volatiles in diamond formation. *Russian Geology and Geophysics* **50**, 1234-1248.
- Sobolev, N. V, Logvinova, A. M., Zedgenizov, D. A., Pokhilenko, N. P., Malygina, E. V., Kuzmin, D. V. & Sobolev, A.V. (2009b). Petrogenetic significance of minor elements in olivines from diamonds and peridotite xenoliths from kimberlites of Yakutia. *Lithos* **112S**, 701-713.
- Sobolev, N.V., Logvinova, A.M., Lavrent'ev, Yu.G., Karmanov, N.S., Usova, L.V., Koz'menko, O.A. & Ragozin, A.L., (2011). Nb-Rutile from Eclogite Microxenolith of the Zagadochnaya Kimberlite Pipe. *Doklady Earth Sciences* **439**, 970-973.
- Solov'eva, L. V. (2007). Reworking of the lithospheric mantle of the Siberian Craton by reduced fluids in the Middle Paleozoic Kimberlite Event: geochemical consequences. *Doklady Earth Science* **413**, 238-243.
- Solov'eva, L. V., Lavrent'ev, Y. G., Egorov, K. N., Kostrovitsky, S. I., Korolyuk, V. N. & Suvorova, L.F. (2008). The genetic relationship of the deformed peridotites and garnet megacrysts from kimberlites with asthenospheric melts. *Russian Geology and Geophysics* **49**, 207-224.
- Solov'eva L. V., Yasnygina, T. A., Korolyuk, V. N. & Egorov, K. N. (2010). Geochemical Evolution of Deep Fluids in the Mantle Lithosphere of the Siberian Craton during the Middle Paleozoic Kimberlite Cycle. *Doklady Earth Science* **434**, 1330-1336.
- Solovjeva, L. V., Egorov, K. N., Markova, M. E., Kharkiv, A. D., Popolitov, K. E. & Barankevich, V. G. (1997). Mantle metasomatism and melting in deep-seated xenoliths from the Udachnaya pipe, their possible relationship with diamond and kimberlite formation. *Russian Geology and Geophysics* **38**, 182-204.
- Stachel, T., Viljoen, K. S., Brey, G. & Harris, J. W. (1998). Metasomatic processes in lherzolitic and harzburgitic domains of diamondiferous lithospheric mantle: REE in garnets from xenoliths and inclusions in diamonds. *Earth and Planetary Science Letters* **159**, 1-12.

- Stachel, T., Aulbach, S., Brey, G. P., Harris, J. W., Leost, I., Tappert, R. & Viljoen, K. S. (2004). The trace element composition of silicate inclusions in diamonds: a review. *Lithos* **77**, 1-19.
- Tomilenko, A. A., Kovyazin, S. V., Pokhilenko, L. N. & Sobolev, N. V. (2011). Silicate Globules in Kyanite from Grospydites of the Zagadochnaya Kimberlite Pipe, Yakutia: The Problem of the Origin. *Doklady Earth Sciences* **436**, 98-101.
- Toramaru, A. & Fuji, N. (1986). Connectivity of melt phase in partially molten peridotite. *Journal of Geophysical Research* **91**, 9239-9252.
- Turkin, A. I. & Sobolev, N. V. (2009). Pyrope–knorringite garnets: overview of experimental data and natural paragenesis. *Russian Geology and Geophysics* **50**, 1169-1182.
- Van Westrenen, W. & Draper, D.S. (2007). Quantifying garnet-melt trace element partitioning using lattice-strain theory: new crystal-chemical and thermodynamic constraints. *Contributions to Mineralogy and Petrology* **154**, 717-730.
- Vernières, J., Godard, M., Bodinier, J. -L. (1997). A plate model for the simulation of trace element fractionation during partial melting and magma transport in the Earth's upper mantle. *Journal of Geophysical Research* **102**, 24771-24784.
- Vielzeuf, D., Baronnet, A., Perchuk, A. L., Laporte, D. & Baker, M. B. (2007). Calcium diffusivity in alumino-silicate garnets: an experimental and ATEM study. *Contributions to Mineralogy and Petrology* **154**, 153-170.
- Walter, M. J. (1998). Melting of garnet peridotite and the origin of komatiite and depleted lithosphere. *Journal of Petrology* **39**, 29-60.
- Wang, L., Essene, E. J. & Zhang, Y. (1999). Mineral inclusions in pyrope crystals from Garnet Ridge, Arizona, USA: implications for processes in the upper mantle. *Contributions to Mineralogy and Petrology* **135**, 164-178.
- Wilson, L. & Head, J. W. (2007). An integrated model of kimberlite ascent and eruption. *Nature* **447**, 53-57.
- Xu, X., O'Reilly, S. Y., Griffin, W. L. & Zhou, X. (1998). The nature of the Cenozoic lithosphere beneath Nushan, East Central China. In: Flower, M. F. J., Chung, S. L., Lo, C. H. & Lee, T. Y. (eds) *Mantle Dynamics and Plate Interactions in East Asia*. *Geodynamics Series 27*, Washington, D. C: American Geophysical Union, 167-196.
- Zack, T., Foley, S. F. & Jenner, G. A. (1997). A consistent partition coefficient set for clinopyroxene, amphibole and garnet from laser ablation microprobe analysis of garnet pyroxenites from Kakanui, New Zealand. *Neues Jahrbuch für Mineralogie, Abhandlungen* **172**, 23-41.

SUPPLEMENTARY FIGURE 1

Element concentration profile across garnet zoning in sample Z6-10.

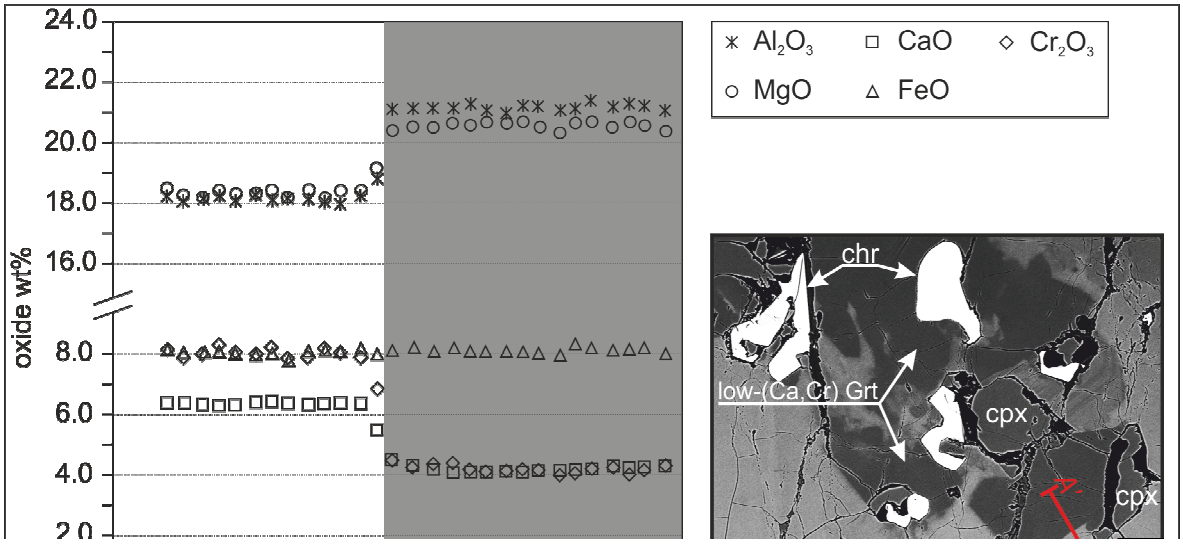

SUPPLEMENTARY FIGURE 2

Element concentration profile in garnet–clinopyroxene microxenolith Z5-15 (Group A).

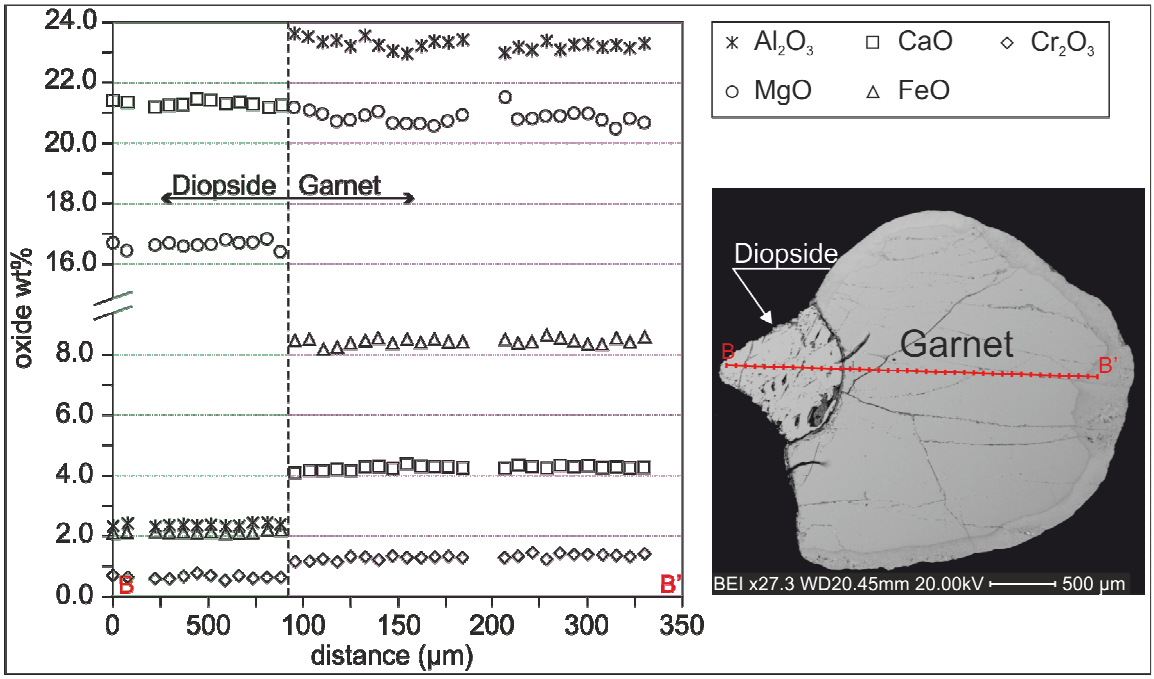

SUPPLEMENTARY TABLE 1

Chemical composition of pyrope grains (< 0.5 mm fraction) randomly selected from the heavy concentrate of the Zagadochnaya kimberlite pipe.

No.	SiO_2	TiO_2	Al_2O_3	Cr_2O_3	FeO	MnO	MgO	CaO	Na_2O	Total
1	41.35	0.06	18.23	6.89	8.02	0.50	18.84	6.34	0.03	100.26
2	41.99	0.33	20.89	3.06	8.42	0.43	20.12	4.57	0.04	99.85
3	41.46	0.36	18.77	5.71	8.57	0.47	19.22	5.38	0.07	100.01
4	42.17	0.25	21.63	2.29	9.02	0.44	20.06	4.44	0.06	100.36
5	42.49	0.18	22.48	1.37	7.33	0.32	21.46	4.41	0.05	100.09
6	42.00	0.10	20.29	4.24	8.42	0.54	20.41	4.33	0.10	100.42
7	41.31	0.30	18.27	5.90	9.12	0.49	17.44	7.19	0.04	100.06
8	41.96	0.13	19.06	5.68	7.62	0.42	19.71	5.51	0.05	100.14
9	42.23	0.01	20.90	3.61	7.49	0.42	19.96	5.56	0.00	100.18
10	41.76	0.25	19.62	4.87	8.22	0.46	20.12	5.12	0.07	100.48
11	41.67	0.22	18.28	6.53	8.00	0.47	18.82	6.21	0.07	100.26
12	41.36	0.12	17.45	7.79	7.82	0.49	18.22	6.66	0.02	99.91
13	42.36	0.14	22.01	1.87	9.07	0.42	20.18	4.46	0.03	100.54
14	41.75	0.17	19.60	4.70	8.57	0.51	19.19	5.63	0.01	100.13
15	42.19	0.29	20.94	3.17	8.40	0.46	20.57	4.50	0.07	100.57
16	42.32	0.00	20.75	3.83	7.79	0.42	19.95	5.59	0.00	100.64
17	42.01	0.22	20.59	3.70	7.98	0.45	20.06	4.88	0.06	99.93
18	41.32	0.29	17.96	6.25	8.26	0.55	18.54	6.44	0.04	99.64
19	41.81	0.15	19.13	5.27	8.10	0.51	19.56	5.19	0.07	99.81
20	41.67	0.13	18.27	6.84	7.64	0.46	19.53	5.35	0.03	99.91
21	42.17	0.16	21.54	2.30	8.54	0.42	20.30	4.47	0.03	99.93
22	41.61	0.20	19.16	5.21	7.87	0.47	19.76	5.19	0.06	99.53
23	40.35	0.07	19.03	4.71	13.14	0.18	12.46	10.33	0.03	100.29
24	42.14	0.37	20.70	3.38	8.41	0.45	20.00	4.70	0.08	100.23
25	41.72	0.29	19.13	5.38	7.81	0.46	19.87	5.16	0.07	99.89
26	41.66	0.07	18.85	5.89	8.25	0.49	19.08	5.71	0.06	100.05
27	42.33	0.00	21.21	3.30	7.37	0.35	19.92	5.55	0.02	100.04
28	41.98	0.25	20.03	4.35	8.21	0.49	20.03	5.06	0.04	100.45
29	41.94	0.02	20.11	4.58	7.68	0.46	19.58	5.70	0.01	100.07
30	41.81	0.23	20.06	4.29	7.98	0.45	19.75	4.99	0.04	99.61
31	41.60	0.15	20.17	4.01	8.32	0.46	19.42	5.16	0.04	99.34
32	41.82	0.19	19.68	4.65	8.06	0.48	19.53	5.20	0.06	99.67
33	41.97	0.26	21.51	2.28	8.51	0.41	20.15	4.63	0.07	99.79
34	41.95	0.00	20.61	4.10	7.60	0.40	19.92	5.59	0.00	100.17
35	42.03	0.17	19.92	4.84	7.04	0.34	21.24	4.41	0.05	100.03
36	41.11	0.17	17.66	7.18	7.98	0.50	18.77	6.29	0.04	99.69
37	42.28	0.30	21.12	2.82	8.59	0.45	20.20	4.58	0.11	100.46
38	41.39	0.31	19.31	4.65	9.21	0.53	18.68	5.47	0.07	99.62
39	40.75	1.09	15.42	7.47	9.80	0.46	17.41	7.09	0.12	99.61
40	41.33	0.01	18.12	6.98	7.84	0.50	18.46	6.82	0.03	100.08
41	41.62	0.24	19.14	5.37	7.95	0.47	20.00	4.93	0.09	99.81
42	41.64	0.02	18.68	6.37	7.27	0.39	19.37	6.42	0.02	100.18
43	42.04	0.28	20.84	3.06	8.51	0.43	20.08	4.75	0.06	100.05
44	41.64	0.25	18.50	6.21	8.53	0.50	18.85	5.61	0.02	100.10
45	42.17	0.18	22.23	1.29	8.68	0.38	20.77	4.13	0.03	99.85
46	41.43	0.21	17.67	7.34	7.57	0.49	19.42	5.60	0.06	99.79
47	41.74	0.28	19.32	5.05	8.07	0.48	19.60	5.38	0.06	99.97

No.	SiO_2	TiO_2	Al_2O_3	Cr_2O_3	FeO	MnO	MgO	CaO	Na_2O	Total
48	41.75	0.11	19.85	4.59	8.17	0.48	19.69	5.02	0.03	99.69
49	42.20	0.05	20.78	3.88	7.10	0.46	22.11	3.39	0.03	99.99
50	41.74	0.09	19.90	4.59	8.33	0.46	19.74	5.17	0.02	100.04
51	41.05	0.13	17.24	7.86	7.91	0.50	18.59	6.21	0.01	99.49
52	41.79	0.20	19.64	4.80	7.96	0.46	19.79	5.24	0.06	99.94
53	42.13	0.03	21.05	3.20	7.39	0.38	20.24	5.41	0.01	99.84
54	41.99	0.02	19.33	5.56	7.62	0.44	20.10	5.14	0.01	100.20
55	41.54	0.35	18.32	6.10	8.34	0.51	18.61	6.03	0.06	99.86
56	41.63	0.29	19.21	5.27	7.89	0.46	19.45	5.80	0.07	100.08
57	41.67	0.23	20.00	4.25	8.18	0.47	19.78	5.27	0.03	99.87
58	41.55	0.22	18.69	5.99	7.89	0.45	19.73	5.15	0.06	99.71
59	41.26	0.07	17.53	7.65	7.76	0.48	19.10	5.90	0.03	99.77
60	41.78	0.13	19.31	5.48	7.65	0.46	21.09	3.54	0.04	99.48
61	41.55	0.27	18.67	5.92	8.20	0.48	19.02	5.85	0.06	100.01
62	41.90	0.24	20.68	3.52	8.35	0.47	20.23	4.62	0.04	100.05
63	41.29	0.12	18.75	6.10	8.12	0.50	19.57	5.27	0.04	99.77
64	41.69	0.26	20.33	3.93	8.06	0.46	20.01	4.95	0.07	99.76
65	41.89	0.31	19.67	4.74	8.14	0.48	20.11	4.71	0.06	100.10
66	41.75	0.02	20.51	4.13	7.71	0.40	19.74	5.81	0.00	100.05
67	42.23	0.23	21.99	1.75	9.19	0.42	20.12	4.47	0.05	100.44
68	41.46	0.04	19.25	5.80	7.65	0.46	19.42	5.80	0.01	99.88
69	41.21	0.24	17.63	7.14	8.56	0.52	17.87	6.54	0.06	99.76
70	41.57	0.01	18.92	6.06	7.18	0.39	19.91	5.72	0.01	99.75
71	41.91	0.05	19.89	4.86	7.71	0.44	19.69	5.64	0.02	100.21
72	41.87	0.35	19.72	4.39	7.97	0.46	19.94	5.00	0.05	99.75
73	41.58	0.23	19.15	5.46	8.17	0.47	19.43	5.55	0.05	100.09
74	41.50	0.02	18.93	5.97	7.41	0.43	19.07	6.39	0.03	99.74
75	41.75	0.02	20.59	3.81	7.75	0.39	19.75	5.72	0.00	99.78
76	41.50	0.01	18.10	6.91	7.49	0.45	18.70	6.60	0.02	99.77
77	42.18	0.00	21.00	3.42	7.51	0.40	19.88	5.54	0.01	99.93
78	41.70	0.07	19.63	5.08	7.71	0.50	20.39	4.56	0.06	99.69
79	41.65	0.10	18.06	7.14	7.87	0.49	18.76	6.17	0.03	100.29
80	42.36	0.28	21.47	2.42	8.68	0.43	20.23	4.58	0.05	100.51
81	42.20	0.22	20.81	3.30	8.46	0.45	19.95	4.89	0.05	100.33
82	41.92	0.02	18.82	6.35	7.65	0.47	18.79	6.44	0.04	100.51
83	41.84	0.21	19.32	5.16	8.15	0.49	19.56	5.00	0.03	99.75
84	42.16	0.19	20.17	4.19	8.25	0.47	19.70	5.28	0.02	100.43
85	41.21	0.34	17.94	6.45	8.45	0.52	18.59	6.14	0.07	99.70
86	40.86	0.35	15.62	9.24	8.19	0.50	18.54	6.37	0.08	99.75
87	41.29	0.22	17.66	6.96	8.51	0.56	18.29	6.15	0.05	99.69
88	41.77	0.29	18.61	6.15	7.62	0.44	19.39	5.80	0.07	100.14
89	41.47	0.12	19.08	5.41	8.28	0.47	19.28	5.85	0.05	100.01
90	41.73	0.29	19.05	5.34	8.45	0.49	19.10	5.71	0.03	100.19
91	41.97	0.01	20.18	4.48	7.30	0.41	19.92	5.89	0.00	100.17
92	41.88	0.17	19.33	5.31	8.36	0.51	19.22	5.38	0.04	100.19
93	42.03	0.30	21.22	2.62	8.59	0.44	20.06	4.58	0.07	99.91
94	41.74	0.07	19.15	5.48	8.03	0.49	19.40	5.59	0.07	100.00
95	41.41	0.02	19.03	5.59	7.90	0.50	18.78	6.28	0.01	99.50
96	41.31	0.11	18.04	6.81	8.05	0.52	18.77	6.41	0.02	100.05
97	42.17	0.24	20.28	4.13	7.77	0.44	20.30	4.77	0.06	100.16
98	41.87	0.23	21.95	1.75	9.44	0.44	20.13	4.34	0.05	100.20
99	41.87	0.07	19.52	4.72	8.30	0.45	19.30	5.56	0.02	99.79
100	41.62	0.00	18.84	6.16	7.38	0.46	19.27	5.91	0.03	99.67
101	41.71	0.35	18.99	5.51	8.16	0.47	19.45	5.38	0.08	100.10

No.	SiO_2	TiO_2	Al_2O_3	Cr_2O_3	FeO	MnO	MgO	CaO	Na_2O	Total
102	41.35	0.06	17.40	7.80	7.44	0.48	19.11	6.17	0.02	99.82
103	41.49	0.06	17.51	7.80	7.40	0.46	19.00	6.21	0.02	99.94
104	41.48	0.24	18.92	5.88	8.06	0.47	19.40	5.40	0.05	99.89
105	41.55	0.06	18.58	6.51	7.74	0.48	18.70	6.36	0.00	99.97
106	41.60	0.01	18.27	6.85	7.61	0.49	18.35	6.66	0.00	99.83
107	41.73	0.01	19.33	5.79	7.41	0.43	19.07	6.25	0.02	100.03
108	41.72	0.25	19.87	4.87	8.12	0.49	19.72	5.24	0.04	100.33
109	41.88	0.24	19.71	4.92	7.86	0.47	19.72	5.29	0.04	100.11
110	41.81	0.03	19.51	5.30	8.04	0.50	19.18	5.88	0.01	100.26
111	41.91	0.22	19.86	4.82	7.82	0.45	19.75	5.41	0.05	100.29
112	41.69	0.22	19.23	5.29	8.38	0.48	19.18	5.79	0.03	100.29
113	41.89	0.02	18.95	6.34	7.37	0.41	19.09	6.24	0.00	100.31
114	41.19	0.26	18.42	6.08	8.32	0.52	18.70	6.06	0.06	99.61
115	41.72	0.35	19.96	4.18	8.25	0.48	19.65	5.09	0.05	99.73
116	41.24	0.12	21.61	1.82	13.87	0.39	17.20	3.88	0.07	100.20
117	41.48	0.00	20.14	4.52	7.86	0.46	19.12	5.84	0.00	99.42
118	41.64	0.04	18.92	6.16	7.59	0.41	19.06	6.35	0.03	100.19
119	41.40	0.05	18.53	6.59	7.99	0.48	18.73	6.24	0.00	100.02
120	41.90	0.01	19.70	5.23	7.11	0.39	20.03	5.87	0.00	100.23
121	42.03	0.32	21.53	2.25	8.60	0.43	20.27	4.48	0.08	99.99
122	41.32	0.14	17.34	7.91	7.52	0.48	18.84	6.29	0.04	99.88
123	41.86	0.28	20.37	3.70	8.95	0.49	19.32	5.14	0.05	100.16
124	42.01	0.29	21.31	2.62	8.42	0.42	20.07	4.70	0.07	99.90
125	40.84	0.09	16.60	8.76	8.18	0.55	17.53	7.39	0.04	99.97
126	41.21	0.20	18.26	6.49	8.24	0.50	18.64	6.29	0.05	99.86
127	42.22	0.16	21.84	2.46	7.17	0.35	21.13	4.55	0.04	99.91
128	41.19	0.09	17.79	7.54	7.60	0.44	18.21	7.01	0.00	99.87
129	41.63	0.18	18.83	6.15	8.00	0.52	19.59	5.53	0.04	100.45
130	41.21	0.20	18.60	6.36	7.83	0.49	19.48	5.61	0.06	99.83
131	41.70	0.22	18.80	5.95	8.15	0.48	19.37	5.55	0.06	100.28
132	41.85	0.29	19.90	4.36	8.48	0.50	19.62	5.24	0.06	100.30
133	40.95	0.32	17.11	7.97	8.37	0.56	18.12	6.63	0.08	100.12
134	41.74	0.29	19.60	4.65	8.35	0.47	19.63	5.39	0.05	100.16
135	41.74	0.00	20.45	4.25	8.57	0.51	18.77	5.98	0.02	100.29
136	41.83	0.29	20.03	4.27	8.20	0.44	20.00	4.86	0.06	99.99
137	42.17	0.30	21.21	2.78	8.02	0.41	20.48	4.67	0.03	100.06
138	41.21	0.15	18.30	6.90	7.88	0.48	19.39	5.61	0.05	99.98
139	41.54	0.26	19.34	5.04	8.33	0.47	19.10	5.58	0.07	99.71
140	41.27	0.05	18.30	6.83	7.91	0.47	18.72	6.15	0.02	99.72
141	41.43	0.13	18.18	7.18	7.90	0.48	19.20	5.83	0.02	100.34
142	41.55	0.12	19.29	5.75	8.05	0.47	19.61	5.49	0.01	100.34
143	41.87	0.20	21.01	3.14	8.33	0.46	20.07	4.83	0.05	99.94
144	41.14	0.09	18.67	6.33	7.93	0.48	19.34	5.59	0.02	99.60
145	41.43	0.23	19.28	5.51	8.24	0.48	19.10	5.57	0.04	99.88
146	41.36	0.26	19.49	5.17	7.91	0.46	19.99	5.01	0.06	99.70
147	41.09	0.00	18.27	6.82	7.72	0.47	18.63	6.73	0.00	99.73
148	41.70	0.30	22.05	1.74	9.29	0.42	19.95	4.39	0.07	99.91
149	41.41	0.21	19.30	5.38	8.31	0.47	18.83	6.03	0.03	99.96
150	41.73	0.24	20.61	3.74	7.85	0.43	20.56	4.99	0.07	100.22
151	41.42	0.23	19.59	4.95	8.17	0.46	19.65	5.28	0.06	99.79
152	41.68	0.19	20.98	3.25	8.56	0.47	20.10	4.83	0.06	100.11
153	40.86	0.05	16.88	8.35	7.82	0.50	17.57	7.52	0.01	99.55
154	41.77	0.30	20.28	4.07	8.15	0.47	20.18	4.76	0.05	100.01
155	40.61	0.06	16.10	9.31	7.98	0.51	17.34	7.84	0.03	99.77

No.	SiO_2	TiO_2	Al_2O_3	Cr_2O_3	FeO	MnO	MgO	CaO	Na_2O	Total
156	42.06	0.16	20.68	3.73	7.89	0.47	20.19	5.02	0.00	100.19
157	41.67	0.24	19.77	4.87	8.42	0.48	19.65	5.15	0.07	100.32
158	41.77	0.01	20.27	4.23	7.40	0.38	20.06	5.34	0.02	99.49
159	42.24	0.33	21.73	2.23	8.58	0.43	20.04	4.56	0.04	100.18
160	41.78	0.33	20.36	3.80	8.52	0.44	19.94	4.90	0.05	100.13
161	41.65	0.29	20.38	3.80	8.27	0.45	19.97	4.73	0.06	99.59
162	41.50	0.25	19.38	5.45	8.00	0.46	19.51	5.48	0.06	100.08
163	41.32	0.26	19.76	4.37	8.34	0.48	19.51	5.32	0.07	99.42
164	41.41	0.02	20.29	4.22	7.37	0.40	20.49	4.89	0.03	99.11
165	41.90	0.18	21.76	2.38	9.00	0.45	19.98	4.59	0.02	100.25
166	41.51	0.00	19.58	5.47	7.62	0.44	19.21	6.19	0.00	100.01
167	41.76	0.19	21.45	2.07	11.47	0.36	18.28	4.80	0.06	100.45
168	41.82	0.32	20.90	3.40	8.30	0.45	20.26	4.57	0.06	100.09
169	41.76	0.18	20.18	4.34	8.17	0.47	19.70	5.30	0.00	100.09
170	41.98	0.00	20.98	3.62	7.24	0.37	19.99	5.63	0.01	99.83
171	40.90	0.09	18.00	7.30	8.23	0.53	18.37	6.47	0.03	99.91
172	41.43	0.02	18.51	6.71	7.35	0.44	18.76	6.66	0.00	99.87
173	41.44	0.11	18.91	5.80	7.96	0.45	19.26	5.90	0.02	99.84
174	41.52	0.10	18.86	5.85	8.04	0.49	19.20	5.94	0.03	100.02
175	41.55	0.29	20.07	4.19	8.39	0.49	19.57	5.44	0.06	100.04
176	41.73	0.16	20.40	3.96	8.18	0.43	19.96	4.93	0.06	99.80
177	41.33	0.19	18.61	6.48	8.02	0.52	19.23	5.70	0.05	100.13
178	41.67	0.12	19.22	5.86	7.59	0.44	20.50	4.61	0.06	100.06
179	42.08	0.32	21.66	2.29	8.62	0.44	20.28	4.51	0.07	100.25
180	41.99	0.26	21.99	1.74	9.09	0.39	19.98	4.33	0.07	99.83
181	41.96	0.18	21.78	2.26	8.36	0.44	20.46	4.49	0.04	99.96
182	41.35	0.13	17.59	7.76	7.72	0.49	19.16	6.04	0.06	100.29
183	41.74	0.06	19.41	5.48	8.16	0.51	19.83	4.94	0.02	100.14
184	41.28	0.17	17.87	7.25	7.65	0.48	19.24	5.86	0.04	99.85
185	41.44	0.16	19.12	5.68	7.91	0.47	19.49	5.59	0.04	99.88
186	41.84	0.00	19.97	5.00	7.65	0.46	19.36	5.95	0.01	100.24
187	40.70	0.02	16.39	9.28	8.12	0.56	17.13	7.83	0.03	100.06
188	42.07	0.28	21.35	2.59	8.66	0.44	20.24	4.55	0.06	100.24
189	41.87	0.29	20.74	3.27	8.10	0.44	20.32	4.71	0.06	99.78
190	41.97	0.30	20.97	3.26	8.27	0.44	20.24	4.62	0.05	100.13
191	41.77	0.30	19.48	4.20	8.97	0.47	19.14	5.31	0.12	99.74
192	41.48	0.17	19.13	5.68	7.86	0.45	19.92	5.19	0.04	99.92
193	41.54	0.08	21.65	1.92	13.91	0.31	17.39	4.09	0.04	100.94
194	41.60	0.09	18.10	7.15	7.73	0.50	19.29	5.76	0.03	100.24
195	41.09	0.19	17.86	7.13	7.98	0.49	18.86	6.40	0.05	100.04
196	41.14	0.13	19.92	3.35	13.02	0.33	17.33	5.26	0.03	100.52
197	41.86	0.16	19.76	4.82	8.07	0.49	19.87	5.13	0.02	100.15
198	42.27	0.02	20.92	4.04	7.04	0.37	22.14	3.16	0.02	99.97
199	41.72	0.27	19.82	4.75	8.05	0.44	19.71	5.04	0.06	99.86
200	41.74	0.21	21.18	2.88	8.74	0.48	20.02	4.53	0.05	99.81
201	41.85	0.04	19.24	5.89	7.69	0.47	20.74	4.18	0.06	100.16
202	41.93	0.17	21.12	3.28	8.27	0.43	20.27	4.77	0.04	100.27
203	41.04	0.14	18.82	6.55	7.88	0.50	19.24	5.72	0.04	99.92
204	41.14	0.13	18.00	6.83	8.04	0.48	18.87	6.26	0.01	99.75
205	42.11	0.24	20.98	3.31	8.12	0.44	20.13	4.80	0.06	100.20
206	41.86	0.29	20.72	3.45	8.43	0.46	20.00	4.99	0.05	100.24
207	41.72	0.24	19.59	4.96	8.13	0.48	19.73	5.20	0.05	100.10
208	41.76	0.00	19.94	4.81	7.58	0.40	20.64	4.80	0.01	99.94
209	41.47	0.29	20.32	3.76	7.88	0.44	20.16	5.09	0.08	99.49

No.	SiO_2	TiO_2	Al_2O_3	Cr_2O_3	FeO	MnO	MgO	CaO	Na_2O	Total
210	41.52	0.06	19.46	5.52	8.09	0.50	19.16	5.87	0.01	100.19
211	41.94	0.01	20.96	3.53	7.67	0.41	19.80	5.47	0.00	99.80
212	41.73	0.00	19.73	5.20	7.42	0.45	19.32	6.07	0.00	99.91
213	41.38	0.00	20.02	4.85	7.60	0.44	19.15	6.00	0.00	99.45
214	41.58	0.36	19.15	5.41	8.05	0.49	19.75	5.33	0.08	100.19
215	41.44	0.06	18.98	5.86	7.75	0.46	19.69	5.65	0.03	99.91
216	41.72	0.33	20.27	3.97	8.17	0.48	20.16	5.14	0.04	100.29
217	41.46	0.25	19.57	4.99	7.81	0.45	19.73	5.27	0.04	99.56
218	41.54	0.30	21.57	2.24	8.82	0.44	20.28	4.42	0.05	99.65
219	41.27	0.11	19.02	6.02	7.66	0.48	19.51	5.43	0.01	99.52
220	41.36	0.26	19.13	5.41	8.30	0.45	19.71	5.29	0.08	99.99
221	42.06	0.30	20.93	3.29	8.36	0.46	20.27	4.85	0.07	100.57
222	41.67	0.25	20.99	2.97	8.53	0.46	20.21	4.53	0.08	99.69
223	41.53	0.14	19.68	4.96	7.83	0.47	19.64	5.62	0.03	99.90
224	41.70	0.22	20.55	3.61	8.30	0.47	20.02	4.95	0.06	99.86
225	41.68	0.19	20.43	3.72	8.24	0.44	19.92	4.92	0.04	99.57
226	41.33	0.35	20.18	3.67	8.45	0.46	19.74	4.84	0.05	99.06
227	41.70	0.29	20.44	3.72	8.39	0.44	19.79	4.81	0.05	99.63
228	41.56	0.18	20.24	4.11	8.30	0.47	19.56	5.25	0.00	99.66
229	41.36	0.25	19.64	4.64	8.08	0.44	19.68	5.21	0.01	99.32
230	41.24	0.31	17.58	7.55	7.63	0.48	19.09	6.10	0.08	100.05
231	41.18	0.31	18.90	5.45	8.10	0.44	19.57	5.55	0.10	99.59
232	41.61	0.29	18.68	6.04	8.02	0.47	19.67	5.05	0.10	99.93
233	41.80	0.30	20.77	3.10	8.36	0.45	20.15	4.76	0.05	99.74
234	41.78	0.01	19.74	5.12	7.64	0.45	19.56	5.73	0.02	100.05
235	41.81	0.20	19.52	4.99	8.26	0.46	19.70	5.09	0.03	100.06
236	41.56	0.72	19.80	3.55	7.57	0.38	19.01	7.04	0.09	99.71
237	41.81	0.01	19.60	5.03	7.58	0.42	20.58	4.59	0.04	99.66
238	41.27	0.11	17.34	7.87	7.75	0.49	18.61	6.28	0.02	99.74
239	41.81	0.29	19.07	5.43	8.31	0.48	18.97	5.78	0.06	100.19
240	41.03	0.22	18.83	5.85	8.04	0.49	19.43	5.80	0.03	99.72
241	40.66	0.18	17.29	7.71	7.76	0.49	18.44	6.52	0.01	99.06
242	40.92	0.25	18.73	5.48	8.14	0.46	19.31	5.58	0.06	98.94
243	41.17	0.12	18.92	5.67	6.59	0.38	20.21	5.71	0.06	98.85
244	41.29	0.22	20.40	3.60	8.08	0.47	19.89	4.97	0.02	98.93
245	41.59	0.26	20.19	3.93	8.32	0.48	19.93	4.91	0.04	99.66
246	41.66	0.21	19.95	4.21	8.18	0.46	20.01	4.79	0.07	99.54
247	41.28	0.00	19.05	5.68	7.63	0.45	19.06	6.22	0.00	99.37
248	41.94	0.16	21.95	1.37	10.18	0.34	19.90	4.50	0.07	100.40
249	41.28	0.13	20.60	3.33	8.53	0.43	19.52	5.09	0.04	98.93
250	41.75	0.12	21.65	2.19	8.71	0.45	20.33	4.53	0.02	99.74
251	41.11	0.04	19.07	5.57	7.94	0.46	18.54	6.48	0.02	99.22
252	40.75	0.12	17.35	7.65	7.38	0.49	18.75	6.20	0.03	98.72
253	40.90	0.11	17.89	7.04	7.57	0.45	18.98	5.92	0.02	98.87
254	40.81	0.19	17.08	7.88	8.03	0.49	18.36	6.45	0.06	99.32
255	41.40	0.08	18.99	5.72	7.68	0.49	19.20	5.58	0.04	99.18
256	40.97	0.03	17.98	7.05	8.05	0.48	18.46	6.45	0.02	99.48
257	41.60	0.24	19.64	4.85	8.04	0.46	19.68	5.10	0.06	99.67
258	41.78	0.26	19.71	4.89	8.00	0.45	19.29	5.09	0.06	99.54
259	41.64	0.25	19.52	4.87	8.11	0.47	19.55	5.08	0.06	99.55
260	41.37	0.16	18.28	6.67	7.72	0.49	19.07	6.02	0.03	99.80
261	41.66	0.18	19.76	4.54	8.09	0.45	20.00	4.87	0.06	99.60
262	41.44	0.06	19.27	5.42	8.13	0.48	19.26	5.80	0.02	99.86
263	41.47	0.06	18.98	6.14	8.00	0.44	19.43	5.62	0.04	100.17

No.	SiO_2	TiO_2	Al_2O_3	Cr_2O_3	FeO	MnO	MgO	CaO	Na_2O	Total
264	41.43	0.07	19.31	5.36	7.68	0.46	19.90	5.38	0.03	99.61
265	41.89	0.00	21.80	2.16	8.53	0.58	19.58	5.01	0.03	99.58
266	41.69	0.18	19.56	5.01	8.34	0.46	19.26	5.57	0.03	100.10
267	41.81	0.10	19.95	4.49	7.90	0.43	20.04	5.23	0.06	100.01
268	41.97	0.03	19.93	4.83	7.39	0.42	19.70	5.90	0.00	100.15
269	41.80	0.26	20.04	4.05	8.28	0.46	19.92	5.04	0.02	99.87
270	41.60	0.06	21.99	1.40	14.25	0.34	17.33	3.58	0.06	100.62
271	40.95	0.17	20.40	2.69	9.33	0.64	15.57	10.34	0.05	100.14
272	41.81	0.01	20.52	3.89	7.74	0.41	19.47	5.58	0.04	99.45
273	41.42	0.17	18.16	6.76	7.95	0.51	18.99	5.76	0.04	99.76
274	42.04	0.18	22.01	1.82	9.01	0.42	20.08	4.48	0.05	100.09
275	41.43	0.09	17.49	7.67	8.25	0.51	18.26	6.46	0.03	100.20
276	41.21	0.09	17.34	7.76	8.11	0.51	18.53	6.50	0.03	100.06
277	41.91	0.08	19.37	5.55	7.73	0.48	21.16	3.68	0.01	99.98
278	41.52	0.08	21.23	2.57	11.93	0.19	16.02	7.17	0.02	100.73
279	41.77	0.19	19.44	5.08	8.01	0.50	19.37	5.28	0.04	99.68
280	41.17	0.16	17.69	7.28	8.03	0.49	18.57	6.36	0.04	99.79
281	42.31	0.17	21.26	2.91	8.49	0.45	19.97	4.71	0.05	100.32
282	41.08	0.06	17.16	7.90	7.78	0.50	17.71	7.58	0.00	99.76
283	41.86	0.18	21.76	1.70	10.83	0.49	18.54	5.07	0.04	100.47
284	41.30	0.03	18.86	5.88	7.95	0.51	20.23	4.31	0.02	99.07
285	41.68	0.28	19.38	5.19	8.26	0.50	19.58	5.41	0.06	100.32
286	41.87	0.26	20.84	3.29	8.35	0.45	20.01	4.87	0.07	100.01
287	41.56	0.25	19.21	5.20	8.46	0.50	19.32	5.12	0.09	99.70
288	42.06	0.16	20.32	4.01	7.89	0.43	20.04	4.94	0.03	99.89
289	41.33	0.23	18.46	5.93	8.12	0.48	19.13	5.87	0.07	99.61
290	41.69	0.24	18.74	5.79	8.07	0.48	19.20	5.80	0.04	100.04
291	41.64	0.00	20.42	4.04	7.53	0.40	19.95	5.71	0.00	99.70
292	42.21	0.00	20.63	3.80	7.78	0.42	19.96	5.53	0.01	100.34
293	41.40	0.06	19.10	5.71	8.13	0.52	18.93	5.71	0.00	99.56
294	41.97	0.00	19.91	4.64	7.70	0.42	19.30	5.93	0.00	99.86
295	41.31	0.25	17.28	7.72	7.94	0.51	18.65	6.56	0.08	100.29
296	42.23	0.00	20.13	4.80	7.38	0.42	20.96	4.08	0.03	100.02
297	42.10	0.00	20.25	4.54	7.30	0.41	21.25	3.86	0.02	99.74
298	41.33	0.37	18.54	5.83	8.41	0.49	19.65	4.81	0.09	99.51
299	41.80	0.19	19.90	4.50	7.82	0.47	19.93	5.07	0.02	99.71
300	41.64	0.10	18.39	6.74	8.22	0.47	19.28	5.31	0.07	100.21
301	42.02	0.02	19.32	5.56	7.28	0.42	19.73	5.73	0.00	100.08
302	41.66	0.27	18.55	6.10	8.20	0.49	18.98	5.59	0.06	99.90
303	41.76	0.19	19.95	4.59	8.18	0.48	19.53	5.20	0.06	99.95
304	41.34	0.03	19.38	5.43	8.15	0.51	18.52	6.30	0.04	99.70
305	41.58	0.22	19.61	4.75	8.20	0.49	19.68	5.26	0.10	99.88
306	42.07	0.15	22.19	1.40	10.54	0.38	19.65	4.07	0.03	100.48
307	41.90	0.19	19.35	5.48	7.41	0.47	19.55	5.70	0.05	100.09
308	41.61	0.29	20.62	3.36	8.55	0.45	20.05	4.71	0.04	99.67
309	41.93	0.27	19.99	4.48	8.21	0.48	20.03	4.80	0.03	100.22
310	42.02	0.26	20.44	3.69	8.12	0.44	19.78	4.97	0.06	99.77
311	41.94	0.01	20.32	4.34	7.44	0.42	19.69	5.48	0.00	99.63
312	42.11	0.14	21.70	2.34	9.09	0.46	19.98	4.46	0.03	100.32
313	41.40	0.01	18.89	5.94	7.70	0.44	18.77	6.44	0.01	99.60
314	41.17	0.15	15.97	9.31	7.63	0.46	18.83	6.29	0.05	99.86
315	42.06	0.30	21.06	2.96	8.80	0.46	19.94	4.73	0.06	100.36
316	41.72	0.00	19.39	5.45	7.22	0.39	19.33	6.19	0.00	99.69
317	42.42	0.22	21.42	2.77	8.27	0.49	20.77	3.81	0.06	100.22

No.	SiO_2	TiO_2	Al_2O_3	Cr_2O_3	FeO	MnO	MgO	CaO	Na_2O	Total
318	41.44	0.01	18.41	6.40	8.25	0.54	19.36	5.35	0.02	99.79
319	41.73	0.17	18.63	6.30	8.01	0.49	19.00	5.88	0.05	100.25
320	41.63	0.01	19.86	4.59	8.04	0.51	18.94	5.99	0.00	99.56
321	42.39	0.06	22.37	1.63	7.71	0.36	20.58	5.18	0.02	100.29
322	41.39	0.05	18.05	6.75	7.53	0.45	18.85	6.85	0.00	99.92
323	41.29	0.00	20.14	4.18	7.91	0.46	19.35	5.55	0.02	98.91
324	41.43	0.02	20.11	4.16	7.95	0.44	19.57	5.58	0.00	99.26
325	41.63	0.33	20.59	3.37	8.45	0.45	19.91	4.79	0.07	99.59
326	41.96	0.35	20.85	3.09	8.08	0.44	20.52	4.37	0.08	99.75
327	41.26	0.13	16.98	8.23	7.88	0.50	18.44	6.49	0.04	99.94
328	41.37	0.14	19.83	4.24	8.57	0.48	19.63	4.87	0.05	99.18
329	41.21	0.28	19.07	5.31	8.39	0.51	19.61	5.20	0.04	99.61
330	41.84	0.29	20.13	4.15	8.27	0.46	20.13	4.88	0.07	100.22
331	41.60	0.01	19.93	4.69	8.23	0.49	19.06	5.86	0.00	99.87
332	41.95	0.12	20.15	4.33	8.35	0.48	19.68	5.09	0.02	100.17
333	41.39	0.19	19.28	5.18	8.00	0.47	19.76	5.33	0.09	99.68
334	42.22	0.23	21.74	1.97	8.53	0.42	20.29	4.35	0.04	99.78
335	42.20	0.16	22.40	1.38	8.62	0.40	20.45	4.13	0.06	99.79
336	42.25	0.23	22.17	1.50	8.70	0.41	20.51	4.26	0.09	100.11
337	41.80	0.04	19.96	4.52	7.41	0.41	20.55	4.59	0.01	99.29
338	41.03	0.20	18.23	6.50	7.75	0.48	19.70	5.40	0.07	99.36
339	41.64	0.19	18.82	5.64	8.22	0.50	19.22	5.90	0.05	100.18
340	41.62	0.21	19.10	5.81	7.67	0.46	19.72	5.36	0.06	100.01
341	41.59	0.02	18.67	6.38	7.75	0.47	19.66	5.37	0.04	99.95
342	41.64	0.20	19.32	5.05	8.37	0.48	19.23	5.53	0.07	99.88
343	41.78	0.18	19.34	5.32	7.94	0.49	19.58	5.38	0.05	100.07
344	41.60	0.22	19.57	4.94	7.84	0.47	20.00	5.15	0.04	99.82
345	41.75	0.03	18.36	6.69	7.51	0.43	19.68	5.65	0.03	100.14
346	41.64	0.12	19.74	4.64	8.36	0.48	19.40	5.58	0.04	99.98
347	41.85	0.21	20.81	3.09	8.88	0.48	19.55	4.99	0.05	99.90
348	42.15	0.24	20.52	3.71	7.87	0.43	20.14	4.95	0.07	100.09
349	41.66	0.06	19.86	4.86	7.84	0.42	19.19	6.06	0.04	99.99
350	42.09	0.15	20.93	3.25	8.14	0.35	20.23	5.22	0.06	100.41
351	40.86	0.39	16.79	7.71	8.91	0.55	17.47	7.16	0.07	99.91
352	41.98	0.06	21.10	2.95	8.83	0.51	20.00	4.40	0.08	99.91
353	41.63	0.00	18.32	6.73	7.35	0.43	19.00	6.55	0.02	100.02
354	41.47	0.17	18.87	5.89	7.92	0.48	19.43	5.49	0.06	99.77
355	41.60	0.29	19.10	5.16	8.49	0.50	19.42	5.46	0.10	100.10
356	41.57	0.02	18.78	6.16	7.91	0.48	18.66	6.26	0.02	99.87
357	42.14	0.36	20.96	3.25	8.46	0.44	20.07	4.71	0.07	100.46
358	41.59	0.01	18.55	6.44	7.59	0.46	19.42	5.71	0.01	99.77
359	41.75	0.17	19.53	5.27	7.85	0.47	19.59	5.43	0.05	100.10
360	41.42	0.09	17.64	7.47	8.08	0.50	18.52	6.31	0.04	100.06
361	40.98	0.15	18.18	6.57	8.06	0.49	18.99	6.23	0.03	99.68
362	41.38	0.00	19.54	5.12	7.42	0.43	19.61	5.85	0.00	99.35
363	41.54	0.27	19.78	4.40	8.08	0.42	19.74	5.28	0.09	99.60
364	41.60	0.02	19.40	5.33	8.18	0.49	18.75	6.17	0.04	99.97
365	41.98	0.18	20.73	3.59	8.07	0.44	20.24	4.95	0.04	100.21
366	42.19	0.01	21.51	2.87	7.12	0.28	20.88	5.11	0.00	99.96
367	41.71	0.01	19.84	4.94	7.77	0.43	19.31	6.01	0.01	100.03
368	41.77	0.04	19.36	5.41	8.36	0.55	18.33	6.11	0.02	99.95
369	42.33	0.32	20.85	3.26	8.39	0.43	20.12	4.54	0.06	100.29
370	41.44	0.09	18.13	6.95	8.03	0.50	18.86	6.10	0.05	100.14
371	42.14	0.20	21.17	2.64	7.79	0.37	20.24	5.09	0.07	99.73

No.	SiO_2	TiO_2	Al_2O_3	Cr_2O_3	FeO	MnO	MgO	CaO	Na_2O	Total
372	42.75	0.10	23.14	0.54	8.73	0.27	21.10	3.87	0.06	100.56
373	42.23	0.21	20.96	3.23	7.89	0.44	20.39	4.84	0.05	100.24
374	42.16	0.00	20.97	3.38	7.78	0.42	20.19	5.24	0.05	100.18
375	40.89	0.02	18.50	6.07	7.75	0.49	18.48	6.58	0.02	98.80
376	41.54	0.13	19.97	4.23	8.33	0.47	19.36	5.19	0.06	99.27
377	42.12	0.33	20.75	3.14	8.56	0.45	19.95	4.62	0.05	99.94
378	42.14	0.24	20.91	3.19	7.96	0.43	20.19	4.86	0.06	99.97
379	41.14	0.03	19.32	5.03	8.20	0.51	18.75	6.03	0.01	99.02
380	41.56	0.10	18.87	5.90	8.17	0.51	19.20	5.77	0.05	100.13
381	42.21	0.19	21.64	2.39	8.88	0.43	20.02	4.61	0.05	100.41
382	41.45	0.07	18.18	7.00	7.49	0.48	18.48	6.80	0.03	99.97
383	41.81	0.00	19.38	5.43	7.69	0.47	19.08	6.25	0.01	100.12
384	41.56	0.19	19.35	4.82	9.53	0.53	19.03	5.16	0.04	100.19
385	41.54	0.28	18.85	5.66	7.95	0.49	19.18	5.46	0.06	99.46
386	41.07	0.20	18.58	5.53	8.47	0.51	19.16	5.67	0.06	99.25

SUPPLEMENTARY TABLE 2

Major and trace element composition of selected garnets and associated minerals from the Zagadochnaya kimberlite. Estimated pressures and temperatures are also reported.

Notes and abbreviations:

mg#: $100*Mg/(Mg + Fe_{tot})_{mol}$;

Cr#: $100*Cr/(Cr + Al)_{mol}$;

b.d.l.: below detection limit;

---: not analyzed;

Zr_{PM}: primitive mantle-normalized concentration after McDonough and Sun (1995);

La_{CI}: condrite-normalized concentration after Anders and Grevesse (1989);

Ti*: $(Eu_{PM}+Gd_{PM})/2$;

Cpx: clinopyroxene

Grt: garnet;

incl: inclusion;

intergr: intergrowth.

Ry96: Ni-in-garnet themometer of Ryan et al. (1996)

Ca99: Ni-in-garnet themometer of Canil (1999)

NT00: Single-clinopyroxene thermobarometer of Nimis and Taylor (2000)

Group A garnets

Sample Notes	Z4-2	Z4-10	z5-02	Z5-11	Z5-15	Z6-2	Z6-14
SiO_2	42.11	41.68	41.53	42.10	42.81	41.66	42.03
TiO_2	0.30	0.29	0.17	0.32	0.14	0.24	0.16
Al_2O_3	21.90	20.57	20.30	21.15	23.03	20.85	21.97
Cr_2O_3	2.85	4.41	5.18	4.11	1.30	4.42	2.56
FeO_{tot}	8.66	8.55	8.26	8.75	8.54	8.48	8.50
MnO	0.39	0.36	0.29	0.38	0.39	0.27	0.42
MgO	20.46	19.68	19.76	19.86	20.68	19.95	20.03
CaO	4.54	5.01	5.03	4.78	4.42	4.99	4.57
Na_2O	0.06	0.03	0.00	0.05	0.04	0.06	0.07
K_2O	0.01	0.00	0.00	0.00	0.00	0.00	0.00
SUM	101.27	100.58	100.53	101.51	101.35	100.90	100.31
Mg#	80.8	80.4	81.0	80.2	81.2	80.7	80.8
Cr#	8.0	12.6	14.6	11.5	3.6	12.4	7.3
T(°C)-Ry96	853	839	822	838	811	813	816
T(°C)-Ca99	952	942	929	941	922	923	903
Li	b.d.l.	0.51	0.21	b.d.l.	b.d.l.	b.d.l.	0.48
B	b.d.l.	b.d.l.	3.58	1.81	b.d.l.	1.83	0.58
Ti	1637	1658	926	1696	740	1250	1029
Co	44.6	42.2	40.2	40.3	40.9	38.9	40.3
Ni	26.3	24.8	23.0	24.7	22.0	22.2	22.4
Zn	11.3	9.41	11.3	10.2	9.41	9.35	9.58
Sc	81.6	105	133	101	83.2	85.2	96.2
V	197	231	236	210	176	211	169
Rb	b.d.l.	0.046	0.071	0.081	b.d.l.	b.d.l.	b.d.l.
Sr	0.18	0.16	0.084	0.11	0.10	0.12	0.071
Y	16.0	13.4	17.4	15.8	25.4	10.1	19.0
Zr	23.2	17.6	11.4	18.5	19.7	14.4	24.6
Nb	0.020	0.029	0.082	0.019	0.024	0.052	0.026
Cs	b.d.l.	0.004	b.d.l.	b.d.l.	b.d.l.	b.d.l.	b.d.l.
Ba	b.d.l.	b.d.l.	b.d.l.	b.d.l.	0.33	0.098	0.040
La	0.010	0.008	0.008	b.d.l.	0.007	0.015	b.d.l.
Ce	0.052	0.080	0.073	0.040	0.066	0.10	0.028
Pr	0.019	0.054	0.028	0.039	0.016	0.024	0.025
Nd	0.35	0.58	0.36	0.47	0.26	0.38	0.32
Sm	0.51	0.57	0.43	0.62	0.35	0.54	0.67
Eu	0.35	0.34	0.22	0.32	0.26	0.30	0.47
Gd	1.53	1.18	1.13	1.29	1.08	1.24	1.55
Tb	0.34	0.30	0.30	0.29	0.32	0.24	0.31
Dy	2.66	2.083	2.55	2.78	2.96	1.82	2.80
Ho	0.61	0.52	0.63	0.63	1.01	0.37	0.73
Er	2.09	1.504	2.36	1.80	2.83	1.11	2.40
Tm	0.28	0.22	0.35	0.28	0.52	0.17	0.36
Yb	2.22	1.96	3.29	2.01	4.04	1.32	3.00
Lu	0.30	0.29	0.59	0.32	0.71	0.19	0.49
Hf	0.47	0.59	0.38	0.31	0.36	0.31	0.34
Ta	b.d.l.	b.d.l.	b.d.l.	b.d.l.	0.008	b.d.l.	b.d.l.
Pb	0.016	0.019	b.d.l.	b.d.l.	b.d.l.	0.147	b.d.l.
Th	b.d.l.	0.003	0.005	0.007	0.008	b.d.l.	b.d.l.
U	b.d.l.	0.011	0.009	b.d.l.	0.005	0.015	0.009
La_{CI}/Sm_{CI}	0.012	0.009	0.012		0.012	0.018	
Sm_{CI}/Yb_{CI}	0.25	0.32	0.15	0.34	0.10	0.45	0.25
Ti_{PM}/Ti^*	0.54	0.63	0.44	0.64	0.33	0.49	0.29
Zr_{PM}/Hf_{PM}	1.33	0.81	0.81	1.63	1.49	1.27	1.94

Group B garnets and associated secondary low-(Ca, Cr) domains (sec.).

Sample	**Z4-3**	**Z4-3**	**Z4-7**	**Z4-7**	**Z4-9**	**Z4-9**	**Z5-5**	**Z5-5**
Notes		**sec.**		**sec.**		**sec.**		**sec.**
SiO_2	41.47	41.47	41.70	42.67	41.69	41.89	41.55	41.14
TiO_2	0.17	0.13	0.16	0.09	0.21	0.09	0.11	0.08
Al_2O_3	19.03	20.15	19.60	21.36	19.22	19.48	19.36	20.87
Cr_2O_3	6.92	5.14	5.78	3.86	6.20	6.18	5.36	4.39
FeO_{tot}	8.25	8.52	8.22	8.16	8.27	8.22	7.94	8.17
MnO	0.33	0.48	0.39	0.45	0.31	0.36	0.40	0.44
MgO	18.73	19.51	19.33	20.44	19.30	20.11	18.80	20.10
CaO	6.10	5.18	5.32	4.18	5.63	4.53	5.20	4.79
Na_2O	0.01	0.05	0.00	0.07	0.04	0.07	0.00	0.02
K_2O	0.00	0.01	0.00	0.01	0.00	0.00	0.26	0.00
SUM	101.01	100.64	100.50	101.30	100.87	100.94	98.97	99.98
Mg#	80.2	80.3	80.7	81.7	80.6	81.4	80.9	81.4
Cr#	19.6	14.6	16.5	10.8	17.8	17.5	15.7	12.4
T(°C)-Ry96	840		692		810		798	
T(°C)-Ca99	943		831		921		912	
Li	0.42	6.54	b.d.l.	b.d.l.	b.d.l.	0.47	0.34	0.43
B	1.55	7.98	b.d.l.	1.43	b.d.l.	b.d.l.	1.57	1.71
Ti	945	778	999	528	1099	595	695	519
Co	40.2	40.4	36.6	38.1	38.1	43.9	36.0	37.6
Ni	24.9	51.2	12.0	36.3	21.8	26.9	20.7	22.6
Zn	8.39	15.8	4.29	15.7	8.46	9.59	7.57	7.55
Sc	145	159	160	167	116	114	112	149
V	299	201	228	126	237	156	211	168
Rb	0.057	0.96	0.11	1.18	0.083	0.09	0.069	b.d.l.
Sr	0.63	23.8	0.79	2.46	0.12	1.01	0.23	4.62
Y	9.78	15.9	12.8	27.0	8.28	10.9	7.76	35.7
Zr	15.4	34.2	20.0	56.5	31.1	68.7	11.6	68.3
Nb	0.200	11.6	0.069	0.92	0.11	0.63	0.084	1.20
Cs	b.d.l.	0.011	b.d.l.	0.025	b.d.l.	0.006	b.d.l.	b.d.l.
Ba	0.37	22.7	9.22	85.7	b.d.l.	0.99	0.18	2.66
La	0.090	2.68	0.071	0.24	0.006	0.15	0.034	0.45
Ce	0.98	7.41	1.01	0.98	0.14	1.02	0.16	1.76
Pr	0.49	1.03	0.39	0.25	0.053	0.37	0.092	0.403
Nd	4.67	7.16	2.91	3.50	0.96	4.02	1.34	4.43
Sm	1.59	3.40	1.20	3.46	0.69	3.42	0.88	4.60
Eu	0.50	1.35	0.52	1.86	0.29	1.36	0.36	2.43
Gd	1.52	3.43	1.58	6.77	0.93	3.02	1.18	8.42
Tb	0.27	0.61	0.33	1.40	0.17	0.37	0.22	1.31
Dy	1.46	3.37	1.95	6.14	1.40	2.11	1.29	8.26
Ho	0.39	0.71	0.52	0.97	0.39	0.38	0.27	1.48
Er	1.23	1.41	1.52	2.18	1.06	1.34	0.87	2.64
Tm	0.22	0.25	0.26	0.34	0.15	0.19	0.13	0.41
Yb	1.63	2.2	1.76	2.23	1.35	1.56	0.99	3.24
Lu	0.26	0.34	0.25	0.36	0.21	0.31	0.19	0.42
Hf	0.35	0.42	0.48	0.35	0.68	0.53	0.31	0.41
Ta	0.004	0.305	0.007	0.046	b.d.l.	0.065	0.003	0.08
Pb	0.040	0.82	0.022	0.19	0.042	0.054	b.d.l.	0.264
Th	0.068	1.33	0.015	0.025	0.003	0.038	0.018	0.044
U	0.074	1.04	b.d.l.	0.053	0.015	0.046	0.016	0.057
La_{CI}/Sm_{CI}	0.036	0.494	0.037	0.044	0.006	0.028	0.024	0.061
Sm_{CI}/Yb_{CI}	1.08	1.71	0.75	1.71	0.56	2.42	0.98	1.57
Ti_{PM}/Ti^*	0.26	0.09	0.26	0.04	0.51	0.07	0.26	0.03
Zr_{PM}/Hf_{PM}	1.19	2.18	1.13	4.31	1.23	3.53	1.02	4.49

Group B garnets and associated secondary low-(Ca, Cr) domains (sec.).

Sample	**Z5-6**	**Z5-13**	**Z6-12**	**Z6-12**	**Z6-17**
Notes				**sec.**	
SiO_2	41.35	41.84	41.18	41.92	41.41
TiO_2	0.35	0.06	0.12	0.08	0.25
Al_2O_3	19.21	18.44	19.80	21.52	18.55
Cr_2O_3	6.67	7.63	5.82	3.75	7.17
FeO_{tot}	7.14	7.98	8.34	8.26	7.88
MnO	0.19	0.35	0.47	0.46	0.33
MgO	20.76	19.28	19.26	20.61	18.59
CaO	4.99	5.47	5.06	4.39	5.96
Na_2O	0.00	0.00	0.04	0.00	0.05
K_2O	0.00	0.01	0.00	0.02	0.00
SUM	100.67	101.06	100.10	101.00	100.20
Mg#	83.8	81.2	80.4	81.6	80.8
Cr#	18.9	21.7	16.5	10.5	20.6
T(°C)-Ry96	1020	792	812		827
T(°C)-Ca99	1065	907	922		933
Li	b.d.l.	b.d.l.	0.99	0.12	0.19
B	2.05	0.98	1.95	1.69	8.193
Ti	1715	407	1294	618	1185
Co	38.8	35.3	34.3	37.9	38.8
Ni	48.3	20.1	22.0	20.4	23.6
Zn	10.1	7.28	9.2	8.75	7.79
Sc	128	168	117	150	133
V	288	241	218	113	290
Rb	0.12	b.d.l.	0.28	0.037	b.d.l.
Sr	0.59	0.15	3.10	0.49	0.21
Y	6.79	3.17	10.3	78.3	8.57
Zr	21.4	8.7	22.5	49.5	29.4
Nb	0.26	0.20	1.75	0.24	0.26
Cs	b.d.l.	b.d.l.	b.d.l.	b.d.l.	b.d.l.
Ba	0.31	b.d.l.	2.62	0.15	0.026
La	0.072	0.039	1.45	0.043	0.044
Ce	0.74	0.37	2.15	0.55	0.34
Pr	0.25	0.12	0.32	0.20	0.18
Nd	2.02	1.22	2.20	2.84	2.10
Sm	0.79	0.40	1.46	3.03	1.29
Eu	0.33	0.21	0.49	1.71	0.55
Gd	1.12	0.56	1.71	6.81	1.38
Tb	0.17	0.11	0.29	1.64	0.24
Dy	1.29	0.66	1.48	13.4	1.69
Ho	0.25	0.12	0.38	3.11	0.32
Er	0.72	0.47	1.26	9.50	0.95
Tm	0.11	0.057	0.19	1.30	0.15
Yb	0.83	0.55	1.18	10.31	1.32
Lu	0.14	0.13	0.27	1.56	0.21
Hf	0.53	0.22	0.48	0.53	0.81
Ta	0.023	0.007	0.096	0.021	0.018
Pb	b.d.l.	0.038	0.192	0.028	0.091
Th	0.029	0.012	0.23	0.040	0.009
U	0.035	0.029	0.097	0.033	0.025
La_{CI}/Sm_{CI}	0.057	0.061	0.624	0.009	0.021
Sm_{CI}/Yb_{CI}	1.04	0.80	1.37	0.32	1.08
Ti_{PM}/Ti^*	0.68	0.28	0.39	0.04	0.32
Zr_{PM}/Hf_{PM}	1.09	1.08	1.27	2.50	0.98

Group C garnets and associated secondary low-(Ca,Cr) domains (sec.).

Sample	**Z4-1**	**Z4-1**	**Z4-4**	**Z4-4**	**Z4-6**	**Z4-8**	**Z4-8**	**Z5-10**	**Z5-10**	**Z5-14**
Notes		**sec.**		**sec.**			**sec.**		**sec.**	
SiO_2	41.07	42.10	40.96	41.58	41.28	41.38	42.06	41.72	41.91	41.49
TiO_2	0.28	0.15	0.04	0.01	0.16	0.06	0.05	0.16	0.05	0.05
Al_2O_3	17.70	20.94	17.78	20.37	18.02	18.58	20.12	17.94	19.23	17.69
Cr_2O_3	7.99	4.41	8.36	5.04	8.27	7.28	4.69	8.13	7.07	8.64
FeO_{tot}	8.11	8.20	8.58	8.49	7.99	8.10	8.01	8.04	8.24	8.23
MnO	0.31	0.49	0.35	0.49	0.30	0.38	0.42	0.35	0.39	0.32
MgO	18.80	20.64	17.78	19.68	18.82	19.03	19.47	18.34	18.98	17.40
CaO	6.36	4.15	6.95	5.06	6.15	6.24	4.34	6.32	5.77	7.38
Na_2O	0.04	0.03	0.01	0.00	0.01	0.08	0.13	0.06	0.07	0.02
K_2O	0.00	0.01	0.01	0.02	0.00	0.00	0.06	0.01	0.00	0.00
SUM	100.66	101.12	100.82	100.73	100.99	101.12	99.35	101.06	101.70	101.21
Mg#	80.5	81.8	78.7	80.5	80.8	80.7	81.3	80.3	80.4	79.0
Cr#	23.2	12.4	24.0	14.2	23.5	20.8	13.5	23.3	19.8	24.7
T(°C)-Ry96	822		738		857	802		805		804
T(°C)-Ca99	930		867		954	915		917		916
Li	b.d.l.	b.d.l.	b.d.l.	b.d.l.	0.14	b.d.l.	b.d.l.	b.d.l.	b.d.l.	0.11
B	b.d.l.	b.d.l.	0.99	2.03	1.35	0.68	1.71	1.26	1.4	1.05
Ti	1415	786	161	141	890	454	199	806	433	384
Co	38.1	42.8	24.3	31.8	40.2	38.7	37.4	36.1	45.9	35.4
Ni	23.0	23.8	15.4	70.1	26.7	21.0	20.3	21.3	23.8	21.2
Zn	9.22	9.57	6.63	10.7	10.8	8.03	8.83	8.29	11.07	8.63
Sc	140	162	115	152	116	204	218	133	169	185
V	273	159	227	172	273	243	130	293	199	313
Rb	0.041	0.037	0.21	2.94	0.22	b.d.l.	b.d.l.	0.11	0.18	0.047
Sr	0.21	0.29	0.36	3.32	0.68	0.32	0.55	0.13	3.69	0.13
Y	6.27	25.4	0.71	44.3	7.94	2.24	17.5	2.39	41.3	1.63
Zr	20.1	39.4	6.2	61.3	18.8	15.4	45.9	18.4	57.7	5.7
Nb	0.19	0.23	0.44	2.01	0.061	0.21	0.30	0.10	1.09	0.13
Cs	0.008	0.007	0.006	0.072	b.d.l.	b.d.l.	0.012	b.d.l.	b.d.l.	0.008
Ba	0.024	0.36	12.8	238	9.26	0.22	0.41	0.15	3.03	b.d.l.
La	0.025	0.050	0.041	0.26	0.10	0.087	0.083	0.012	0.62	0.042
Ce	0.30	0.44	0.24	1.39	0.82	0.67	0.68	0.17	1.89	0.25
Pr	0.13	0.24	0.11	0.45	0.42	0.21	0.23	0.10	0.36	0.074
Nd	1.44	2.78	1.22	4.36	4.64	1.96	4.19	1.76	4.34	0.55
Sm	1.00	3.24	0.46	3.97	1.96	0.85	3.99	1.86	3.97	0.37
Eu	0.48	1.75	0.18	2.06	0.69	0.30	1.84	0.46	1.91	0.13
Gd	1.58	5.66	0.31	6.86	1.65	0.72	5.26	1.5	7.01	0.33
Tb	0.28	1.09	0.036	1.30	0.31	0.11	0.80	0.11	1.42	0.027
Dy	1.59	6.18	0.18	9.11	1.77	0.49	4.41	0.40	8.66	0.25
Ho	0.29	1.01	0.023	1.86	0.29	0.087	0.70	0.094	1.58	0.072
Er	0.60	2.02	0.057	4.46	0.55	0.21	1.43	0.18	3.64	0.18
Tm	0.059	0.24	0.005	0.56	0.11	0.028	0.19	0.035	0.47	0.030
Yb	0.45	1.57	0.074	5.92	0.46	0.50	1.08	0.34	4.00	0.60
Lu	0.079	0.22	0.021	0.52	0.059	0.09	0.21	0.063	0.56	0.083
Hf	0.32	0.34	0.15	0.91	0.36	0.43	0.28	0.24	0.44	0.09
Ta	0.002	0.006	0.022	0.11	b.d.l.	0.006	0.032	0.007	0.084	0.008
Pb	0.13	b.d.l.	0.02	b.d.l.	b.d.l.	0.050	0.061	b.d.l.	0.046	b.d.l.
Th	0.004	0.009	0.015	0.06	0.075	0.019	0.035	0.015	0.103	0.008
U	0.004	0.021	0.036	0.304	0.097	0.023	0.026	0.041	0.082	0.030
La_{CI}/Sm_{CI}	0.015	0.010	0.056	0.041	0.033	0.064	0.013	0.004		0.071
Sm_{CI}/Yb_{CI}	2.42	2.27	6.87	0.74	4.70	1.89	4.08	5.97	1.10	0.68
Ti_{PM}/Ti^*	0.39	0.06	0.16	0.01	0.20	0.23	0.02	0.23	0.03	0.44
Zr_{PM}/Hf_{PM}	1.69	3.11	1.14	1.82	1.41	0.96	4.48	2.04	3.52	1.70

Group C garnets and associated secondary low-(Ca,Cr) domains .

Sample	**Z6-9**	**Z6-9**	**Z6-10**	**Z6-10**	**Z6-11**
Notes		**sec.**		**sec.**	
SiO_2	41.49	42.31	41.45	42.34	41.13
TiO_2	0.17	0.05	0.14	0.01	0.09
Al_2O_3	18.17	20.94	18.39	21.42	18.26
Cr_2O_3	8.06	4.24	7.76	3.97	7.83
FeO_{tot}	7.54	7.54	7.80	7.99	7.67
MnO	0.30	0.36	0.39	0.43	0.38
MgO	18.85	21.08	18.47	20.40	18.06
CaO	6.33	4.29	6.49	4.36	6.88
Na_2O	0.07	0.04	0.09	0.02	0.03
K_2O	0.00	0.00	0.00	0.01	0.01
SUM	100.97	100.85	100.97	100.95	100.34
Mg#	81.7	83.3	80.8	82.0	80.8
Cr#	22.9	12.0	22.1	11.1	22.3
T(°C)-Ry96	830		728		811
T(°C)-Ca99	935		859		922
Li	b.d.l.	0.31	0.24	0.62	b.d.l.
B	0.98	0.38	1.62	b.d.l.	0.47
Ti	852	295	483	269	374
Co	38.8	43.9	25.9	56.5	37.5
Ni	23.8	29.9	14.6	30.6	21.9
Zn	9.290	8.660	5.95	12.9	7.255
Sc	143	132	135	278	358
V	261	154	198	217	202
Rb	0.051	0.33	0.13	0.079	0.052
Sr	0.94	4.36	0.56	0.83	0.20
Y	5.85	12.9	2.04	13.9	4.76
Zr	43.3	59.3	13.5	59.3	43.4
Nb	0.64	2.57	0.20	0.37	0.21
Cs		0.009	0.002	b.d.l.	b.d.l.
Ba	0.83	7.57	0.14	0.082	b.d.l.
La	0.12	0.26	0.091	0.13	0.093
Ce	0.54	1.32	0.34	0.83	0.66
Pr	0.24	0.35	0.083	0.51	0.20
Nd	2.33	3.77	1.26	4.66	2.24
Sm	1.38	2.40	0.72	3.98	1.61
Eu	0.41	1.22	0.17	1.68	0.66
Gd	0.97	3.51	0.33	6.45	1.77
Tb	0.15	0.58	0.060	0.84	0.29
Dy	0.97	2.80	0.37	4.37	1.18
Ho	0.23	0.55	0.082	0.58	0.18
Er	0.69	1.21	0.21	1.1	0.37
Tm	0.10	0.16	0.042	0.13	0.035
Yb	1.07	1.40	0.42	0.82	0.26
Lu	0.17	0.24	0.11	0.23	0.036
Hf	0.69	0.43	0.33	0.21	0.88
Ta	0.016	0.18	0.004	b.d.l.	0.003
Pb	0.056	0.16	0.065	0.21	b.d.l.
Th	0.067	0.076	0.028	0.057	0.026
U	0.045	0.062	0.044	0.084	0.073
La_{CI}/Sm_{CI}	0.055	0.068	0.080	0.021	0.036
Sm_{CI}/Yb_{CI}	2.42	1.89	1.88	5.36	6.86
Ti_{PM}/Ti^*	0.32	0.03	0.47	0.02	0.08
Zr_{PM}/Hf_{PM}	1.68	3.70	1.09	7.76	1.33

Garnets wherein inclusion-rich domains apparently extend pervasively throughout the grain, and garnet in amphibole-garnet intergrowth Z4-11.

Sample **Notes**	**Z5-3** **sec.**	**Z4-5** **sec.**	**Z5-9** **sec.**	**Z4-11**	**Z4-11** **sec.**
SiO_2	42.10	41.93	42.09	41.77	41.97
TiO_2	0.07	0.10	0.15	0.00	0.02
Al_2O_3	21.47	20.72	21.18	19.71	20.25
Cr_2O_3	3.97	4.34	4.62	6.17	5.17
FeO_{tot}	8.68	8.12	8.33	8.77	8.51
MnO	0.42	0.40	0.41	0.51	0.50
MgO	20.67	20.64	19.94	19.63	19.78
CaO	4.26	4.39	4.68	4.79	4.53
Na_2O	0.03	0.00	0.01	0.06	0.02
K_2O	0.01	0.00	0.00	0.02	0.01
SUM	101.67	100.64	101.42	101.43	100.77
Mg#	80.9	81.9	81.0	80.0	80.6
Cr#	11.0	12.3	12.8	17.4	14.6
T(°C)-Ry96				779	
T(°C)-Ca99				898	
Li	b.d.l.	b.d.l.	0.94	0.23	b.d.l.
B	b.d.l.	b.d.l.	1.22	0.67	b.d.l.
Ti	472	780	847	20.5	45.9
Co	38.9	45.7	33.0	37.4	64.0
Ni	19.6	26.3	23.2	18.9	32.5
Zn	9.74	10.5	7.18	6.42	12.4
Sc	173	116	121	155	370
V	127	203	191	286	140
Rb	0.088	b.d.l.	0.12	b.d.l.	0.14
Sr	0.32	1.58	3.85	1.06	4.37
Y	69.8	12.4	12.5	0.69	116
Zr	57.9	36.0	46.8	0.36	61.43
Nb	0.10	0.82	1.16	1.03	1.81
Cs	b.d.l.	0.004	0.020	0.010	b.d.l.
Ba	0.093	0.68	2.60	0.57	1.72
La	0.080	0.14	0.55	0.096	0.23
Ce	0.65	0.95	1.58	0.57	2.11
Pr	0.24	0.34	0.41	0.031	0.85
Nd	2.91	3.12	4.47	0.071	9.51
Sm	3.12	1.93	3.49	0.043	9.04
Eu	1.82	0.81	1.79	0.062	5.53
Gd	6.91	2.07	5.09	0.18	20.0
Tb	1.61	0.33	0.55	0.014	3.98
Dy	12.1	1.94	3.02	0.11	22.9
Ho	2.67	0.51	0.58	0.015	4.27
Er	7.08	1.48	1.33	0.078	9.93
Tm	1.13	0.21	0.24	0.014	1.22
Yb	7.37	2.01	1.04	0.44	8.15
Lu	1.08	0.29	0.24	0.090	1.34
Hf	0.42	0.35	0.55	b.d.l.	0.23
Ta	0.012	0.051	0.020	0.015	0.13
Pb	0.07	0.022	0.091	0.047	0.052
Th	0.063	0.022	0.32	0.026	0.079
U	0.038	0.049	0.11	b.d.l.	0.047
La_{CI}/Sm_{CI}	0.016	0.045	0.098	1.399	0.016
Sm_{CI}/Yb_{CI}	0.47	1.06	3.71	0.11	1.23
Ti_{PM}/Ti^*	0.03	0.14	0.07	0.05	0.00
Zr_{PM}/Hf_{PM}	3.76	2.77	2.31		7.17

Clinopyroxenes associated with Group A garnets

Sample Notes	Z4-2	Z5-02	Z5-11	Z5-15
SiO_2	54.98	55.24	54.90	55.62
TiO_2	0.24	0.15	0.34	0.10
Al_2O_3	3.11	2.58	2.58	2.48
Cr_2O_3	1.70	2.74	2.27	0.57
FeO_{tot}	2.19	1.80	1.89	2.08
MnO	0.03	0.00	0.06	0.07
MgO	15.32	15.71	15.87	16.72
CaO	19.94	19.52	19.76	21.31
Na_2O	2.43	2.51	2.49	1.60
K_2O	0.00	0.03	0.02	0.01
SUM	99.95	100.27	100.18	100.57
Mg#	92.6	94.0	93.7	93.5
Cr#	26.9	41.7	37.1	13.4
Ko	0.049	0.078	0.065	0.016
Jd (+Ae)	0.122	0.097	0.109	0.094
Di	0.758	0.738	0.740	0.808
T(°C)-NT00	803	875	841	885
P(GPa)-NT00	3.23	3.71	3.80	3.37
Li	0.62	1.97	1.64	0.99
B	b.d.l.	1.74	1.31	1.32
Ti	1285	706	1695	505
Co	14.6	15.2	16.4	15.5
Ni	259	267	261	299
Zn	7.89	8.85	8.95	8.78
Sc	24.5	29.3	31.3	18.7
V	389	475	424	363
Rb	b.d.l.	0.081	0.20	0.021
Sr	141	70.8	133	156
Y	1.98	1.29	1.88	2.68
Zr	18.2	6.17	19.1	14.0
Nb	0.050	0.75	1.29	1.38
Cs	0.004	b.d.l.	0.005	b.d.l.
Ba	0.14	0.98	2.92	0.81
La	4.81	2.77	3.04	10.0
Ce	11.8	6.43	9.66	23.9
Pr	1.53	0.72	1.54	2.57
Nd	7.38	3.15	7.80	8.91
Sm	1.77	0.78	2.03	1.49
Eu	0.55	0.26	0.54	0.52
Gd	1.15	0.63	0.86	0.98
Tb	0.15	0.066	0.15	0.10
Dy	0.58	0.41	0.58	0.86
Ho	0.10	0.043	0.091	0.13
Er	0.15	0.11	0.10	0.19
Tm	0.017	0.005	0.014	0.025
Yb	0.08	0.12	0.10	0.13
Lu	0.008	b.d.l.	0.007	0.017
Hf	0.95	0.31	0.93	0.45
Ta	b.d.l.	0.027	0.039	0.027
Pb	0.70	0.27	0.62	0.71
Th	0.58	0.086	0.17	0.54
U	0.086	0.024	0.059	0.15
La_{CI}/Ce_{CI}	1.1	1.1	0.8	1.1
La_{CI}/Sm_{CI}	1.7	2.2	0.9	4.2
Sm_{CI}/Yb_{CI}	24	7	22	13
Ti_{PM}/Ti^*	0.37	0.41	0.55	0.16
Nb_{PM}/Ta_{PM}		1.54	1.84	2.87
Zr_{PM}/Hf_{PM}	0.52	0.54	0.55	0.83

Clinopyroxenes associated with secondary low-(Ca, Cr) domains

Sample	**Z4-3**	**Z4-7**	**Z5-5**	**Z6-12**	**Z4-9**	**Z5-3**	**Z4-5**	**Z5-9**
Notes								
SiO_2	54.76	55.39	53.89	54.89	54.73	54.28	54.51	54.55
TiO_2	0.07	0.16	0.07	0.19	0.14	0.10	0.21	0.23
Al_2O_3	3.98	4.34	2.88	3.14	4.45	2.68	3.83	4.19
Cr_2O_3	3.74	3.77	2.69	3.47	4.43	3.08	4.02	3.74
FeO_{tot}	2.59	2.48	2.33	2.11	2.56	2.15	2.43	2.54
MnO	0.01	0.00	0.00	0.00	0.00	0.00	0.00	0.00
MgO	13.58	13.25	14.96	14.18	13.18	15.03	13.69	13.35
CaO	17.21	16.38	18.83	18.54	16.40	19.27	16.53	16.62
Na_2O	3.86	4.38	2.84	3.21	4.54	2.52	3.99	4.09
K_2O	0.00	0.01	0.01	0.00	0.00	0.00	0.00	0.00
SUM	99.79	100.17	98.51	99.73	100.43	99.11	99.20	99.31
Mg#	90.4	90.5	92.0	92.3	90.2	92.6	90.9	90.3
Cr#	38.7	36.8	38.6	42.6	40.0	43.5	41.3	37.4
Ko	0.107	0.107	0.078	0.099	0.125	0.089	0.115	0.107
Jd (+Ae)	0.164	0.197	0.123	0.126	0.190	0.090	0.165	0.180
Di	0.644	0.620	0.709	0.711	0.591	0.735	0.626	0.628
T(°C)-NT00	788	788	809	764	730	845	840	793
P(GPa)-NT00	3.20	3.37	3.58	3.30	3.05	3.41	3.48	3.25
Li	---	1.20	1.43	1.54	---	0.58	5.30	0.47
B	---	b.d.l.	1.96	1.00	---	0.65	5.98	10.60
Ti	---	1087	519	913	---	546	1003	1696
Co	---	17.6	13.9	14.6	---	15.0	12.5	11.7
Ni	---	170	231	229	---	250	211	237
Zn	---	7.36	6.22	8.35	---	8.29	14.8	7.27
Sc	---	45.7	36.1	49.7	---	54.4	39.3	55.4
V	---	605	369	359	---	368	591	700
Rb	---	0.64	0.14	b.d.l.	---	0.047	b.d.l.	0.18
Sr	---	451	337	594	---	636	516	651
Y	---	2.50	5.32	6.04	---	3.27	0.99	2.04
Zr	---	40.9	50.9	65.0	---	59.1	55.7	101
Nb	---	2.53	7.11	1.03	---	0.41	3.18	6.41
Cs	---	b.d.l.	b.d.l.	b.d.l.	---	b.d.l.	b.d.l.	0.019
Ba	---	7.59	22.6	b.d.l.	---	0.28	3.09	5.34
La	---	19.1	45.0	22.2	---	41.4	18.5	28.4
Ce	---	75.5	103	72.1	---	102	62.8	103
Pr	---	13.1	11.8	10.8	---	12.7	9.33	18.2
Nd	---	42.6	48.1	50.1	---	52.0	37.0	77.4
Sm	---	6.93	8.29	8.78	---	7.47	7.40	12.1
Eu	---	1.50	2.21	2.51	---	1.77	1.39	2.41
Gd	---	2.59	4.08	5.43	---	3.19	1.36	4.07
Tb	---	0.15	0.48	0.59	---	0.31	0.21	0.21
Dy	---	0.31	1.63	2.18	---	1.06	0.17	0.85
Ho	---	0.081	0.29	0.23	---	0.15	b.d.l.	0.044
Er	---	b.d.l.	0.48	0.36	---	0.40	0.18	0.45
Tm	---	b.d.l.	0.052	0.032	---	0.025	b.d.l.	0.017
Yb	---	b.d.l.	0.28	0.35	---	0.17	0.38	b.d.l.
Lu	---	0.040	0.046	0.010	---	0.018	b.d.l.	b.d.l.
Hf	---	1.43	1.13	2.11	---	2.74	2.25	2.52
Ta	---	0.12	0.38	0.073	---	0.064	0.26	0.46
Pb	---	0.99	3.56	1.73	---	1.76	1.37	1.52
Th	---	0.24	1.45	0.71	---	1.31	0.33	0.67
U	---	0.033	0.10	0.093	---	0.12	0.13	0.12
La_{CI}/Ce_{CI}		0.7	1.1	0.8		1.0	0.8	0.7
La_{CI}/Sm_{CI}		1.7	3.4	1.6		3.5	1.6	1.5
Sm_{CI}/Yb_{CI}			32	28		50	22	
Ti_{PM}/Ti^*		0.12	0.04	0.06		0.05	0.14	0.12
Nb_{PM}/Ta_{PM}		1.24	1.06	0.80		0.36	0.69	0.79
Zr_{PM}/Hf_{PM}		0.77	1.21	0.83		0.58	0.67	1.08

Clinopyroxenes associated with secondary low-(Ca, Cr) domains

Sample	**Z4-6**	**Z4-1**	**Z4-4**	**Z4-8**	**Z5-10**	**Z6-9**	**Z6-10**	**Z6-11**
Notes								
SiO_2	55.00	55.05	54.78	54.78	55.36	55.13	54.88	54.76
TiO_2	0.07	0.27	0.04	0.05	0.10	0.09	0.04	0.02
Al_2O_3	2.67	4.05	2.09	3.54	4.67	3.47	3.38	3.06
Cr_2O_3	3.18	4.13	2.21	3.73	4.13	3.69	3.22	3.45
FeO_{tot}	1.89	2.43	1.81	2.34	2.55	2.30	2.30	1.94
MnO	0.02	0.02	0.07	0.00	0.00	0.00	0.00	0.00
MgO	15.18	13.27	16.20	13.97	13.10	14.19	14.26	14.63
CaO	19.12	16.58	20.46	16.93	16.03	18.07	18.53	18.72
Na_2O	2.75	4.10	1.90	3.66	4.63	3.39	3.21	2.95
K_2O	0.01	0.01	0.01	0.03	0.01	0.00	0.00	0.00
SUM	99.90	99.91	99.57	99.04	100.58	100.33	99.80	99.53
Mg#	93.5	90.7	94.1	91.4	90.2	91.7	91.7	93.1
Cr#	44.4	40.6	41.5	41.4	37.2	41.6	39.0	43.0
Ko	0.091	0.118	0.063	0.107	0.116	0.105	0.092	0.099
Jd (+Ae)	0.102	0.169	0.070	0.151	0.204	0.131	0.133	0.108
Di	0.727	0.633	0.778	0.650	0.592	0.682	0.702	0.713
T(°C)-NT00	843	814	888	874	777	817	778	822
P(GPa)-NT00	36.0	33.0	37.6	36.2	31.9	32.8	32.2	33.0
Li	1.65	---	b.d.l.	15.7	---	---	0.65	---
B	2.95	---	1.79	13.6	---	---	5.19	---
Ti	434	---	106	291	---	---	192	---
Co	15.3	---	16.2	14.1	---	---	16.6	---
Ni	290	---	293	230	---	---	263	---
Zn	8.83	---	15.2	27.8	---	---	13.7	---
Sc	32.2	---	23.9	67.8	---	---	47.8	---
V	514	---	420	491	---	---	516	---
Rb	2.19	---	2.01	0.33	---	---	0.13	---
Sr	567	---	622	544	---	---	583	---
Y	0.54	---	1.48	2.23	---	---	0.92	---
Zr	13.3	---	30.0	65.1	---	---	57.4	---
Nb	0.81	---	3.01	3.63	---	---	1.18	---
Cs	0.042	---	0.027	0.016	---	---	b.d.l.	---
Ba	218	---	170	14.1	---	---	0.22	---
La	26.6	---	28.8	24.7	---	---	25.9	---
Ce	62.9	---	85.7	91.8	---	---	89.3	---
Pr	8.63	---	10.4	14.7	---	---	14.2	---
Nd	35.8	---	42.6	64.1	---	---	60.4	---
Sm	2.66	---	6.35	9.70	---	---	10.8	---
Eu	0.54	---	1.78	2.79	---	---	1.84	---
Gd	0.77	---	2.21	5.53	---	---	4.47	---
Tb	0.052	---	0.28	0.37	---	---	0.36	---
Dy	0.22	---	0.71	1.17	---	---	0.53	---
Ho	0.033	---	0.059	0.080	---	---	0.14	---
Er	0.051	---	0.097	0.22	---	---	0.28	---
Tm	0.005	---	0.011	0.010	---	---	b.d.l.	---
Yb	b.d.l.	---	0.28	0.15	---	---	b.d.l.	---
Lu	0.002	---	b.d.l.	b.d.l.	---	---	b.d.l.	---
Hf	0.67	---	1.39	1.74	---	---	3.27	---
Ta	0.016	---	0.069	0.11	---	---	0.030	---
Pb	3.25	---	1.65	2.51	---	---	1.53	---
Th	1.68	---	1.30	0.69	---	---	0.41	---
U	0.28	---	0.38	0.21	---	---	0.13	---
La_{CI}/Ce_{CI}	1.1		0.9	0.7			0.7	
La_{CI}/Sm_{CI}	6.3		2.8	1.6			1.5	
Sm_{CI}/Yb_{CI}			25	70				
Ti_{PM}/Ti^*	0.15		0.01	0.02			0.02	
Nb_{PM}/Ta_{PM}	2.87		2.45	1.91			2.21	
Zr_{PM}/Hf_{PM}	0.54		0.58	1.01			0.47	

Phlogopites in veinlets and included in or associated with secondary domains of Group A (Z5-2 and Z6-2) and Group B (from Z4-5 to Z6-12) garnets.

Sample	**Z5-2**	**Z6-2**	**Z4-5**	**Z4-7**	**Z4-9**	**Z5-3**	**Z5-5**	**Z5-6**	**Z6-12**
Notes	veinlet	veinlet	veinlet	veinlet	veinlet	veinlet	assoc. to rim	veinlet	big assoc.
SiO_2	41.27	39.59	40.36	41.62	41.79	39.90	42.01	39.00	40.66
TiO_2	0.24	0.15	0.20	0.21	0.29	0.27	0.17	2.62	0.39
Al_2O_3	13.81	13.50	14.63	13.16	13.07	16.35	13.29	16.09	12.97
Cr_2O_3	1.30	0.93	1.28	0.88	2.26	1.82	0.90	2.52	0.84
FeO_{tot}	3.41	4.15	3.62	2.70	3.46	4.04	2.75	3.61	2.78
MnO	0.00	0.06	0.00	0.00	0.00	0.00	0.07	0.00	0.01
MgO	24.71	25.77	24.58	25.94	24.56	22.75	24.83	21.85	25.33
CaO	0.03	0.14	0.00	0.00	0.04	0.03	0.04	0.01	0.05
Na_2O	0.78	0.70	0.46	0.66	0.31	2.66	0.60	0.62	0.55
K_2O	8.29	8.80	9.59	8.90	9.46	4.93	8.76	9.52	9.14
Cl	0.06	0.05	0.03	0.05	0.05	0.05	0.03	0.00	0.11
SUM	93.91	93.85	94.75	94.12	95.29	92.81	93.46	95.83	92.83
Mg#	92.8	91.7	92.4	94.5	92.7	90.9	94.1	91.5	94.2
Li	2.53	---	---	4.13	---	b.d.l.	4.51	b.d.l.	2.3
B	b.d.l.	---	---	11.06	---	b.d.l.	b.d.l.	b.d.l.	5.1
Ti	1463	---	---	1462	---	2135	1202	12322	2095
Co	45.59	---	---	44	---	56.7	49	39.1	48
Ni	367	---	---	1351	---	880	1408	473	1364
Zn	23.7	---	---	28	---	15.5	26.9	15.3	33
Sc	3.58	---	---	1.5	---	19.9	1.73	18.9	3.04
V	92.1	---	---	60	---	122	38.2	251	63
Rb	227	---	---	223	---	34.7	166	294	167
Sr	66.1	---	---	79	---	490	84.6	88.3	98
Y	0.061	---	---	*0.07*	---	*0.55*	*0.14*	b.d.l.	*0.85*
Zr	2.99	---	---	3.2	---	12.8	3.78	13.4	2.7
Nb	35.0	---	---	31.5	---	117	23.3	35.7	21.7
Cs	3.7	---	---	4.0	---	0.88	4.05	3.35	2.8
Ba	4138	---	---	5704	---	1433	6295	2757	6953
La	0.32	---	---	*0.26*	---	*0.77*	*0.12*	*0.06*	*5.0*
Ce	0.65	---	---	*0.13*	---	*0.69*	b.d.l.	b.d.l.	*7.7*
Pr	0.038	---	---	*0.07*	---	b.d.l.	0.023	*0.04*	*0.37*
Nd	0.37	---	---	*0.24*	---	*0.22*	b.d.l.	b.d.l.	*1.7*
Sm	b.d.l.	---	---	b.d.l.	---	b.d.l.	*0.19*	b.d.l.	*0.34*
Eu	b.d.l.	---	---	*0.09*	---	*0.11*	*0.16*	*0.18*	*0.23*
Gd	b.d.l.	---	---	b.d.l.	---	b.d.l.	b.d.l.	b.d.l.	b.d.l.
Tb	b.d.l.	---	---	*0.04*	---	b.d.l.	b.d.l.	b.d.l.	b.d.l.
Dy	b.d.l.	---	---	b.d.l.	---	b.d.l.	*0.18*	b.d.l.	*0.23*
Ho	0.052	---	---	b.d.l.	---	b.d.l.	b.d.l.	b.d.l.	*0.06*
Er	b.d.l.	---	---	b.d.l.	---	b.d.l.	b.d.l.	b.d.l.	*0.30*
Tm	b.d.l.	---	---	b.d.l.	---	b.d.l.	*0.085*	b.d.l.	b.d.l.
Yb	0.16	---	---	b.d.l.	---	b.d.l.	b.d.l.	b.d.l.	b.d.l.
Lu	0.026	---	---	b.d.l.	---	b.d.l.	b.d.l.	*0.06*	b.d.l.
Hf	0.13	---	---	0.54	---	0.81	b.d.l.	0.29	*0.55*
Ta	2.45	---	---	1.80	---	23.4	1.65	3.71	0.71
Pb	0.35	---	---	2.06	---	2.0	0.45	0.76	8.0
Th	0.28	---	---	1.93	---	*0.15*	*1.19*	b.d.l.	*5.5*
U	0.021	---	---	0.43	---	*0.13*	0.29	b.d.l.	*0.53*

Phlogopites in veinlets and included in or associated with secondary domains of Group C garnets.

Sample	**Z4-4**	**Z4-6**	**Z4-8**	**Z5-9**	**Z5-10**	**Z6-10**
Notes	big incl.	big incl.	incl.	small incl.	incl.	veinlet
SiO_2	40.97	41.02	41.61	40.36	40.88	39.87
TiO_2	0.08	0.26	0.07	0.68	0.90	0.16
Al_2O_3	13.07	13.18	13.06	14.54	12.47	14.79
Cr_2O_3	0.94	0.94	1.12	1.25	0.40	1.30
FeO_{tot}	3.39	2.96	2.60	3.92	4.72	4.02
MnO	0.03	0.03	0.00	0.02	0.01	0.03
MgO	25.00	24.99	25.80	24.04	25.34	25.59
CaO	0.02	0.00	0.08	0.00	0.01	0.08
Na_2O	0.19	0.28	0.49	0.71	0.87	0.65
K_2O	9.57	9.42	8.93	8.98	8.57	8.47
Cl	0.46	0.42	0.07	0.05	0.02	0.03
SUM	93.73	93.50	93.83	94.54	94.19	94.99
Mg#	92.9	93.8	94.7	91.6	90.5	91.9
Li	2.1	1.7	---	5	---	---
B	1.6	2.2	---	2	---	---
Ti	680	1641	---	3802	---	---
Co	66	60	---	47	---	---
Ni	1792	1749	---	431	---	---
Zn	37	30	---	21	---	---
Sc	1.3	1.2	---	2.2	---	---
V	105	103	---	108	---	---
Rb	159	126	---	168	---	---
Sr	45	53	---	62	---	---
Y	*0.19*	0.18	---	b.d.l.	---	---
Zr	2.1	0.44	---	2.0	---	---
Nb	64	2.3	---	47	---	---
Cs	4.1	3.0	---	3.2	---	---
Ba	10689	9620	---	3761	---	---
La	*0.56*	*0.039*	---	b.d.l.	---	---
Ce	*0.87*	*0.052*	---	*0.05*	---	---
Pr	*0.031*	*0.007*	---	b.d.l.	---	---
Nd	*0.12*	*0.015*	---	b.d.l.	---	---
Sm	b.d.l.	*0.041*	---	b.d.l.	---	---
Eu	*0.05*	*0.072*	---	b.d.l.	---	---
Gd	b.d.l.	b.d.l.	---	*0.09*	---	---
Tb	*0.01*	b.d.l.	---	b.d.l.	---	---
Dy	*0.03*	b.d.l.	---	b.d.l.	---	---
Ho	*0.01*	*0.001*	---	b.d.l.	---	---
Er	b.d.l.	b.d.l.	---	*0.08*	---	---
Tm	b.d.l.	*0.002*	---	b.d.l.	---	---
Yb	*0.05*	*0.008*	---	b.d.l.	---	---
Lu	*0.017*	b.d.l.	---	b.d.l.	---	---
Hf	0.14	0.04	---	b.d.l.	---	---
Ta	4.1	0.26	---	3.2	---	---
Pb	1.1	1.59	---	0.80	---	---
Th	*1.59*	*4.51*	---	*0.081*	---	---
U	*0.45*	*0.64*	---	*0.011*	---	---

Amphiboles, carbonates and serpentines

Sample	Z4-3	Z4-9	Z5-5	Z4-1	Z4-8	Z4-11	Z4-10	Z6-2	Z5-15	Z6-2	Z5-5	Z4-6
	amphibole						carbonate		serpentine			
Notes	Grt rim intergr	veinlet	intergr with Cpx	veinlet	veinlet	grt-amph intergr	incl	incl with serp	incl in Cpx	incl with carb	incl	incl
SiO_2	48.30	45.02	47.37	45.34	43.55	49.21	0.05	0.03	49.33	40.12	45.61	48.78
TiO_2	0.23	0.15	0.20	0.91	0.11	0.05	---	---	0.02	0.04	0.07	0.06
Al_2O_3	9.20	16.87	7.92	12.40	13.78	9.18	---	---	5.35	1.71	1.28	1.98
Cr_2O_3	2.77	4.94	2.25	1.78	3.59	2.29	---	---	1.36	0.15	0.34	0.09
FeO_{tot}	2.89	6.25	2.69	4.47	5.39	2.96	0.04	0.05	3.57	7.73	8.81	3.03
MnO	0.01	0.33	0.00	0.19	0.24	0.06	0.09	0.09	0.00	0.06	0.03	0.02
MgO	19.21	16.55	18.27	18.47	18.35	19.92	0.14	0.19	25.16	33.55	30.44	33.31
CaO	7.43	7.28	7.13	8.85	8.63	7.51	54.65	54.85	1.32	0.47	0.35	0.25
Na_2O	5.18	1.07	4.56	3.61	3.79	5.36	---	---	0.11	0.00	0.03	0.01
K_2O	1.42	0.28	1.37	0.29	0.32	0.97	---	---	0.05	0.04	0.01	0.01
Cl	---	---	---	---	---	---	---	---	0.07	0.08	0.16	0.10
CO_2[a]	---	---	---	---	---	---	43.12	43.34	---	---	---	---
SUM	96.66	98.72	91.79	96.32	97.75	97.51	98.09	98.55	86.33	83.94	87.14	87.63
Li	5.73	---	2.03	---	---	1.39	2.62	24.9	---	---	---	---
B	13.1	---	7.18	---	---	2.14	9.24	2.29	---	---	---	---
Cr		---		---	---		88.4	32.3	---	---	---	---
Ti	1458	---	1092	---	---	210	15.5	6.04	---	---	---	---
Co	30.0	---	23.0	---	---	26.7	2.54	1.43	---	---	---	---
Ni	675	---	555	---	---	623	16.7	18.0	---	---	---	---
Zn	19.6	---	14.0	---	---	10.7	2.51	29.2	---	---	---	---
Sc	42.1	---	31.9	---	---	39.4	0.6	1.9	---	---	---	---
V	195	---	133	---	---	222	1.43	b.d.l.	---	---	---	---
Rb	4.97	---	3.65	---	---	1.98	b.d.l.	0.38	---	---	---	---
Sr	341	---	288	---	---	604	71.2	76.4	---	---	---	---
Y	8.86	---	8.41	---	---	10.4	2.69	7.3	---	---	---	---
Zr	115	---	89.2	---	---	97.1	0.86	2.45	---	---	---	---
Nb	41.2	---	31.6	---	---	97.1	1.61	1.26	---	---	---	---
Cs	0.067	---	0.022	---	---	b.d.l.	b.d.l.	b.d.l.	---	---	---	---
Ba	227	---	162	---	---	254	1.92	15.3	---	---	---	---
La	15.5	---	8.37	---	---	27.3	116.9	236	---	---	---	---
Ce	49.2	---	30.9	---	---	106	119	286	---	---	---	---
Pr	6.9	---	5.22	---	---	16.7	10.7	22.8	---	---	---	---
Nd	35.1	---	26.2	---	---	78.7	32.5	73.8	---	---	---	---
Sm	8.58	---	6.18	---	---	15.31	3.67	6.24	---	---	---	---
Eu	2.35	---	1.77	---	---	4.57	1.02	1.73	---	---	---	---
Gd	4.2	---	4.42	---	---	8.69	1.88	3.28	---	---	---	---
Tb	0.56	---	0.50	---	---	0.88	0.21	0.38	---	---	---	---
Dy	2.66	---	2.19	---	---	3.47	0.64	1.69	---	---	---	---
Ho	0.41	---	0.42	---	---	0.37	0.13	0.20	---	---	---	---
Er	0.79	---	0.91	---	---	0.54	0.11	0.42	---	---	---	---
Tm	0.12	---	0.069	---	---	0.065	b.d.l.	0.052	---	---	---	---
Yb	0.76	---	0.39	---	---	0.34	0.086	0.26	---	---	---	---
Lu	0.055	---	0.048	---	---	0.030	0.042	b.d.l.	---	---	---	---
Hf	2.59	---	2.88	---	---	1.46	b.d.l.	0.043	---	---	---	---
Ta	3.36	---	2.84	---	---	7.65	0.028	0.18	---	---	---	---
Pb	0.98	---	0.59	---	---	1.18	0.29	0.31	---	---	---	---
Th	0.63	---	0.12	---	---	0.46	0.068	0.45	---	---	---	---
U	0.26	---	0.018	---	---	0.100	0.13	0.052	---	---	---	---

[a] Calculated from stoichiometry.

Chromian spinels included in secondary, low-(Ca-Cr) garnet domains.

Sample	**Z4-1**	**Z4-3**	**Z4-4**	**Z4-6**	**Z4-7**	**Z4-8**	**Z4-9**	**Z4-11**	**Z5-3**	**Z5-5**	**Z5-9**	**Z5-13**
Notes	incl.[1]	on Grt rim[2]	incl	incl[3]	incl	incl	incl	incl[2]	incl	incl	incl	incl
SiO_2	0.11	0.05	0.12	0.08	0.09	0.10	0.12	0.10	0.07	0.08	0.14	0.05
TiO_2	1.35	0.53	0.15	0.46	0.62	0.22	0.82	0.10	0.80	0.54	1.28	0.17
Al_2O_3	8.71	10.17	8.99	8.80	9.60	9.94	9.01	11.99	9.59	10.12	7.44	8.72
Cr_2O_3	56.19	55.43	58.98	58.89	55.89	56.27	55.75	53.83	55.18	55.67	56.86	59.35
FeO_{tot}	22.22	22.01	20.31	21.12	22.18	21.39	22.54	22.22	23.28	22.72	22.93	21.33
MnO	0.37	0.34	0.35	0.35	0.29	0.29	0.32	0.37	0.34	0.43	0.33	0.33
MgO	11.73	10.70	10.91	11.05	11.05	11.22	11.29	11.26	10.77	10.95	10.49	11.11
V_2O_3	0.35	0.15	0.33	0.31	0.25	0.27	0.23	0.14	0.18	0.12	0.34	0.31
NiO	0.14	0.11	0.11	0.12	0.08	0.16	0.12	0.09	0.10	0.10	0.08	0.10
SUM	101.16	99.48	100.25	101.16	100.06	99.86	100.21	100.10	100.32	100.74	99.88	101.47
Mg#	55.4	52.4	53.7	53.6	53.51	54.91	54.43	54.67	52.0	52.97	50.71	54.1
Cr#	81.2	78.5	81.5	81.8	79.61	79.15	80.59	75.08	79.4	78.67	83.68	82.0
Li	*1.5*	*1.9*	---	0.8	---	---	---	---	0.31	---	---	*0.5*
B	*2.9*	*2.5*	---	2.2	---	---	---	---	b.d.l.	---	---	*1.1*
Ti	7965	3399	---	2967	---	---	---	---	4548	---	---	1118
Co	345	319	---	*330*	---	---	---	---	328	---	---	326
Ni	1032	825	---	*785*	---	---	---	---	914	---	---	714
Zn	1414	1573	---	*1420*	---	---	---	---	1484	---	---	1267
Sc	4.5	4.1	---	*1.4*	---	---	---	---	6.77	---	---	1.8
V	2306	977	---	*1862*	---	---	---	---	1775	---	---	1874
Rb	*1.1*	*2.7*	---	*5.3*	---	---	---	---	*0.4*	---	---	*0.52*
Sr	*0.12*	*4.8*	---	*1.9*	---	---	---	---	*14*	---	---	*0.09*
Y	*0.19*	*0.46*	---	b.d.l.	---	---	---	---	*1.2*	---	---	b.d.l.
Zr	2.5	5.7	---	0.35	---	---	---	---	2.5	---	---	1.11
Nb	3.50	11.2	---	0.44	---	---	---	---	0.98	---	---	0.81
Cs	*0.01*	*0.03*	---	*0.13*	---	---	---	---	b.d.l.	---	---	*0.01*
Ba	*0.23*	*33*	---	*239*	---	---	---	---	*0.88*	---	---	b.d.l.
La	*0.10*	*1.6*	---	*0.072*	---	---	---	---	*0.78*	---	---	b.d.l.
Ce	*0.41*	*3.2*	---	*0.22*	---	---	---	---	*2.64*	---	---	b.d.l.
Pr	*0.033*	*0.49*	---	*0.039*	---	---	---	---	*0.27*	---	---	b.d.l.
Nd	*0.19*	*0.61*	---	*0.094*	---	---	---	---	*1.11*	---	---	b.d.l.
Sm	b.d.l.	*0.14*	---	b.d.l.	---	---	---	---	*0.19*	---	---	b.d.l.
Eu	b.d.l.	*0.031*	---	b.d.l.	---	---	---	---	*0.083*	---	---	b.d.l.
Gd	*0.040*	*0.17*	---	*0.020*	---	---	---	---	*0.22*	---	---	b.d.l.
Tb	*0.008*	*0.038*	---	b.d.l.	---	---	---	---	0.058	---	---	*0.014*
Dy	*0.058*	*0.21*	---	b.d.l.	---	---	---	---	*0.27*	---	---	b.d.l.
Ho	*0.015*	*0.022*	---	*0.003*	---	---	---	---	0.054	---	---	b.d.l.
Er	b.d.l.	*0.072*	---	b.d.l.	---	---	---	---	*0.12*	---	---	b.d.l.
Tm	b.d.l.	*0.021*	---	b.d.l.	---	---	---	---	0.022	---	---	b.d.l.
Yb	b.d.l.	b.d.l.	---	b.d.l.	---	---	---	---	0.18	---	---	*0.061*
Lu	*0.026*	b.d.l.	---	b.d.l.	---	---	---	---	0.030	---	---	b.d.l.
Hf	0.045	0.16	---	b.d.l.	---	---	---	---	b.d.l.	---	---	b.d.l.
Ta	0.078	0.40	---	*0.05*	---	---	---	---	0.079	---	---	0.020
Pb	*0.181*	*7.8*	---	*0.32*	---	---	---	---	0.46	---	---	*0.17*
Th	*0.041*	*0.88*	---	*0.061*	---	---	---	---	*0.022*	---	---	b.d.l.
U	*0.043*	*0.25*	---	*0.030*	---	---	---	---	*0.012*	---	---	b.d.l.

[1] big (ca. 400 μm) inclusion associated with serpentine and amphibole, connected to late veinlets;

[2] associated with amphibole;

[3] associated with a big inclusion of phlogopite.

Here Mg# = 100*Mg/(Mg+Fe^{2+}).

Late spinels in veinlets, and one Ti-oxide of the crichtonite series included in the secondary domain of garnet Z4-1.

Sample	**Z4-5**	**Z4-8**	**Z4-9**	**Z4-9**	**Z5-2**	**Z5-6**	**Z5-10**	**Z5-11**	**Z5-13**		**Z4-1**
Notes											cric
SiO_2	0.12	0.14	0.22	0.20	0.10	0.32	0.13	0.08	0.08		0.07
TiO_2	0.74	0.82	0.17	0.85	0.70	0.47	0.43	1.54	0.33		53.16
Al_2O_3	18.85	16.98	39.54	18.16	22.10	47.06	18.57	16.80	20.02		1.67
Cr_2O_3	43.95	43.17	22.22	41.40	39.07	19.44	45.17	41.15	44.69		20.78
FeO_{tot}	24.03	25.64	23.06	27.63	26.20	15.40	23.76	29.96	23.56		8.71
MnO	0.39	0.40	0.61	0.46	0.50	0.36	0.44	0.59	0.43		0.11
MgO	12.39	11.72	14.56	10.72	11.51	18.55	12.03	9.61	11.90		3.99
V_2O_3	0.27	0.27	0.03	0.24	0.15	0.11	0.20	0.32	0.19		---
NiO	0.07	0.09	0.01	0.04	0.02	0.00	0.16	0.12	0.04		---
CaO	---	---	---	---	---	---	---	---	---		0.66
SrO	---	---	---	---	---	---	---	---	---		2.94
Zr_2O_3	---	---	---	---	---	---	---	---	---		2.27
La_2O_3	---	---	---	---	---	---	---	---	---		1.01
Ce_2O_3	---	---	---	---	---	---	---	---	---		1.31
Nb_2O_5	---	---	---	---	---	---	---	---	---		0.37
Na_2O	---	---	---	---	---	---	---	---	---		0.00
K_2O	---	---	---	---	---	---	---	---	---		0.13
BaO	---	---	---	---	---	---	---	---	---		0.00
SUM	100.82	99.24	100.43	99.68	100.34	101.72	100.89	100.18	101.23		97.18
Mg#	56.73	54.90	61.69	61.69	52.67	73.06	55.84	44.91	54.85		
Cr#	61.01	63.05	27.38	27.38	54.26	21.70	62.01	62.16	59.96		

Here Mg# = 100*Mg/(Mg+Fe^{2+}).

SUPPLEMENTARY TABLE 3

Chemical and modal parameters used in Plate Model numerical simulations and trace element composition (ppm)of model garnets

Chemical parameters

	$^{Ol/L}D$	$^{Opx/L}D$	$^{Cpx/L}D$	$^{Grt/L}D$	Infiltrated Melt Model 1 (ppm)	Infiltrated Melt Model 2 and 3 (ppm)	Initial Peridotite Model 1 and 2 (ppm)	Initial Peridotite Model 3 (ppm)
Th	1.00E-07	3.00E-05	1.20E-02	1.37E-03	5.8	49	0.0000004	0.0000004
U	1.00E-07	4.00E-05	1.00E-02	5.88E-03	0.78	13	0.0000005	0.0000006
Nb	2.00E-04	5.00E-04	7.70E-03	3.10E-03	7.6	65	0.000003	0.000003
La	1.00E-04	2.00E-04	5.40E-02	1.60E-03	4.1	56	0.000008	0.000010
Ce	2.00E-04	4.00E-04	8.60E-02	5.00E-03	13.3	195	0.00005	0.00006
Sr	1.00E-04	3.00E-04	1.28E-01	2.50E-03	41.2	252	0.0013	0.0015
Nd	4.00E-04	1.00E-03	1.87E-01	5.20E-02	4.9	89.8	0.0002	0.0002
Zr	4.00E-03	5.00E-03	1.30E-01	2.70E-01	72.9	57.1	0.0033	0.0087
Hf	6.00E-03	1.00E-02	2.00E-01	2.40E-01	1.5	1.5	0.0002	0.0002
Sm	4.40E-04	3.00E-03	2.91E-01	2.50E-01	1.4	6.4	0.0002	0.0003
Gd	7.60E-04	1.28E-02	4.00E-01	7.54E-01	1.4	2.0	0.0009	0.0010
Ti	7.00E-03	7.00E-02	3.30E-01	2.90E-01	2553	3258	2.6	2.1
Dy	1.40E-03	2.61E-02	4.42E-01	2.20E+00	1.3	0.66	0.0025	0.0029
Ho	1.84E-03	3.56E-02	4.39E-01	3.18E+00	0.32	0.12	0.00073	0.00084
Er	2.36E-03	4.74E-02	4.36E-01	3.60E+00	0.79	0.34	0.0037	0.0027
Yb	3.64E-03	7.87E-02	4.30E-01	6.60E+00	0.61	0.25	0.020	0.0034
Lu	4.40E-03	9.86E-02	4.27E-01	7.10E+00	0.10	0.04	0.0041	0.0010

Modal parameters (mass ratio)

	Ol	Opx	Cpx	Grt
Initial modal composition of country peridotite	0.772	0.16	0.06	0.042
Crystallising mineral mode in *Model 1*			0.8	0.2
Assimilated mineral in *Model 2* & *3**		1		

*Orthopyroxene assimilation in Model 2 & 3 was designed to progressively vary in each run increment from 0.5% of solid mass in the first cell at the bottom of the mantle column to 0.01‰ of solid mass at the top of the mantle column

Trace element composition (ppm)of model garnet from each cell of the hypothetical mantle column after 20 process increments in the numerical simulation Cell 1 is the bottom of the mantle column, Cell 20 is the top.

Model 1

cell	Th	U	Nb	La	Ce	Sr	Nd	Zr	Hf	Sm	Gd	Ti	Dy	Ho	Er	Yb	Lu
1	0.0081	0.0046	0.024	0.0067	0.067	0.10	0.26	19.9	0.36	0.35	1.09	745	2.97	1.01	2.83	4.01	0.70
2	0.0085	0.0049	0.025	0.0070	0.070	0.11	0.27	20.8	0.38	0.37	1.12	773	3.00	1.00	2.81	3.78	0.65
3	0.0089	0.0051	0.026	0.0073	0.074	0.11	0.28	21.6	0.39	0.38	1.14	797	3.01	0.98	2.72	3.27	0.56
4	0.0093	0.0054	0.028	0.0077	0.077	0.12	0.29	22.6	0.41	0.39	1.18	831	2.96	0.92	2.47	2.54	0.42
5	0.0098	0.0057	0.029	0.0081	0.081	0.13	0.31	24.0	0.43	0.41	1.23	875	2.79	0.80	2.08	1.89	0.31
6	0.0104	0.0060	0.031	0.0086	0.086	0.13	0.33	25.6	0.46	0.44	1.27	924	2.52	0.67	1.70	1.43	0.24
7	0.0110	0.0063	0.032	0.0092	0.092	0.14	0.35	27.7	0.50	0.47	1.30	975	2.23	0.55	1.38	1.12	0.19
8	0.0118	0.0068	0.035	0.0098	0.099	0.15	0.38	30.1	0.54	0.51	1.31	1027	1.97	0.46	1.13	0.93	0.16
9	0.0127	0.0073	0.037	0.0106	0.108	0.17	0.42	33.5	0.59	0.56	1.33	1087	1.75	0.39	0.95	0.79	0.14
10	0.0137	0.0079	0.040	0.0115	0.117	0.19	0.47	37.3	0.66	0.61	1.35	1147	1.58	0.34	0.83	0.71	0.12
11	0.0147	0.0085	0.043	0.0125	0.129	0.21	0.53	42.0	0.73	0.67	1.37	1210	1.47	0.31	0.76	0.68	0.12
12	0.0160	0.0092	0.047	0.0138	0.145	0.24	0.61	48.4	0.83	0.75	1.40	1288	1.38	0.29	0.71	0.65	0.11
13	0.0174	0.0100	0.051	0.0154	0.167	0.30	0.73	56.4	0.94	0.84	1.43	1373	1.35	0.28	0.70	0.65	0.11
14	0.0190	0.0110	0.056	0.0180	0.204	0.39	0.91	67.1	1.09	0.96	1.48	1470	1.34	0.29	0.70	0.67	0.12
15	0.0212	0.0122	0.062	0.0229	0.272	0.55	1.17	81.6	1.27	1.10	1.53	1581	1.38	0.30	0.73	0.69	0.12
16	0.0241	0.0139	0.070	0.0322	0.392	0.80	1.52	99.8	1.49	1.25	1.58	1698	1.41	0.31	0.78	0.74	0.13
17	0.0297	0.0172	0.085	0.0503	0.592	1.16	1.96	119.6	1.71	1.40	1.63	1800	1.45	0.32	0.81	0.77	0.13
18	0.0426	0.0249	0.119	0.0832	0.901	1.66	2.44	137.5	1.88	1.50	1.66	1854	1.55	0.35	0.88	0.82	0.14
19	0.0777	0.0456	0.211	0.1406	1.353	2.27	2.88	150.2	1.97	1.53	1.67	1849	1.66	0.38	0.96	0.89	0.15
20	0.2046	0.1196	0.570	0.2466	2.023	3.02	3.25	156.1	1.97	1.50	1.64	1796	1.73	0.41	1.03	0.95	0.16

Model 2

cell	Th	U	Nb	La	Ce	Sr	Nd	Zr	Hf	Sm	Gd	Ti	Dy	Ho	Er	Yb	Lu
1	0.0650	0.0713	0.192	0.0864	0.936	0.60	4.48	14.8	0.34	1.52	1.46	908	1.39	0.37	1.17	1.52	0.24
2	0.0608	0.0667	0.179	0.0808	0.875	0.56	4.19	13.8	0.31	1.42	1.36	851	1.28	0.33	1.03	1.21	0.19
3	0.0554	0.0608	0.163	0.0736	0.797	0.51	3.81	12.5	0.28	1.29	1.22	772	1.05	0.25	0.73	0.77	0.13
4	0.0490	0.0538	0.145	0.0651	0.704	0.45	3.35	10.9	0.25	1.13	1.02	664	0.69	0.14	0.38	0.48	0.09
5	0.0420	0.0461	0.124	0.0557	0.602	0.39	2.84	9.1	0.20	0.93	0.75	520	0.34	0.06	0.16	0.39	0.08
6	0.0347	0.0381	0.102	0.0459	0.494	0.32	2.30	6.9	0.15	0.71	0.46	351	0.14	0.02	0.08	0.37	0.08
7	0.0276	0.0302	0.081	0.0363	0.389	0.25	1.76	4.8	0.10	0.49	0.23	198	0.06	0.01	0.06	0.38	0.08
8	0.0211	0.0231	0.062	0.0275	0.293	0.19	1.26	2.9	0.06	0.29	0.09	93	0.04	0.01	0.06	0.39	0.08
9	0.0156	0.0170	0.046	0.0200	0.210	0.13	0.83	1.5	0.03	0.15	0.03	39	0.04	0.01	0.06	0.39	0.08
10	0.0111	0.0122	0.033	0.0140	0.144	0.09	0.51	0.7	0.01	0.07	0.01	19	0.04	0.01	0.06	0.40	0.08
11	0.0078	0.0085	0.023	0.0095	0.095	0.06	0.28	0.3	0.00	0.03	0.01	13	0.04	0.01	0.07	0.41	0.08
12	0.0053	0.0058	0.015	0.0063	0.060	0.03	0.15	0.1	0.00	0.01	0.01	12	0.04	0.01	0.07	0.41	0.08
13	0.0036	0.0039	0.010	0.0041	0.037	0.02	0.07	0.0	0.00	0.00	0.01	13	0.04	0.01	0.07	0.42	0.08
14	0.0025	0.0026	0.007	0.0026	0.022	0.01	0.03	0.0	0.00	0.00	0.01	14	0.04	0.01	0.07	0.42	0.09
15	0.0017	0.0018	0.005	0.0016	0.013	0.01	0.01	0.0	0.00	0.00	0.01	15	0.05	0.01	0.07	0.43	0.09
16	0.0012	0.0012	0.003	0.0010	0.007	0.00	0.00	0.0	0.00	0.00	0.01	16	0.05	0.01	0.07	0.43	0.09
17	0.0008	0.0009	0.002	0.0006	0.004	0.00	0.00	0.0	0.00	0.00	0.01	17	0.05	0.01	0.08	0.43	0.09
18	0.0006	0.0006	0.002	0.0004	0.002	0.00	0.00	0.0	0.00	0.00	0.01	18	0.05	0.01	0.08	0.44	0.09
19	0.0004	0.0004	0.001	0.0002	0.001	0.00	0.00	0.0	0.00	0.00	0.01	19	0.05	0.01	0.08	0.44	0.09
20	0.0003	0.0003	0.001	0.0001	0.000	0.00	0.00	0.0	0.00	0.00	0.01	20	0.05	0.02	0.08	0.44	0.09

Model 3

cell	Th	U	Nb	La	Ce	Sr	Nd	Zr	Hf	Sm	Gd	Ti	Dy	Ho	Er	Yb	Lu
1	0.0650	0.0713	0.192	0.0864	0.936	0.60	4.48	14.8	0.34	1.52	1.46	908	1.39	0.37	1.17	1.52	0.24
2	0.0608	0.0667	0.179	0.0808	0.875	0.56	4.19	13.8	0.31	1.42	1.36	851	1.28	0.33	1.03	1.14	0.18
3	0.0554	0.0608	0.163	0.0736	0.797	0.51	3.81	12.5	0.28	1.29	1.22	772	1.05	0.25	0.72	0.59	0.09
4	0.0490	0.0538	0.145	0.0651	0.704	0.45	3.35	10.9	0.25	1.13	1.02	664	0.69	0.14	0.37	0.22	0.04
5	0.0420	0.0461	0.124	0.0557	0.602	0.39	2.84	9.1	0.20	0.93	0.75	519	0.34	0.06	0.15	0.09	0.02
6	0.0347	0.0381	0.102	0.0459	0.494	0.32	2.30	6.9	0.15	0.71	0.46	350	0.14	0.02	0.07	0.07	0.02
7	0.0276	0.0302	0.081	0.0363	0.389	0.25	1.76	4.8	0.10	0.49	0.23	197	0.06	0.02	0.05	0.06	0.02
8	0.0211	0.0231	0.062	0.0275	0.293	0.19	1.26	2.9	0.06	0.29	0.09	92	0.04	0.01	0.05	0.06	0.02
9	0.0156	0.0170	0.046	0.0200	0.210	0.13	0.83	1.5	0.03	0.15	0.03	38	0.04	0.01	0.05	0.07	0.02
10	0.0111	0.0122	0.033	0.0140	0.144	0.09	0.51	0.7	0.01	0.07	0.02	17	0.04	0.01	0.05	0.07	0.02
11	0.0078	0.0085	0.023	0.0095	0.095	0.06	0.28	0.3	0.00	0.03	0.01	11	0.05	0.01	0.05	0.07	0.02
12	0.0053	0.0058	0.015	0.0063	0.060	0.03	0.15	0.1	0.00	0.01	0.01	10	0.05	0.02	0.05	0.07	0.02
13	0.0036	0.0039	0.010	0.0041	0.037	0.02	0.07	0.1	0.00	0.00	0.01	10	0.05	0.02	0.05	0.07	0.02
14	0.0025	0.0026	0.007	0.0026	0.022	0.01	0.03	0.1	0.00	0.00	0.01	11	0.05	0.02	0.05	0.07	0.02
15	0.0017	0.0018	0.005	0.0016	0.013	0.01	0.01	0.1	0.00	0.00	0.01	12	0.05	0.02	0.05	0.07	0.02
16	0.0012	0.0012	0.003	0.0010	0.007	0.00	0.00	0.1	0.00	0.00	0.01	13	0.05	0.02	0.05	0.07	0.02
17	0.0008	0.0009	0.002	0.0006	0.004	0.00	0.00	0.1	0.00	0.00	0.01	14	0.06	0.02	0.06	0.07	0.02
18	0.0006	0.0006	0.002	0.0004	0.002	0.00	0.00	0.1	0.00	0.00	0.02	15	0.06	0.02	0.06	0.07	0.02
19	0.0004	0.0004	0.001	0.0002	0.001	0.00	0.00	0.1	0.00	0.00	0.02	15	0.06	0.02	0.06	0.07	0.02
20	0.0003	0.0003	0.001	0.0001	0.000	0.00	0.00	0.1	0.00	0.00	0.02	16	0.06	0.02	0.06	0.07	0.02

DISCUSSION AND CONCLUSIONS

Single-mineral thermobarometry for mineral concentrates in kimberlites and diamond inclusions and robustness of thermobarometric estimates for Zagadochnaya

As discussed in the introduction chapter, mantle assemblages suitable for conventional thermobarometry are scarce in many kimberlites, even if abundant remnants of disaggregated xenoliths can be found as discrete xenocrysts or in heavy-mineral concentrates. The same problem concerns mineral inclusions in diamonds: polymineralic inclusions are uncommon, and even more rarely do they contain the appropriate mineral assemblage for reliable thermobarometry (e.g. Stachel and Harris 2008). To obtain information on pressure and temperature from isolated xenocrysts and diamond inclusions, single-mineral thermobarometers remain the only viable option (e.g. Ryan et al. 1996; Canil 1999; Nimis and Taylor 2000; Ashchepkov 2006; Grütter et al. 2006; Simakov 2008, 2012; Creighton 2009; Turkin and Sobolev 2009).

One of the most widely used geothermometers for isolated garnets is the Ni-in-garnet thermometer, which is based on Ni partitioning between garnet and mantle olivine. . Two versions of this thermometer are available: that of Ryan et al. (1996) is based on an empirical calibration against the somewhat unreliable olivine–garnet geothermometer of O'Neill and Wood (1979) (cf. Nimis and Grütter 2010); that of Canil (1999) was calibrated against experimental data. Application to Zagadochnaya garnets associated with clinopyroxenes showed a good agreement of the Ryan et al. (1996) version with temperatures estimated with the enstatite-in-Cpx thermometer of Nimis and Taylor (2000) (see *Manuscript 3*), which is considered to be one of the most reliable thermometers for garnet peridotites (Nimis and Grütter 2010). The Canil (1999) version gave temperatures up to 120°C higher than that of Ryan et al. (1996), the discrepancy being greater at low estimated T, suggesting possible overestimation with this thermometer in the low temperature region.

In many studies, the Ni-in-garnet thermometer is coupled with a Cr-in-garnet geobarometer (e.g., Ryan et al. 1996; Grütter et al. 2006; Turkin and Sobolev 2009), which allows one to estimate P for garnets in equilibrium with spinel (e.g., Griffin et al. 1999c, 2003b, 2004, 2005; Zheng et al. 2006; Batumike et al. 2009; Tappert et al. 2011; Kahoui et al. 2012). If spinel is not present, only minimum pressures can be estimated. This limitation typically produces considerable scatter in P–T diagrams (see, for example, Fig. 4 in Griffin et al. 1999c), even if a palaeogeotherm can still be estimated by the envelope of maximum P at each T using large garnet datasets (Ryan et al., 1996). For the Zagadochnaya xenocrysts, for which coexistence

with primary spinel could not be verified, only minimum pressures could be estimated with these methods.

The Cr-in-Cpx geobarometer (Nimis and Taylor, 2000) requires coexistence with garnet, therefore it allows quantitative estimation of equilibrium P for many mantle-derived chromian clinopyroxenes. Its application requires careful screening of clinopyroxene composition (Nimis 2002; Grütter 2009; *Manuscript 1*). In this work, I quantitatively evaluated the propagation of analytical errors on P uncertainties for a large range of clinopyroxene compositions, and I defined the appropriate EMP analytical conditions that should be adopted for optimum Cr-in-cpx geobarometry (*Manuscript 1*). I showed that 22% of the 764 clinopyroxenes in the mantle xenolith database of Nimis and Grütter (2010) and 40% of reported clinopyroxene inclusions in ultramafic-type diamonds (cf. Stachel and Harris 2008) have unfavorable compositions for geobarometry and are likely to yield unreliable P–T estimates. However, if appropriate analytical conditions are used, the application of the barometer can be safely extended to at least 90% of clinopyroxenes from mantle xenoliths and 80% of diopside inclusions in ultramafic-type diamonds.

The progressive underestimation with the Cr-in-Cpx barometer at pressures greater than 4.5 GPa (Nimis 2002) remains an unresolved limitation. Despite my attempts, owing to a lack of consistent thermodynamic data for Cr-bearing clinopyroxenes, a thermodynamic approach to investigating pressure dependence of clinopyroxene composition in natural peridotitic systems is not yet viable (*Manuscript 2*), indicating the need for new high-pressure, high-temperature experiments on Cr-bearing clinopyroxenes.

Taking into account this limitation and the results reported in *Manuscript 1*, the single-clinopyroxene thermobarometers could be safely applied to the Zagadochnaya xenocryst population (*Manuscript 3*). The low pressures and temperatures obtained in the present work and in previous work by Nimis et al. (2009) (3.0–4.0 GPa, 741–885°C), consistent with the low Ni-in-garnet temperatures (691–857°C; Ryan et al. 1996) and *minimum* Cr-in-garnet pressures (1.3 to 3.9 GPa; Grütter et al. 2006, Turkin and Sobolev 2009) reported here (*Manuscript 3*), suggest derivation of Zagadochnaya xenocrystic material from a relatively shallow mantle section (ca. 100–130 km), thus offering a simple possible explanation for the absence of diamond at Zagadochnaya. The above estimates are reliable, because the composition of the Zagadochnaya diopsides is well within the limits for optimum thermobarometry (i.e., a_{Cr}/Cr# $\geq$ 0.027 and Cr# $\geq$ 0.13) defined in the present work (cf. *Manuscript 1*) and P estimates are not affected by systematic deviations in the estimated pressure range (Nimis 2002).

Ca-Cr and REE variations in garnets

It is common practice to classify mantle garnet compositions on the basis of their Ca and Cr contents (Dawson and Stephens 1975; Sobolev et al. 1973; Gurney 1984; Schulze 2003; Grütter et al. 2004). The compositions of lherzolitic garnets from individual kimberlites typically show a positive correlation between Ca and Cr (i.e., the so-called *lherzolitic trend*). This correlation may be the result of Ca–Cr interaction in the garnet crystal lattice and of Ca buffering operated by coexistent clinopyroxene (Griffin et al. 1999d). The compositional variation along the lherzolitic trend is commonly interpreted as the result of variations in the Cr/Al ratio of the host rock, which is in turn a measure of the degree of depletion or enrichment in basaltic components (e.g. Griffin et al. 1999d; Burgess and Harte 1999, 2004).

The results of thermodynamic modelling of natural peridotitic compositions (*Manuscript 2*) showed that, as long as garnet coexists with spinel, Ca–Cr variations along this trend can also be obtained by varying P and T along a continental geotherm under isochemical bulk conditions. This suggests that the particular position of some garnets along the lherzolitic trend can be related to their P–T conditions of equilibrium rather than to bulk chemical variations. In the case of the Zagadochnaya primary garnets (Fig. 3 in *Manuscript 3*), however, the concurrent variations of Ca–Cr *and* trace elements (cf. Fig. 11 in *Manuscript 3*), the restricted range of estimated P–T conditions, and the apparent absence of primary spinel, still suggest a major role of metasomatic processes on garnet compositional variations. In the absence of detailed geochemical and thermobarometric data, the significance of the observed Ca–Cr trend would have remained uncertain.

The wide spectrum of geochemical compositions of Zagadochnaya garnets gave also the opportunity to investigate the effect of melt/rock interactions on garnet REE composition. Numerical simulations (Plate Model; Vernières et al., 1997), which take into account the combined effects of fractional crystallization and of chromatographic and assimilation processes, allowed to place quantitative constraints on peridotite–melt processes in the Zagadochnaya mantle section. The results show that the wide spectrum of REE compositions observed in the different garnet groups can be produced by a unique episode of melt injection and percolation through a refractory mantle column, whereby the melt progressively changes its composition due to chromatographic ion exchange, fractional crystallization and assimilation of peridotitic minerals, under decreasing melt/rock ratios.

Lessons for future mantle studies

The results obtained in this work provide valuable information for future thermobarometric and geochemical studies of peridotitic garnets and clinopyroxenes from kimberlites. Thanks

to a detailed evaluation of electron microprobe uncertainties using different analytical conditions and of their propagation on pressure estimates, single-clinopyroxene geobarometry can now be applied with reasonable confidence to a wider variety of clinopyroxene compositions, thus allowing better definition of mantle geotherms and diamond potential. On the other hand, doubts are cast on the reliability of many previous thermobarometric data, which were obtained using non-optimized chemical analyses. For instance, the large scatter of P–T estimates obtained so far for inclusions of chromian diopside in diamonds (see Fig. 27 in Stachel and Harris 2008) probably mainly reflects non-optimized electron microprobe analyses of clinopyroxenes with unfavorable compositions. High-quality analyses will not eliminate recognized underestimation of pressure at P > 4.5 GPa (cf. Nimis 2002), but a robust recalibration of the geobarometer is not possible at present, due to the lack of accurate thermodynamic data for Cr-bearing clinopyroxenes.

New constraints and modelling hints were also provided for the quantitative petrochemical characterization of peridotitic garnets from cratonic settings:

(a) The new thermodynamic model, which uses improved thermodynamic data for some Cr-bearing endmembers, allows a more reliable assessment of garnet–spinel relationships and compositional variations in minerals in a variety of compositions relevant to Earth's mantle (from strongly depleted harzburgitic to fertile lherzolitic) and a variety of thermal regimes.

(b) Numerical simulations using the Plate Model emphasized the importance of certain critical petrochemical parameters (fractional crystallization, assimilation of peridotitic minerals, time-integrated melt/rock ratio, chromatographic ion exchange processes, mineral/melt partition coefficients, composition of the ambient peridotite) for a correct interpretation of trace element variability in mantle-derived peridotitic garnets. In common practice, although some of these parameters cannot be directly measured, reasonable constraints can be obtained using the most extreme among the garnet compositions observed. For instance, the progressive decrease in HREE and increase in LREE observed in Zagadochnaya Group A and Group B garnets was reproduced assuming percolation of a melt in equilibrium with the most HREE-rich garnets through a mantle column containing a garnet with extremely fractionated REE (HREE/LREE >> 1 xCI), and simulating interactions with progressive decreasing time-integrated melt/rock ratio and fractional crystallization of clinopyroxene and garnet. The sinusoidal REE patterns in Group C garnets were instead reproduced by percolation of a melt in equilibrium with the most LREE-rich Group B garnet, which was assumed to represent the residual melt of the reactions that produced Group A and Group B garnets. In this case, the best fit was obtained assuming chromatographic-type chemical exchange at low time-integrated melt/rock ratios, with no fractional crystallization,

but allowing for orthopyroxene assimilation. Such assimilation was found to be necessary to reproduce the progressive decrease in LREE contents (with similar LREE fractionation) observed in group C garnets. The numerous attempts to reproduce the REE composition of Group C garnets showed that, if no or only minor fractional crystallization is assumed during melt percolation, the calculated HREE contents of the garnet strongly depend on the initial HREE composition of the ambient peridotite. The degree of MREE/HREE fractionation of the modeled garnet compositions is instead strongly dependent on the adopted $^{Grt/melt}D$ values. Numerous attempts indicated that the HREE depletion rates and MREE/HREE fractionations observed in Group A and Group B garnets could be obtained only using $^{Grt/melt}D_{HREE}$ values higher than those estimated based on Grt/Cpx partitioning (Burgess and Harte, 2004; Gibson et al. 2008). The best fit with the observed data were obtained the high-T experimental dataset of Johnson (1998). The best fit with the composition of Zagadochnaya primary garnets was obtained using the high-*T* experimental $^{Grt/melt}D$ values of Johnson (1998). Future numerical simulations for other case studies can be designed taking into account these tips.

The study of mantle fragments from the diamond-free Zagadochnaya kimberlite, and the comparison with the nearby, highly diamondiferous Udachnaya kimberlite, gave the opportunity to investigate the possible factors that controlled the diamond potential. The shallow origin of Zagadochnaya mantle samples (< 130 km), as constrained by the results of single-clinopyroxene thermobarometry and Ni-in-garnet thermometry, suggests a significant sampling bias for the kimberlite compared to its highly diamondiferous neighbor, and therefore provides a simple first-order explanation for the absence of diamonds at Zagadochnaya. The lack of deeper mantle material, however, poses new questions on the volcanology of the Zagadochnaya kimberlite, since a similar sampling bias has never been reported for other Paleozoic kimberlites from the Siberian Craton (cf. Griffin et al. 1999c; Ashchepkov et al. 2010; Ionov et al. 2010). Arndt et al. (2010) suggested that type-II kimberlites such as Zagadochnaya, due to their low CO_2 contents, may have slower ascent rates than type-I kimberlites. A slow ascent of the kimberlitic magma to shallow lithospheric levels before eruption would explain the absence of deep mantle material, the abundance of secondary mineral assemblages, and the high-Mg composition of the kimberlite (cf. Kostrovitsky and de Bruin 2004).

The late-stage, pervasive reactions with melts related to the host kimberlite, recorded by secondary assemblages in garnet and clinopyroxene grains, may have constituted an additional unfavorable condition for diamond. These pervasive reactions, which occurred at mantle depths shortly before the kimberlite eruption, may have led to resorption of any small diamond load originally present. Understanding which was the dominant factor that controlled

the diamond potential of this kimberlite is not straightforward, and requires further investigations from different prospective. Future studies on other type-II kimberlite pipes from the Daldyn Field (Bukovinskaya, Gornyatskaya, and Kusov), which are known to have very low diamond grades (<0.5 ct/ton; Kargin et al. 2011) and contain secondary assemblages very similar to those at Zagadochnaya (Kostrovitsky and de Bruin 2004), may provide further insight into specific relationships between metasomatic processes and type-II kimberlite magmatism and into volcanological factors that controlled mantle sampling by these kimberlites.

REFERENCES

- Afonso JC, Ranalli G, Fernàndez M, Griffin WL, O'Reilly SY, Faul, U (2010) On the Vp/Vs–Mg# correlation in mantle peridotites: Implications for the identification of thermal and compositional anomalies in the upper mantle. Earth Planet Sci Lett 289:606–618
- Andersen T, O'Reilly SY, Griffin WL (1984) The trapped fluid phase in upper mantle xenoliths from Victoria, Australia: implications for mantle metasomatism. Contrib Mineral Petrol 88:72–85.
- Arndt NT, Coltice N, Helmstaedt H, Gregoire M (2009) Origin of Archean subcontinental lithospheric mantle: some petrological constraints. Lithos 109:61–71
- Arndt NT, Guitreau M, Boullier AM, Le Roex A, Tommasi A, Cordier P, Sobolev A (2010) Olivine, and the origin of kimberlite. J Petrol 51:573–602
- Ashchepkov IV (2006) Empirical garnet thermobarometer for mantle peridotites. Russ Geol Geophys 47:1071–1085
- Aulbach S, Griffin WL, Pearson NJ, O'Reilly SY, Doyle BJ (2007) Lithosphere formation in the central Slave Craton (Canada): Plume subcretion or lithosphere accretion? Contrib Mineral Petrol 154:409–427
- Bascou J, Doucet LS, Saumet S, Ionov DA, Ashchepkov IV, Golovin AV (2011) Seismic velocities, anisotropy and deformation in Siberian cratonic mantle: EBSD data on xenoliths from the Udachnaya kimberlite. Earth Planet Sci Lett 304:71–84
- Batumike JM, Griffin WL, O'Reilly SY (2009) Lithospheric mantle structure and the diamond potential of kimberlites in southern D.R. Congo. Lithos 112:166–176
- Bleeker W (2003) The late Archean record: a puzzle in ca. 35 pieces. Lithos 71:99–134
- Boyd FR (1973) A pyroxene geotherm. Geochim Cosmochim Acta 37:2533–2546
- Boyd FR (1989). Compositional distinction between oceanic and cratonic lithosphere. Earth Planet Sci Lett 96 (1999).
- Boyd FR, Mertzman SA (1987) Composition and structure of the Kaapvaal lithosphere, Southern Africa. In: Mysen, B.O. (ed.) Magmatic Processes: Physicochemical Principles. Geochem Soc Spec Publ 1:3–12
- Boyd FR, Pokhilenko NP, Pearson DG, Mertzman SA, Sobolev NV, Finger LW (1997) Composition of the Siberian cratonic mantle: evidence from Udachnaya peridotite xenoliths. Contrib Mineral Petrol 128:228–246
- Brey GP, Köhler T (1990) Geothermobarometry in four-phase lherzolites. II. New thermobarometers, and practical assessment of existing thermobarometers. J Petrol 31:1353–1378
- Brey G, Köhler T, Nickel K (1990) Geothermobarometry in four-phase lherzolites I. Experimental results from 10 to 60 kb. J Petrol 31:1313–1352
- Brey GP, Bulatov VK, Girnis V (2008) Geobarometry for Peridotites: Experiments in simple and natural systems from 6 to 10 GPa. J Petrol 49:3–24
- Brey GP, Doroshev AM, Girnis AV, Turkin AI (1999) Garnet-spinel-olivine-orthopyroxene equilibria in the FeO-MgO-Al2O3-SiO2-Cr2O3 system: I. Composition and molar volumes of minerals. Eur J Mineral 11:599–617
- Burgess SR, Harte B (1999) Tracing lithosphere evolution through the analysis of heterogeneous G9/G10 garnet in peridotite xenoliths, I: Major element chemistry. In: Gurney JJ, Gurney JL, Pascoe MD, Richardson SH (eds) Proceedings of the 7th Kimberlite Conference (Dawson volume). Cape Town, Red Roof Design, 66–80

- Burgess SR, Harte B (2004) Tracing lithosphere evolution through the analysis of heterogeneous G9-G10 garnets in peridotite xenoliths, II: REE chemistry. J Petrol 45:609–634
- Canil D (2004) Mildly incompatible elements in peridotites and the origins of mantle lithosphere. Lithos 77:375–93
- Carswell DA (1991) The garnet–orthopyroxene Al barometer: problematic application to natural garnet lherzolite assemblages. Mineral Mag 55:19–31
- Cawood PA, Hawkesworth CJ, Dhuime B (2013) The continental record and the generation of continental crust. GSA Bulletin 125:14–32
- Chatterjee ND, Terhart L (1985) Thermodynamic calculation of peridotite phase relations in the system MgO-Al_2O_3-SiO_2-Cr_2O_3, with some geological applications. Contrib Mineral Petrol 89:273–284
- Connolly JAD (1990) Multivariable phase diagrams: An algorithm based on generalized thermodynamics. Am J Sci 290:666–718
- Connolly JAD, Petrini K (2002) An automated strategy for calculation of phase diagram sections and retrieval of rock properties as a function of physical conditions. J Metamorph Geol 20: 697–708
- Cookenboo HO, Grütter HS (2010) Mantle-derived indicator mineral compositions as applied to diamond exploration. Geochemistry: Exploration, Environment, Analysis, 10:81–95
- Creighton S, Stachel T, McLean H, Muehlenbachs K, Simonetti A, Eichenberg D, Luth R (2008) Diamondiferous peridotitic microxenoliths from the Diavik Diamond Mine, NT. Contrib Mineral Petrol 155:541-554
- Creighton S, Stachel T, Matveev S, Höfer HE, McCammon C, Luth RW (2009) Oxidation of the Kaapvaal lithospheric mantle driven by metasomatism. Contrib Mineral Petrol 157:491–504
- Dawson JB (1984) Contrasting types of upper mantle metasomatism. In: Kornprobst J (ed) Kimberlites II: The Mantle and Crust-Mantle Relationships. Amsterdam, Elsevier, pp 289–294
- Dawson JB, Stephens WE (1975) Statistical classification of garnets from kimberlite and associated xenoliths J Geol 83:589–607
- Doroshev A, Brey G, Girnis A, Turkin A, Kogarko L (1997) Pyrope-knorringite garnets in the Earth's mantle: Experiments in the MgO-Al2O3-SiO2-Cr2O3 system. Russ Geol Geophys 38:559-586
- Doucet LS, Ionov DA, Golovin AV, Pokhilenko NP (2012) Depth, degrees and tectonic settings of mantle melting during craton formation: Inferences from major and trace element compositions of spinel harzburgite xenoliths from the Udachnaya kimberlite, central Siberia. Earth Planet Sci Lett 359-360:206–218
- Ellis DJ and Green DH (1979) An experimental study of the effect of Ca upon garnet-clinopyroxene Fe–Mg exchange equilibria. Contrib Mineral Petrol 71:13–22
- Erlank AJ, Waters FG, Hawkesworth CJ, Haggerty SE, Allsopp HL, Rickard RS, Menzies M (1987) Evidence for mantle metasomatism in peridotite nodules from the Kimberley pipes, South Africa. In: Menzies M, Hawkesworth CJ (eds) Mantle metasomatism. New York, Academic, pp 221–311
- Gasparik T (1984) Two-pyroxene thermobarometry with new experimental data in the system CaO-MgO-Al_2O_3-SiO_2. Contrib Miner Petrol 87:87–97
- Gibson SA, Malarkey J, Day AA (2008) Melt Depletion and Enrichment beneath the Western Kaapvaal Craton: Evidence from Finsch Peridotite Xenoliths. J Petrol 49:1817–1852

- Girnis AV, Brey GP, Doroshev AM, Turkin AI, Simon N (2003) The system MgO-Al_2O_3-SiO_2-Cr_2O_3 revisited: reanalysis of Doroshev et al.'s (1997) experiments and new experiments. Eur J Mineral 15:953–964
- Giuliani A, Kamenetsky VS, Kendrick MA, Phillips D, Goemann K (2013) Nickel-rich metasomatism of the lithospheric mantle by pre-kimberlitic alkali-S-Cl-rich C-O-H fluids. Contrib Miner Petrol, 165:155–171
- Grégoire M, Bell DR, Le Roex AP (2002) Trace element geochemistry of phlogopite-rich mafic mantle xenoliths: their classification and their relationship to phlogopite-bearing peridotites and kimberlites revisited. Contrib Mineral Petrol 142:603–625
- Griffin WL, Ryan CG (1995) Trace elements in indicator minerals: area selection and target evaluation in diamond exploration. J Geochem Explor 53:311–337
- Griffin WL, O'Reilly SY, Ryan CG, (1999a) The composition and origin of subcontinental lithospheric mantle. In: Fei Y, Bertka CM, Mysen BO (Eds) Mantle Petrology: Field Observations and High Pressure Experimentation: a Tribute to Francis R. (Joe) Boyd. The Geochemical Society, Special Publication, pp 13–45
- Griffin WL, Shee SR, Ryan CG, Win TT, Wyatt BA (1999b) Harzburgite to lherzolite and back again: metasomatic processes in ultramafic xenoliths from the Wesselton kimberlite, Kimberley, South Africa. Contrib Mineral Petrol 134:232–250
- Griffin WL, Ryan CG, Kaminsky FV, O'Reilly SY, Natapov LM, Win TT, Kinny PD, Ilupin IP (1999c) The Siberian lithosphere traverse. Mantle terranes and the assembly of the Siberian craton. Tectonophysics 310:1–35
- Griffin WL, Fisher NI, Friedman JH, Ryan CG, O'Reilly SY (1999d) Cr-pyrope garnets in the lithospheric mantle: I. Compositional systematics and relations to tectonic setting. J Petrol 40:679–704
- Griffin WL, Fisher NI, Friedman JH, O'Reilly SY, Ryan CG (2002) Cr-pyrope garnets in the lithospheric mantle 2. Compositional populations and their distribution in time and space. Geochemistry Geophysics Geosystems 3, doi:10.1029/2002GC000298
- Griffin WL, O'Reilly SY, Abe N, Aulbach S, Davies RM, Pearson NJ, Doyle BJ, Kivi K (2003a) The origin and evolution of Archean lithospheric mantle. Precambrian Res 127:19–41
- Griffin WL, O'Reilly SY, Natapov LM, Ryan CG (2003b) The evolution of lithospheric mantle beneath the Kalahari Craton and its margins. Lithos 71:215–242
- Griffin WL, O'Reilly SY, Doyle BJ, Pearson NJ, Coopersmith H, Kivi K, Malkovets V and Pokhilenko N (2004). Lithosphere mapping beneath the North American plate. Lithos 77:873–922
- Griffin WL, Natapova LM, O'Reilly SY, van Achterbergh E, Cherenkova AF, Cherenkov VG (2005) The Kharamai kimberlite field, Siberia: Modification of the lithospheric mantle by the Siberian Trap event. Lithos 81:167–187
- Grütter HS, Gurney JJ, Menzies AH, Winter F (2004) An updated classification scheme for mantle-derived garnet, for use by diamond explorers. Lithos 77:841–857
- Grütter H (2006) Cr-saturation arrays in concentrate garnet compositions from kimberlite and their use in mantle barometry. J Petrol 47:801-820
- Grütter HS (2009) Pyroxene xenocryst geotherms: techniques and application. Lithos 112:1167–1178
- Gurney JJ (1984) A correlation between garnets and diamonds in kimberlites. In: Glover JE, Harris PG (Eds) Kimberlites: Occurrence and Origin: A Basis for Conceptual Models in Exploration. University of Western Australia, Extension Services, Perth, pp 143–166

- Harley SL, Green DH (1982) Garnet-orthopyroxene barometry for granulites and garnet peridotites. Nature 300:697–700.
- Harte B (1983) Mantle peridotites and processes – the kimberlite sample. In: Hawkesworth CJ, Norry M J (eds) Continental Basalts and Mantle Xenoliths. Nantwich, Shiva, pp. 46–91
- Herzberg C, Rudnick R (2012) Formation of cratonic lithosphere: An integrated thermal and petrological model. Lithos 149:4–15
- Hoal KEO, Hoal BG, Erlank AJ, Shimizu N (1994) Metasomatism of the mantle lithosphere recorded by rare earth elements in garnets. Earth Planet Sci Lett 126:303–313
- Holland TJB, Powell R (1998) An internally consistent thermodynamic data set for phases of petrological interest. J Metamorph Geol 16:309–343
- Ionov DA, Doucet LS, Ashchepkov IV (2010) Composition of the Lithospheric Mantle in the Siberian Craton: New Constraints from Fresh Peridotites in the Udachnaya-East Kimberlite. J Petrol 51:2177–2210
- James DE, Boyd FR, Schutt D, Bell DR, Carlson RW (2004) Xenolith constraints on seismic velocities in the upper mantle beneath southern Africa. Geochem Geophys Geosyst 5, doi:10.1029/2003GC000551
- Jenkins DM, Newton RC (1979) Experimental determination of the spinel peridotite to garnet peridotite inversion at 900°C and 1000°C in the system CaO-MgO-Al_2O_3-SiO_2, and at 900°C with natural garnet and olivine. Contrib Mineral Petrol 68:407–419
- Kahoui M, Kaminsky FV, Griffin WL, Belousova E, Mahdjoub Y, Chabane M (2012) Detrital pyrope garnets from the El Kseibat area, Algeria: A glimpse into the lithospheric mantle beneath the north-eastern edge of the West African Craton. J Afr Earth Sci 63:1–11
- Kargin AV, Golubeva Yu. Yu. & Kononova VA (2011) Kimberlites of the Daldyn–Alakit Region (Yakutia): Spatial Distribution of the Rocks with Different Chemical Characteristics. Petrology 19:496–520
- Kinny PD, Dawson JB (1992) A mantle metasomatic injection event linked to late Cretaceous kimberlite magmatism. Nature 360:726–728
- Klemme S (2004) The influence of Cr on the garnet–spinel transition in the Earth's mantle: experiments in the system MgO–Cr_2O_3–SiO_2 and thermodynamic modelling. Lithos 77:639–646
- Klemme S, Ivanic TJ, Connolly JAD, Harte B (2009) Thermodynamic modelling of Cr-bearing garnets with implications for diamond inclusions and peridotite xenoliths. Lithos 112:986–991
- Klemme S, O'Neill HSC (2000) The near-solidus transition from garnet lherzolite to spinel lherzolite. Contrib Mineral Petrol 138:237–248
- Kober L (1921) Der Bau der Erde (The construction of the Earth). Gebrüder Borntraeger, Berlin, 353 pp
- Kostrovitsky SI, de Bruin D (2004) Chromium assemblage of minerals in micaceous kimberlites of Yakutian province. Russ Geol Geophys 45:565–576
- Lee C-TA, Luffi P, Chin EJ (2011) Buliding and destroying continental mantle. An Rev Earth Planet Sci 39:59–90
- Lee C-TA (2006) Geochemical/petrologic constraints on the origin of cratonic mantle. In: Benn K, Mareschal J-C, Condie KC (eds) Archean Geodynamics and Environments. Geophys Monogr. Washington DC, AGU, pp 89–114
- Lenardic A, Moresi L-N, Muhlhaus H-B (2003) Longevity and stability of cratonic lithosphere: insights from numerical simulations of coupled mantle convection and continental tectonics. J Geophys Res B Solid Earth 108:9–15

- MacGregor ID (1965) Stability fields of spinel and garnet peridotites in the synthetic system $MgO–CaO–Al_2O_3–SiO_2$. Carnegie Inst Wash Year Book 64:126–134
- MacGregor ID (1974) The system $MgO–Al_2O_3–SiO_2$: solubility of Al_2O_3 in enstatite for spinel and garnet peridotite compositions. Am Mineral 59:110–119
- MacKenzie JM, Canil D (1999) Composition and thermal evolution of cratonic mantle beneath the central Archean Slave Province, NWT, Canada. Contrib Mineral Petrol 134:313–324
- Malkovets VG, Griffin WL, O'Reilly SY, Wood BJ (2007) Diamond, subcalcic garnet, and mantle metasomatism: Kimberlite sampling patterns define the link. Geology 35:339–342
- Mather KA, Pearson DG, McKenzie D, Kjarsgaard BA, Priestley K (2011) Constraints on the depth and thermal history of cratonic lithosphere from peridotite xenoliths, xenocrysts and seismology. Lithos 125:729–742
- Menzies MA (1983) Mantle ultramafic xenoliths in alkaline magmas: evidence for mantle heterogeneity modified by magmatic activity. In: Hawkesworth CJ, Norry MJ (eds) Continental Basalts and Mantle Xenoliths. Nantwich, Shiva, pp 92–110
- Menzies M, Xu Y, Zhang H, Fan W (2007) Integration of geology, geophysics and geochemistry: A key to understanding the North China Craton. Lithos 96:1–21
- Mitchell RH (1995) Kimberlites, Orangeites and Related Rocks. Plenum Press, New York, N.Y.
- Nickel KG, Green DH (1985) Empirical geothermobarometry for garnet peridotites and implications for the nature of the lithosphere, kimberlites and diamonds. Earth Planet Sci Lett 73:158–170
- Nickel KG (1986) Phase equilibria in the system SiO2–MgO–Al2O3–CaO–Cr2O3 (SMACCR) and their bearing on spinel/garnet lherzolite relationships. Neues Jahrb Mineral Abh 155:259–287
- Nickel KG (1989) Garnet-pyroxene equilibria in the system SMACCR ($SiO_2–MgO–Al_2O_3–CaO–Cr_2O_3$): The Cr-geobarometer. In: Ross J, Jaques AL, Ferguson J, Green DH, O'Reilly SY, Danchin RV, Janse AJA (eds) Kimberlites and Related Rocks, Vol. 2, Their Mantle/Crust Setting, Diamonds and Diamond Exploration. Geological Society of Australia Special Publication 14. Blackwell Scientific, Victoria, pp 901–912
- Nimis P (2002) The pressures and temperatures of formation of diamond based on thermobarometry of chromian diopside inclusions. Can Mineral 40:871–884
- Nimis P, Grütter H (2010) Internally consistent geothermometers for garnet peridotites and pyroxenites. Contrib Mineral Petrol 159:411–427
- Nimis P, Taylor WR (2000) Single-clinopyroxene thermobarometry for garnet peridotites. Part I. Calibration and testing of a Cr-in-Cpx barometer and an enstatite-in-Cpx thermometer. Contrib Mineral Petrol 139:541–554
- Nimis P, Zanetti A, Dencker I, Sobolev NV (2009) Major and trace element composition of chromian diopsides from the Zagadochnaya kimberlite (Yakutia, Russia): Metasomatic processes, thermobarometry and diamond potential. Lithos 112:397–412
- Nimis P, Grütter H (2012) Discussion of "The applicability of garnet–orthopyroxene geobarometry in mantle xenoliths", by Wu C.-M. and Zhao G. (Lithos, v. 125, p. 1–9). Lithos 142–143:285–287
- Nixon PH (1987) Mantle xenoliths. John Wiley, Chichester.
- O'Neill HSC (1981) The transition between spinel lherzolite and garnet lherzolite, and its use as a geobarometer. Contrib Mineral Petrol 77:185–194

- O'Reilly SY, Griffin WL, Poudjom Djomani YH and Morgan P (2010). Are lithosphere forever? Tracking changes in subcontinental lithospheric manle through time. GSA Today 11:4–10
- Parman SW, Grove TL, Dann JC, de Wit MJ (2004) A subduction origin for komatiites and cratonic lithospheric mantle. S Afr J Geol 107:107–118
- Pearson DG, Nowell GM (2002) The continental lithospheric mantle: characteristics and significance as a mantle reservoir. Philosoph Trans Royal Soc Lond 360:2383–2410
- Pearson DG, Wittig N (2008) Formation of Archean continental lithosphere and its diamonds: the root of the problem. J Geol Soc 165:895–914
- Pearson DG, Canil D, Shirey SB (2003) Mantle Samples Included in Volcanic Rocks : Xenoliths and Diamonds. In: Holland HD, Turekian KK (eds) Treatise on Geochemistry. Elsevier, Amsterdam, pp 171–275
- Pearson DG, Shirey SB, Carlson RW, Boyd FR, Pokhilenko NP, Shimizu N (1995) Re-Os, Sm-Nd, and Rb-Sr isotope evidence for thick Archean lithospheric mantle beneath the Siberian craton modified by multistage metasomatism. Geochim Cosmochim Acta 59:959–77
- Pivin M, Féménias O and Demaiffe D (2009) Metasomatic mantle origin for Mbuji-Mayi and Kundelungu garnet and clinopyroxene megacrysts (Democratic Republic of Congo). Lithos 112:951–960
- Robinson JAC, Wood BJ (1998) The depth of the spinel to garnet transition at the peridotite solidus. Earth Planet Sci Lett 164:277–284
- Ryan CG, Griffin WL, Pearson NJ (1996) Garnet geotherms: pressure–temperature data from Cr-pyrope garnet xenocrysts in volcanic rocks. J Geophys Res 101:5611–5625
- Shimizu N, Richardson SH (1987) Trace element abundance patterns of garnet inclusions in peridotite suite diamonds. Geochim Cosmochim Acta 51:755–758
- Shimizu N, Pokhilenko NP, Boyd FR, Pearson DG (1997) Geochemical characteristics of mantle xenoliths from the Udachnaya kimberlite pipe. Russ Geol Geophys 38:205–217
- Schulze DJ (1989) Constraints on the abundance of eclogite in the upper mantle. J Geophys Res 94:4205–4212
- Schulze DJ (2003) A classification scheme for mantle-derived garnet in kimberlite: a tool for investigating the mantle and exploring for diamonds. Lithos 71:195–213
- Simakov SK (2008) Garnet–clinopyroxene and clinopyroxene geothermobarometry of deep mantle and crust eclogites and peridotites. Lithos 106:125–136
- Simakov SK (2012) A New Garnet Thermometer for Mantle Peridotites and Estimation of the Diamond Potential on Its Basis. Dokl Earth Sci 445: 1003–1005
- Simon NSC, Carlson RW, Pearson DG, Davies GR (2007) The origin and evolution of the Kaapvaal cratonic lithospheric mantle. J Petrol 48:589–625
- Sleep NH (2004) Evolution of the continental lithosphere. Ann Rev Earth Planet Sci 33:369–93
- Sobolev NV, Kuznetsova IK, Zyuzin NI (1968) Petrology of grospydite xenoliths from the Zagadochnaya kimberlite pipe in Yakutia. J Petrol 9:253–280
- Sobolev NV, Lavrent'ev YG, Pokhilenko NP, Usova LV (1973) Chrome-rich garnets from the kimberlites of Yakutia and their paragenesis. Contrib Mineral Petrol 40:39–52
- Sobolev NV, Mankenda SA, Kaminskiy FV, Sobolev VN (1990) Garnets from kimberlites of Northeastern Angola and correlations between their compositions and diamond content. Dokl Earth Sci 315:238–242

- Stachel T, Harris JW, (2008) The origin of cratonic diamonds – constraints from mineral inclusions. Ore Geol Rev 34:5–32
- Stachel T, Aulbach S, Brey GP, Harris JW, Leost I, Tappert R, Viljoen KS (2004) The trace element composition of silicate inclusions in diamonds: a review. Lithos 77:1–19
- Tappert R, Foden J, Muehlenbachs K, Wills K (2011) Garnet peridotite xenoliths and xenocrysts from the Monk Hill kimberlite, South Australia: Insights into the lithospheric mantle beneath the Adelaide Fold Belt. J Petrol 52:1965–1986
- Taylor WR (1998) An experimental test of some geothermometer and geobarometer formulations for upper mantle peridotites with application to the thermobarometry of fertile lherzolite and garnet websterite. N Jb Min Abh 172:381–408
- Turkin AI, Sobolev NV (2009) Pyrope–knorringite garnets: overview of experimental data and natural parageneses: Russ Geol Geophys 50:1169–1182
- Vernières J, Godard M, Bodinier J-L (1997) A plate model for the simulation of trace element fractionation during partial melting and magma transport in the Earth's upper mantle. J Geophys Res 102:24771–24784
- Walter M, Katsura T, Kubo A, Shinmei T, Nishikawa O, Ito E, Lesher C, Funakoshi K (2002) Spinel–garnet lherzolite transition in the system CaO-MgO-Al2O3-SiO2 revisited: an in situ X-ray study. Geochim Cosmochim Acta 66:2109–2121
- Walter MJ (1998) Melting of Garnet Peridotite and the Origin of Komatiite and Depleted Lithosphere. J Petrol 39:29–60
- Webb SAC, Wood BJ (1986) Spinel-pyroxene-garnet relationships and their dependence on Cr/Al ratio. Contrib Mineral Petrol 92:471–480
- Weiss Y, Griffin WL, Bell DR, Navon O (2011) High-Mg carbonatitic melts in diamonds, kimberlites and the sub-continental lithosphere. Earth Planet Sci Lett 309:337–347
- Woolley AR, Bergman SC, Edgar AD, Le Bas MJ, Mitchell RH, Rock NMS, Scott Smith BH (1996) Classification of lamprophyres, lamproites, kimberlites, and the kalsilitic, melilitic, and leucitic rocks. Can Mineral 34:175–186
- Wu C, Zhao G, (2011) The applicability of garnet–orthopyroxene geobarometry in mantle xenoliths. Lithos 125:1–9
- Zheng J, Griffin WL, O'Reilly SY, Yang J, Li T, Zhang M, Zhang RY, Liou JG (2006) Mineral chemistry of peridotites from Paleozoic, Mesozoic and Cenozoic lithosphere: Constraints on mantle evolution beneath Eastern China. J Petrol 47:2233–2256

APPENDIX 1

BACK-SCATTERED ELECTRON IMAGES OF GARNET XENOCRYSTS FROM THE ZAGADOCHNAYA KIMBERLITE AND MAJOR ELEMENT CONCENTRATION PROFILES

This appendix include back-scattered electron images and major element concentration profiles of garnet xenocrysts from Zagadochnaya. Only zoned garnets showing clear zonation trends are reported. The source data of the element concentration profiles are reported in Appendix 2.

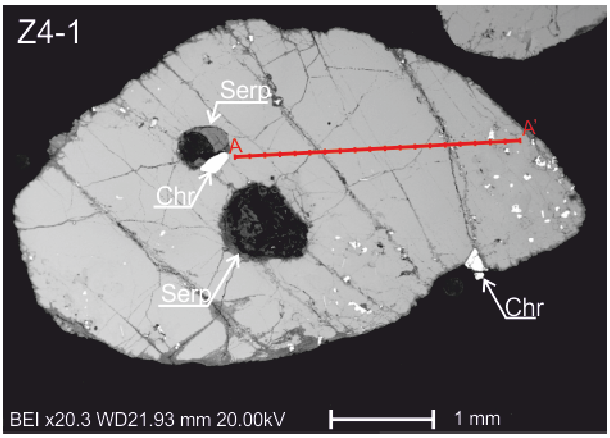
Z4-1
Serp
A
A'
Chr
Serp
Chr
BEI x20.3 WD21.93 mm 20.00kV
1 mm

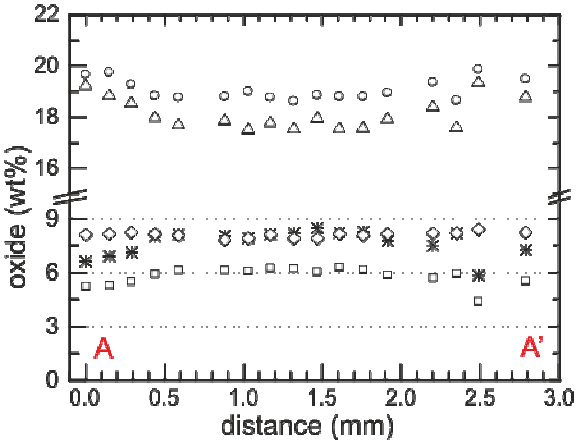
oxide (wt%)
distance (mm)
A
A'

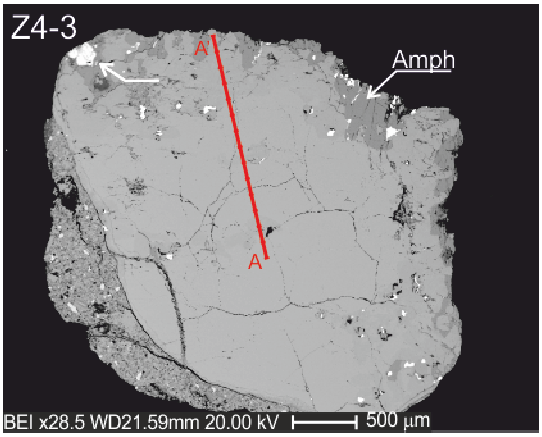
Z4-3
A'
Amph
A
BEI x28.5 WD21.59mm 20.00 kV
500 µm

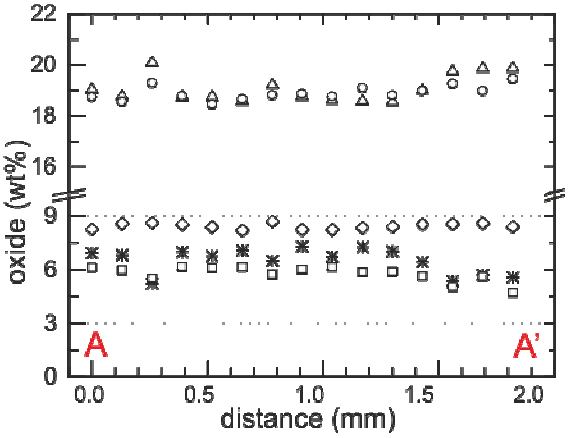
oxide (wt%)
distance (mm)
A
A'

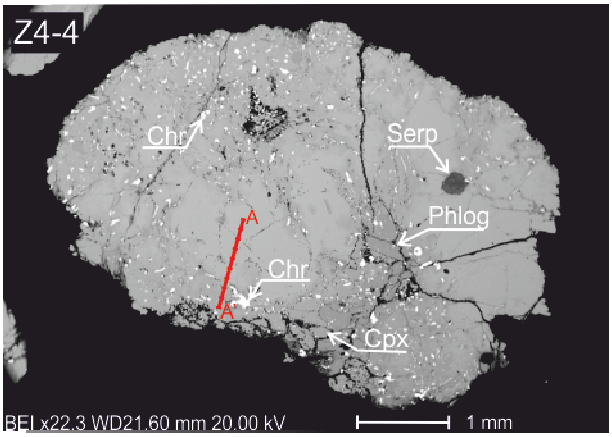
Z4-4
Chr
Serp
Phlog
A
Chr
A'
Cpx
BEI x22.3 WD21.60 mm 20.00 kV
1 mm

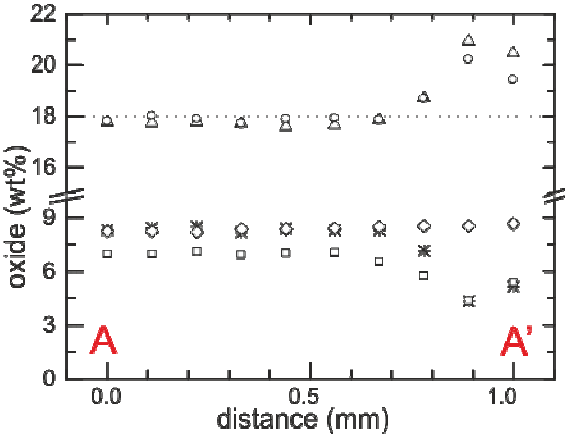
oxide (wt%)
distance (mm)
A
A'

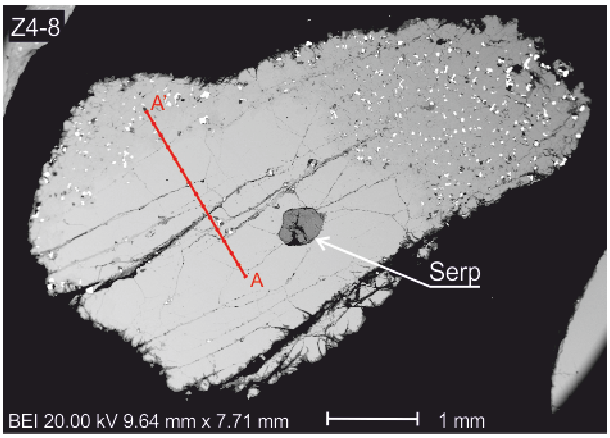
Z4-8
A'
A
Serp
BEI 20.00 kV 9.64 mm x 7.71 mm
1 mm

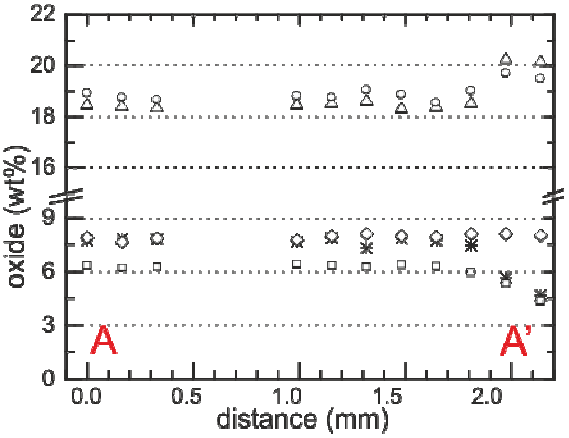
oxide (wt%)
distance (mm)
A
A'

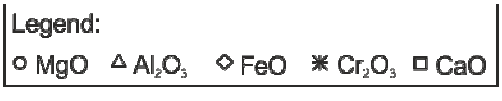
Legend:
MgO
Al2O3
FeO
Cr2O3
CaO

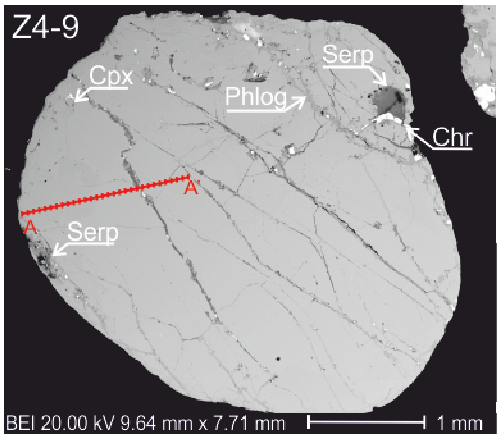
Z4-9
Cpx
Phlog
Serp
Chr
A
A'
Serp
BEI 20.00 kV 9.64 mm x 7.71 mm
1 mm

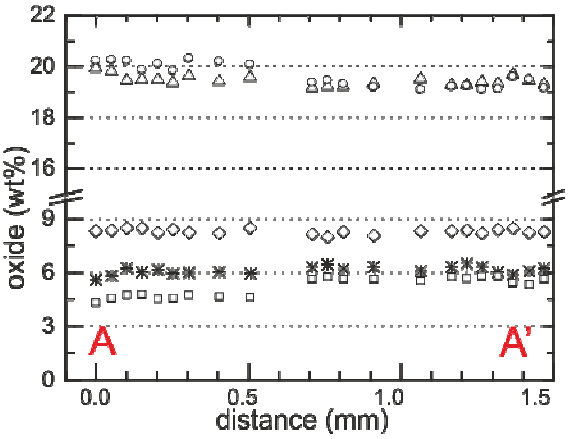
oxide (wt%)
distance (mm)
A
A'

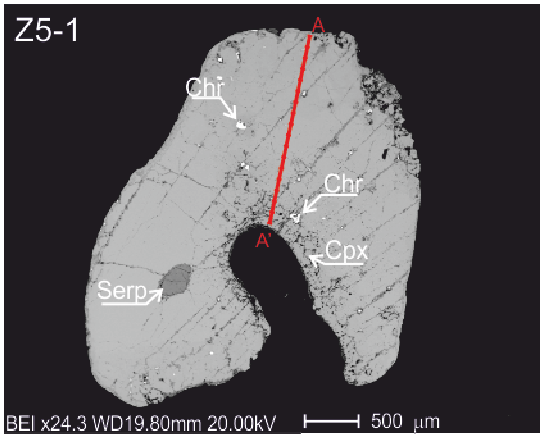
Z5-1
A
Chr
Chr
A'
Cpx
Serp
BEI x24.3 WD19.80mm 20.00kV
500 µm

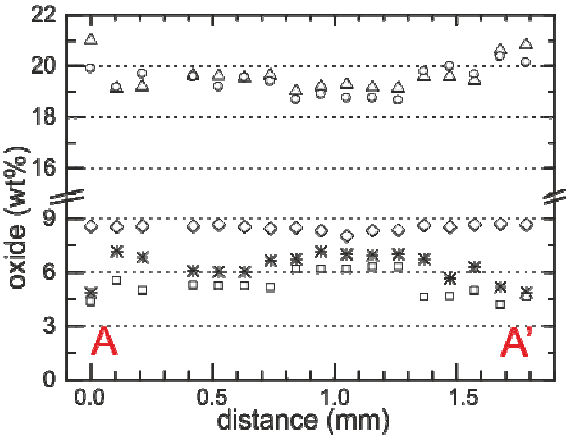
oxide (wt%)
distance (mm)
A
A'

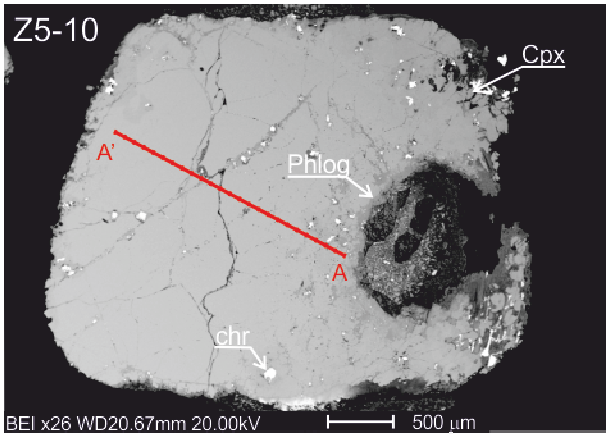
Z5-10
Cpx
A'
Phlog
A
chr
BEI x26 WD20.67mm 20.00kV
500 µm

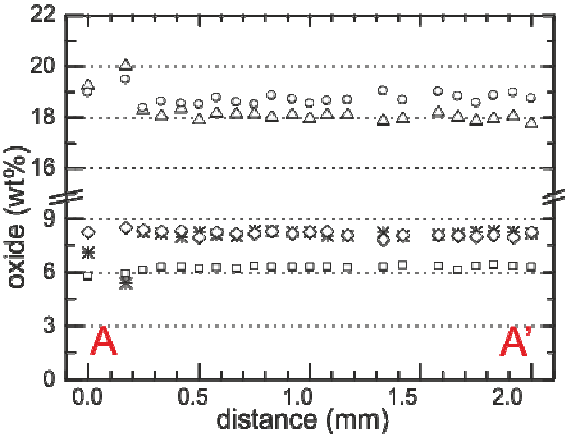
oxide (wt%)
distance (mm)
A
A'

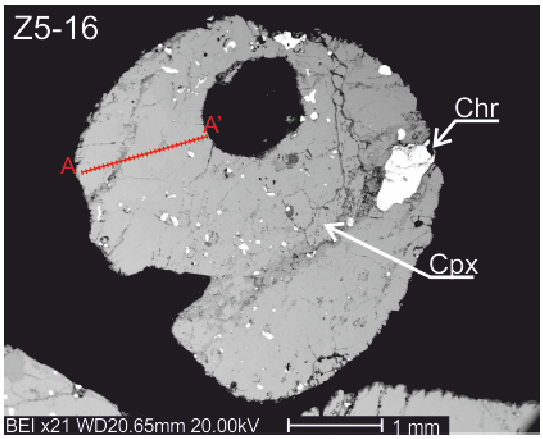
Z5-16
A'
A
Chr
Cpx
BEI x21 WD20.65mm 20.00kV
1 mm

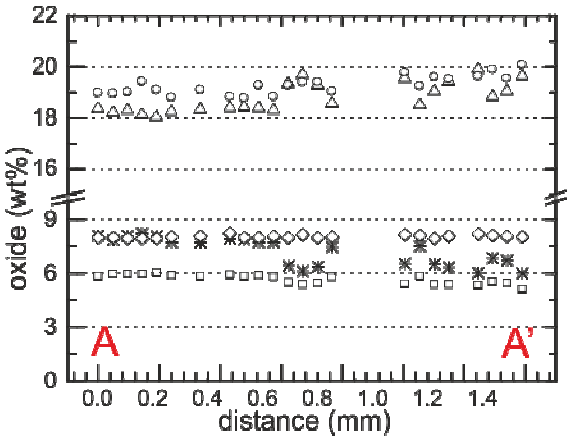
oxide (wt%)
distance (mm)
A
A'

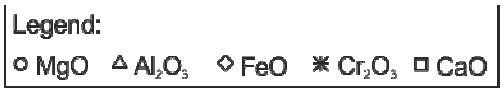
Legend:
MgO
Al2O3
FeO
Cr2O3
CaO

APPENDIX 2

RESULTS OF ELECTRON MICROPROBE TRAVERSES USED FOR MAJOR ELEMENT CONCENTRATION PROFILES

Garnet Z4-1

Label	01	02	03	04	05	07	08	09	10	11	12	13	14	16	17	18	20
SiO_2	41.43	41.93	41.56	41.33	40.94	41.19	41.23	41.29	41.73	41.36	40.93	41.03	41.20	41.41	41.14	41.76	41.32
TiO_2	0.23	0.22	0.26	0.25	0.33	0.33	0.28	0.32	0.34	0.33	0.38	0.35	0.21	0.21	0.29	0.21	0.18
Al_2O_3	19.22	18.83	18.54	17.96	17.67	17.85	17.48	17.75	17.53	17.94	17.51	17.54	17.92	18.37	17.57	19.33	18.78
Cr_2O_3	6.61	6.93	7.11	8.02	8.15	8.07	7.93	8.13	8.18	8.50	8.22	8.26	7.75	7.52	8.17	5.87	7.28
FeO_{tot}	8.10	8.16	8.24	8.12	8.06	7.81	7.87	8.11	7.91	7.88	8.14	8.06	8.14	8.20	8.19	8.40	8.24
MnO	0.35	0.39	0.41	0.32	0.34	0.24	0.42	0.36	0.35	0.30	0.31	0.27	0.39	0.36	0.45	0.33	0.38
MgO	19.65	19.76	19.28	18.82	18.78	18.79	19.00	18.77	18.62	18.86	18.80	18.79	18.95	19.35	18.65	19.85	19.49
CaO	5.24	5.29	5.48	5.90	6.14	6.11	6.07	6.23	6.20	6.04	6.31	6.17	5.87	5.71	5.93	4.38	5.51
Na_2O	0.00	0.04	0.00	0.05	0.09	0.10	0.06	0.08	0.17	0.01	0.15	0.05	0.06	0.06	0.00	0.04	0.09
K_2O	0.01	0.00	0.04	0.00	0.00	0.00	0.20	0.02	0.02	0.00	0.00	0.00	0.01	0.00	0.00	0.01	0.01
SUM	100.84	101.56	100.89	100.77	100.50	100.48	100.35	101.03	101.02	101.22	100.73	100.52	100.48	101.19	100.39	100.17	101.25
Mg#	81.2	81.2	80.7	80.5	80.6	81.1	81.2	80.5	80.8	81.004	80.5	80.6	80.6	80.8	80.2	80.8	80.8
Cr#	18.8	19.8	20.5	23.1	23.6	23.3	23.3	23.5	23.8	24.1	23.9	24.0	22.5	21.5	23.8	16.9	20.6

Garnet Z4-3

Label	01	02	03	04	05	06	07	08	09	10	11	12	13	14	15
SiO_2	41.47	41.60	41.64	41.39	41.37	41.57	41.43	41.47	41.48	41.28	41.33	41.27	41.42	41.47	41.79
TiO_2	0.17	0.18	0.15	0.15	0.22	0.15	0.15	0.19	0.21	0.18	0.19	0.12	0.09	0.12	0.08
Al_2O_3	19.03	18.74	20.08	18.73	18.73	18.55	19.20	18.75	18.60	18.56	18.53	18.99	19.74	19.86	19.86
Cr_2O_3	6.92	6.81	5.24	6.98	6.75	7.07	6.49	7.31	6.74	7.26	7.03	6.42	5.36	5.72	5.56
FeO_{tot}	8.25	8.56	8.61	8.52	8.37	8.18	8.69	8.23	8.23	8.33	8.39	8.53	8.54	8.59	8.40
MnO	0.33	0.41	0.43	0.46	0.24	0.33	0.42	0.36	0.30	0.32	0.31	0.39	0.44	0.51	0.43
MgO	18.73	18.54	19.28	18.76	18.43	18.64	18.81	18.85	18.75	19.08	18.79	18.96	19.25	18.97	19.44
CaO	6.10	5.94	5.48	6.14	6.07	6.11	5.72	6.00	6.12	5.85	5.86	5.62	5.03	5.59	4.69
Na_2O	0.01	0.00	0.11	0.03	0.07	0.01	0.07	0.00	0.02	0.05	0.04	0.00	0.06	0.00	0.11
K_2O	0.00	0.02	0.00	0.01	0.02	0.00	0.01	0.00	0.01	0.00	0.05	0.01	0.01	0.03	0.00
SUM	101.01	100.77	101.02	101.16	100.25	100.60	100.98	101.15	100.44	100.90	100.46	100.31	99.92	100.84	100.38
Mg#	80.2	79.4	80.0	79.7	79.7	80.2	79.4	80.3	80.2	80.3	80.0	79.8	80.1	79.7	80.5
Cr#	19.6	19.6	14.9	20.0	19.5	20.4	18.5	20.7	19.5	20.8	20.3	18.5	15.4	16.2	15.8

Garnet Z4-4

Label	01	02	03	04	05	06	07	08	09	10
SiO_2	40.89	40.90	40.98	41.02	41.16	40.96	41.01	41.29	42.06	41.51
TiO_2	0.04	0.05	0.05	0.05	0.03	0.01	0.05	0.04	0.03	0.03
Al_2O_3	17.76	17.73	17.76	17.69	17.58	17.63	17.86	18.70	20.94	20.47
Cr_2O_3	8.33	8.44	8.49	8.18	8.39	8.31	8.30	7.17	4.34	5.13
FeO_{tot}	8.24	8.24	8.18	8.35	8.34	8.40	8.50	8.51	8.54	8.66
MnO	0.35	0.34	0.37	0.28	0.30	0.33	0.48	0.34	0.42	0.42
MgO	17.79	18.00	17.89	17.70	17.88	17.92	17.86	18.68	20.23	19.43
CaO	6.97	6.98	7.10	6.94	6.99	7.05	6.56	5.74	4.34	5.36
Na_2O	0.00	0.02	0.02	0.00	0.00	0.00	0.06	0.00	0.00	0.00
K_2O	0.01	0.01	0.01	0.01	0.00	0.01	0.01	0.00	0.01	0.00
SUM	100.36	100.70	100.82	100.20	100.67	100.62	100.69	100.46	100.88	101.02
Mg#	79.4	79.6	79.6	79.1	79.3	79.2	78.9	79.6	80.9	80.0
Cr#	23.9	24.2	24.3	23.7	24.2	24.0	23.8	20.5	12.2	14.4

Garnet Z4-8

Label	01	02	03	07	08	09	10	11	12	13	14
SiO_2	41.61	41.22	41.39	41.44	41.32	41.38	41.29	41.21	41.27	41.49	42.06
TiO_2	0.10	0.11	0.10	0.13	0.08	0.06	0.09	0.09	0.04	0.05	0.05
Al_2O_3	18.45	18.37	18.33	18.45	18.50	18.58	18.30	18.36	18.51	20.22	20.12
Cr_2O_3	7.71	7.83	7.80	7.70	7.87	7.28	7.84	7.72	7.48	5.66	4.69
FeO_{tot}	7.91	7.64	7.83	7.75	7.98	8.10	7.96	7.94	8.09	8.12	8.01
MnO	0.35	0.35	0.32	0.38	0.32	0.38	0.38	0.35	0.34	0.40	0.42
MgO	18.93	18.73	18.64	18.79	18.75	19.03	18.86	18.52	18.99	19.69	19.47
CaO	6.31	6.22	6.26	6.41	6.31	6.24	6.37	6.27	5.97	5.32	4.34
Na_2O	0.04	0.07	0.02	0.05	0.03	0.08	0.04	0.03	0.07	0.05	0.13
K_2O	0.02	0.00	0.01	0.00	0.02	0.00	0.00	0.01	0.01	0.01	0.06
SUM	101.40	100.54	100.69	101.08	101.16	101.12	101.12	100.51	100.76	101.02	99.29
Mg#	81.02	81.4	80.9	81.2	80.7	80.7	80.8	80.6	80.7	81.2	81.3
Cr#	21.9	22.2	22.2	21.9	22.2	20.8	22.3	22.0	21.3	15.8	13.5

Garnet Z4-9

Label	01	02	03	04	05	06	07	09	11	15	16
SiO_2	41.81	41.89	41.98	41.83	41.89	41.66	41.91	41.63	41.50	41.34	41.75
TiO_2	0.09	0.14	0.15	0.12	0.09	0.09	0.08	0.10	0.11	0.19	0.19
Al_2O_3	19.91	19.81	19.45	19.49	19.48	19.36	19.64	19.42	19.57	19.16	19.22
Cr_2O_3	5.61	5.81	6.25	6.05	6.18	5.94	5.99	6.03	5.94	6.27	6.45
FeO_{tot}	8.32	8.34	8.46	8.50	8.22	8.40	8.23	8.19	8.49	8.14	7.99
MnO	0.42	0.39	0.40	0.36	0.36	0.39	0.36	0.30	0.37	0.43	0.33
MgO	20.21	20.24	20.22	19.87	20.11	19.83	20.32	20.18	20.08	19.36	19.45
CaO	4.32	4.56	4.72	4.78	4.53	4.57	4.72	4.65	4.59	5.62	5.72
Na_2O	0.04	0.03	0.04	0.05	0.07	0.04	0.01	0.06	0.04	0.02	0.04
K_2O	0.00	0.00	0.00	0.00	0.00	0.01	0.02	0.02	0.00	0.01	0.00
SUM	100.74	101.21	101.67	101.04	100.94	100.28	101.28	100.60	100.69	100.54	101.14
Mg#	81.2	81.2	81.0	80.6	81.4	80.8	81.5	81.5	80.8	80.9	81.3
Cr#	15.9	16.4	17.7	17.2	17.5	17.1	17.0	17.2	16.9	18.0	18.4

Garnet Z4-9 continued

Label	17	19	22	24	25	26	27	28	29	30
SiO_2	41.69	41.59	41.82	41.63	41.48	41.80	41.46	41.78	41.85	41.51
TiO_2	0.21	0.20	0.18	0.16	0.15	0.19	0.15	0.09	0.11	0.13
Al_2O_3	19.22	19.32	19.51	19.26	19.26	19.40	19.34	19.68	19.46	19.30
Cr_2O_3	6.20	6.34	6.08	6.34	6.51	6.29	6.04	5.92	6.06	6.24
FeO_{tot}	8.27	8.07	8.30	8.30	8.37	8.20	8.38	8.47	8.22	8.26
MnO	0.31	0.37	0.34	0.29	0.33	0.40	0.34	0.38	0.35	0.34
MgO	19.30	19.18	19.08	19.22	19.25	19.09	19.12	19.59	19.49	19.14
CaO	5.63	5.61	5.53	5.73	5.66	5.76	5.78	5.42	5.31	5.60
Na_2O	0.04	0.01	0.04	0.04	0.00	0.06	0.03	0.00	0.00	0.00
K_2O	0.00	0.03	0.01	0.01	0.01	0.00	0.00	0.00	0.00	0.00
SUM	100.87	100.70	100.89	100.97	101.01	101.19	100.64	101.32	100.84	100.51
Mg#	80.6	80.9	80.4	80.5	80.4	80.6	80.3	80.5	80.9	80.5
Cr#	17.8	18.0	17.3	18.1	18.5	17.9	17.3	16.8	17.3	17.8

Garnet Z5-1

Label	01	02	03	05	06	07	08	09	10	11	12	13	14	15	16	17	18
SiO_2	41.96	41.88	41.33	41.54	41.46	41.33	41.68	41.18	41.18	41.30	41.46	41.27	41.12	41.60	41.32	42.03	42.19
TiO_2	0.02	0.02	0.02	0.03	0.02	0.03	0.00	0.02	0.00	0.03	0.04	0.03	0.00	0.02	0.05	0.01	0.02
Al_2O_3	20.98	19.11	19.18	19.62	19.59	19.54	19.62	19.01	19.17	19.28	19.14	19.12	19.57	19.57	19.41	20.61	20.82
Cr_2O_3	4.87	7.18	6.85	6.06	6.04	6.03	6.67	6.76	7.18	6.99	6.98	6.99	6.77	5.67	6.30	5.19	4.89
FeO_{tot}	8.57	8.53	8.58	8.58	8.64	8.53	8.45	8.47	8.32	8.02	8.33	8.35	8.60	8.54	8.63	8.70	8.65
MnO	0.40	0.38	0.30	0.31	0.47	0.30	0.32	0.39	0.36	0.33	0.27	0.25	0.38	0.46	0.39	0.38	0.38
MgO	19.89	19.16	19.69	19.56	19.18	19.55	19.38	18.67	18.90	18.73	18.73	18.66	19.79	19.99	19.67	20.38	20.14
CaO	4.35	5.52	5.00	5.26	5.22	5.22	5.13	6.16	6.14	6.14	6.29	6.30	4.62	4.66	4.98	4.17	4.60
Na_2O	0.00	0.02	0.05	0.02	0.00	0.05	0.06	0.06	0.00	0.01	0.01	0.06	0.00	0.00	0.03	0.00	0.08
K_2O	0.00	0.01	0.03	0.00	0.03	0.01	0.00	0.00	0.00	0.01	0.01	0.02	0.01	0.03	0.09	0.11	0.02
SUM	101.04	101.81	101.04	101.00	100.64	100.60	101.31	100.72	101.25	100.84	101.27	101.04	100.85	100.54	100.85	101.58	101.78
Mg#	80.5	80.0	80.4	80.2	79.8	80.3	80.3	79.7	80.2	80.6	80.0	79.9	80.4	80.7	80.3	80.7	80.6
Cr#	13.5	20.1	19.3	17.2	17.1	17.2	18.6	19.3	20.1	19.6	19.7	19.7	18.8	16.3	17.9	14.5	13.6

Garnet Z5-10

Label	01	03	04	05	06	07	08	09	10	11	12	13	14	15
SiO_2	41.91	41.66	41.15	41.39	41.17	41.18	41.50	41.28	41.44	41.35	41.24	41.22	41.10	41.61
TiO_2	0.05	0.11	0.10	0.11	0.15	0.15	0.14	0.12	0.15	0.14	0.12	0.17	0.15	0.15
Al_2O_3	19.23	20.02	18.26	18.04	18.31	17.89	18.13	18.12	18.12	18.01	18.09	17.95	18.09	18.07
Cr_2O_3	7.07	5.42	8.25	8.18	7.98	8.24	8.11	8.02	8.31	8.33	8.25	8.25	8.06	8.08
FeO_{tot}	8.24	8.48	8.34	8.25	8.30	7.95	8.23	8.15	8.13	8.29	8.13	8.23	8.26	8.08
MnO	0.39	0.33	0.39	0.36	0.24	0.33	0.34	0.38	0.28	0.31	0.24	0.26	0.28	0.33
MgO	18.98	19.47	18.36	18.62	18.52	18.49	18.78	18.59	18.49	18.85	18.72	18.52	18.65	18.67
CaO	5.77	5.92	6.13	6.28	6.27	6.19	6.23	6.22	6.31	6.29	6.28	6.30	6.30	6.24
Na_2O	0.07	0.00	0.05	0.07	0.03	0.00	0.01	0.01	0.05	0.00	0.05	0.01	0.00	0.05
K_2O	0.00	0.00	0.00	0.01	0.00	0.00	0.01	0.00	0.00	0.00	0.00	0.00	0.01	0.00
SUM	101.70	101.41	101.03	101.31	100.96	100.42	101.49	100.90	101.28	101.56	101.11	100.91	100.89	101.27
Mg#	80.4	80.4	79.7	80.1	79.9	80.6	80.3	80.3	80.2	80.2	80.4	80.0	80.1	80.5
Cr#	19.8	15.4	23.3	23.3	22.6	23.6	23.1	22.9	23.5	23.7	23.4	23.6	23.0	23.1

Garnet Z5-10 continued

Label	17	18	20	21	22	23	24	25
SiO_2	41.39	41.16	41.17	41.07	41.37	41.55	41.39	41.13
TiO_2	0.14	0.15	0.14	0.17	0.19	0.16	0.13	0.15
Al_2O_3	17.86	17.94	18.18	17.99	17.85	17.93	18.04	17.74
Cr_2O_3	8.24	8.00	8.10	8.14	8.25	8.33	8.28	8.18
FeO_{tot}	7.80	8.05	8.07	8.00	7.96	8.08	7.94	8.21
MnO	0.37	0.30	0.36	0.37	0.29	0.36	0.33	0.37
MgO	19.02	18.69	18.99	18.82	18.57	18.87	18.97	18.74
CaO	6.28	6.36	6.32	6.12	6.31	6.40	6.31	6.27
Na_2O	0.00	0.00	0.00	0.01	0.01	0.05	0.01	0.00
K_2O	0.00	0.00	0.00	0.00	0.00	0.01	0.00	0.00
SUM	101.11	100.67	101.34	100.68	100.80	101.75	101.41	100.82
Mg#	81.3	80.5	80.7	80.7	80.6	80.6	81.0	80.3
Cr#	23.6	23.0	23.0	23.3	23.7	23.8	23.5	23.6

Garnet Z5-16

Label	01	02	03	04	05	06	08	10	11	12	13	14	15	16	17	22
SiO_2	41.95	41.98	41.67	41.75	41.48	41.85	41.90	41.95	41.74	42.22	42.02	42.25	42.22	42.20	41.89	41.92
TiO_2	0.19	0.18	0.21	0.20	0.21	0.14	0.13	0.21	0.21	0.19	0.18	0.19	0.13	0.16	0.18	0.14
Al_2O_3	18.34	18.21	18.28	18.12	18.02	18.22	18.32	18.38	18.40	18.39	18.28	19.34	19.69	19.26	18.55	19.54
Cr_2O_3	8.09	7.86	8.08	8.23	8.07	7.71	7.72	7.94	7.87	7.72	7.74	6.42	6.12	6.37	7.48	6.54
FeO_{tot}	7.96	7.97	7.94	7.95	7.92	8.03	8.05	8.23	7.97	7.99	8.08	7.98	8.15	7.97	8.03	8.15
MnO	0.35	0.23	0.31	0.30	0.28	0.33	0.34	0.30	0.37	0.34	0.33	0.37	0.45	0.36	0.41	0.34
MgO	18.97	18.95	19.00	19.43	19.08	18.79	19.10	18.83	18.77	19.28	18.84	19.28	19.39	19.38	19.03	19.77
CaO	5.81	5.94	5.95	5.94	6.05	5.87	5.84	5.90	5.82	5.88	5.78	5.50	5.36	5.44	5.80	5.41
Na_2O	0.07	0.00	0.00	0.01	0.10	0.00	0.03	0.00	0.04	0.10	0.00	0.03	0.02	0.03	0.12	0.04
K_2O	0.02	0.00	0.00	0.01	0.02	0.00	0.05	0.03	0.02	0.00	0.00	0.01	0.00	0.00	0.02	0.01
SUM	101.72	101.32	101.43	101.94	101.24	100.94	101.47	101.76	101.21	102.11	101.25	101.37	101.53	101.17	101.49	101.88
Mg#	81.0	80.9	81.0	81.3	81.1	80.7	80.9	80.3	80.8	81.1	80.6	81.2	80.9	81.3	80.9	81.2
Cr#	22.8	22.4	22.9	23.4	23.1	22.1	22.0	22.5	22.3	22.0	22.1	18.2	17.3	18.2	21.3	18.3

Garnet Z5-16 continued

Label	23	24	25	27	28	29	30
SiO_2	41.82	42.17	42.10	42.16	41.88	42.06	42.51
TiO_2	0.10	0.11	0.13	0.07	0.09	0.09	0.10
Al_2O_3	18.49	19.02	19.41	19.89	18.83	19.04	19.62
Cr_2O_3	7.50	6.49	6.34	6.04	6.83	6.70	6.01
FeO_{tot}	8.09	7.95	8.06	8.18	8.10	8.04	8.03
MnO	0.38	0.34	0.30	0.25	0.40	0.38	0.31
MgO	19.24	19.60	19.52	19.62	19.89	19.53	20.07
CaO	5.82	5.37	5.35	5.31	5.51	5.43	5.09
Na_2O	0.01	0.06	0.05	0.05	0.10	0.01	0.00
K_2O	0.00	0.00	0.00	0.01	0.00	0.00	0.00
SUM	101.45	101.12	101.27	101.60	101.63	101.28	101.73
Mg#	80.9	81.5	81.2	81.0	81.4	81.2	81.7
Cr#	21.4	18.6	18.0	16.9	19.6	19.1	17.0